

**PhD Thesis**

**Theoretical Condensed Matter Physics**

**Inna Bashta**



PhD Thesis XXXIV Cycle

**Structural anomalies of supercooled water in LiCl solution**

Molecular Dynamics Simulations Study

Supervisors: Prof. Paola Gallo

A thesis submitted for the degree of Doctor of Philosophy in the  
Department of Mathematics and Physics  
Università degli Studi Roma Tre  
Rome, Italy  
January 2022

Copyright © 2022 by Inna Bashta

The thesis of Inna Bashta was reviewed and approved\* by the following:

Professor Paola Gallo  
Full Professor of Theoretical Condensed Matter Physics  
Dipartimento di Matematica e Fisica  
Università degli Studi Roma Tre

Professor Mauro Rovere  
Professor of Theoretical Condensed Matter Physics  
Dipartimento di Matematica e Fisica  
Università degli Studi Roma Tre

\*Signatures are on file in the Graduate School

Date approved:

I hereby declare that this submission is my own work and that, to the best of my knowledge and belief, it contains no material previously published or written by another person nor material which to a substantial extent has been accepted for the award of any other degree or diploma of the university or other institute of higher learning, except where due acknowledgment has been made in the text.



/Inna Bashta

/January 31<sup>st</sup>, 2022

For my Papá - the best man of mankind.

## Abstract

A molecular dynamic study on structural properties of water in correlation between water molecules upon supercooling and hydrated LiCl ions was performed. In connection with the study of the anomaly of supercooled water, two ionic solutions, dilute LiCl:24H<sub>2</sub>O and concentrated LiCl:7H<sub>2</sub>O, were used. Both solutions are readily supercooled, and the liquid state was maintained over a large decrease in temperature. In order to investigate how the presence of salts modifies the behaviour of supercooled water, simulations were performed at ambient pressure from 300 K down to 200 K. The analysis of the changes in structural properties in water induced by the salts revealed that while the salts preserve hydrogen bonds in the systems, the tetrahedral hydrogen bond network is significantly affected. Nonetheless, the anomalies of water found to be intact together with existence of a high density and a low density liquid. Moreover, the modification of the oxygen radial distribution function of the hydrogen bonds in water indicate that LiCl is the high density liquid component in water enhancer with respect to low density component. This observation is indeed in agreement with experimental findings on aqueous ionic solutions.

## Acknowledgements

My deepest thanks to my supervisor Professor Paola Gallo, Full Professor of Theoretical Condensed Matter Physics at the Università degli Studi Roma Tre for her unwavering support in the development and completion of this study. Sincere thanks to Professor Mauro Rovere at the Università degli Studi Roma Tre for guiding me to better understanding of my topic and participation in my success. You both are incredible people and the best mentors anyone could ask for. Thank you for your time, support, patience, dedication to my success and help in accomplishing my goal.

Special recognition is given to the individuals who served on the thesis committee and contributed to the completion of this study:

Special thanks to my friend and colleague, Chiara Nardoni - without your unconditional love, help and support I could not have concurred this task. You have been my rock.

I would like to express my sincere appreciation to my lifetime mentor - Professor Ken Czerwinski for his unwavering support, help and encouragement.

My sincere thanks to my friends: Michael Ashton, Lisa Gentile and Alisa Steinhauer - you are the best support team anyone could have ever asked for.

Lastly, I would like to extend love and appreciation to Mamá for her understanding and unending support to see this PhD degree through completion.



*Water is clearly a mystery to me.*

*A solid? A liquid? A gas? It's all three.*

*Freeze it. Warm it. Boil it. You'll see.*

*Water is clearly a mystery to me.*

*Amy Ludwig VanDerwater*

# Contents

<b>Acronyms</b> .....	<b>xi</b>
<b>Symbols and Constants</b> .....	<b>xiii</b>
<b>Introduction</b> .....	<b>1</b>
<b>1 Water: ubiquitous but deceptive liquid</b> .....	<b>6</b>
1.1 Molecular structure.....	8
1.2 Hydrogen Bond.....	12
1.3 Properties of water molecule.....	16
1.3.1 Physical properties.....	17
1.3.2 Chemical properties.....	18
1.3.3 Polarity.....	18
1.3.4 Heat capacity and heat of vaporization.....	19
1.3.5 Cohesiveness and adhesiveness.....	19
1.3.6 Density paradox.....	20
1.3.7 Phase transitions.....	20
1.3.8 Triple and critical points.....	22
1.3.9 Solvation.....	23
1.3.10 Conductivity.....	26
1.4 Peculiarities of water.....	26
1.4.1 Thermodynamics.....	27
1.4.1.1 Volume.....	27
1.4.1.2 Density.....	27
1.4.1.3 Pressure.....	30
1.4.1.4 Thermodynamic response functions.....	32
1.4.2 Diffusion.....	38
1.4.3 Structure.....	39
1.5 States of water.....	41
1.5.1 The phase diagram of water.....	41
1.5.2 Stable states.....	42
1.5.2.1 Widom line: liquid-gas critical point.....	43
1.5.3 Metastable state.....	44
1.5.3.1 Polyamorphism: Three forms of solid amorphous ice.....	48
1.5.3.2 Supercooled water.....	51
1.5.3.3 Fragile to strong crossover in water.....	60

<b>2</b>	<b>Molecular Dynamics.....</b>	<b>63</b>
2.1	Foundation, Theory and Principles.....	64
2.2	Integration algorithms.....	69
2.2.1	Translational motion.....	70
2.2.2	Rotational motion.....	73
2.3	Thermostats and Barostats.....	76
2.4	Ewald summation.....	78
2.5	Running MD simulations.....	83
2.5.1	System setup.....	84
2.5.2	Equilibration.....	85
2.5.3	Production.....	86
2.5.4	Data analysis and error estimation.....	86
2.6	Force fields.....	87
<b>3</b>	<b>Molecular Dynamics of Water and Ionic Aqueous Solutions.....</b>	<b>92</b>
3.1	General concepts.....	93
3.2	Water models.....	93
3.2.1	Simple water models.....	94
3.2.2	Challenges in implementing models of water.....	97
3.3	MD simulations of water.....	97
3.3.1	Prerequisites.....	98
3.3.2	Periodic Boundary Condition (PBC) of water.....	99
3.3.3	Input to MD simulation program.....	100
3.3.4	Potential models of water under consideration.....	101
3.3.4.1	SPC/E potential model for water.....	101
3.3.4.2	TIP4P/2005 potential model for water.....	103
3.4	MD simulations of ionic aqueous solutions.....	105
3.4.1	JC-TIP4P/2005 potential model for LiCl-water solution.....	107
3.5	Molecular Dynamics identifiers.....	108
3.5.1	Dynamic observables.....	108
3.5.1.1	Self-Intermediate Scattering Function, SISF.....	108
3.5.1.2	Mean Square Displacement, MSD.....	109
3.5.2	Structural observables.....	110
3.5.2.1	Radial Distribution Function, RDF.....	111
3.5.2.1.1	Statistics on RDF.....	117
3.5.2.2	Orientalional Tetrahedral Parameter, $P(Q)$ .....	118
3.5.2.3	Local Structure Index, LSI.....	119
3.5.2.4	Angular Distribution Function, $P(\cos \gamma)$ .....	122
3.5.2.5	Structural Order Parameter, $P(\zeta)$ .....	123
3.5.2.6	Translational Tetrahedral Parameter, $S_k$ .....	124

<b>4</b>	<b>LiCl:RH<sub>2</sub>O solutions in supercooled water regime.....</b>	<b>125</b>
4.1	Significancy of LiCl:RH <sub>2</sub> O solutions.....	126
4.1.1	Features of LiCl: RH <sub>2</sub> O solutions.....	128
4.1.2	Influence of LiCl on dynamics of water.....	129
4.1.3	Impact of LiCl on the molecular structure of water molecule.....	130
4.1.3.1	Properties of aqueous ionic solutions: ionic hydration.....	136
4.1.3.2	Effects on HB network: Hofmeister classification scheme for anions and cations in the HB network of H <sub>2</sub> O.....	137
4.2	LiCl:RH <sub>2</sub> O solutions: a gateway for probing water in a supercooled regime.....	138
4.2.1	Recent experimental findings.....	140
4.2.2	Latest MD simulations results.....	143
<b>5</b>	<b>Water and hydrated ions correlations: investigating structural properties.....</b>	<b>148</b>
5.1	MD simulations.....	151
5.1.1	Model potential.....	152
5.1.2	Simulation constituents.....	152
5.2	Structure and thermodynamics of water in presence of ions.....	155
5.2.1	Correlation between TMD anomaly and ionic concentrations.....	156
5.2.2	Structural properties of water.....	158
5.2.2.1	RDFs for O-O.....	160
5.2.2.2	RDFs for O-H.....	162
5.2.2.3	RDFs for H-H.....	164
5.3	Ion-water correlations.....	166
5.3.1	RDFs for Cl-X.....	167
5.3.2	RDFs for Li-X.....	171
5.3.3	RDFs for ion-H.....	175
5.4	Calculations of structural trajectories and variables.....	178
5.4.1	Local Structure Index, LSI.....	178
5.4.2	Tetrahedral Parameter, $P(Q)$ .....	182
5.5	Hydrogen Bond network.....	185
5.5.1	Angular Distribution Function, $P(\cos \gamma)$ .....	185
5.5.2	HBs distribution.....	189
	<b>Conclusion.....</b>	<b>192</b>
	<b>References.....</b>	<b>197</b>
	<b>Appendices.....</b>	<b>222</b>
	<b>Vita.....</b>	<b>237</b>

## Acronyms

Acronym	Definition
ASW	Amorphous Solid Water
CIP	Contact Ion Pair
CN	Coordination Number
CP	Critical Point
DFT	Density Function Theory
FF	Force Field
FSC	Fragile to Strong Crossover
HB	Hydrogen Bond
HDA	High Density Amorphous Ice
HDL	High Density Liquid
HGW	Hyperquenched Glassy Water
HN	Hydration Number
HOMO	Highest Occupied Molecular Orbital
LDA	Low Density Amorphous Ice
LDL	Low Density Liquid
LJ	Lennard-Jones
LLCP	Liquid-Liquid Critical Point
LSI	Local Structure Index
LUMO	Lowest Unoccupied Molecular Orbital
MCT	Mode Coupling Theory
MD	Molecular Dynamics
MO	Molecular Orbital
MSD	Mean Squared Displacement
NPT	Isobaric-Isothermal Ensemble
NVE	Microcanonical Ensemble
NVT	Canonical Ensemble
OTO ( $P(q)$ )	Orientalional Tetrahedral Order
PB	Poisson-Boltzmann
PBC	Periodic Boundary Conditions
PMF	Potential of Mean Force
PME	Particle Mesh Ewald Method
RDF ( $g(r)$ )	Radial Distribution Function
SIP	Solvent-shared Ion Pair
SISF	Self Intermediate Scattering Function
SO ( $P(\zeta)$ )	Structural Order
SPC	Simple Point Charge (3-site water model)
SPC/E	Simple Point Charge Extended 3-site water model
TIP	Transferable Intermolecular Potential
TIP4P	Transferable Interaction Potential with 4 Points
TMD	Temperature of Maximum Density
TP	Triple Point

TTO ( $S_k$ )	Translational Tetrahedral Order
VHDA	Very High Density Amorphous Ice
$\mu$ VT	Grand Canonical Ensemble

---

## Symbols and Constants

Symbol/ Constant	Definition	Value
$c_p$	Specific heat capacity	$4184 \text{ J} \cdot \text{kg}^{-1} \cdot \text{K}^{-1}$
$c$	Concentration in moles per litre (molality)	
$c$	Velocity of light	$2 \cdot 997925 \times 10^{10} \text{ cm sec}^{-1}$
$C_p$	Isobaric specific heat	
$D$	Self-diffusion coefficient	$2.299 \cdot 10^{-9} \text{ m}^2 \cdot \text{s}^{-1}$ at 25 °C $1.261 \cdot 10^{-9} \text{ m}^2 \cdot \text{s}^{-1}$ at 4 °C
$d_{\text{HB}}$	Distance to the furthest HB neighbour	
$d_{\text{-HB}}$	Distance to the nearest non-HB neighbour	
$e$	Electronic charge	
$F$	Faraday constant	$96486 \cdot 8 \text{ coulomb (g} \cdot \text{equivalent)}^{-1}$
$G$	Gibbs free energy	
$g(r)$	RDF	
$H$	Enthalpy	$104.83 \text{ kJ} \cdot \text{kg}^{-1}$ at 25 °C
$\mathcal{H}$	Hamiltonian of the system	
$h$	Hydration number	
$I$	Ionic strength	
$I_h$	Hexagonal ice	
$K - K_w$	Equilibrium constant →	
$-k$	Ionization constant of water → Rate constant	$K_w = 1.01 \times 10^{-14}$ at 25 °C
$\mathcal{K}$	Kinetic energy of the system	
$k_B$	Boltzmann's constant	$1.38064852 \times 10^{-23} \text{ m}^2 \text{ kg s}^{-2} \text{ K}^{-1}$
$k_C$	Electrostatic constant used in MD modelling	$332.1 \text{ \AA} \cdot \text{kcal/mol}$
$k_T$	Isothermal compressibility of water	$4.6 \times 10^{-10} \text{ m}^2 \cdot \text{N}^{-1}$ at 25 °C
$L$	Specific latent heat	
$L_f$	Molar latent heat of melting/fusion	$334 \text{ kJ} \cdot \text{kg}^{-1}$ at 0 °C
$L_v(L_c)$	Specific latent heat of vaporization (boiling)	$2264.705 \text{ kJ} \cdot \text{kg}^{-1}$ at 100 °C
$\mathcal{L}$	Lagrangian of the system	
$l$	Length	
$M$	Abbreviation for <i>molal</i>	
$m$	Mass	

$m$	Moles of solute per kg of solvent (molality)	
$N$	Avogadro number	$6 \cdot 02252 \times 10^{23} \text{ mol}^{-1}$
$N_i$	Total number of ions of species $i$	
$n_i$	Number of ions of species $i$ per volume; in particular of bulk water	
$p$	Pressure	
$Q$	Electric charge	
$q$	Critical distance for ion-pair formation	
$q$	Orientational parameter	
<b>q</b>	Quaternion	
$q_i$	Partial charge related to charges of electrons	
$r$	Distance or radius	
$r_{ij}$	Distance between two atoms or charged sites	
$S$	Entropy	$0.36722 \text{ kJ} \cdot (\text{kg} \cdot \text{K})^{-1}$ at 25 °C
$s$	Solubility	
$\Delta s$	Specific entropy change of the phase transition	
$T$	Absolute temperature	
$T$	Temperature	
$T_g(p)$	Glass transition temperature	136 K
$T_H(p)$	Homogeneous nucleation temperature	232 K
$T_M(p)$	Melting temperature	273 K
$T_S(p)$	Singular divergence of temperature upon cooling	228 K
$T_x(p)$	Spontaneous crystallization temperature	150 K
$t$	Time	
$t$	Translational parameter	
$U$	Potential energy	
$u$	Many-body interaction potential	
$u_{ij}$	Radial potential of pair of particles	
$\mathcal{V}$	Virial	
$v$	Velocity	
$v$	Molar volume	
$\Delta v$	Specific volume change of the phase transition	

$v_L$	Molar volume of liquid phase	
$v_S$	Molar volume of solid phase	
$X$	Generic response function of the power law	
$\Lambda$	Equivalent conductivity of electrolyte	
$\alpha$	Degree of dissociation	
$\alpha_P$	Coefficient of thermal expansion	$207 \times 10^{-6} \cdot \text{K}^{-1}$ at 20 °C
$\gamma$	Activity coefficient on molality scale	
$\lambda$	Latent heat of fusion	
$\rho$	Density of water	$0.997 \text{ g} \cdot \text{m}^{-3}$ at 25 °C
$\varepsilon$	Dielectric constant/extinction coefficient	
$\varepsilon$	Molar absorption coefficient	
$\varepsilon_r$	Relative permittivity	87.9 at 0 °C for visible light: 1.77
$\eta$	Viscosity	0.89 mPa. s at 25 °C
$\mu$	Dipole moment	
$\mu$	Mobility coefficient	
$\tau_1$	Nucleation time	

## Introduction



Water is the most abundant substance in all living cells without which life simply would cease to exist. As the main constituent of Earth's hydrosphere and the fluids of all known living organisms, water is the global solvent, essential for all living organisms [1]. In fact, life is believed to have originated in aqueous solutions of the world's oceans, and all living organisms depend on aqueous solutions.

Mankind's quest for life on other planets is primarily initiated by looking for water as it is had been consented to be the foundation of life on Earth. Thus, all life forms in our universe are water-dependent [2, 3]. Water has already been found on other planets in our solar system (e.g., Mars) and their moons, on asteroids and comets [4].

Water is established to be a solvent, reactant, product, catalyst, chaperone, messenger, and controller. In some ways, water behaves as an ordinary liquid but in other ways water is very complex and anomalous substance. Interestingly, as a key to existence of life, water is the strangest liquid in the universe with many peculiar counterintuitive properties.

Many of water's anomalous macroscopic properties originate from its ability to form up to four hydrogen bonds (HBs), in addition to the non-directional interactions observed in simple liquids. Among the most

---

famous examples of water's unusual properties are an increased density on melting, decreased viscosity under pressure, density maximum at 4 °C, high surface tension, to name a few. For decades water's anomalies are observed in many experiments, and are called for explanations by applying various theories, experiments, modelling and simulations [5, 6].

Up to date, more than 75 anomalies have been reported for water, however amongst most striking anomalies are probably the existence of a maximum on the density and on the viscosity versus temperature [7]. In other words, unlike in most other liquids, the density and viscosity of water do not evolve monotonously with temperature. To explain these behaviours, over 30 years ago, Poole *et al.* [8] postulated the existence of two different liquid states of water, a *low-density liquid* (LDL) and a *high-density liquid* (HDL), with a *critical point* (CP), also called *liquid-liquid CP* (LLCP) located at low temperature in the *supercooled* region where water exists in a state of precarious equilibrium. [9, 10, 11, 12, 13, 14, 15, 16, 17, 18].

Below the homogeneous nucleation temperature,  $T_H = 232$  K, water crystallizes rapidly [19, 20, 21, 22], which presents a great challenge for accessing it experimentally with bulk liquid water region of temperature below  $T_H$  and above the glass-transition temperature,  $T_g = 136$  K. Because of this difficulty, that region of temperature,  $T_H > T > T_g$ , is called the *no-man's land*. Given that the putative liquid-liquid (LL) transition between the HDL, and the LDL, is located inside the no-man's land, it is difficult to observe experimentally, hence, the subject of the metastability of these two liquid states of water continues to be studied a lot. According to the LLCP hypothesis the anomalous behaviour of water can be justified by treating liquid water as a mixture of two defined groups of molecules, relating to two different arrangements of the HB network, i.e., LDL and HDL. The characteristics of the LDL are : it prevails on the low temperature

---

side of the diagram, it has stronger tetrahedral order locally, and has more cage-like structure. The features of the HDL are : it is mostly located at higher temperature side, it contains broken HBs, and its structure is less cage-like.

In order to obtain a deep understanding of how water's properties are encoded within its molecular structures, *Molecular Dynamics* (MD) simulation investigations are by far more surpassive. Indeed, in probing and interpreting observable properties of water in terms of molecular structure, energetics, and population distribution, modelling is far more superior method.

The general aim of the MD simulations is to probe the dynamic and structural trajectories for a system composed of  $N$  particles by integrating Newton's equations of motion. To examine the physics in the system under MD study, four essential steps must be taken - setup of initial system, equilibration run, production run, data analysis, and error estimation. The specific aim of the MD simulations of water is to calculate as many macroscopic physical properties as possible from the simulated trajectories.

Water is the universal solvent. Thus, addition of ions into water significantly impacts its properties as they interrupt the HB network of water.

Many properties of the electrolyte solutions are the consequences of the way in which the solvent molecules behave to get close to and to interact with the ions. For instance, the selectivity of the ionic channels is a direct consequence of the hydration of the ions since the dimensions of the channels are particularly dependent on the specific dimensions of the

---

hydrated ions. The presence of the ion and their hydration shells may destroy locally, or at least may perturb the water hydrogen bond (HB) network which is responsible for many properties of the aqueous solutions [23, 24, 25, 26].

The MD simulations of ionic solutions allow to determine the orientation of the water molecules in the hydration shell of ions based on the location of the first maxima in the ion-oxygen and ion-hydrogen structural arrangement.

In the present study, lithium chloride is selected because of its high solubility in water and its ease in supercooling. Aqueous solutions of LiCl are also of great use in studying the properties of bulk water in the supercooled regime up to eutectic temperatures of 200 K, and far into no man's land. Furthermore, in the presence of LiCl, the HDL component of water is enhanced which prevents possibility of crossover from fragile (more HDL) to strong (more LDL) dynamic behaviour. Yet, overall, as a representative member of alkali halides, LiCl has surprisingly received far less attention regarding its association/dissociation properties on the molecular level. Thus, much knowledge about structural properties of water in aqueous LiCl solutions is yet to be gained.

MD simulations of aqueous LiCl solution are of a particular importance because they can reveal the vital aspects of how presence of LiCl in aqueous solutions affects the structure of water molecules. Moreover, the small size of the cation's salt is attributed to high solubility of LiCl in water, presumed modified behaviour in supercooled water and revelation of water's behaviour in no man's land, all of which are advantageous not only in probing structural properties of water but also in finding explanations for water's anomalies.

There are many unanswered questions in the field of aqueous LiCl behaviour hence investigation of structural properties of water by examining correlations between water molecules and hydrated LiCl ions is of a great interest. By employing MD simulations with an appropriate model potential, this study examines water interactions and aims to answer some of the prominent questions such as: How does the presence of LiCl modify the behaviour of water in approaching the supercooled liquid region? How does the presence of LiCl influences the HDL - LDL transition in the solutions of different concentrations? Does decrease in temperature leads to increase in tetrahedral order in water? How does the presence of LiCl ions modifies the tetrahedrality of H<sub>2</sub>O and impacts the HB network of H<sub>2</sub>O? Is tetrahedral order only able to become stabilized in the system of low ionic concentration? How does the LiCl concentration affects the strength of ionic electrostriction in H<sub>2</sub>O? This study is dedicated to finding answers to these open questions.

## Chapter 1

### Water: ubiquitous and eccentric liquid



Water is an inorganic, tasteless, odorless, transparent and almost colourless liquid at room temperature. It forms the world's streams, lakes, oceans, rains, and is the major constituent of the fluids in living organisms. Arguably, it is the strangest liquid in the universe with many peculiar counterintuitive properties.

Water is a chemical compound and a polar molecule, which adopts liquid form at standard temperature and pressure. The chemical formula for water molecule is  $\text{H}_2\text{O}$ ; with Molar mass of 18.015 g/mol at ambient pressure; liquid density of 0.997 g/mL [27] at room temperature ( $25^\circ\text{C}$ ); melting point of  $0^\circ\text{C}$  (273.15 K); and boiling point of  $99.98^\circ\text{C}$  (373.13 K) [28]. Water is relatively small molecule comprised of two hydrogen atoms and one oxygen atom joined by the covalent bond with molecular radius of 1.4 Å [26]. The geometry of water molecule is non-linear V-shape, and in isolated scenario, the H-O-H angle is about  $104.5^\circ$  with the O-H length of 0.958 Å in the gas phase [27, 30].

Water exists in gaseous (vapour or steam), liquid and solid (ice) states [31]. Even though, water molecule is simple in structure, the physical and chemical properties of this unique compound are extraordinarily complex in comparison to all other substances. Being the most abundant liquid on the planet, it is simultaneously the most bizarre one as it exhibits a surprising array of unusual properties, the most famous of which are its maximum density at 4 °C (277 K) at ambient pressure and its unusually high thermal capacity. Furthermore, unlike any solids on the planet, the solid form of water, ice, floats. This behaviour is attributed to water molecule's hydrogen bonding (HB) which creates perfect tetrahedrally coordinated network, linking them into six-membered rings with much empty space between the molecules.

Based on the importance of water and the necessity to understand its behaviour, it is extensively studied in broad spectrum of science [30], e.g., condensed matter physics, chemical physics, physical chemistry. The findings of the academic studies are of a considerable importance in real life practical applications in material sciences, geochemistry and geophysics, industrial chemistry, radiochemistry, biology, agriculture, mining, food processing, medicine and engineering.

This chapter covers Molecular structure of water (1.1); Hydrogen Bond (1.2); Properties of water molecule (1.3); Peculiarities of water (1.4) and States of water (1.5).

## 1.1 Molecular structure

The key to understanding water's properties and behaviour is its molecular structure. Water is a simple molecule consisting of one oxygen atom bonded to two different hydrogen atoms. Due to the higher *electronegativity* of the oxygen atom, the bonds in water molecule are *polar bonds*, i.e., polar covalent. The oxygen atom attracts the shared electrons of the covalent bonds to a much greater extent than the hydrogen atoms. Consequently, the oxygen atom requires a partial negative charge ( $\delta^-$ ), while each of the hydrogen atoms acquires a partial positive charge ( $\delta^+$ ) (Figure 1).

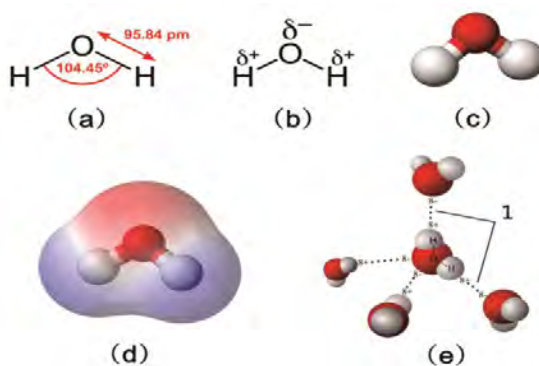


Figure 1: Basic physical and chemical models of water (a) Model: experimental H-O-H angle is  $104.5^\circ$  and the intramolecular distance O-H is  $0.957 \text{ \AA}$ ; (b) Partial charges on the atoms in a molecule; (c) ball-and-stick model; (d) Separation of charge: negative charge (red), positive charge at the ends (blue); (e) Model of hydrogen bonds between molecules where lone pair of oxygen electrons arranged together with two hydrogen atoms into locally formed tetrahedral structure.

The water molecule adopts a *bent* structure because of the two lone pairs of electrons on the oxygen atom. In principle, this bent structure is due to the fact that the oxygen atom, in addition to forming bonds with the hydrogen atoms, also carries two pairs of unshared electrons. All the electron pairs - shared and unshared - repel each other (Figure 2).

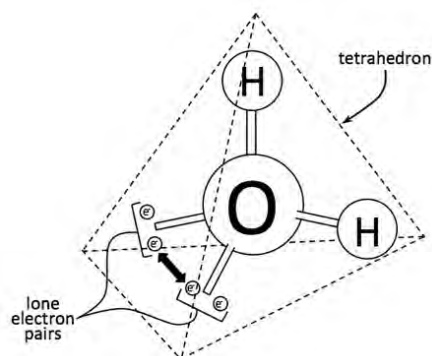


Figure 2: Bent structure of the tetrahedral geometry of water molecule.

The bent shape of the water molecule is crucial because the polar O-H bonds do not cancel one another, and the molecule, as a whole, is polar. Figure 3 illustrates the net polarity of the water molecule.

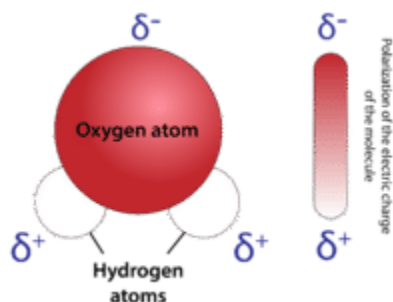
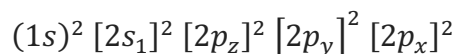


Figure 3: Depiction of greater electron density around the more electronegative oxygen atom in water molecule.

The H-O-H bond angle is  $104.5^\circ$ , which is slightly smaller than the ideal  $109.5^\circ$  of an  $sp^3$  hybridized atomic orbital.

The hybridization of the molecular orbitals is  $sp^3$  is responsible for the *tetrahedral structure* of water molecule, even though the three atoms are coplanar. This tetrahedral structure is reflected in the network-like structures in condensed phases of water.

The molecular orbitals (MOs) of water are shown in Figure 4. Each of the four orbitals to the left of the dashed line contain two electrons. The complete orbital description is:



To the right of the dashed line the first empty orbital is shown, i.e., the lowest occupied molecular orbital (LUMO). This particular arrangement is solely responsible for water's HB. The *lone-pair orbitals* of water are a linear combination of the 1b1, i.e., highest occupied molecular orbital (HOMO) and 3a1 MOs. The two lone pairs are perpendicular to the molecular plane. The two covalent bonding orbitals are directed along the O-H bond orientations and are a linear combination of the first two orbitals. These four orbitals have maximum electron densities along the tetrahedral directions ( $sp^3$  hybridization) [32].

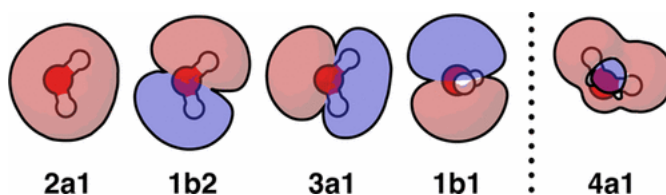
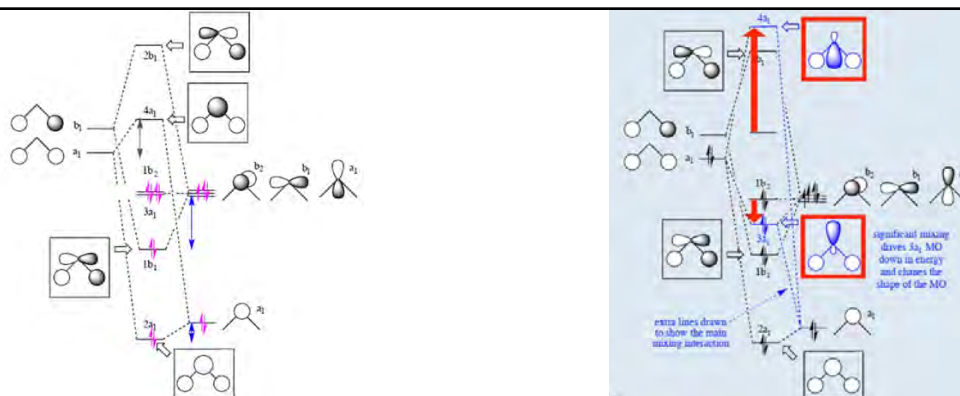


Figure 4: Molecular orbitals of water with their symmetries.

More detailed representation of simple and hybridized MOs in water molecule is shown in Figure 5.

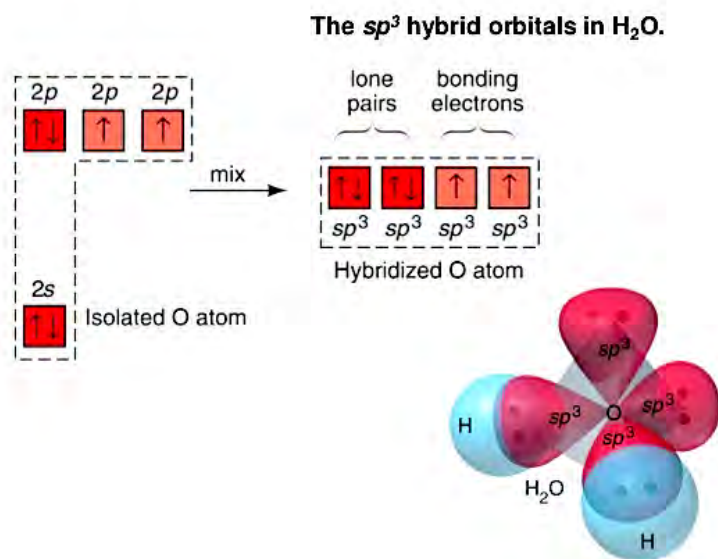


(a) Simple MO of water.

(b) Hybridized MO of water.

Figure 5: Simple and hybridized MOs of water molecule.

In addition, Figure 6 contains graphical depiction of  $sp^3$  hybridization of molecular structure of water.

Figure 6:  $sp^3$  hybridization of water molecule.

The water molecule is not the static entity: the molecule is in continuous internal motion, with the constituent atoms vibrating against each other. However, these vibrational interactions are perturbed by the HB.

---

## 1.2 Hydrogen Bonds

Water is an extraordinary liquid in comparison to other liquids because of its strong directional character of the intermolecular interaction potential. This potential is attributed to the HB which is an intermediate of the strength between the stronger covalent bond and the weaker dipole-induced interaction.

As we know, opposite charges attract one another. The slight positive charges on the hydrogen atoms that is bound covalently to an electronegative atom, oxygen, in water molecule shifts its charge distribution when another nearby electronegative atom attracts slight negative charges on the oxygen atoms of the other water molecules. This tiny force of attraction is indeed the HB. This bond is very weak. Thus, the HB forms between the positively charged hydrogen atom of the donor molecule and the lone pair electrons of the acceptor molecule. This bond is very weak. HBs are formed easily when two water molecules come close together, but they are just easily broken when the water molecules move apart. HBs are only a small fraction of the strength of a covalent bond, but there are a lot of them, and they impact some very special properties of water.

The HB occurs when a hydrogen atom that is bound covalently to an electronegative atom - oxygen - shifts its charge distribution when another nearby electronegative atom attracts it. The HB is regarded as an intramolecular and intermolecular electrostatic polarization [33] with a quantum mechanical charge-transfer component.

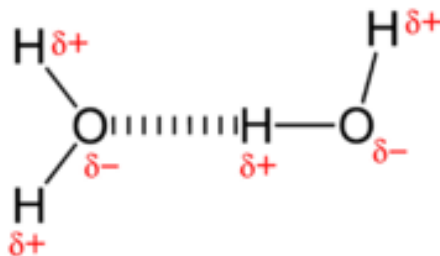


Figure 7: Schematic representation of the HB as the attraction between a lone pair of electrons on the oxygen atom of the water molecule and the electron-deficient hydrogen atom of a nearby molecule.

Another words, the HB requires a hydrogen atom pointing toward a close-by oxygen atom. The strength of the HB is maximized when the hydrogen atom is colinear with the acceptor and donor oxygen and progressively weakens on increasing the H-O-O angle [34].

Since each hydrogen atom has two lone pairs, it can make HBs to the hydrogen atoms of two separate other molecules. The most stable arrangement within water molecule is the one where repelling shared and unshared electrons hydrogen atoms are placed far enough apart from each other, with the O-H bonds forming two out of four *legs*. Since, the lone pairs are slightly more repulsive than the bond electrons, the angle between the O-H bonds is slightly less than  $109.5^\circ$  of a perfect tetrahedron and is around  $104.5^\circ$  Figure 8 below shows the result of an approximately tetrahedral geometry around each oxygen atom, consisting of two covalent bonds and two HBs.

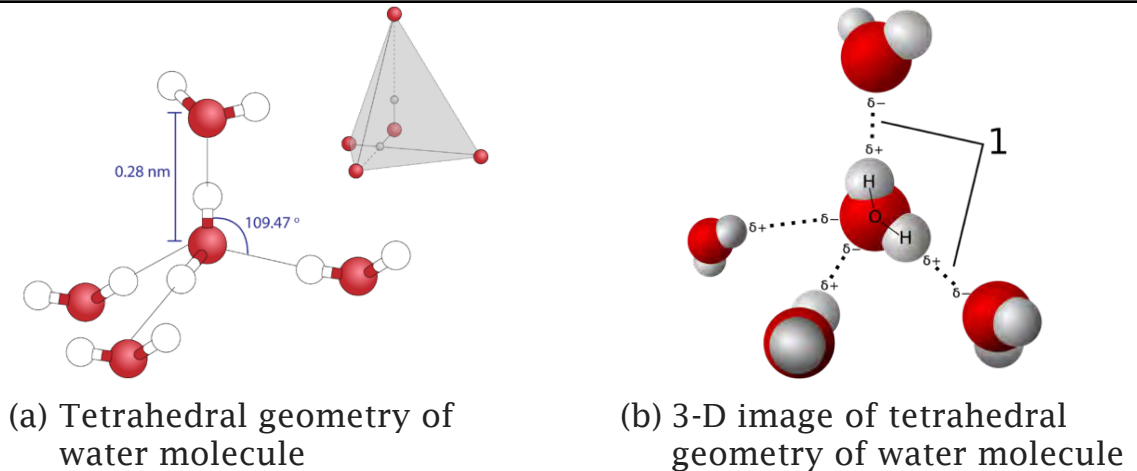


Figure 8: Tetrahedral geometry of water molecule based on the nature of HBs in water molecule.

Polar molecules attract one another by dipole-dipole forces, as the positive end of one molecule is attracted to the negative end of the nearby molecule. In case of water, the highly polar O-H bonds result in very small electron density around the hydrogen atoms. Each hydrogen atom is strongly attracted to the lone-pair electrons on an adjacent oxygen atom. Thus, the HBs are stronger than conventional dipole-dipole forces.

The energy affiliated with the HB is  $\sim 20$  kJ/mol. This value is much larger than the energy value of dipole-dipole interactions ( $\sim 1$  kJ/mol), yet much smaller than the energy value of a covalent bond ( $\sim 400$  kJ/mol). Thus, in liquid state of water molecules HBs are preserved since the latent heat of fusion in water is low with respect to the latent heat of sublimation [35].

The strength of the HB and its directionality are the key elements in thermodynamic and dynamic behaviour of water. In fact, the directionality of the HB interaction is responsible for the peculiar correlation between local energy, density, and entropy.

The HB has a strong impact on stabilizing temperature of liquid water. HBs in water allow to absorb and release heat energy more slowly than many other substances. Since temperature is a measure of the motion, i.e., kinetic energy of molecules, as the motion increases, the energy and thus the temperature increase. Water has shown to absorb a great deal of energy before its temperature rises. This increased energy, in turn, disrupts HBs between water molecules. Because these bonds can be created and disrupted rapidly, water absorbs an increase in energy and temperature changes only minimally. This implies that water acts as a moderator of the temperature changes within organisms and within their environments. With continuing input of energy, the balance between the HB formation and destruction shifts toward the destruction mode. Hence, more bonds are broken than are formed. This course of action results in the release of individual water molecules at the surface of liquid. This process is called *evaporation*.

Conversely, when a molecular motion decreases and the temperature drops, less energy is present to break the HBs between water molecules. These bonds remain intact and begin to form a rigid, lattice-like structure, e.g., ice (Figure 9). When frozen, the water molecules are further apart and formed ice is less dense than liquid water [33].

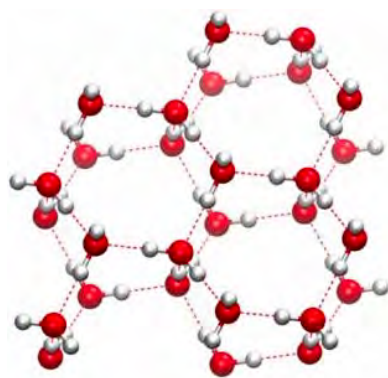


Figure 9: The lattice structure of low-density ice created by unbroken HBs in molecules of liquid water.

Furthermore, when the phase of water changes from liquid to solid, the HB enhances ice to take up more space as shown in Figure 10. In ice,  $I_h$ , each water molecule forms four HBs with O-O distance of 2.76 Å to the nearest oxygen neighbour. Due to the ordered structure of ice, there are less H<sub>2</sub>O molecules in a given space of volume.

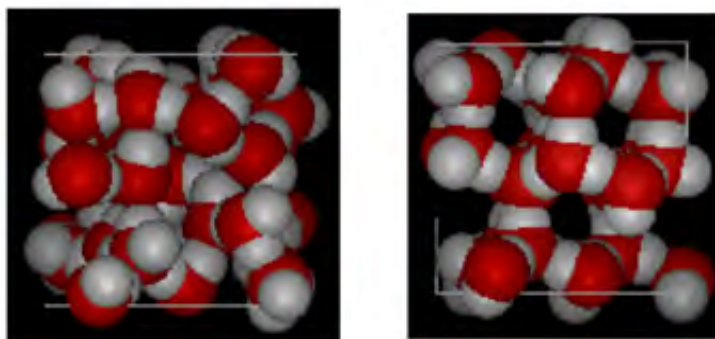


Figure 10: Side-by-side comparison of water's HBs box of 10 Å across.

### 1.3 Properties of water molecule

Water is the only universal compound that supports life due to its unusual chemically structural and physical properties.

Water has distinctive liquid and solid properties [28, 37], such as:

- high cohesiveness
- volumetric anomalies: solid form of water - ice - floats on its liquid; pressure melts the solid instead of freezing the liquid; heating shrinks the liquid
- number of solid phases of water supersedes the number of solid phases of other substances
- water's supercooled liquid has apparent divergent thermodynamic response functions

---

The most important property of liquid water is comparatively high boiling point which points out to the presence of strong intermolecular forces in its liquid state. This is a subsequent reason why it is difficult for the water molecule in a liquid state to migrate into the vapour phase.

Furthermore, the high melting point of water indicates that there exists some sort of quasi-crystalline structure in the liquid water which promotes the formation of the solid state regardless of the presence of the significantly high thermal energy of the system.

Like simple liquids, water molecules are almost spherical, and their self-interactions are subject to van der Waals forces. But unlike simpler liquids, water's HB, which determines its molecular orientation, results in formation of the tetrahedral cage-like structure that is responsible for remarkable volumetric and thermal properties of water.

Physical and chemical properties of water, its molecular structure and the nature of the HB reveal the behaviour of water.

### 1.3.1 Physical properties

Physical properties of water describe its appearance:

- Density: weight of a certain amount of water ( $\text{kg/m}^3$ )
- Thermal property: state of water when it's heated; at which its temperature becomes gaseous
- Conductivity: amount of electricity that water can conduct expressed in a chemical magnitude

- 
- Viscosity: syrupiness of water which determines the mobility of water - when the temperature rises, the viscosity decreases; this means that water is more mobile at higher temperatures

### 1.3.2 Chemical properties

Chemical properties of water address its state:

- Light absorption: certain amount of light can be absorbed by a certain amount of water over time
- The pH: number of H atoms determines pH; more H atoms = lower pH; substance with many H atoms = acidic (1-6); neutral = pH (7); basic = pH (8-14)
- Alkalinity: excellent capacity of water to neutralize acid or a base, so that the pH will not change

### 1.3.3 Polarity

Polarity is responsible for water's organization. Water molecules are polar with partial positive charges on two hydrogen atoms and a partial negative charge on the oxygen atom. The overall bent structure of water molecule is due to the stronger electronegativity on the oxygen atom which, subsequently, attracts electrons better than hydrogen atoms, as shown in Figure 11.

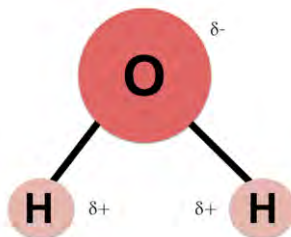


Figure 11: Geometrical representation of polarity of water molecule

#### 1.3.4 Heat capacity and heat of vaporization

Water plays an important role in regulating temperature in the environment as it takes a lot of energy to raise the temperature of a certain amount of water by a degree. Thus, its heat capacity is very high.

Similarly, water's heat of vaporization is also very high since it is rapidly converting from liquid state to a steam upon reaching the heat of vaporization. In fact, living beings use of water's high heat of vaporization to cool off, is known as *evaporative cooling*.

#### 1.3.5 Cohesiveness and adhesiveness

The tendency of a liquid surface to resist a rupture upon been placed under tension or stress, is attributed to the cohesive forces which are responsible for the *surface tension* in liquids. Water's ability to form the HBs with one another, in addition to van der Waals interactions, is attributed to surpassing presence of strong *cohesiveness* and subsequent *surface tension* in water molecules. This makes water more cohesive than simple liquids. Furthermore, water's ability to bind to substances other than itself is dependable on its *adhesive* properties.

### 1.3.6 Density paradox

Usually, when substances freeze, their molecules come closer together. Water has an anomaly in this regard: it freezes below 0 °C but when the temperature drops below 4 °C, water begins to expand again, and its density becomes lower. Thus, water is less dense as a solid than as a liquid. Upon freezing, water molecules form a crystalline structure that spaces the molecules further apart than in liquid water. The reason why ice floats is because it is less than liquid water.

### 1.3.7 Phase transitions

There are three common states of matter of water: liquid, H<sub>2</sub>O; solid, ice; and gas, vapor or steam (Figure 12).

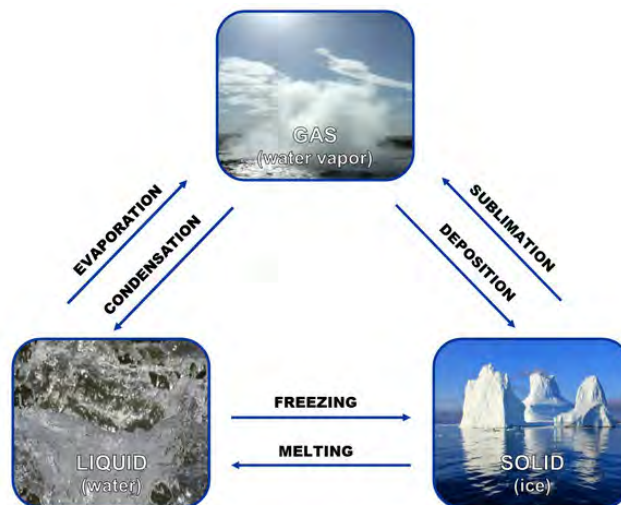


Figure 12: Three common states of matter of water and their phase transitions.

The changes from a liquid to a solid or to a gas are called *phase changes* [38]. The addition or removal of heat can bring on these phase transitions, i.e.:

- freezing which leads to the transformation of the liquid water to ice (at a pressure of 1 atm freezing is found at 0 °C temperature)
- melting which makes ice to become liquid water (at a pressure of 1 atm melting is found at 0 °C temperature)
- vaporizing (boil) which turns liquid water into a vapour (at 100 °C at the pressure of 1 atm)
- undergoing condensation which reverses vapour to liquid water (at 100 °C at the pressure of 1 atm)
- undergoing sublimation which turns ice into vapour
- undergoing deposition which results in inversion of vapor into ice

Noteworthy, the phase transition diagram for most materials between liquid and solid phases have positive slopes. Au contraire, water's phase transition diagram's slope is indeed negative. This is shown in Figure 13 (courtesy of Martelli).

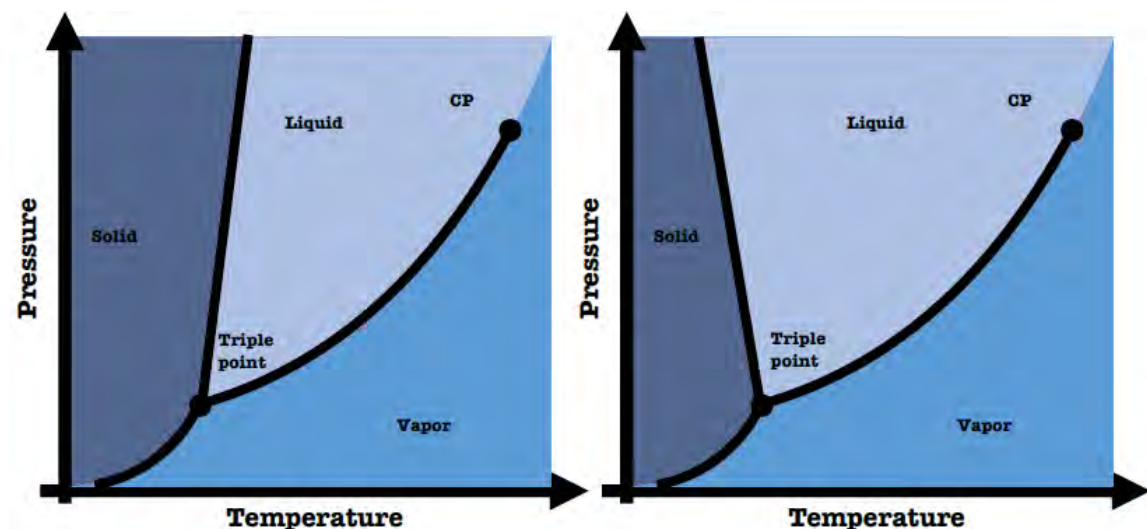


Figure 13: Slopes of Solid-Liquid transition phases. Left: most materials - (+) slope. Right: water - (-) slope.

Since both, melting and boiling points of water depend on the pressure, the rate of change of melting temperature with pressure is explained by Clausius-Clapeyron relation [39, 40]

$$\frac{dP}{dT} = \frac{T(v_L - v_S)}{L_f} \quad (1.1)$$

where  $v_L$  and  $v_S$  are the molar volumes of the liquid and solid phases,  $L_f$  is the molar latent heat of melting.

As a rule, in most substances, the volume increases upon melting, thus the melting temperature increases with pressure. However, since ice is less dense than liquid water, its melting temperature decreases [41].

Interestingly, the Clausius-Clapeyron relation also applies to the boiling point of water which increases with pressure due to the fact that in the liquid - phase transition the density of the vapour phase is significantly lower than that one of a liquid phase [39, 40, 41, 42].

### 1.3.8 Triple and critical points of water

Figure 14 depicts water's separation curves: solid from vapour, vapour from liquid, liquid from solid. Notably, these curves adjoin at a single point where the temperature is 0.01 °C and the pressure is 6.12 kPa - the lowest pressure for liquid to exist [43]. This point is called the *triple point* (TP) where all three phases of water coexist.

When water - vapour phase terminates at higher temperature and pressure, i.e., 647 K (374 °C) and 22 Mpa (218 atm), respectively, a collection of water molecules arrives at the *critical point* (CP). In this

vicinity the liquid and vapour phases form a continuous phase - *supercritical fluid* which can be incrementally compressed or expanded between density-sensitive gas-like and liquid-like phases. Here, liquid-like clusters float within a vapour-like phase.

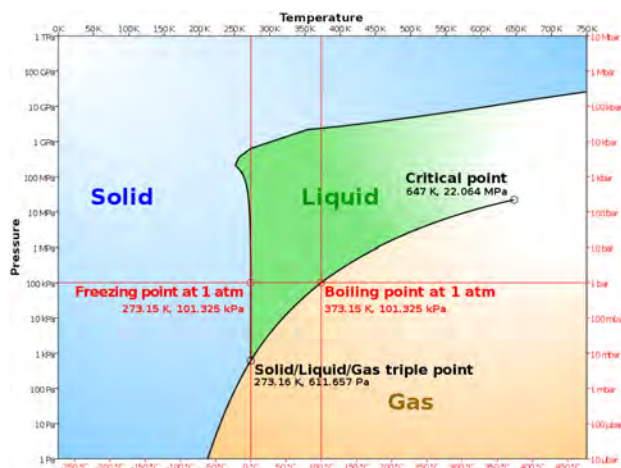


Figure 14: Pressure - temperature phase diagram of water.

When water changes phases, its physical appearance changes, but its chemical properties do not. This is because the chemical structure of water remains the same.

### 1.3.9 Solvation

Polarity determines if a substance is water-soluble or not. Water is called the universal solvent because it dissolves a wide variety of substances due to its polarity. Liquid water has surpassing ability to dissolve variety of polar and ionic substances which is vital for all living matter.

Each water molecule attracts other water molecules due to the positive and negative charges in the different parts of the molecule. Furthermore, water molecules are also attracted to other polar molecules and to ions. The

charged particles will form HBs with a surrounding layer of water molecules. This is referred to as a *sphere of hydration* and serves to keep the particles separated or dispersed in the water. The relatively small size of water molecules typically allows many water molecules to surround one molecule of *solute*. A charged or polar substance that interacts with and dissolves in water is *hydrophilic* (water-loving). In contrast, the nonpolar molecules separate and do not dissolve in water – they are *hydrophobic* (water-fearing). Figure 15 shows an image of the lack of solubility of a nonpolar compound (oil) in water as they do not mix. Overall, ionic and polar substances such as acids, alcohols, and salts are easily soluble in water, while nonpolar substances such as fats and oils are not. This is due to the fact that nonpolar molecules stay together in water because it is energetically more favourable for the water molecules to HB to each other than to engage in van der Waals interactions with nonpolar molecules.



Figure 15: Microscopic image of non-solubility of oil in water.

Water's behaviour as a solvent for nonpolar and charged molecules can be explained through a combination of its *caging structures* and water's electric dipole.

Special attention is given to water's propensity to dissolve ionic salts. When two ions interact in water, both solvation shells determine the solution properties. The water structure around an ion pair depends on

the cation-anion distance. When two ions come together, the *potential of mean force* (PMF) which is the free energy of bridging two particles together in a solvent from a large original distance apart to a separation  $r$  from each other is shown in Figure 16, i.e., how the solvation-shell waters are structured at different separations. When the ions are far apart, each ion's solvation shell is structured as for isolated ions. On the other hand, when two ions are separated by around one layer of water, the *bridging waters* between them are structured by multiple interactions. Then, each bridging water interacts with other bridging waters via HB, and each bridging water interacts with each ion via its water dipole. When the two mobile ions come into contact, the ion-ion electrostatics can also contribute substantially to the free energy. The shape of the PMF depends on all these factors, as has been shown by extensively performed computer simulations. The resulting free energy from the sum of the factors can be quite different for ions of different sizes and shapes [43].

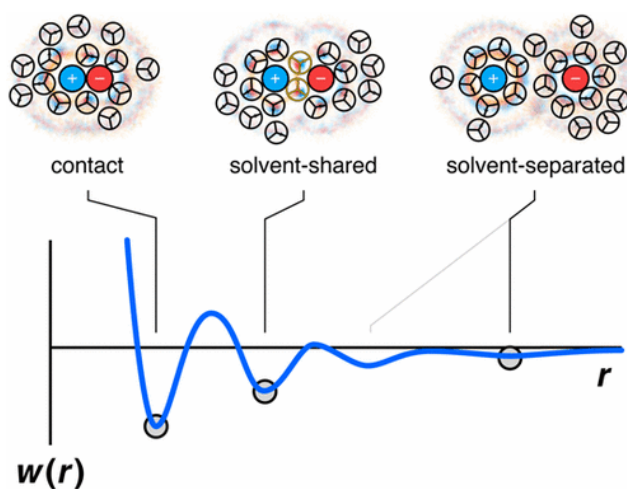


Figure 16: Main frame: Solvation-shell waters at different separations. Ion-ion contacts of opposite charges are stabilized by electrostatic attractions, in addition to the water sources. Top frames: Positive charge density of the waters (blue). Negative charge density of the water (red). Density of water-water HB arms (orange) [Adopted from 43].

### 1.3.10 Conductivity

Pure water is a good insulator (poor conductor) - it does not conduct electricity well. However, since water is such a good solvent, it often has some solute dissolved in it. As salts are the most common substances dissolved in water, an electric current can flow in salty aqueous solutions because salts are comprised of free ions which are easily subjected to electric conductivity. As a result, aqueous salt solutions are good electricity conductors.

### 1.4 Peculiarities of water

The intrinsic peculiarities of water are best understood by physicists. Up to date, there are at least 74 properties of water molecule,  $H_2O$ , which are different from those of a simple liquid. In addition, there are more than 60 thermodynamic and dynamical anomalies of water due to its peculiar ability to form the HBs network [44, 45, 46, 47, 48].

For example, water is more cohesive than any other substances made of molecules of the same size and shape. And because water molecules are packed tightly with one another, water has high value of surface tension, melting and boiling points.

In addition, anomalous properties of water stem from the cage-like features of its molecular structure, arising from the tetrahedral HB among neighbouring molecules.

## 1.4.1 Thermodynamics

### 1.4.1.1 Volume

Volumetric anomalies of water arise from a competition between van der Waals attractive forces and the HB-driven expansion. Volume anomaly of water can be related as: when liquid H<sub>2</sub>O becomes ice, its volume increases

$$\frac{dP}{dT} = \frac{1}{T} \frac{\lambda}{\Delta V} \quad (1.2)$$

where  $\lambda$  is the latent heat of fusion.

In most liquids, volume and entropy are positively correlated, i.e., an increase in volume subsequently results in increase in entropy. However, in water below 277 K volume and entropy fluctuations are anticorrelated, i.e., as volume increases, entropy decreases.

### 1.4.1.2 Density

Density of a simple liquid increases with decreasing temperature, and this is also true for water when it is hot. However, as liquid water enters its ambient regime zone, the rate of increase drops and the maximum in density is observed at 277 K (4 °C) at ambient pressure, after which the density decreases upon further cooling [49, 50, 51]. Thus, in water, density ( $\rho$ ), as well as entropy ( $S$ ) fluctuations become more pronounced at lower temperatures, i.e., density anomaly is revealed at  $T = 277$  K.

The temperature at which density exhibits a maximum is also 277 K and is known as a *temperature of maximum density* (TMD). The TMD line obtained by varying the pressure serves as a border between a simple liquid water state and an anomalous liquid water state which expands upon cooling.

Water's density anomaly is manifested in various ways. One example being ice floating in a liquid water versus in other materials where solid sinks in a liquid. This is due to the fact that water's solid (ice) form is less dense than its liquid form because cold water is dominated by its tetrahedral HBs which prompt to have only four neighbours of any given water molecule. Cold water at low pressure has a tendency to maximize its HBs which results in its open and loose structure (Figure 17).

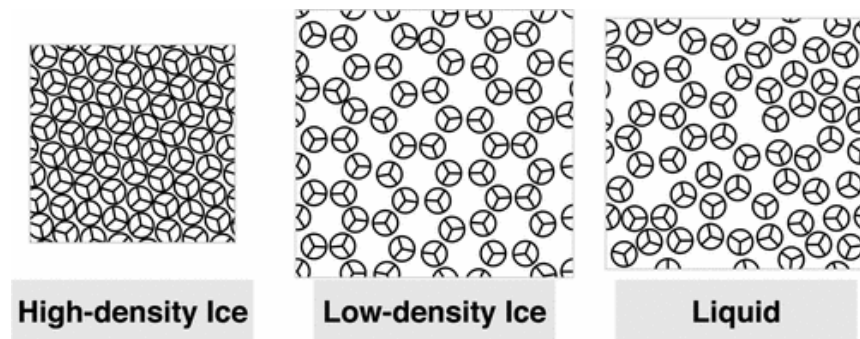


Figure 17: Densities of some phases of water illustrated in 2D model. At high pressures, ices are dense with some broken HBs. At low pressure (1 bar), ices are less dense with more optimal HBs. Liquid water is more disordered yet has much residual cage-like structuring [Figure adopted from 43].

As a rule, the slope of  $p - T$  equilibrium phase boundary between the solid and liquid for most materials is positive. However, in phase diagram the slope of coexistence line between solid and liquid phases for water is negative. Upon applying pressure, most liquids freeze. When pressure is applied on water, it causes water's solid to melt into liquid. In fact, water

has over 12 phases of its solid, ice, while typical materials have only one or two solid phases [43].

Both, volume and density anomalies of water are shown and discussed in Figure 18. The thermodynamic response functions will be presented in more detail in 1.4.1.4.

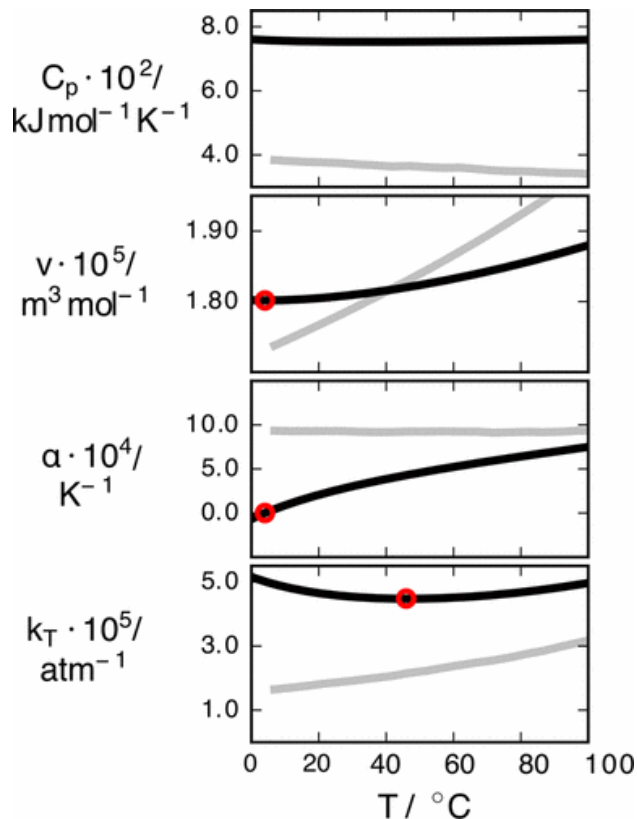


Figure 18: Volumetric anomalies of water. Temperature dependences of liquid water on its heat capacity ( $C_p$ ), molar volume ( $v$ ), thermal expansion coefficient ( $\alpha$ ), isothermal compressibility ( $k_T$ ) for water is shown in black lines; and a LJ simple fluid ( $\sigma = 2.9\text{\AA}$ ,  $\epsilon = 0.8 \text{ kcal mol}^{-1}$ ) shown in gray lines. The heat capacity of water is relatively large because water stores energy in both van der Waals and HBs. Red circles represent water's minimum volume, i.e., a Temperature of Maximum Density (TMD) at  $4^\circ \text{C}$  ( $277 \text{ K}$ ) as opposed to monotonical increase in volumes of simpler liquids. Cold water has a negative thermal expansion coefficient (red circle): between  $0$  and  $4^\circ \text{C}$  which means that heating shrinks it. Water has a negative derivative of compressibility at temperatures below  $46^\circ \text{C}$  (red circle) which means that heating makes water less compressible [Data adopted from 52].

---

Both, density and volumetric anomalies of water are present in stable liquid phase of water and become incrementally elevated upon supercooling water to its final state.

#### 1.4.1.3 Pressure

If liquid water is sufficiently cold, its diffusivity increases, and its viscosity decreases upon compression. Pressure disrupts the tetrahedral HB network and the molecular mobility consequently increases. The anomalous pressure dependence of water's transport coefficients [52] occurs below 283 K for the diffusivity and below 306 K for the viscosity, persistent up to pressure nearly 2 kbar. The qualitative physical explanation for this anomalous water's pressure behaviour is Le Chatelier's principle.

According to Le Chatelier's principle, applying pressure squeezes a system into a denser state. However, in case of water, applying pressure shifts water structure, crunching cage-like waters into van der Waals clusters. This breakage of the HB frees up water molecules to move faster [45, 47, 53, 54, 55, 56].

Cold and supercooled water diffusion and viscosity depend on the relative population of high- and low-density water. In simple liquids (and in hot water), increasing the pressure increases the viscosity and decreases the diffusivity due to applied pressure which leads to crowding of the molecules, thus making their motion sluggish. However, cold water behaves differently: at temperature below 306 K the viscosity of water *decreases* with increasing pressure [54, 57]. Below 283 K the diffusivity of water molecules *increases* upon increasing the pressure of the system [58].

Anomalous behaviour is also observed in the sound velocity in cold water [59].

The line of coexistence of water and its vapour has a positive slope which means that a pressure lower than 1 atm boiling occurs at lower temperatures than normal (100 °C). Using Clausius-Clapeyron relation this can be viewed as [39, 40]

$$\frac{dP}{dT} = \frac{L}{T\Delta v} = \frac{\Delta s}{\Delta v} \quad (1.3)$$

where  $dP / dT$  is the slope of the tangent to the coexistence curve at any point,  $L$  is the specific latent heat,  $T$  is the temperature,  $\Delta v$  is the specific volume change of the phase transition, and  $\Delta s$  is the specific entropy change of the phase transition.

Walking along the liquid-vapor coexistence line of a pure substance into direction of high pressures and high temperatures, the vapor density increases, and the liquid density decreases to the point where the densities of the two phases become equal. This point determines the end of the coexistence line and corresponds to the state in which the two phases become identical, i.e., the *critical point* (CP).

The CP  $(T_c, p_c)$  lies in the terminal point of the liquid-vapour coexistence line. Near the CP the coexistence line is represented by semi-straight line

$$p - p_c = A(T - T_c), \quad T < T_c \quad (1.4)$$

where  $A$  is a constant strictly positive which is identified as  $(\partial p / \partial T)_v$  calculated at CP.

Using the Clausius-Clapeyron equation again, the coexistence relation between the differences in molar entropy and molar volume in both phases is

$$(s_G - s_L) = A(v_G - v_L) \quad (1.5)$$

Therefore, at CP molar volumes,  $v_G$  and  $v_L$ , and molar entropies  $s_G$  and  $s_L$  are all become identical. As a result, the boiling latent heat  $l_c$  disappears.

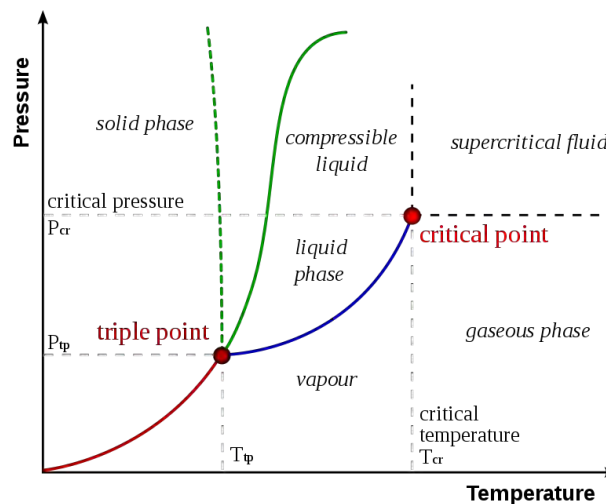


Figure 19: Phase diagram for water. The dotted green line depicts the anomalous behaviour of water. The Clausius-Clapeyron relation is applicable to derive the relationship between pressure and temperature along the phase boundaries.

#### 1.4.1.4 Thermodynamic response functions

Since thermodynamic properties of water measure the response to external perturbations, they are referred to as thermodynamic response functions [60]. Their unusual behaviour for water is denoted anomalous where the anomaly becomes strongly pronounced upon cooling.

The three most important thermodynamic response functions for water are *isobaric heat capacity*,  $C_p$ , *isothermal compressibility*,  $k_T$ , and *coefficient of thermal expansion*,  $\alpha_p$ .

Isobaric heat capacity,  $C_p$ , is related to the entropy ( $S$ ) fluctuation in the liquid [48, 59], and is one of the important thermodynamic response functions of water.

The isobaric specific heat,  $C_p$ , is expressed as

$$C_p = \frac{T}{N} \left( \frac{\partial S}{\partial T} \right)_p = \frac{\langle (\delta S)^2 \rangle}{Nk_B} \quad (1.7)$$

The isothermal compressibility,  $k_T$ , is related to volume ( $V$ ), or equivalently density ( $\rho$ ) fluctuations of the liquid [48, 59]. To derive the response of the volume of water to the increase in pressure, the following equation is employed

$$k_T = -\frac{1}{V} \left( \frac{\partial V}{\partial p} \right)_T = \frac{\langle (\delta V)^2 \rangle}{Vk_B T} \quad (1.6)$$

The coefficient of thermal expansion,  $\alpha_p$ , which defines the measure of the cross-correlations between the volume ( $V$ ) and entropy ( $S$ ) is

$$\alpha_p = \frac{1}{V} \left( \frac{\partial V}{\partial T} \right)_p = \frac{\langle \delta V \cdot \delta S \rangle}{Vk_B T} \quad (1.8)$$

In fact, the density variation can be derived from the *coefficient of thermal expansion*,  $\alpha_p$ , dependent on the cross-correlation between fluctuations in density and entropy, which thus become negative for water below the density maximum [48, 59].

The above equations connect all three thermodynamic response functions, i.e., the isothermal compressibility,  $k_T$ , isobaric heat capacity coefficient,  $C_p$ , to the volume and entropy fluctuation of the system. In simple liquids upon lowering the temperature only small fluctuations of the thermodynamical response functions occur. Au contraire, in liquid water upon decrease in temperature, the self-correlation of these response functions anomalously increases.

Figure 20 shows the summary of the anomalous behaviour of the thermodynamic response functions of water (courtesy of Martelli).

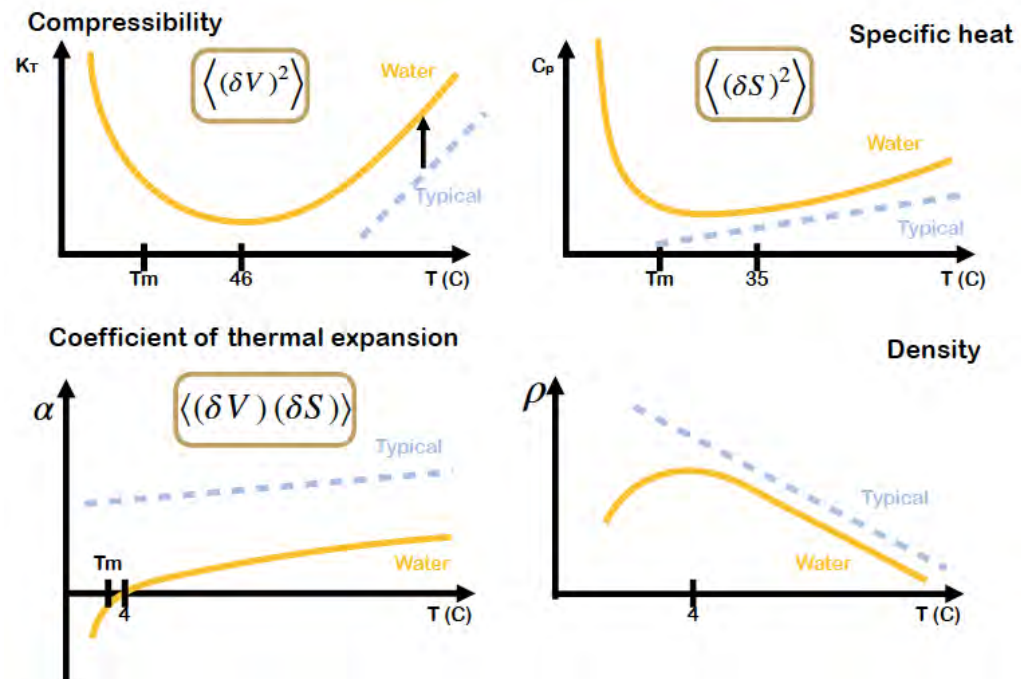


Figure 20: Thermodynamic response functions of water. Top (left): isothermal compressibility ( $k_T$ ); Top (right): isobaric specific heat,  $C_p$ ; Bottom (right): density ( $\rho$ ); Bottom (left): coefficient of thermal expansion,  $\alpha_p$ .

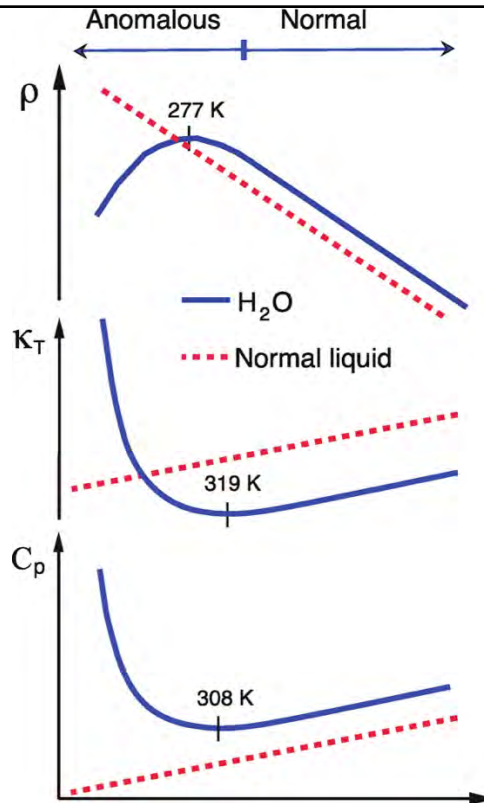


Figure 21: Comparison of the density ( $\rho$ ), isothermal compressibility ( $k_T$ ), and heat capacity ( $C_p$ ) for  $H_2O$  (full line) with that of typical liquids (dashed line) showing the onset of anomalous behaviour already at ambient temperatures and pressure [Adopted from 61].

Unlike in simple liquids, where  $C_p$  and  $k_T$  initially decrease monotonically when the temperature is decreased, in water, just above the ambient temperature regime, a deviation occurs and both, the heat capacity and compressibility begin to increase on further cooling. This results a minimum of in water these response functions exhibit a minimum at 308 K (35 °C) and 319 K (46 °C), respectively [50, 62, 63, 64, 65].

Furthermore, in a simple liquid the coefficient of thermal expansion,  $\alpha_p$  is also expected to decrease monotonically with decreasing temperature yet remains greater than zero. But in water at a fixed pressure,  $\alpha_p$ , becomes

zero in conjunction of the TMD. Also,  $\alpha_p$  of water becomes negative and rapidly decreases.

Overall, all three response functions of water deviate from those of simple liquids upon further decrease in temperature, transitioning toward the deep supercooled phase via rapid increase or decrease in values. The steep increase upon cooling of these response functions is described by the power law [66, 67]

$$X = A \left( \frac{T - T_S}{T_S} \right)^{\lambda_X} \quad (1.9)$$

where  $X$  is the generic response function,  $T_S$  is the singular temperature for occurring divergence,  $\lambda_X$  is the associated exponent to the divergent quantity  $X$ .

At pressure of 1 bar, the estimated divergent temperature,  $T_S$ , is 228 K, as is for all the response functions. Because  $T_S$  is of nine degrees below homogeneous nucleation temperature  $T_H$ , the divergence of thermodynamic response functions is predicted to take place within *no man's land* region. Thus these functions are known as *apparent divergences*.

Figure 22 shows alternative representation of thermodynamic response functions in reference to water anomalies where the behaviour of water is indicated by the solid line and that for a typical liquid is shown by the dashed lines. Each of these thermodynamic response functions is proportional to the corresponding fluctuations in the entropy or volume parameters. The anomalous thermodynamics and fluctuations of liquid water are apparent above the melting temperature,  $T_M$ , and become more pronounced as water supercools below  $T_M$ .

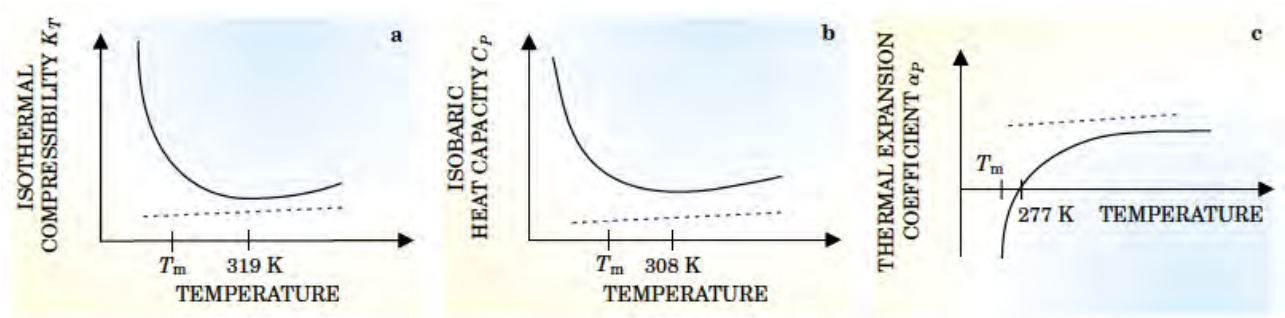


Figure 22 : Water anomalies represented by schematic dependence on temperature. (a) the isothermal compressibility,  $k_T$ ; (b) the constant-pressure specific heat,  $c_p$ ; (c) the coefficient of thermal expansion,  $\alpha_p$  [Adopted from 48].

To complete the picture of water’s thermodynamical anomalies at ambient pressure, graphical representation of behaviour of water’s density ( $\rho$ ), isothermal compressibility ( $k_T$ ), coefficient of thermal expansion ( $\alpha_p$ ), and isobaric specific heat ( $C_p$ ) in comparison to a simple liquid is shown in Figure 23.

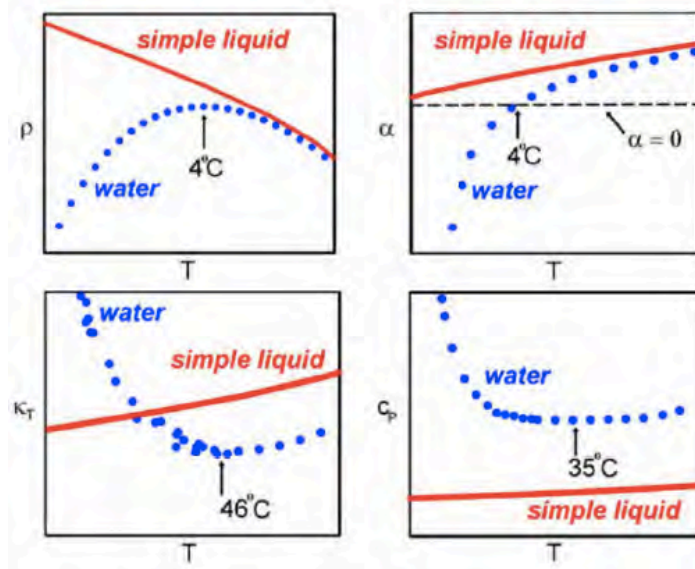


Figure 23 : Temperature trends of density  $\rho$  (top left), thermal expansion coefficient  $\alpha_p$  (top right), isothermal compressibility  $k_T$  (bottom left), isobaric heat capacity  $C_p$  (bottom right).

---

 1.4.2 Diffusion

Water has anomalous dynamics which stem from unusual diffusion behaviour. In simple liquids upon increased compression, the diffusion coefficient decreases. However, at 283 K the diffusivity of water increases as the pressure increases up to its reached maximum at 150 Mpa (at that temperature). Computer simulations show that the application of pressure somehow breaks the HB network, hence aiding the diffusion process [68]. Furthermore, upon further decrease in temperature, water diffusivity passes through a minimum which causes it to be restored to its normal behaviour. A line of a diffusivity extrema can be visualized when maxima and minima of the diffusivity are co-joined.

In terms of diffusivity, the main dynamical anomaly of water involves the *self-diffusion coefficient*  $D$  which is defined through the *mean square displacement* (MSD)

$$D = \lim_{t \rightarrow \infty} \frac{\langle |\mathbf{r}_j(t' + t) - \mathbf{r}_j(t')|^2 \rangle}{6t} \quad (1.10)$$

and is related to the liquid viscosity through the Stokes-Einstein (SE) equation [69].

$$D = \mu k_B T \quad (1.11)$$

where  $\mu$  is the *mobility coefficient*, i.e., the ratio of the particle's drift velocity to an applied force ( $\mu = v_d / F$ );  $k_B$  is the Boltzmann's constant;  $T$  is the absolute temperature.

Based on the notion that compression is correlated to a loss of fluidity, in simple liquids the self-diffusion coefficient  $D$  should decrease upon

---

pressure increase. Yet again, liquid water behaves oppositely. This diffusivity anomaly of water has been detected in number of simulated water potentials [63, 68, 70, 71], as well as has been observed in experimental studies [72, 73].

### 1.4.3 Structure

To gain fundamental understanding of the origin of water's anomalies, the instantaneous local structure of the liquid at various thermodynamic state points is addressed and the comprehension of how this structure couples to the dynamics of the molecular motion is sought out. The inquiry into this field begins with the notion that on a larger scale liquid water is homogeneous, yet the question is: is it also locally homogeneous or can it be heterogeneous? Perhaps, it is not heterogeneous in terms of a static structural picture but maybe induced by fluctuations on some length and time scales between specific classes of local structures? Overall, many different plausible explanations exist for the unusual properties of water where possibly both homogeneous and heterogeneous models could be viable. Studies to obtain sophisticated structural and dynamical experimental data to confirm their validity are ongoing.

The other major question is: how large are the distortions in the HB network? In a locally homogeneous model, the distortions should be around a near-tetrahedral HB arrangement, whereas in a heterogeneous model there would be distortions within each class of configurations in addition to the distinction in local structure between the classes. The more popular heterogeneous models build on fluctuations between two main classes of contrasting structures with notations such as tetrahedral and distorted [74], symmetrical and asymmetrical [75, 76], locally favoured

---

and normal [77], and low-density liquid (LDL) and high-density liquid (HDL) [55, 59, 78, 79] to mention the recent proposals inspired by number of experimental studies [55, 59, 60, 74, 78, 79] and modelling techniques [75, 76, 77].

Current knowledge about structure of water is comprised from both, experimental and theoretical investigations. The experimental data employs bulk measurements to probe relationships of water's properties such as enthalpies, entropies, and heat capacities of pure water in its various phases; changes in thermal quantities upon melting or boiling; alterations due to dissolving solutes; affects due to applied pressure; modifications of electrical properties in applied electric fields, and measurements of the surface tensions. In order to gain a deep understanding of how water's properties are encoded within its molecular structures experimental techniques like x-ray or neutron diffraction give information on the microscopic arrangements of the molecules in the different states of water.

Investigations beyond experiments are of great relevance to test models based on hypothetical molecular force fields. The main tool of such investigations is computer simulations.

In theoretical approaches the structural anomalies region of water has been described by two order parameters: *orientation parameter*,  $q$ , which measures the degree of tetrahedrality of arrangement of four first nearest neighbour molecules, and the *translation parameter*,  $t$ , which accounts for tendency of two water molecules to adopt preferential separation [71]. The cause of water's structural anomaly is the decrease of translational and orientational orders upon compression vs. normal liquids where this

---

behaviour is reversed. Thus, the structure of water becomes more disordered when it is compressed.

## 1.5 States of water

### 1.5.1 The phase diagram of water

A typical way to observe behaviour of water is to visualize its  $p - T$  phase diagram. The phase diagram of water shows its preferred physical states at different temperatures and pressure. The common key aspects of such diagram are:

- Fusion (melting or freezing) curve which represents the transition between liquid and solid states
- Vaporization (or condensation) curve which represents the transition between gaseous and liquid state
- Sublimation (or deposition) curve which represents the transition between gaseous and solid state
- Critical point (CP) at which water is indistinguishable between liquid and gaseous state, and when critical pressure is applied, supercritical fluid is formed
- Triple point at which all three states of water, i.e., gas, solid and liquid coexist

The phase diagram of stable states of water is rather complex (Figure 24). At ambient condition water is stable in the liquid phase. Above the temperature of 373 K and pressure at 1 bar water becomes steam. This means that above this temperature is the only stable phase. When the temperature drops below 273 K at 1 bar it becomes one of the stable solid phases, i.e., hexagonal ice ( $I_h$ ). In the diagram, each line represents the

conditions when two phases coexist. However, if a temperature and/or pressure change, an abrupt change of one phase to another may occur. Similarly, upon change of temperature and/or pressure, the three phases existing at triple point may suddenly and entirely change into each other. As mentioned above, phase diagram of water also contains a CP.

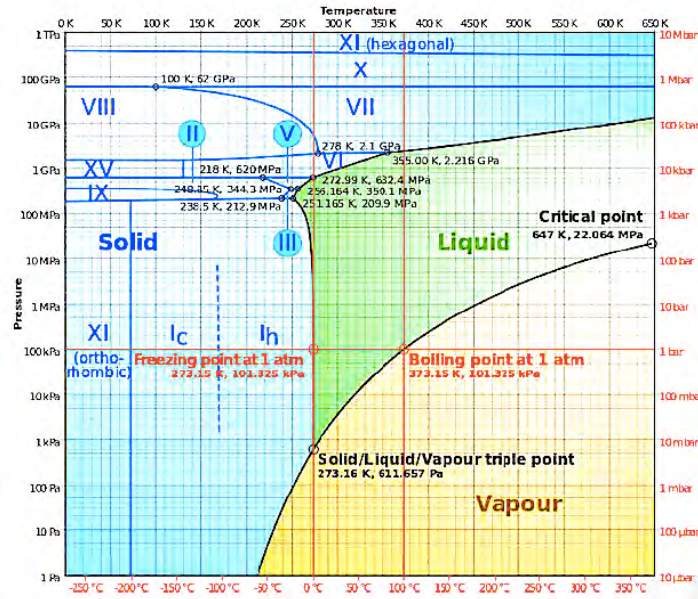


Figure 24: Phase diagram of the stable phases of water in the  $p - T$  plane.

### 1.5.2 Stable states

Stable form of water at sufficiently low temperature is invariably crystalline.

Due to the *polymorphism*, crystalline water has several triple points, aside from the known one - the solid-liquid-vapour triple point. Up to date, there are 17 known different crystalline phases of solid water (ice) [80]. The most familiar form of solid water is hexagonal ice,  $I_h$ , which has a relatively open structure and lower density than that of other liquids.

Figure 25 shows many solid phases of water in  $p - T$  region of the phase diagram.

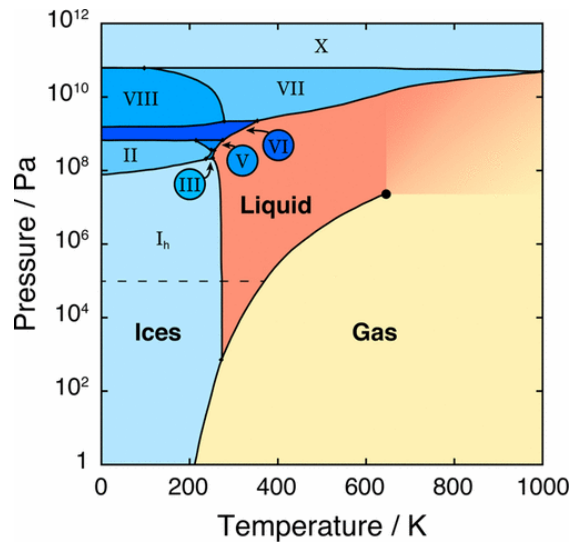


Figure 25: Solid phases of water in  $p - T$  region of the phase diagram of water.

#### 1.5.2.1 Widom line for the gas-liquid CP

The gas-liquid phases of water system are determined by the water's critical temperature,  $T_c$ , and critical pressure,  $p_c$ . For temperatures  $T > T_c$  and pressures  $p > p_c$ , the CP is reached, the two phases merge and, consequently, become indistinguishable. Thus, beyond gas-liquid CP only single fluid can be defined. However, these are some thermophysical quantities with maxima that define a line emanating from CP that diverges a region with a more liquid-like vapour from a region with a more gas-like form of a steam. This line is called *Widom line*. It is the locus of maximum of the correlation length in the single phase region [93, 94]. This line was first introduced in the supercooled state in connection with the liquid-liquid CP [96].

### 1.5.3 Metastable states

The incomplete understanding of the origin of numerous water anomalies motivates scientific research of liquid water in all states but particularly in its metastable liquid state. When water remains in liquid form below its melting point, it is in a metastable supercooled state. If the cooling occurs fast enough in this region, crystallization can be prevented, regardless of the fact that the supercooled water contains crystals in a stable state. The physical conditions at which the system is kept in metastable state are explained by the thermodynamical equations in addition to the conditions of the presence of impurities and/or perturbations in the liquid water. Moreover, the exploration of the existence of more than one disarrayed amorphous form of disordered solid state of water due to polymorphism is of a large pursuit.

Presence of metastable liquid water is not forbidden by thermodynamic constraints. If the cooling occurs fast enough in this region, crystallization can be prevented. The physical conditions at which the system is kept in metastable state are determined by the thermodynamics but in addition the stability of the supercooled liquid state is conditioned by the presence of impurities. Fast crystallization rate and subsequent decrease of metastable liquid's lifetime prevents observations of liquid water with available experimental techniques. In water due to the presence of impurities the fast crystallization rate and subsequent decrease of metastable liquid lifetime make difficult to study supercooled liquid water with the available experimental techniques.

The depiction of the phase diagram of water with the emphasis on liquid metastable phases of water, divided by their boundaries is shown in Figure 26.

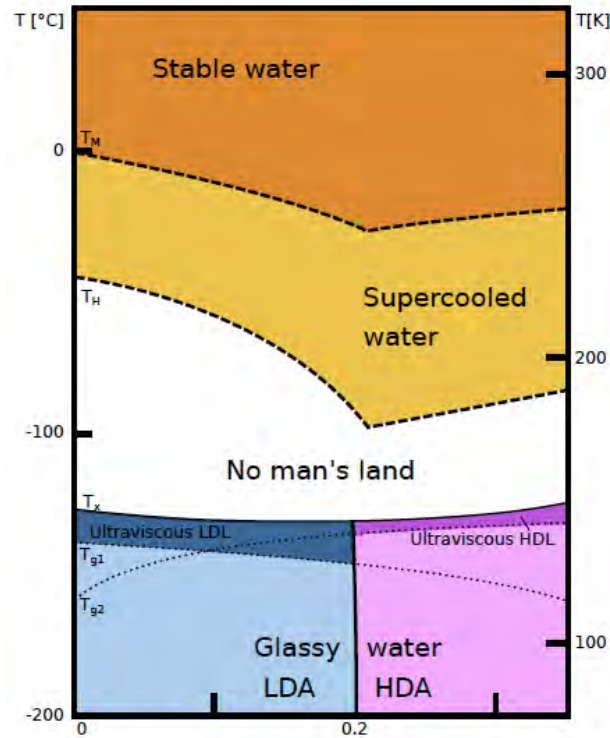


Figure 26: Schematic representation in the  $p - T$  plane of the phase diagram of water with emphasis on metastable state of supercooled and glassy water (units of pressure are GPa). [Figure adopted from 6].

Metastable state of water is reached when the stable state water is rapidly cooled (frozen) below its melting temperature ( $T_M(p) = 273$  K) and water enters into metastable liquid phase - *supercooled water*.

Further cooling down to the temperature of the homogeneous nucleation ( $T_H(p) = 231$  K) causes water to reach its kinetic limit (*supercooling limit*) which brings about a rapid turn of supercooled liquid water into ice by spontaneous thermal fluctuations below this temperature. Notably, the

---

homogeneous nucleation temperature is a kinetic limit and not a thermodynamic one.

With appropriate experimental techniques it is possible to quench water and get amorphous ice. As we explain more later there are two forms of amorphous ice, the low density amorphous (LDA) and the high density amorphous (HDA), as indicated in the figure 26. The glass transition temperature  $T_g$  is slightly different for LDA and HDA, around  $T_g = 136$  K at 1 bar. It is important that, at variance with other glass former, if we start from the glassy states and increase the temperature above the glass transition temperatures at a temperature  $T_H(p)$  it is observed the formation of ultraviscous liquid metastable states. These metastable states are bounded by a line of spontaneous crystallization temperature  $T_x$  (at 1 bar  $T_x = 150$  K), at which the ultraviscous liquid turns into ice.

The interval between the homogeneous nucleation temperature and the temperature of spontaneous crystallization is the so-called *no man's land*.

In general, it is difficult to experimentally probe water deep in the supercooled regime due to rapid ice crystallization. But recent experimental study by Nilsson *et al.* in probing structural anomalies of water by X-rays spectroscopies produced the schematic picture of a hypothetical phase diagram of liquid water showing the liquid-liquid coexistence line between LDL and HDL in terms of simple regions, the CP (real or virtual), the Widom line in the one-phase region and fluctuations on different length scale emanating from the CP giving rise to local spatially separated regions in the anomalous region, as presented in Figure 29.

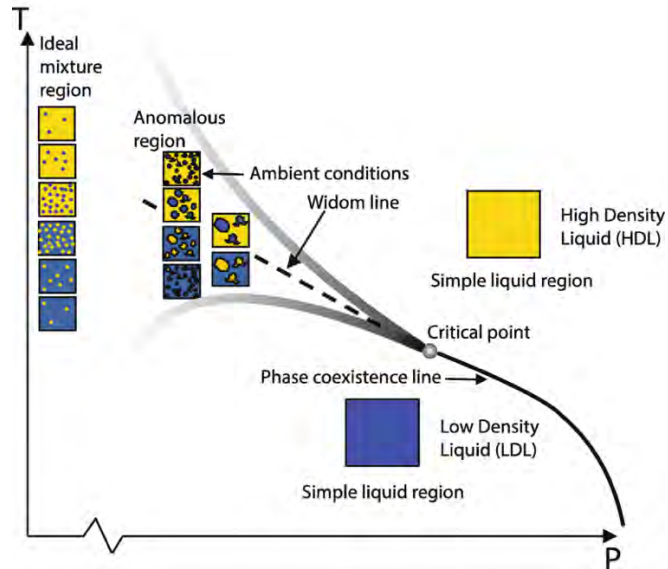


Figure 29: The shaded lines indicate how far in temperature the fluctuations extend at the various pressure defining the anomalous region [Figure adopted from 61].

Overall, in between  $T_H(p)$  and  $T_x(p)$  fast ice nucleation prevents any experimental attempts to keep water in a liquid form. Therefore, *Molecular Dynamics* (MD) simulations, using very fast cooling rates, can enter the no man's land.

The other two ultraviscous liquid metastable phases of water are bounded by spontaneous crystallization temperature ( $T_x(p) = 150$  K) from above, at which the ultraviscous liquid turns into ice, and by the glass transition temperature of water ( $T_g(p) = 136$  K) from below. Heating glassy water above glass transition temperature ( $T_g(p) = 136$  K) creates ultraviscous liquid metastable phase.

The non-crystalline metastable states of water are (some overlap):

1. Superheated liquid water
2. Supercooled liquid water
3. Stretched water (liquid under tension)

4. Glassy water (liquid rapidly cooled below a glass transition temperature)
5. Cold film produced by water vapour deposition
6. Pressure-amorphized ice (*amorphous ice*)

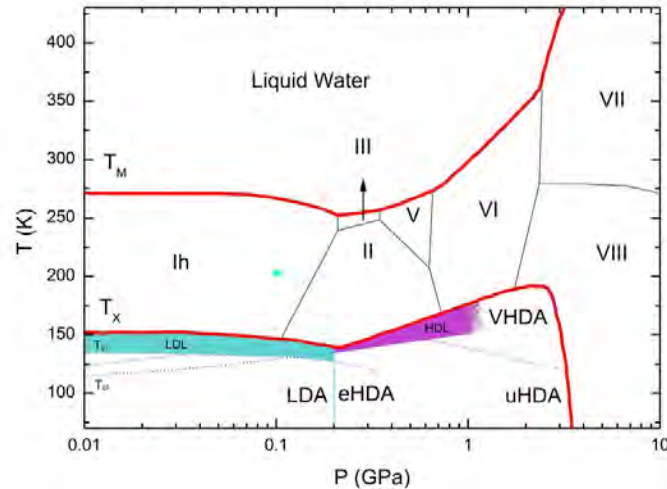


Figure 27: Phase diagram of non-crystalline water.

#### 1.5.3.1 Polyamorphism: Three forms of solid amorphous ice

As a rule, cooling a liquid slowly causes it to freeze to a stable crystalline state. However, by rapidly cooling water can cause it to enter into kinetically trapped states that are *glassy*, i.e., the kind that do not have regular order and where the transport is sluggish [81].

One of the most intriguing findings in the physics of amorphous water (ice) is *polyamorphism* which depicts the arrested disordered states of water below the *no man's land*. By definition, polyamorphism in water is the existence of more than one amorphous phase.

---

Glasses are nonequilibrium materials. Different experimental approaches are utilized to produce different forms of polyamorphic solid glassy water. However, unlike other materials, glassy water is very unusual because its transformation between different forms is essentially sharp, practically reversible and is accompanied by the large changes in fundamental physical properties such as density, which is indicative of a thermodynamic phase transition.

Molecular structure of water governs its properties. Based on the studies of water's diffusion and viscosity properties, water diffuses more rapidly above glass transition than below. Hence, water is a complex glassy material. As a rule, cooling a liquid slowly causes it to freeze to a stable crystalline state. However, rapid cooling a liquid water can cause it to enter into kinetically trapped states that are *glassy*, i.e., the kind that do not have regular order and where the transport is sluggish [81].

Furthermore, in case of water - it undergoes such a glass transition to an amorphous solid. In water, the characteristic relaxation times become of the order of 100s, and the rate of change of the volume and entropy decreases abruptly (yet continuously) to that of a crystalline solid [82]. To explore glassy water dynamics, computer simulations of supercooled water are engaged.

As one of the most intriguing findings in the physics of amorphous water (ice) is polyamorphism which depicts the arrested disordered states of water below the no man's land. Polyamorphism in water is the existence of more than one amorphous phase in metastable equilibrium [6]. Different amorphous phases should differ in their properties, as well as phase boundaries to stable or metastable phases have to exist.

---

Since glasses are nonequilibrium materials, different experimental approaches are utilized to produce different forms of polyamorphic solid glassy water. However, unlike other materials, glassy water is very unusual because its transformation between different forms is essentially sharp, practically reversible and is accompanied by the large changes in fundamental physical properties such as density, which is indicative of a thermodynamic phase transition.

Extensive studies of glassy water have been performed for *low-density* (LDA) and *high-density* (HDA) *amorphous ices* [49, 83, 84, 85] which are separated by the first order phase transition, and recently, *very-high-density* third glassy state *amorphous ice* (VHDA) has been introduced and explored as a new distinct form of glassy water [86]. The temperature of glass transition is slightly different in the two cases.

Three amorphous ices of water are considered according to their respective density. Low density amorphous ice, LDA, is produced by vapour deposition on a cold surface, or by extremely rapid supercooling of liquid droplets ( $> 10^6 \text{ K / s}$ ). High density amorphous ice, HDA, is produced by pressuring ice,  $I_h$ , at 77 K, or by quenching and compressing emulsions of pure liquid water. Very-high-density amorphous ice, VHDA, is produced by raising up the density above the latter (Figure 28).

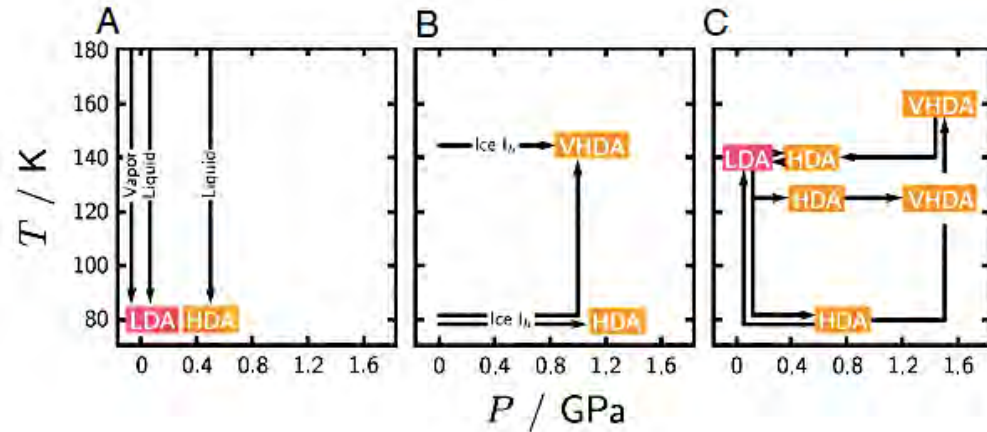


Figure 28: Laboratory schematics for amorphous ices. Path starting from vapour or liquid water is shown in A; path starting from hexagonal ice ( $I_h$ ) is shown in B; path in which an amorphous form is prepared starting from a specific amorphous ice is presented in C; where horizontal arrows represent isothermal compression/decompression paths, and vertical arrows indicate isobaric cooling/heating paths [Data adopted from 95].

### 1.5.3.2 Supercooled water

The metastable states of water are very complex. The liquid state of water below its melting point and below its freezing temperature is known as a *supercooled water* - water in its liquid metastable state with a finite lifetime below its melting temperature,  $T_M(p)$ . In liquid supercooled water, the crystal remains in the stable state, yet the crystallization can be bypassed if the cooling occurs expediently. Thus, supercooled water exists in a state of precarious equilibrium. Slight perturbations such as dissolved or suspended impurities would lead to a sudden appearance of the stable crystalline phase.

Supercooled water shows some anomalies, both experimentally and in simulation. It has been observed that the anomalous behaviour of water is substantially more pronounced in the deep supercooled water region. The

---

hypothesis that water could exist as HDL and LDL macroscopic phases [9], which connects the presence and transformation between the two amorphous glassy states of water, i.e., HDA and LDA [59, 87]. This hypothesis has been found more successfully in explaining the anomalies of supercooled water with respect to other theoretical approaches like the *stability liquid conjecture* [67], the *critical point free scenario* [89], and the *singularity free* approach [89].

In principle, supercooled water could be produced by restraining water from freezing and keeping it in a liquid form even below its normal freezing point and its melting temperature,  $T_M(p)$ , i.e., meticulous prevention of nucleation by experimental techniques. Based on evaporative cooling experiments, so far, the temperature limit is reached at about 227 K [90]. As described above, the region between the spontaneous crystallization temperature of devitrified water and the homogeneous nucleation temperature is the no-man's land.

The three amorphous ices discussed above (HDA, LDA, VHDA) are the products of further rapid cooling of the supercooled water. Since the lifetime of the supercooled water in metastable state is finite, it either crystallizes in a solid stable state or turns into a glass state [91]. The driving force behind these two scenarios is based on innate characteristics of the supercooled liquid itself, i.e., the *nucleation time* ( $\tau_1$ ) - the time required for a fraction of volume to crystallize, and the *relaxation time* ( $\tau_2$ ).

Based on anomalous thermodynamic properties of water, relations between glasses and supercooled water can be perceived from the HDA and LDA transitions. The sudden transition between HDA and LDA upon heating at low pressure or decompressing at adequately high temperature

---

is a clear manifestation of the possibility that such transition is indicative of the out-of-equilibrium thermodynamic coexistence curve between two arrested liquids of different density. Subsequently, the existence of more than one glass of water coincides with the notion of existence of more than one liquid form [88]. The existence of two distinct liquids is attributed to one important precondition: the time of relaxation must be shorter than the time of transformation.

The exothermic nature of the changes involved in HDA to LDA transition implies that HDA has a larger entropy. Clausius-Clapeyron relation [39, 40] connects the slope of the coexistence curve to the entropy and volume change of the phase transition. Based on that, a transition in which the denser phase is more disordered has a coexistence line with a negative slope in the  $p - T$  plane. Therefore, the second liquid-liquid CP would occur at the low-pressure and high-temperature and of the LDA-HDA equilibrium point.

The transition between LDA and HDA is a low-temperature indication of a first-order transition between two phases of liquid water: LDL and HDL. Thus, LDA and HDA are simply the corresponding vitreous forms.

According to *Liquid-liquid phase transition hypothesis*, the transition between LDL and HDL terminates at a LLC. At higher temperatures, the HDL and LDL phases are indistinguishable, similar to the gas and liquid phases above a liquid-gas CP. Above the critical temperature and in association with any CP, *critical fluctuations* occur. Both, HDL and LDL (Figure 30) become identical at a LLC in supercooled water [92]. Therefore, the LLC explains the drastic increase in the compressibility, specific heat, and thermal expansion coefficient.

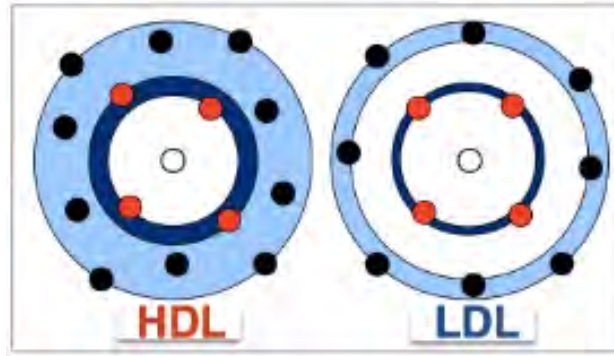


Figure 29: Graphical representation of molecular constitution of HDL and LDL.

Theoretical and computational studies have located the LLCPP below the homogeneous nucleation temperature, and, once again, it is difficult to probe experimentally due to the rapid crystallization.

Figure 31 shows the phase diagram of water with the emphasis on supercooled and non-crystalline forms of water based on the computationally obtained LLCPP deduction. As seen here, the second LLCPP and the coexistence line along which LDL and HDL are coinciding within the no man's land. In addition, at low temperatures, both liquid phases become structurally arrested into their glassy forms, i.e., LDA and HDA. Upper homogeneous ice nucleation locus line representing  $T_H(p)$  and lower line representing the temperature of the spontaneous crystallization,  $T_x(p)$ , are shown. Given that the slope of the LDL-HDL is negative, it means that the LDL is significantly less denser than the HDL [42].

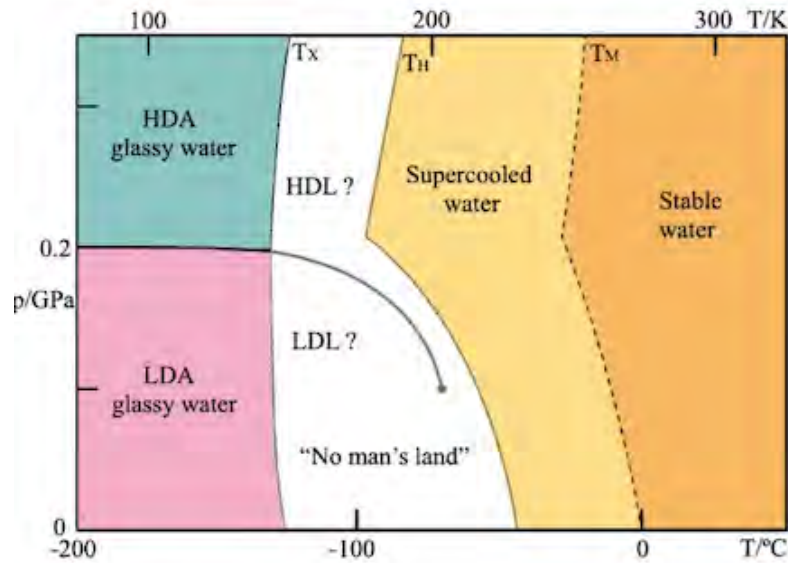


Figure 30 : The phase diagram of water with emphasis on supercooled and non-crystalline forms of water showing the second LLCP [Figure adopted from 6].

As noted, based on the observations, there exist two separate liquid phases, HDL and LDL with a coexistence line in the  $p - T$  diagram deep in the supercooled regime and at elevated pressure [9, 59]. This LLT line ends with decreasing pressure in the LLCPP which has been detected at positive high pressure and low temperature, way deep inside the no man's land. The uniqueness of water lays in the fact that at ambient pressure the location of the LLCPP is such that the anomalous region with fluctuations extends up to approximately 320 K (47 °C).

The line of the thermodynamic response function originates from LLCPP extends into the one-phase region and it is known as *Widom line* [93], alike to the Widom line of the liquid-gas CP [94]. The existence of two different liquid states of supercooled water via LLCPP and Widom line has been long predicted by theory and simulations [94, 95, 96]. At the Widom line the density fluctuations reach a maximum which is consistent with equal population of water molecules in HDL and LDL [97]. Given that the

---

anomalous behaviour of water can be justified by treating liquid water as a mixture of two distinct groups of molecules, pertained to two different arrangements of the HB network, i.e., LDL and HDL [55, 74, 80, 98, 99, 100, 101]. The LDL phase is found to be on the low-temperature side and is characterized locally by a stronger tetrahedral order. On the other hand, the HDL is prevalent to the ambient temperature side where the HB structure is broken. This is a classic example of the high-density, HB-distorted species' domination at ambient conditions [61]. Moreover, the anomalous properties of water originate in fluctuations of the HBs as their tetrahedral specks are growing in size of the directional HBs and become more dominant [55, 102].

The similarities in mechanisms, features and behaviour between LDL-HDL and LDA-HDA phases are straight forward analogous. Thus, previously mentioned, Widom line is indeed separates the dominance of HDL over LDL and vice versa. Recent experimental confirmation of existence of the Widom line, and subsequent second-order CP in the supercooled region of the water phase diagram has been presented by Kim *et al.* [102] (See Figure 31).

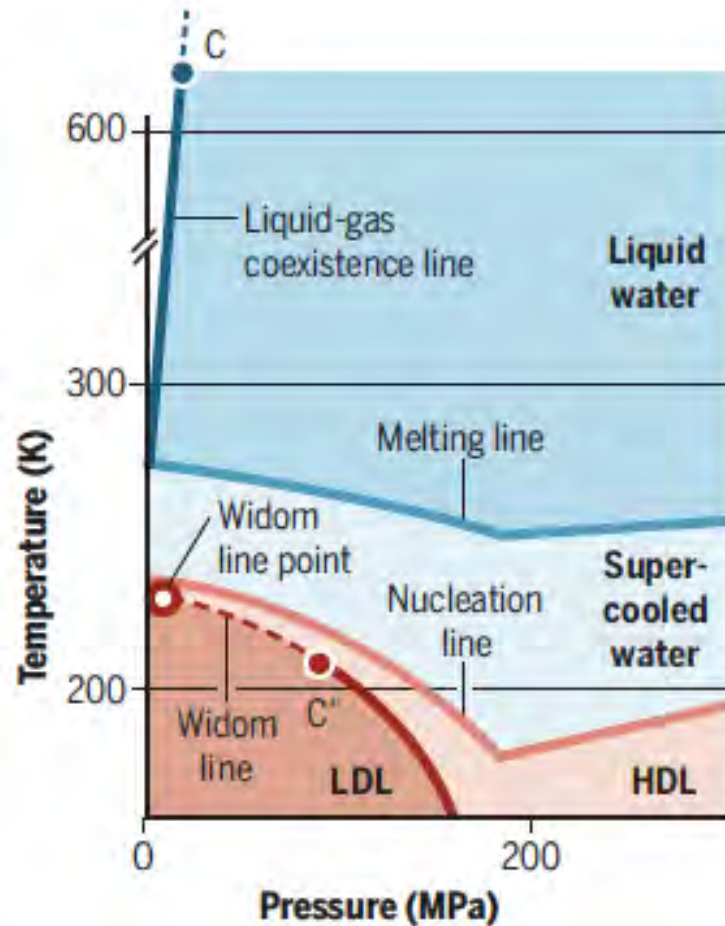


Figure 31: The first red point is the experimental evidence of the Widom line as a thermodynamic response function originated from LLCP in glassy water [Figure adopted from 103].

Structurally, supercooled water is created by clusters of water molecules coming together in intrinsically different ways which result in formation of HDL and LDL, as depicted in Figure 32.

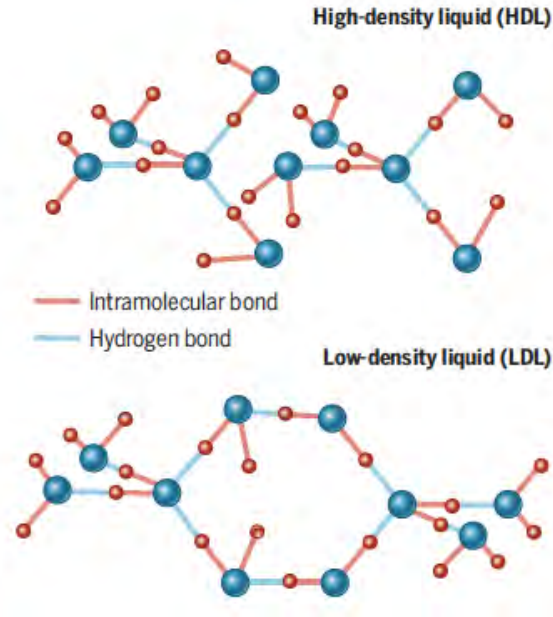


Figure 32: Molecular structure of HDL and LDL [Figure adopted from 103].

The key properties of interest of supercooled water are:

- ◆ isothermal compressibility

$$k_T = \left( \frac{\partial \ln \rho}{\partial \ln p} \right)_p \quad (1.12)$$

- ◆ isobaric heat capacity

$$C_p = T \left( \frac{\partial S}{\partial T} \right)_p \quad (1.13)$$

where  $p$  is the pressure,  $T$  is the temperature,  $\rho$  is water's density,  $S$  is the entropy.

One hypothesis is that this divergence simply implies that a system is reaching a *spinodal point*, beyond which there is no metastable state hence, the system must freeze. An alternative hypothesis is based on idea

---

that this divergence reflects a phase transition between two different metastable phases of liquid [93, 104, 105].

One interesting concept of a liquid-liquid coexistence is that there are two species of water, A and B, with temperature-dependent concentrations  $x_A(T)$  and  $x_B(T)$  [24] of the disordered liquid phases, HDL and LDL [106]. Here, the difference in two liquids is attributed to both, density and local order. The latter had suggested that the thermodynamics of water are controlled by two order parameters [107].

In terms of cage geometry, LDL can be visualized as more cage-like and HDL is less cage-like. These hypothetical liquids stem from experimental results on studies of LDA and HDA. The results show that LDA is formed by depositing water vapor on a single-crystal metallic surfaces, while HDL is obtained by applying pressure to hexagonal ice,  $I_h$ . Moreover, the notion that the LLCP is partially motivated by the observation of a first-order phase transition between LDA and HDA is implied [48].

Nowadays, the properties of supercooled water are widely explored by computer simulations of liquid water in no-man's land [100, 108, 109]. Recent results of computer simulations modelling clearly show that supercooled water undergoes a liquid-liquid phase transition [8, 14, 49, 110]. If liquid water is cooled fast enough, freezing can be avoided and water, consequently, will become a noncrystalline solid, i.e., a glass [111, 112, 113]. Besides, in 2015 Smallenburg and Sciortino successfully proved that tetrahedral model systems, similar to water, have two stable supercooled liquid phases [114].

## 1.5.3.3 Fragile to strong crossover in water

Angell *et al.* gave a precise classification of the glass former liquids. In approaching the glassy state the viscosity increases many order of magnitude and Angell defines the glass transition temperature when the viscosity reaches the value of  $10^{13}$  poise corresponding to a relaxation time of 100 s. Glass formers are classified as strong liquid if the viscosity increases exponentially, the Arrhenius behaviour,

$$\ln k(T) = \ln A - \frac{E_a}{RT} \quad (1.14)$$

where

$k$  is the rate constant (frequency of collisions resulting in a reaction),

$T$  is the absolute temperature (in degrees Kelvin or Rankine),

$A$  is the pre-exponential factor,

$E_a$  is the activation energy for the reaction (in the same units as  $RT$ ),

$R$  is the universal gas constant.

The activation energy,  $E_a$ , represents the energy barrier that particles must cross in order to diffuse and is temperature-dependent. The  $1 / RT =$  additional quadratic term associated with deviation of linearity in an Arrhenius plot.

In other systems, called fragile liquids, the viscosity increases with a super-Arrhenius formula, i.e.,

$$\ln k(T) = \ln A + \frac{B}{RT} + \frac{C}{(RT)^2} \quad (1.15)$$

where

$C$  dictates if the plot is “concave” or “convex” [114].

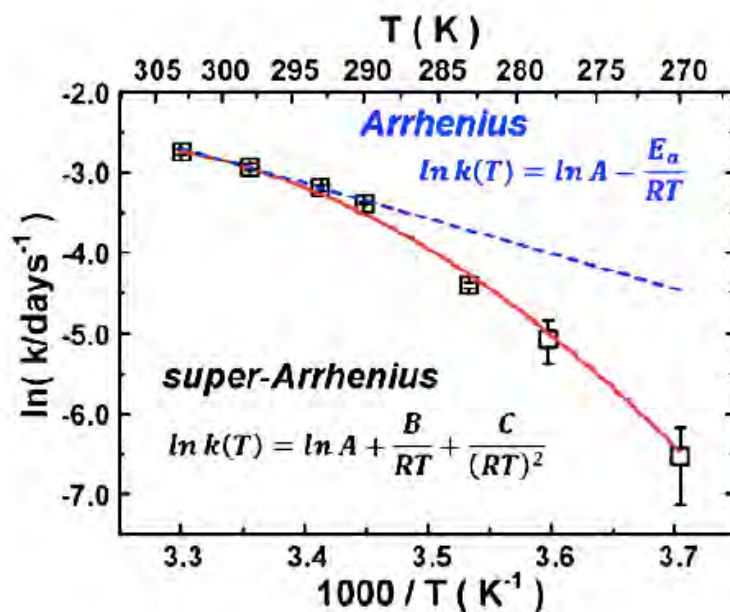


Figure 33. Arrhenius plot of logarithm of reaction rate constants as a function of inverse absolute temperature  $K$ . The dashed line in blue indicates the linear Arrhenius plot as a reference. The convex line in red indicates the super-Arrhenius plot as a reference [Data adopted from 116].

According to Angell's classification, water is a fragile liquid as its viscosity increases (diffusion decreases) more than exponentially when the temperature drops below its melting temperature ( $T_M = 273$  K). Most molecular liquids are fragile, but water is a highly exceptional fragile liquid. In fact, the super-Arrhenius evolution of the viscosity with temperature is larger in water than in most liquids.

Fragility is usually related to the extent of cooperative motions, i.e., the increase of the activation energy,  $E_a(T)$ , by the need for an increasing number of molecules to cross energy barriers cooperatively to reach diffusion. Consequently, the large super Arrhenius behavior of water indicates that cooperative motions are particularly large for water.

Increasing the pressure or the density leads to a decrease of the super-Arrhenius behaviour [117, 118, 119] in water. Since fragility relates to the

---

cooperative motions, when the pressure or density is increased, the cooperative motions are decreased - this, in turn, accelerates the dynamics (i.e., decreases the viscosity) in supercooled water. Teboul *et al.* 2019 had interpreted this effect from the pressure induced structural modifications in the liquid. His MD study deduced that increasing the pressure promotes the high-density structure and as a result decreases the structural fluctuations that are responsible for the large cooperative motions in water [119].

A fragile to strong crossover has been found in supercooled water to take place at the crossing of the liquid-liquid Widom line. According to the interpretation of the LLCP water remains fragile in the HDL state while the LDL component is associated to a strong behaviour [41, 72, 93, 120, 121, 122, 123, 124].

---

## Chapter 2

### Molecular Dynamics



Classic Molecular Dynamics (MD) is the most ubiquitous and highly proficient scientific tool for execution of the detailed modelling of microscopic state of matter. Nowadays, many scientific disciplines employ the MD simulations to study matter and subsequently benefit from it. Some of these are: theoretical physics of matter, chemical physics, physical chemistry, chemical engineering, radiochemistry, biophysics, biochemistry, material sciences, to name a few. It is particularly the most extensive computational technique in condensed matter physics as it delivers a solution of the classical equations of motions for atoms and molecules throughout the time evolution of the system. The principle of the MD is based on the calculations of the *real* dynamics of the system which enables the calculations of the time averages of the properties within the system under investigation. The MD is a *deterministic* method at its core, i.e., the state of the system at any future time can be predicted from its current state. Moreover, the MD method is designed to constructively replicate microscopic behaviour by employing model systems, as opposed to trying to derive it from an experiment.

---

Fundamentally, in the MD simulations the evolution of the system of interest is derived by employing numerical integration of the Newton's law of motion.

This chapter is dedicated to presenting the Foundation, Theory and Principles of the MD method (2.1); Integration algorithms employed (2.2) application to different molecular system ensembles such as Thermostats and Barostats (2.3); implementation of Ewald summation (2.4); steps in Running MD simulations (2.5); and Force fields applied to depict particles interactions (2.6).

## 2.1 Foundation, Theory and Principles

Molecular Dynamics method was developed within the field of theoretical physics in the late 1950s [125, 126]. At the offset (and thereon), the premises of the MD are attributed to Newton's laws of motion.

Conjunctively, the origins of the MD are embedded in the relic of atomism. The implication of the solution to many-body problem was compiled by the genius of Laplace, i.e.: "Given for one instant an intelligence which could comprehend all the forces by which nature is animated and the respective situation of the beings who compose it - an intelligence sufficiently vast to submit these data to analysis - it would embrace in the same formula the movements of the greatest bodies of the universe and those of the lightest atom; for it, nothing would be uncertain and the future, as the past, would be present to its eyes" [127].

---

The theoretical basis for the MD constitutes an immense body of scientific results in analytical mechanics delivered by the great minds such as Euler, Hamilton, Lagrange, Newton [128]. For structureless particles, the simplest form of the MD requires more than Newton's second law. For instance, rigid molecules depend on the use of Euler equations expressed in terms of Hamilton's *quaternions*. Lagrange method of including the geometric constraints into the dynamic equation is highly efficient in applications to molecules with internal degrees of freedom, as they are also subject to structural constraints. In general, normal equilibrium MD is related to the *microcanonical ensemble* of statistical mechanics. But in some cases, properties at constant temperature and pressure are required [129].

Decisively, the equations of motions can only be solved numerically. The nature of interatomic interactions is described by classic potentials. One of the most used, in combination with the Coulomb potential is Lennard-Jones (LJ) potential with strongly repulsive core. It is unreasonable to seek even moderate accuracy in trajectories, even over limited period of time. Thus, comparatively low-order numerical integration method such as the MD is much more effective than any other [130].

The concept of the MD simulation is very logical and rather straightforward [131, 132]. In classical theory, the motion of molecules is governed by Newton's equations of motion. In the MD simulations, particles motion in a microscopic system is simulated on a computer corresponding to the equations of motion [133]. Then, the thermodynamic, static, dynamic and structural properties of a many-body system can be easily calculated and plainly understood by utilizing the MD simulations in a classical deterministic fashion [134]. Straightforward Newton's equation of motion for the single molecule  $i$ , with mass  $m_i$  and an external field  $f_i$  is

$$m_i \frac{d^2 \mathbf{r}_i}{dt^2} = \mathbf{f}_i \quad (2.1)$$

In a system composed of  $N$  molecules, there  $N$  is a sets of similar equations, and the motion of  $N$  molecules interacts through forces acting among the molecules. Thus, for a system of fixed number of atoms and molecules in MD simulation the general Hamiltonian  $H$  is given by

$$H(\{\mathbf{r}_i\}_N, \{\mathbf{p}_i\}_N) = K(\{\mathbf{p}_i\}_N) + U(\{\mathbf{r}_i\}_N) \quad (2.2)$$

or, alternatively

$$H = (\mathbf{r}^N, \mathbf{p}^N) = K(\mathbf{p}_1, \mathbf{p}_2, \dots, \mathbf{p}_N) + U(\mathbf{r}_1, \mathbf{r}_2, \dots, \mathbf{r}_N) = \sum_{i=1}^N \frac{p_i^2}{2m} + \sum_{i=1}^N \sum_{j>i}^N u(\mathbf{r}_i - \mathbf{r}_j) \quad (2.3)$$

where  $K$  is kinetic energy and  $U$  is many-body interaction potential, counted as the sum of radial potentials  $u_{ij}$  between pairs of particles

$$U(\{\mathbf{r}_i\}_N) = \frac{1}{2} \sum_i \sum_{j \neq i} u_{ij}(|\mathbf{r}_i - \mathbf{r}_j|) \quad (2.4)$$

Based on Newton's second law, the trajectories of the particles in the system are derived by solving the following differential equations

$$m_i \ddot{\mathbf{r}}_i = \frac{d\mathbf{p}_i}{dt} = \mathbf{F}_i = -\nabla_{\mathbf{r}_i} U \quad (2.5)$$

$$\mathbf{v}_i = \dot{\mathbf{r}}_i = \frac{\mathbf{p}_i}{m_i} \quad (2.6)$$

A finite difference method is applied for the integration of the above equations which consist of distinctly separate parts of the temporal axis in a series of time steps of length  $\delta t$ . If the positions and velocities of a particles at defined time  $t$  are known, the translated positions, velocities and trajectories of the particles at time  $t + \delta t$  are then calculated in deterministic fashion.

Microscopic evolution of a system (position and velocities) is generated by the MD simulation which produces a sequence of points in the phase space as a function of time. As these points belong to the same ensemble, they satisfy conditions of a specific thermodynamic state. In order to evaluate quantities of the system, its properties must be transformed from microscopic to macroscopic state. Hence, quantities of the system in motion can be probed by the MD with statistical mechanics principles such as *ergodic hypothesis*. If  $A$  is a generic thermodynamic quantity under ergodic hypothesis, its calculated average within the system at a certain time is equivalent to its value over steps in time, i.e.

$$\langle A \rangle = \int A(\mathbf{r}^N, \mathbf{p}^N) \rho[H(\mathbf{r}^N, \mathbf{p}^N)] d\mathbf{r}^N d\mathbf{p}^N = \bar{A} = \lim_{t \rightarrow \infty} \frac{1}{t} \int_0^t A(\mathbf{r}^N, \mathbf{p}^N) dt' \quad (2.7)$$

Established correlation between the temperature and the kinetic energy leads to configuring the velocity from extracting random values from the Maxwell-Boltzmann distribution. The probability of a particle  $i$  of mass  $m_i$  and temperature  $T$  has velocity  $\mathbf{v}_{ix}$  along the  $x$ -axis is

---

$$P(\mathbf{v}_{ix}) = \sqrt{\frac{m_i}{2\pi k_B T}} \exp\left[-\frac{m_i \mathbf{v}_{ix}}{2k_B T}\right] \quad (2.8)$$

The trajectories produced in the MD simulations are correlated by a sequence of points in the phase space as a function of time. The time of running the MD simulations on the sampling of specific phase space must exceed the time of movements attributed to molecular motions.

Based on specific thermodynamic configuration of a given system, several common statistical ensembles with different characteristics have been established within the MD. These are:

- *NVE* - Microcanonical Ensemble in which the thermodynamical state of a system is distinguished by a fixed number of particles  $N$ , a fixed volume  $V$ , and a fixed total energy  $E$ .
- *NVT* - Canonical Ensemble in which the thermodynamical state of a system is distinguished by a fixed number of particles  $N$ , a fixed volume  $V$ , and a fixed temperature  $T$ .
- *NPT* - Isobaric-Isothermal Ensemble in which the thermodynamical state of a system is distinguished by a fixed number of particles  $N$ , a fixed pressure  $P$ , and a fixed temperature  $T$ .

Due to the conservation of the total energy of the system in *NVE* ( $E = K + U$ ), this natural ensemble does not require rescaling of velocity in the MD. Thus, quantities such as temperature and pressure of the system can be easily calculated. For temperature calculation, the *equipartition theorem* is employed, and the temperature is represented as

$$T = \frac{2 \langle K \rangle}{3 k_B} = \frac{1}{3} \frac{\sum_{i=1}^N m_i v_i^2}{k_B N} \quad (2.9)$$

where  $N_c$  is the number of constraints.

Similarly, the pressure is calculated via *virial theorem*

$$P = \frac{Nk_B - \frac{1}{3} \langle \mathcal{V} \rangle}{V} \quad (2.10)$$

where the *virial* is

$$\mathcal{V} = \sum_{i=1}^N \mathbf{r}_i \cdot \mathbf{F}_i \quad (2.11)$$

Another important aspect in the MD simulations is *periodic boundary conditions*, PBC, which are applied to calculations of properties of bulk gases, liquids and crystals. The significance of PBC resides in prevention of entrance of artifacts due to the presence of surfaces in the box in study, as well as access to performing the MD simulations with comparatively small number of molecules [135].

## 2.2 Integration algorithms

In the MD integration of the equation of motion and calculation of particle' trajectories in accordance with Newton's laws, algorithms of *finite difference method* are required. In general, a successful MD simulation

algorithm should be fast, must require little memory; should allow the use of a long-time step  $\delta t$  (fs) ought to replicate classical trajectory closely; must obey energy and momentum conservation laws; and has to act in time-reversible fashion [136].

### 2.2.1 Translational motion

The positions, velocities and accelerations of particles are treated as an approximation, e.g., Taylor series expansions [137]

$$\mathbf{r}_i(t + \delta t) = \mathbf{r}_i(t) + \mathbf{v}_i(t)\delta t + \frac{1}{2}\mathbf{a}_i(t)\delta t^2 + \frac{1}{6}\mathbf{b}_i(t)\delta t^3 + \dots \quad (2.12)$$

$$\mathbf{v}_i(t + \delta t) = \mathbf{v}_i(t) + \mathbf{a}_i(t)\delta t + \frac{1}{2}\mathbf{b}_i(t)\delta t^2 + \dots \quad (2.13)$$

$$\mathbf{a}_i(t + \delta t) = \mathbf{a}_i(t) + \mathbf{b}_i(t)\delta t + \dots \quad (2.14)$$

where  $\delta t$  is the Dirac delta function of identity constraints.

One of the most commonly used algorithms in MD is the *Verlet algorithm* [138]. This algorithm calculates particle's position at time  $t + \delta t$  and its velocities at a time  $t$  by taking its position  $\mathbf{r}(t)$  and acceleration  $\mathbf{a}(t)$  at time  $t$  and position at the previous step  $\mathbf{r}(t - \delta t)$

$$\mathbf{r}(t + \delta t) = \mathbf{r}(t) + \mathbf{v}(t)\delta t + \frac{1}{2}\mathbf{a}(t)\delta t^2 + \dots \quad (2.15)$$

$$\mathbf{r}(t - \delta t) = \mathbf{r}(t) - \mathbf{v}(t)\delta t + \frac{1}{2}\mathbf{a}(t)\delta t^2 - \dots \quad (2.16)$$

Then, addition and subtraction of the two above equations 2.15 and 2.16 results in

$$\mathbf{r}(t + \delta t) = 2\mathbf{r}(t) - \mathbf{r}(t - \delta t) + \mathbf{a}(t)\delta t^2 \quad (2.17)$$

$$\mathbf{v}(t) = [\mathbf{r}(t + \delta t) - \mathbf{r}(t - \delta t)] / (2\delta t) \quad (2.18)$$

Although the Verlet algorithm is efficient in terms of its storage capacity, it does have a disadvantage in quality of precision when small terms  $\sim \delta t^2$  are added to the difference of two significantly larger terms to obtain  $\mathbf{r}(t + \delta t)$  position. Moreover, the simultaneously generated velocities at the same time of particle's position are lagging in one time-step.

Since the original postulate of Verlet algorithm in 1967, and on the basis of it, a number of modified algorithms have been developed in order to improve the velocity and precision executions.

One of the surpassing MD algorithms is the *leapfrog* algorithm which utilizes velocity quantity at half-time intervals and integrates the translational motion of the particles. Contrary to Euler first-order integration, leapfrog integration is of a second order, yet it requires the same number of function evaluation per each step. This iteration algorithm operates in two steps:

1. Velocity at time  $(t + \frac{1}{2}\delta t)$  is computed from  $\mathbf{a}_i(t)$  and  $\mathbf{v}_i(t - \frac{1}{2}\delta t)$  as

$$\mathbf{v}_i\left(t + \frac{1}{2}\delta t\right) = \mathbf{v}_i\left(t - \frac{1}{2}\delta t\right) + \mathbf{a}_i(t)\delta t \quad (2.19)$$

2. Position at time  $(t + \frac{1}{2}\delta t)$  is derived as

$$\mathbf{r}_i(t + \delta t) = \mathbf{r}_i(t) + \mathbf{v}_i\left(t + \frac{1}{2}\delta t\right)\delta t \quad (2.20)$$

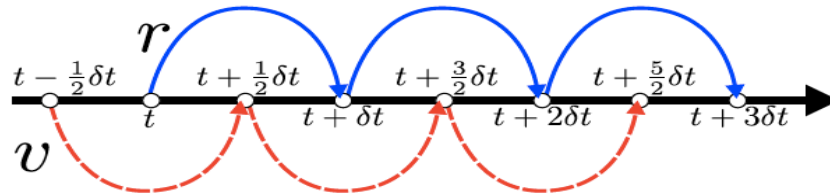


Figure 2.1. Schematic representation of the leapfrog algorithm. Continuous (blue) lines represent storage in position. Dashed (red lines) indicate storage in velocities. The position and velocities of the particle leapfrog over each other upon being stored [137].

Since leapfrog algorithm uses velocities at closer time, the resultant computed positions are much more precise.

Finally, the half-time behind velocity which is not at the same time as of the position at time  $t$ , is calculated as

$$\mathbf{v}_i(t) = \frac{\mathbf{v}_i\left(t + \frac{1}{2}\delta t\right) - \mathbf{v}_i\left(t - \frac{1}{2}\delta t\right)}{\delta t} \quad (2.21)$$

### 2.2.2 Rotational motion

While the translational motion integration in the MD is rather straightforward, the rotational motion of a particles is somewhat complex.

The torque with respect to the center of mass of the molecule at position  $\mathbf{r}_i$  is described by the vector  $\tau_i$

$$\tau_i = \sum_a ((\mathbf{r}_{ia} - \mathbf{r}_i) \wedge \mathbf{F}_{ia}) = \sum_a \mathbf{d}_{ia} \wedge \mathbf{F}_{ia} \quad (2.22)$$

where  $\mathbf{d}_{ia}$  denotes the position of the atom  $a$  within the molecule  $i$  in reference to its center of mass.

To describe the transformation of the rigid body in space from the laboratory frame of reference to that one of the center of mass, a rotation matrix is employed. This matrix is defined by the three independent angular parameters - *Euler angles* ( $\varphi, \theta, \psi$ ). A function of the Euler angles is a quadri-dimensional vector with unitarity norm, a.k.a., *quaternion*,  $\mathbf{q}$  which permits convergent equations of motion.

$$\mathbf{q} = (q_0, q_1, q_2, q_3) \quad (2.23)$$

If  $q_0^2 + q_1^2 + q_2^2 + q_3^2 = 1$ , then the rotational matrix is written in terms of  $\mathbf{q}$  as:

$$R = \begin{pmatrix} q_0^2 + q_1^2 - q_2^2 - q_3^2 & 2(q_1q_2 + q_0q_3) & 2(q_1q_3 - q_0q_2) \\ 2(q_1q_2 - q_0q_3) & q_0^2 - q_1^2 + q_2^2 - q_3^2 & 2(q_2q_3 + q_0q_1) \\ 2(q_1q_3 + q_0q_2) & 2(q_2q_3 - q_0q_1) & q_0^2 - q_1^2 - q_2^2 + q_3^2 \end{pmatrix} \quad (2.24)$$

Since  $\mathbf{d}_{ia}$  is the position of the atom  $a$  at the center of mass frame, then its position in the laboratory frame is

$$\mathbf{d}_{ia} = R^T \widehat{\mathbf{d}}_{ia} \quad (2.25)$$

Each molecule represented by quaternion is in accord with the equation of motion

$$\begin{pmatrix} \dot{q}_0 \\ \dot{q}_1 \\ \dot{q}_2 \\ \dot{q}_3 \end{pmatrix} = \frac{1}{2} \begin{pmatrix} q_0 & -q_1 & -q_2 & -q_3 \\ q_1 & q_0 & -q_3 & q_2 \\ q_2 & q_3 & q_0 & -q_1 \\ q_3 & -q_2 & q_1 & q_0 \end{pmatrix} \begin{pmatrix} 0 \\ \omega_x \\ \omega_y \\ \omega_z \end{pmatrix} \quad (2.26)$$

where  $0, \omega_x, \omega_y, \omega_z$  are the 3-D components of the angular velocity vector  $\omega$  in the center of mass frame.

Since the system at hand does not contain singularities, it can be simply solved by implementing the same procedure as the one used in translational motion integration. For solving the rotational motion, the following equation is employed

$$\frac{d\mathbf{J}}{dt} = \frac{d}{dt} (I\omega) = \tau \quad (2.27)$$

where  $\mathbf{J}$  is the total angular momentum of the molecule,  $I$  is the momentum of inertia matrix,  $\tau$  is the torque of the molecule.

If  $\mathbf{J}\left(t - \frac{1}{2}\delta t\right)$ ,  $\mathbf{q}(t)$  and  $\tau(t)$  are stored, iterative approach is taken to solve the equations for rotational motion. First, the angular momentum should be updated by

$$\mathbf{J}(t) = \mathbf{J}\left(t - \frac{1}{2}\delta t\right) + \tau(t)\frac{1}{2}\delta t \quad (2.28)$$

Then quaternion  $\mathbf{q}$  can be calculated by

$$\mathbf{q}\left(t + \frac{1}{2}\delta t\right) = \mathbf{q}(t) + \dot{\mathbf{q}}(t)\frac{1}{2}\delta t \quad (2.29)$$

The latter two auxiliary equations allow to determine  $\mathbf{q}\left(t + \frac{1}{2}\delta t\right)$  and calculate  $\dot{\mathbf{q}}$  at the half-step time. Finally, deduced equations for calculating the total angular momentum of the molecule,  $\mathbf{J}$  and the quadri-dimensional vector with unitarity norm,  $\mathbf{q}$  are

$$\mathbf{J}\left(t + \frac{1}{2}\delta t\right) = \mathbf{J}\left(t - \frac{1}{2}\delta t\right) + \tau(t)\frac{1}{2}\delta t \quad (2.30)$$

$$\mathbf{q}(t + \delta t) = \mathbf{q}(t) + \dot{\mathbf{q}}\left(t + \frac{1}{2}\delta t\right)\delta t \quad (2.31)$$

Additional methods to generate the motion of a rigid body are the constraints algorithms in which the precise constraints between positions of the atoms in the molecule are defined and the performed procedure is

- 
1. The particle is permitted to move separately.
  2. Explicit constraint forces are imposed.
  3. Employing techniques of Lagrange multipliers (or similar), the forces are minimized.

### 2.3 Thermostats and Barostats

Amongst statistical ensembles in the MD, most algorithms are applied to the Microcanonical *NVE* ensemble. However, Canonical *NVT* and Isothermal-isobaric *NPT* ensembles can also be subjected to MD algorithms in order to simulate thermostat and barostat, respectively.

For the Canonical *NVT* ensemble (thermostat), the most popular techniques are Nosé-Hoover [139], Berendsen [140] and Gaussian constraints [140]. For the Isothermal-isobaric *NPT* ensemble (barostat), the most applied algorithms are Berendsen [141] and Hoover [139].

For a given system, coupling to thermostat and/or barostat can be successfully obtained by adding terms to Lagrangian which will result in modification of the equations of motion.

The classic Lagrangian for a system is

$$\mathcal{L} = \frac{1}{2}m \sum_{i=1}^N |\dot{\mathbf{r}}_i|^2 - U \quad (2.32)$$

For thermostat, *thermal bath* is inserted, and velocities are rescaled as  $\dot{\mathbf{r}}_i \rightarrow s\dot{\mathbf{r}}_i$ .

Then, the new Lagrangian with rescaled quantities becomes

$$\mathcal{L} = \frac{1}{2}m \sum_{i=1}^N s^2 |\dot{\mathbf{r}}_i|^2 - U + \frac{Q}{2}s^2 - (3N + 1)k_B T_0 \ln s \quad (2.33)$$

where  $Q$  is the “mass” related to thermal bath.

Thus, the modified equations of motion are

$$\ddot{\mathbf{r}}_i = -\frac{1}{m_i s^2} \frac{\partial U}{\partial \mathbf{r}_i} - \frac{2\dot{s}}{s} \dot{\mathbf{r}}_i \quad (2.34)$$

$$Q\ddot{s} = \frac{1}{s} \left[ \sum_i m_i s \dot{\mathbf{r}}_i^2 - (3N + 1)k_B T_0 \right] \quad (2.35)$$

Here, the accumulative energy of the entire system, i.e., the energy of the system itself plus the thermal energy of the bath, is conserved. Yet, the energy of the system itself is not conserved.

In case of the Isothermal-isobaric  $NPT$  ensemble (barostat), the pressure is set to a specific value, the volume is modulated dynamically, and the shape of the simulation box is calibrated to desired size by using applicable algorithms, such as Hoover [139], Berendsen [140], amongst the many.

## 2.4 Ewald summation

The MD method is highly efficient in probing variety of particles interactions. Because it is study-specific, corrections methods need to be applied to one kind of interaction or the other, based on objectives of the study. The long-range particles interactions, i.e., electrostatic type, require particular approach for dealing with the slow convergence of the system pertinent to the long-range interactions and truncation of their potentials [140]. In fact, if these interactions are left unattended and not accounted for, the results of MD simulations will be tainted by inaccuracies [145].

The most prominent method for computing long-range interactions between ions and their periodic images in the system is *Ewald summation*. It is an effective method to handle long-range interactions for simulations carried in PBC which rely on suppression of boundary effects [145].

In principle, Ewald summation is a version of the *Poisson summation* formula in which the summation of real space interaction energies is replaced with an equivalent summation of *Fourier space*. Here, the long-range interaction is divided in two parts: (1) *short-range component* (calculated in real space); (2) *long-range contribution*, in which singularity is absent and it is calculated via Fourier transform. The advantage of this method is that it allows the comparison of the rapid convergence of the energy with direct summation. In order to accurately calculate the sum of all Coulombic interactions within the system, the charge neutrality of the molecular system must be taken into consideration [146].

In Ewald summation, the electrostatic energy term of the interaction potential for the system with periodic boundary condition is expressed as

$$U_E = \frac{1}{2} \sum_{i=1}^N q_i \phi_E(\mathbf{r}_i) \quad (2.36)$$

where  $\phi_E$  is

$$\phi_E = \sum_{j=1}^N \sum_{\mathbf{R}} \frac{q_j}{|\mathbf{r}_{ij} + \mathbf{R}|} \quad (2.37)$$

and  $\mathbf{R} = \mathbf{n}L$ ,  $n = (n_x, n_y, n_z)$ , with  $n_x, n_y, n_z \in \mathbb{Z}$ .

The summation is performed with the condition that  $i \neq j$  if  $\mathbf{R} = 0$ .

Ewald summation rewrites the interaction potential as the sum of two terms (addition and subtraction of screening charges would apply), i.e.

$$U_E = U_{\text{SR}} + U_{\text{LR}} \quad (2.38)$$

In Eq.2.38,  $U_{\text{SR}}$  is the short-range part which is evaluated in the real space and includes the original point charges, screened by diffuse clouds of opposite charges; and  $U_{\text{LR}}$  is the long-range part evaluated in the Fourier space and is set to compensate for added screening charges from which it is generated via summing screening densities with opposite charges. Screening charges are handled by *Gaussian distribution*, i.e.

$$\rho_s(r) = -q_i \left(\frac{\alpha}{\pi}\right)^{3/2} e^{-\alpha r^2} \quad (2.39)$$

First step is the calculation of the long-range part ( $U_{LR}$ ) in the summation. As screening charges have already been taken into consideration (Eq.2.39), the compensating charge distribution is expressed as

$$\rho_c(\mathbf{r}) = \sum_{j=1}^N \sum_{\mathbf{R}} q_j \left(\frac{\alpha}{\pi}\right)^{3/2} \exp\left[-\alpha|\mathbf{r} - (\mathbf{r}_j + \mathbf{R})|^2\right] \quad (2.40)$$

where,  $\rho_c(\mathbf{r})$  is the charge density field at position  $\mathbf{r}$ ,  $q_j$  charge in the central unit cell, and  $\alpha$  is Gauss criterion term for integral convergence, i.e., series converges if  $\alpha > 1$  and diverges if  $\alpha \leq 1$  [147].

Its Fourier transform is:

$$\tilde{\rho}_c(\mathbf{k}) = \int_V d\mathbf{r} e^{-i\mathbf{k}\cdot\mathbf{r}} \rho_c(\mathbf{r}) = \sum_{j=1}^N q_j e^{-i\mathbf{k}\cdot\mathbf{r}_j} e^{-k^2/4\alpha} \quad (2.41)$$

Poisson's equation in the Fourier space is

$$k^2 \tilde{\phi}(\mathbf{k}) = 4\pi \tilde{\rho}(\mathbf{k}) \quad (2.42)$$

and is used to calculate the charge distribution in Eq.2.40, along with anti-transforming obtained field and plugging it into the long-range ( $U_{LR}$ ) part of the summation, i.e.

$$U_{LR} = \frac{1}{2} \sum_{i=1}^N q_i \phi_c(\mathbf{r}_i) = \frac{1}{2V} \sum_{\mathbf{k} \neq 0} \frac{4\pi}{k^2} |\tilde{\rho}(\mathbf{k})|^2 e^{-k^2/4\alpha} \quad (2.43)$$

In the long-range interaction potential, the point charges and the compensating charges interact simultaneously at position  $\mathbf{r}_i$ , thus giving rise to an ersatz self-interactions terms which correspond to value of the potential at the center of the Gaussian charge distribution. Therefore, in order to obtain an accurate value for Coulombic energy, these self-interaction terms have to be subtracted from the final expression for entire interaction potential of the system.

The second step in Ewald summation is the calculation of the short-range interaction potential,  $U_{\text{SR}}$ . With Poisson's equation in the real space

$$-\nabla^2 \phi(\mathbf{r}) = 4\pi\rho(\mathbf{r}) \quad (2.44)$$

the screening potential is expressed as

$$\phi_s(r) = \frac{q_i \text{erf}(\alpha^{1/2}r)}{r} \quad (2.45)$$

where the error function  $\text{erf}$  is defined as

$$\text{erf}(x) = \frac{2}{\pi^{1/2}} \int_0^x e^{-t^2} dt \quad (2.46)$$

The self-interaction terms are written as follows

$$\phi_{\text{self}} = \phi_s(0) = 2 \left(\frac{\alpha}{\pi}\right)^{1/2} q_i \quad (2.47)$$

and the total self-interaction energy, which has to be subtracted from the total electrostatic energy, is expressed by

$$U_{\text{self}} = \left(\frac{\alpha}{\pi}\right)^{1/2} \sum_{i=1}^N q_i^2 \quad (2.48)$$

The short-range part of summation is derived as

$$U_{\text{SR}} = \frac{1}{2} \sum_{\mathbf{R}} \sum_{i \neq j}^N q_i q_j \left[ \frac{1}{|\mathbf{r}_{ij} + \mathbf{R}|} - \frac{\text{erf}[\alpha^{1/2} |\mathbf{r}_{ij} + \mathbf{R}|]}{|\mathbf{r}_{ij} + \mathbf{R}|} \right] = \frac{1}{2} \sum_{\mathbf{R}} \sum_{i \neq j}^N q_i q_j \frac{\text{erfc}[\alpha^{1/2} |\mathbf{r}_{ij} + \mathbf{R}|]}{|\mathbf{r}_{ij} + \mathbf{R}|} \quad (2.49)$$

where the *erf* function is

$$\text{erfc}(x) = \frac{2}{\pi^{1/2}} \int_x^{+\infty} e^{-t^2} dt \quad (2.50)$$

Finally, the complete summation for the electrostatic potential of the system is

$$U_E = U_{\text{SR}} + U_{\text{LR}} + U_{\text{self}} = \frac{1}{2} \sum_{\mathbf{R}} \sum_{i \neq j}^N q_i q_j \frac{\text{erfc}[\alpha^{1/2} |\mathbf{r}_{ij} + \mathbf{R}|]}{|\mathbf{r}_{ij} + \mathbf{R}|} + \frac{1}{2V} \sum_{\mathbf{k} \neq 0} \frac{4\pi}{k^2} |\tilde{\rho}(\mathbf{k})|^2 e^{-k^2/4\alpha} - \left(\frac{\alpha}{\pi}\right)^{1/2} \sum_{i=1}^N q_i^2 \quad (2.51)$$

To reiterate, in Ewald summation the short-range interactions are calculated in the real space, while long-range interactions are derived from Fourier space. The convergence of the integrals is highly dependent on

---

proper tuning of the Gauss parameter  $\alpha$  which must be large in the short-range (real space) and small in long-range (Fourier space). In order to reach required balance between these two potentials in summation, the values of  $\alpha$  parameter is usually set to the order of  $5/L$  and for the computation of the summation over  $\mathbf{k}$ , preferable number of wave vectors is of the order of ten [136, 148].

In summary, the implementation of the Ewald summation method is rather essential for successful run of the MD simulation. Its contribution in ability to handle long-range interactions for simulations carried in PBC which rely on suppression of boundary effects upon computing long-range interactions between ions and their periodic images in the system by summing two fundamental parts of particles interactions, i.e., short-range and long-range, is unprecedented.

## 2.5 Running MD simulations

The aim of the MD simulations is to compute macroscopic properties of a chemical system using essential assumption that the microscopic interaction potentials are known, i.e.:

- The atoms or molecules constituting the system under study are represented (modelled) by point masses or rigid bodies subject to classical mechanics.
- All interaction potentials between these masses and/or rigid bodies are known.
- The classical trajectories of the point masses and rigid bodies under the influence of their mutual forces and torques are representative of the motions of the atoms and molecules in the system.

- 
- Statistical averages taken over the ensemble of phase space points of the trajectories over a sufficient length of time reproduce the structural and dynamic properties of the system.

To examine the physics in the system of interest, four essential steps must be taken in the MD simulations. The first step is dedicated to the initial system setup where an initial space configuration of a particle is defined. This is done by placing particle at the vertices of standard lattices. Notably, crystallographic data provides point of reference for more complex solute-solvent systems which require significantly realistic molecular conformations. The next three steps are equilibration run, production run, data analysis and error estimation [149].

### 2.5.1 System setup

During the system setup, the following steps must be taken:

- plausible configuration should be created: positions of atoms and initial velocities (Boltzmann with random directions)
- valid force field must be adopted
- cut-off radius and the method to treat electrostatic interactions (if partial charges are present) must be designated
- integration algorithm and a correct time step must be chosen
- working ensemble must be selected
- size of the system should be properly defined.

---

### 2.5.2 Equilibration

At this stage, the system is allowed to run for a period of time from its initial configuration up to its full relaxation state. During this stage, proper equilibration of the system and monitoring of the total and potential energies throughout time of the run must be observed. Upon minimization of the system's energy, all counters should be set to zero and the system must be allowed to continue evolving further.

Subsequently, the trajectories are produced during an equilibrium run, all the way up to until an equilibrium is reached, upon which the algorithms for rescaling of the velocities are applied.

In order to allow the system to reach the equilibrium density corresponding to the desired pressure and temperature, the use of the *NPT* simulation is required.

The choice of the thermostat and barostat is not critical since this part of the simulation is not applicable for computing of any property. However, upon reaching an equilibrated state, attention must be paid to pressure, density and different energy components which would fluctuate around some average value without showing any drift.

Furthermore, independence of the status of some standard properties, such as Radial Distribution Function (RDF), Mean Square Displacement (MSD), from the segment of the trajectory used to compute them must be assured. This will hold only for lengthy segment where the ergodic hypothesis will apply.

---

### 2.5.3 Production

When the system under study has reached an equilibrium state at the selected temperature and pressure, production run can begin. To avoid any undesired influence from the thermostat or the barostat within the system, the choice of working with the *NVE* ensemble is optimal. In general, working with a fixed cell and avoiding an incommodity of dealing with volume fluctuations during the trajectory analysis is the best approach. Yet, there are some exceptional cases such as simulating a phase transition [150, 151].

The run time of the simulation must be longer than the relaxation time of the property of interest. And, the simulation time should also be long enough to substantiate ergodic hypothesis, i.e., the average simulation time of a given property must coincide with the average simulation time of the ensemble [152].

Consequently, production run produces equilibrated trajectories which are stored for further calculations of quantities of interest.

### 2.5.4 Data analysis and error estimation

The properties of interest in the study can finally be analysed from obtained by simulation trajectories. Here, any statistical mechanical property that can be expressed in terms of obtained variables, such as atomic positions, velocities, force as a function of time, etc., can be computed.

---

Analysis of an experimental results include an associated error for each computed value obtained from a simulation. In general, for a given property calculated as the average of the value of a given observable during the simulation, the error as a variance of the set of data can be estimated. However, unlike most experimental procedures, the set of data produced by the simulations does not represent independent measurements. Hence, in order to calculate the error corresponding to averaging over a series of correlated data, several tailored to the MD simulations statistical techniques have been implemented, e.g., *block method*, integration of the *autocovariance* [152, 153, 154, 155].

## 2.6 Force fields

A *force field* (FF) is a mathematical expression describing the dependence of the energy of a system on the coordinates of its particles.

In the force field methods, a.k.a. *molecular mechanics methods*, the electronic degrees of freedom of the molecules are not considered, and only motions of the nuclei are calculated. The foundation of all molecular mechanics is the Born-Oppenheimer approximation which allows separation of nuclear and electronic motions on different scales. Subsequently, the energy of the system is written as a function of nuclear coordinates alone.

In addition, two other assumptions are included in treating all common force fields: *additivity* and *transferability*. The former contains the sum of different potentials which comprise the total potential energy of the system, e.g., bond deformations, electrostatics, dispersion forces, etc. The latter represents the notion that potential energy functions pertaining to a

small set of molecules can be applied to a much wider range of molecules having similar chemical groups constituents. The validity of these assumptions is responsible for correctness of estimating the molecular mechanics force fields [136].

Most classical force fields are comprised of five simple physical entities. These are: (1) potential energy of bond deformation; (2) potential energy of angle geometry (bonds stretching/compression, bending of angles); (3) rotation about specific dihedral angles (torsions); (4) non-bonded term which describes the electrostatic interactions; (5) terms describing the dispersion interactions and repulsion which occur when atoms overlap (van der Waals forces).

A typical expression for FF is

$$\begin{aligned}
 u = & \sum_{\text{bonds}} \frac{1}{2} k_b (r - r_0)^2 + \sum_{\text{angles}} \frac{1}{2} k_a (\theta - \theta_0)^2 + \sum_{\text{torsions}} \frac{V_n}{2} [1 + \cos(n\phi - \delta)] \\
 & + \sum_{\text{improper}} V_{\text{imp}} + \sum_{\text{LJ}} 4 \epsilon_{ij} \left( \frac{\sigma_{ij}^{12}}{r_{ij}^{12}} - \frac{\sigma_{ij}^6}{r_{ij}^6} \right) + \sum_{\text{elec}} \frac{q_i q_j}{r_{ij}}
 \end{aligned} \tag{2.52}$$

where the first four terms refer to intramolecular or local contributions to the total energy (bond stretching, angle bending, dihedral and improper torsions), and the last two terms describe the repulsive Van der Waals interactions (in this case by means of 12-6 Lennard-Jones potential) and the Coulombic interactions [149].

More specifically, the first, bond stretching term represents harmonic potential that controls the length of covalent bonds;  $k_b$  represents the force constant of the bond (generally very high indicating large uptake of energy required significantly stretch or compress chemical bond);  $r_0$  is the

reference bond length, i.e., the value of the bond length when all other terms in the potential energy function are zero.

- Four intramolecular terms

Angle bending in Eq.2.52 is usually represented by harmonic potential

$$u_{\text{bending}} = \frac{1}{2} k_a (\cos \theta - \cos \theta_0)^2 \quad (2.53)$$

For the potential energy change upon deformation of angles, values of force constraints are typically lower in magnitude compare to those for bond stretching. This implies that it takes less energy for a bond angle to deviate from its reference value.

Torsional motions play crucial role in determining the local structure of macromolecule. Their potential (part of the Eq.2.52) is calculated as follows [150]

$$u_{\text{tors}} = \sum_{\text{torsion}} k_0 + \frac{k_1}{2} (1 + \cos \phi) + \frac{k_2}{2} (1 - \cos 2\phi) + \frac{k_3}{2} (1 + \cos 3\phi) \quad (2.54)$$

The last intramolecular term in Eq.2.52 is improper potential which describes the positive contribution to the energy for *out-of-plane motions*. It is represented by

$$u_{\text{imp}} = \sum_{\text{impropers}} \frac{k_{\text{imp}}}{2} [1 + \cos(2\omega - \pi)] \quad (2.55)$$

- Two intermolecular terms

Van der Waals interactions between atoms emerge from the balance between repulsive and attractive forces. The overlap of the electron clouds of both atoms yields repulsion, while induced dipoles' interaction produces an attractive component which varies as  $r^{-6}$ . Lennard-Jones (LJ) 12-6 potential is one of the most effective representation of these interactions [151, 152, 153]. The LJ potential is widely used in the study of liquids, and is expressed as

$$u_{\text{LJ}}(r) = 4\epsilon \left[ \left( \frac{\sigma}{r} \right)^{12} - \left( \frac{\sigma}{r} \right)^6 \right] \quad (2.56)$$

where  $r$  is the distance between two interacting particles,  $\epsilon$  is the depth of the potential well (dispersion energy), and  $\sigma$  is the distance at which the particle-particle potential energy  $\mathcal{U}$  is zero (size of the particle). The minimum of LJ potential is at a distance  $r = r_m = 2^{1/6}\sigma$ , where the potential energy has a value of  $\mathcal{U} = -\epsilon$ .

The final term in Eq.2.52 describes the electrostatic intermolecular interactions. Due to the fact that different atoms have different electronegativity, electric charge in molecules is not evenly distributed. This presents a challenge for electrostatic potential calculations. One approach is to derive electrostatic properties of molecules via first principles, i.e., calculate the electrostatic potential directly from the electron density, defined by the wave function. In this case, the electrostatic potential of a molecule can be obtained by summation of electrostatic potentials induced by charges placed on atomic nuclei, i.e., partial atomic charges. In this case, electrostatic potential can be calculated as

$$U(r) = \sum_{\substack{\text{non-bonded} \\ \text{pairs } i,j}} \frac{q_i q_j}{4\pi\epsilon_0 r_{ij}} \quad (2.57)$$

where  $r_{ij}$  is the distance between nuclei  $i$  and  $j$ .

Calculation of non-bonded interactions is the most consuming part of MD simulation.

---

## Chapter 3

# Molecular Dynamics of Water and Ionic Aqueous Solutions



In nature, the liquid state of matter is an intermediate between a gas and a solid state. To study behaviour of water and its ionic solutions, all the employed empirical tools are specifically applied to liquid state, allowing to acquire deep insight of matter on a molecular level. In particular, the MD simulations are very effective in the theoretical exploration of the dynamic and structural properties of liquids when it comes to exploration of the molecular arrangements inside the system, they can perform microscopical exploration deeper than any of its experimental counterparts. Ability to calculate trajectories and obtain time-variant depiction of positions and velocities of the particles in the various systems is what makes this technique so powerful.

This chapter will present the General concepts of the MD of water (3.1); Water models (3.2); MD simulations of water (3.3); MD simulations of ionic solutions (3.4); Molecular Dynamics identifiers - dynamic and structural observables (3.5).

### 3.1 General concepts

MD simulation for molecular liquids is optimal when applied to the systems in which the molecules consist of independent atoms bound together by continuous intramolecular forces. In the calculation for small molecules (such as water) the molecule is often treated as a system of rigid particles.

### 3.2 Water models

Many different water models have been developed up to date and they all rely on the MD approximations. These water models are classified by the number of interaction points (site); distinction of whether the model is rigid or flexible, i.e., atoms plus dummy sites; validation of whether the model includes polarization effects or not. The geometry of the water molecule is essential in all water models and is shown in Figure 1.

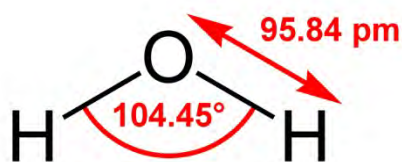


Figure 1: Geometry of water molecule by Water model and other parameters: atomic charges and LJ.

Planar and almost tetrahedral geometries of water models are represented in Figure 2.

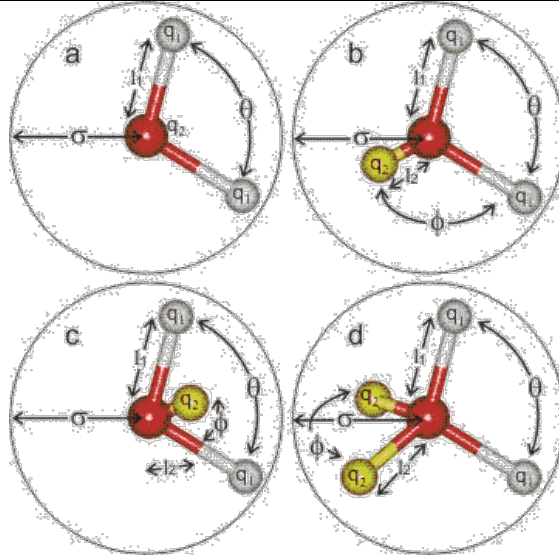


Figure 2: Representation of model types: planar - (a), (b), (c); ~ tetrahedral: (d).

Three main types of classic water models have been developed: (1) simple interaction-site models in which rigid geometry is maintained for each water molecule and the interaction between molecules is described using pairwise Coulombic and LJ expressions; (2) flexible models which permit internal changes in conformation of the molecule; (3) models which explicitly include the effects of polarization and many-body effects [156].

### 3.2.1 Simple water models

The simplest water models treat water molecule as a rigid entity and depend only on non-bonded interactions. The dispersion and repulsion forces are described by LJ potential and the electrostatic interaction represented by Coulomb's law, i.e.

$$E_{ab} = \sum_i^{\text{on a}} \sum_j^{\text{on b}} \frac{k_c q_i q_j}{r_{ij}} + \frac{A}{r_{00}^{12}} - \frac{B}{r_{00}^6} \quad (3.1)$$

where  $k_c = 332.1 \text{ \AA} \cdot \text{kcal/mol}$  is the electrostatic constant used in molecular modelling;  $q_i$  are the partial charges relative to the charges of electron;  $r_{ij}$  is the distance between two atoms or charged sites;  $A$  and  $B$  are the LJ parameters. The charged sites may be on the atoms or on the dummy sites, e.g., lone pairs. In most water models, the LJ term exclusively represents the interaction between the oxygen atoms.

There are 5 main  $n$ -sites water models with  $n = 2, 3, 4, 5$  and  $6$ . Figure 3 shows the general shape of the 3- to 6-site water models where the exact geometric parameters, i.e., the O-H distance and the H-O-H angle, vary depending on the model. There are also other models such as MW model which represents water as a monoatomic liquid states [157]. Coarse-grained models in which each site of  $n$ -sited water molecule is represented by several water molecules.

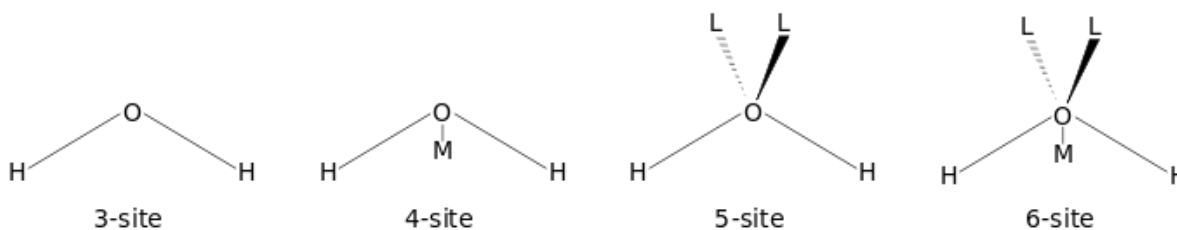


Figure 3: General shape of 3- to 6-site water models. Note: In a 4-site model,  $M$  represents a dummy atom; in a 5-site model,  $L$  represents a dummy atom, and in the 6-site model, both  $M$  and  $L$  represent dummy atoms.

#### ◆ 3-site model of water

These model have three interaction sites, each of which corresponds to the 3-atoms of water molecule. Each atom is assigned a point charge, while

---

oxygen atom gets the LJ parameters. The 3-site models are frequently employed by MD simulations due to its simplicity and computation efficiency. In particular, the SPC model is an exception because it assumes an ideal tetrahedral shape - H-O-H angle of  $109.47^\circ$ , instead of the observed angle of  $104.5^\circ$ .

Popular 3-site models have been: TIPS [158], SPC [159], TIP3P [160], SPC/E [161]. Of these, SPC/E model is the one that better reproduces bulk water features.

- ◆ 4-site model of water

In these models the negative charge is placed on a dummy atom ( $M$ ) located near the oxygen along the bisector of the H-O-H angle. This enhances the electrostatic distribution around the water molecule.

The first 4-site model - BF [162] did not reproduce bulk properties of water (density, heat of vaporization) and, therefore, was succeeded by more proficient TIP4P models.

From the original TIP4P model [158], the TIP4P models are specifically parameterized, such as the TIP4P-Ew model [163]; the TIP4P/Ice model [164] is employed for simulation of solid water ice; the TIP4P/2005 model [165] which mostly produces the entire phase diagram of water more similar to the experiments and which is nowadays is the most used potential for water.

- ◆ 5-site model of water

---

In these models, negatively charged dummy atoms,  $L$ , represent the lone pairs of the oxygen atom with a tetrahedral-type geometry. Initially developed TIP5P models were costly in computation. However, the latest TIP5P models [166] are highly sufficient in probing the geometry for the water dimer, tetrahedrality of water structure which produces the experimental Radial Distribution Function (RDF) from neutron diffraction, and the temperature of maximum density of water. Moreover, the TIP5P-E model is an extended parametrization of TIP5P [167].

### 3.2.2 Challenges in implementing water models

The unique properties of liquid water stem from water molecules' ability to create a hydrogen-bonded structure based on electropositive hydrogen atoms and electronegative oxygen atoms attraction [168].

Sometimes it may be challenging to study water molecule if the chosen model is not suitable. Therefore, the most efficient model for studying liquid water is the one that delivers accurate yet simplified description of the charge distribution of the water molecule which would account for the hydrogen bonding in a liquid phase [169].

### 3.3 MD simulations of water

The initial setup of MD simulation of water requires generation of initial space configuration of its constituents. This is commonly achieved by placing the constituents at the vertices of the standard lattices.

---

One of the most popular simulation packages today is GROMACS [167]. It is a versatile tool which includes the topology of many common solvents as well as allows to add the solvent molecules around the solute.

### 3.3.1 Prerequisites

For the simulation of a continuous (bulk) water a few assumptions must be implemented, such as:

- The liquid water is represented by a finite number point masses/rigid bodies located in a regular cell (cube).
- The cell and all the particles replicate themselves infinitely in all directions. This construction avoids surface effects which would otherwise dominate the behaviour of such small sample (*vide infra*).
- The walls of the cell are transparent, and particles can move freely between the cell and its periodic replica, thus keeping the density in the cell constant.
- Particles in the replica cells are often called *mirror particles*, and as they are replica of particles in the cell, their motions are the same and do not have to be computed. This construction is called *Periodic Boundary Condition* (PBC) and is discussed in Section 3.3.2.
- Once the number of particles in the simulation is known, the volume of the cell is obtained by choosing desired density of the system.
- Overall, the outcome of the simulated results is greatly dependent on the number of particles used and thus on the cell size.
- The *minimum distance convention* is applied. This is a prescription for the interaction potentials and interparticle forces exerted by all particles in the system that are to be computed. Combined with PBC,

---

this procedure avoids surface effects and allows the simulation of an infinitely extended system with a finite number of particles.

- The interaction potentials between water molecules are assumed to be pair-wise additive.
- If electric charges or dipole occur in the system under study, like the point charges of the water (*vide infra*) and the ions, the long-range Coulomb forces must be dealt with (Ewald summation).

### 3.3.2 Periodic Boundary Condition (PBC) of water

Water molecules behave differently near surfaces (either a vacuum or a wall), creating special structures. When water is simulated in a box with walls, the water molecules near the walls create pressure on the water molecules in the simulation box, i.e., *Laplace pressure* - the pressure difference between the inside and the outside of a curve surface that forms the boundary between gas and liquid regions [171]. The challenge of this approach lays in dealing with Coulomb (electrostatic) interactions between water molecules. In order to accurately determine the forces that water molecules experience in real water, the interactions between molecules that occur at the distances greater than the size of the simulation box must be accounted for. This phenomenon is characteristic for water molecule as it is polar molecule with non-zero electric dipoles. This problem is usually solved by employing Ewald summation method which creates many replicas of the box arranged in a periodic fashion.

However, since water is not a periodic system, some concerns still exist which prompted to investigate other than cubes boxes for water. For example, a polyhedral with regular polygon sides which fills space in regular way is one of very suitable candidate for water.

The general representation of PBC for water molecules is shown in Figure 4.

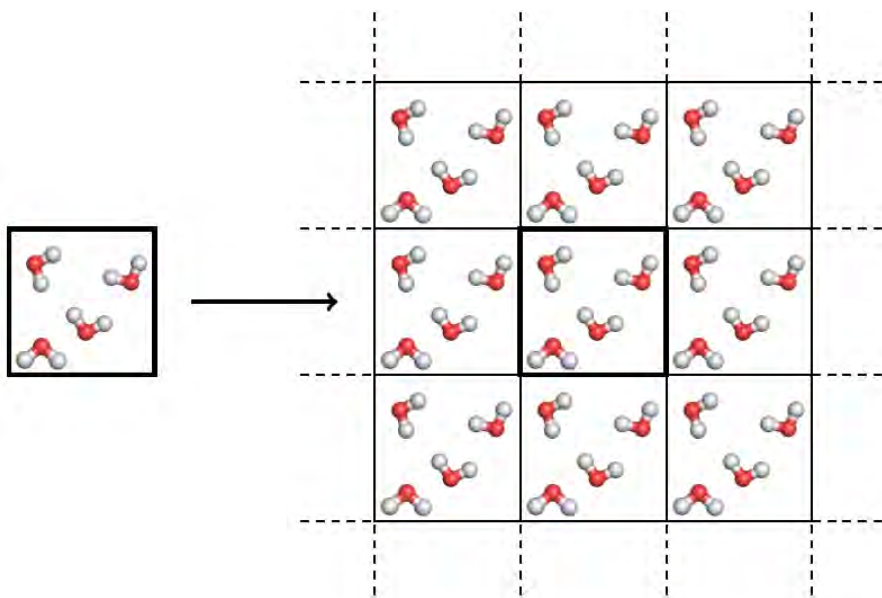


Figure 4: PBC for water (image adopted from TeXmple.net).

### 3.3.3 Input to MD simulation program

To begin running the MD simulation for water the following must be defined:

- number of particles in the cell
- particles' masses and moments of inertia
- desired density
- interaction potentials (most important)

Considering stated above prerequisites, the results of the MD simulations depend only on the microscopic interactions between the atoms and

---

molecules in the system. The MD simulations will deliver the classical trajectories of the particles under the influence of their mutual forces calculated by numerical integration of Newton's equation or any other set of equivalent equations.

Overall, the aim of the MD simulations of water is to calculate as many macroscopic physical properties as possible from the simulated trajectories.

### 3.3.4 Potential models of water under consideration

In the recent studies of properties and behaviour of water using MD method, the two most popular models are SPC/E potential model for water and TIP4P/2005 potential model for water.

#### 3.3.4.1 SPC/E potential model for water

Several classic rigid model potential have been successfully used to study water. The SPC/E potential model for water is one of such examples. The SPC (*Simple Point Charge*) 3-site water model [172], i.e., flexible SPC water model was initially the most accurate 3-site water model without taking into an account the polarization (Figure 5).

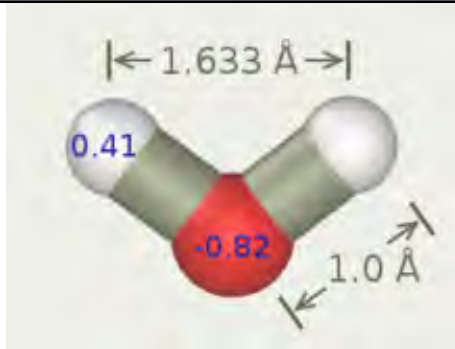


Figure 5: Molecular structure of water in flexible SPC water model [161].

Nevertheless, the SPC water model served as a precursor for more improved SPC/E (*Simple Point Charge Extended*) model of water [160] which included a polarization correction of the energy and subsequent reparameterization of the SPC model. Such modifications allow for more accurate reproduction of polar liquids attributes. In addition, the SPC/E model is superior to the SPC model because it results in better density and diffusion constant.

An average polarization correction to the potential function in the SPC/E model is added as

$$E_{pol} = \frac{1}{2} \sum_i \frac{(\mu - \mu^0)^2}{\alpha_i} \quad (3.2)$$

where  $\mu$  is the dipole of the effectively polarized water molecule (2.35 D from model);  $\mu^0$  is the dipole moment of an isolated water molecule (1.85 D from experiment);  $\alpha_i = 1.608 \times 10^{-40}$  Fm is an isotropic polarizability constant. Given that the charges in this model are constant, the resulted correction is obtained by addition of 1.25 kcal/mol (5.22 kJ/mol) to the total energy.

Special attention is given to utilizing the SPC/E model to the tetrahedral water molecule as shown in Figure 6. This geometry contains three interaction coplanar sites with the O-H distance of 1 Å and the H-O-H angle of 109.5°. Point charges are lying on the oxygen and hydrogen position with  $q_O = -0.8476e$  and  $q_H = +0.4238e$ , respectively. Furthermore, the only LJ interaction site of the molecule with  $\epsilon_{OO} = 0.650$  kJ/mol and  $\sigma_{OO} = 3.166$  Å lie on the oxygen position only.

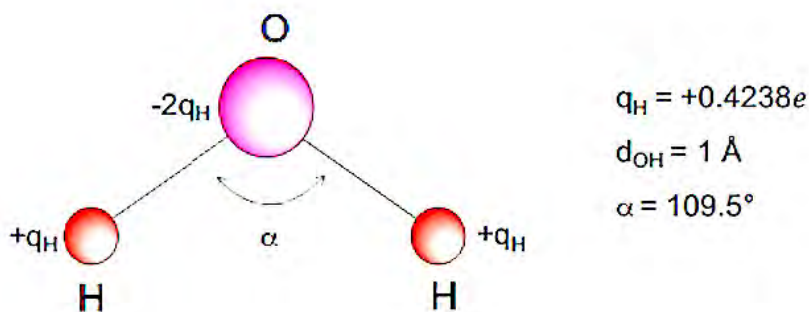


Figure 6: Geometry of the SPC/E model of water.

The full interaction potential for the  $i$ -th water molecule is

$$u(r_{ij}) = 4\epsilon_{ij} \left[ \left( \frac{\sigma_{ij}}{r_i - r_j} \right)^{12} - \left( \frac{\sigma_{ij}}{r_i - r_j} \right)^6 \right] + \frac{e^2}{4\pi\epsilon_0} \frac{q_i q_j}{|r_i - r_j|} \quad (3.3)$$

#### 3.3.4.2 TIP4P/2005 potential model for water

The TIP4P models belong to the 4-site series of models for water. They contain several potentials of water within the same water molecule geometry and different parameters. The first TIP4P model [173] laid the ground for the more advanced and study-specific models, such as the re-

parametrization TIP4P/Ice [164] model which provides better results for reproducing phase diagram of water competing with the various solid phases of crystallin and amorphous water; the re-parametrization models: TIP4P/Ew [158] and TIP4P/2005 [165] which deliver big improvement in such quantities as Temperature Maximum Density (TMD), diffusion coefficient, and description of an entire phase diagram and dynamics of water. Moreover, the TIP4P/2005 water model has been shown to accurately reproduce structural and dynamical properties of hydrophobic hydration shells [174].

Currently, the TIP4P/2005 is the best suited model to study rigid potential interactions of water [158].

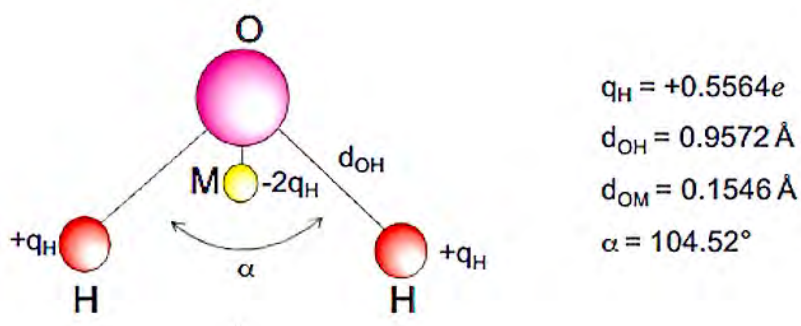


Figure 7: Geometry of the TIP4P/2005 model of water.

The water molecule is represented by four interaction sites. Both hydrogen atoms contain charge site  $q_H$ . The oxygen atom is of electrostatic nature, depicted by the LJ interaction site in the water molecule and is spatially separated from the charge point. Along the bisector of the H-O-H angle, the negative site  $M$  with  $q_M = -2q_H$  is placed, and coplanar with the other three interaction sites.

In the TIP4P/2005 potential model of water, the O-H distance and the H-O-H angle are fixed to the experimental values of 0.9572 Å and 104.52°, respectively. The O-M distance is 0.1546 Å, and the LJ interaction parameters are adopted as  $\epsilon_{OO} = 0.7749$  kJ/mol and  $\sigma_{OO} = 3.1589$  Å. The charge  $q_H = +0.5564e$ . Figure 3-8 shows all of the constituents with their parameters for TIP4P/2005 potential model for water molecule.

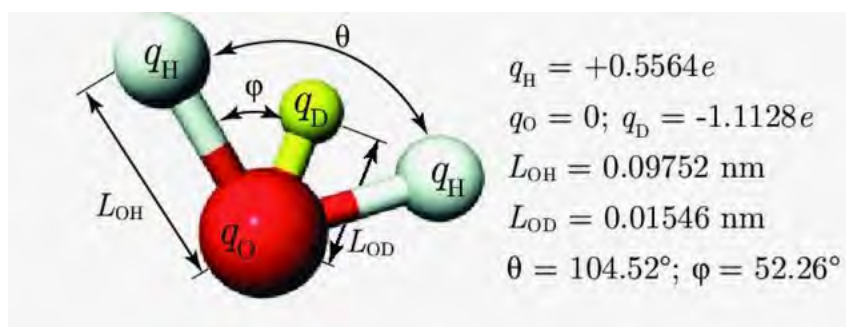


Figure 8: TIP4P/2005 molecular model potential with its parameters for water [151].

### 3.4 MD simulations for ionic aqueous solutions

Understanding the behaviour of polar polarizable solvents and the features of the solution of salts in these systems is of a great interest in various fields of physics, chemistry and engineering. Within ionic liquid systems, the ionic charge induces a dipole on the neighbouring ion. Thus, induction interactions must be taken into consideration. However, as this term is not pairwise additive, it presents a challenge for incorporating it into MD simulation.

Overall, polarizability of solvent molecules is an essential part in studying ionic solutions [175]. If polar solvent molecules have a finite polarizability, calculations in the liquid phase must include an effective

---

dipole moment which is the sum of the permanent dipole moment and a contribution enhanced by the local electrostatic field of the surrounding molecules. As a crude attempt to account for this ion polarizability, the *shell model* was proposed in which each ion is represented as a core surrounded by a shell [176]. In this model, the ionic charge is partially set to be located at the shell and its remaining part was to rest at the core. Such division of charges is specifically contrived to assure that the negative charge is always placed on the shell because it contains the electronic cloud. Then, the sum of the Coulombic shell-shell, core-core, and shell-core contributions depicts the nature of ionic interactions. In addition, the shell and core of a given ion are coupled by a harmonic string potential. During simulation, the mass of the shell is set to zero, with their positions adjusted iteratively to zero as well to obtain the net force acting on each shell. In addition, ionic solutions are challenging to simulate due to their long-range Coulombic interactions and elevated strength of the intermolecular forces which affect their structure [175].

Implicit solvent model, a.k.a., *continuum model*, is a specific water model for the MD simulations of ionic solutions. It is generally combined with CHARMM force field [177] and is widely used in probing behaviour of ions, peptides and small proteins in aqueous solutions [178].

In setting up MD simulation of solute-solvent systems, such as water-ions, realistic conformation of molecules is gathered from crystallographic data.

MD simulations of aqueous solutions of salts, such as LiCl, are of particular interest because their small-size cation is attributed to excellent solvation properties, i.e., LiCl has considerably high solubility [179]. This is indeed advantageous for probing thermodynamic and structural properties of water.

### 3.4.1 JC-TIP4P/2005 potential model for LiCl-water solutions

The JC-TIP4P/2005 potential model describes particles interactions in LiCl-water solutions [180].

In this force field a LJ site and a point charge site are placed on each ion position. The LJ parameters on ions are defined by Joung and Cheatham [179], while the electrostatic charges are  $+e$  for  $\text{Li}^+$  ion and  $-e$  for  $\text{Cl}^-$  ion. Overall, the LJ interaction parameters and charge sites of water molecule are adopted from the TIP4P/2005 potential model for water.

The accumulative potential of ionic solution is a sum of two potentials: LJ and Coulombic electrostatic interactions, i.e.

$$u(r_{ij}) = 4\epsilon_{ij} \left[ \left( \frac{\sigma_{ij}}{r_{ij}} \right)^{12} - \left( \frac{\sigma_{ij}}{r_{ij}} \right)^6 \right] + \frac{q_i q_j}{4\pi\epsilon_0 r_{ij}} \quad (3.4)$$

where  $r_{ij}$  is the distance between two interacting particles, and  $q_i$  is the charge of an ion or the charge of a water site.

The crossed interactions between ions within JC-TIP4P/2005 potential model are obtained by modifying the commonly used Lorentz-Berthelot (LB) combining rules

$$\epsilon_{ij} = \chi \cdot \sqrt{\epsilon_{ii} \cdot \epsilon_{jj}} \quad \sigma_{ij} = \eta \cdot \frac{\sigma_{ii} + \sigma_{ij}}{2} \quad (3.5)$$

where  $\chi = 1.88$  and  $\eta = 0.934$  [28] vs.  $\chi = 1$  and  $\eta = 1$  values of LB which corrects the ion pairing structure;  $\epsilon$  is the potential depth of a particle;  $\sigma$  is the diameter of a particle.

### 3.5 Molecular Dynamics identifiers

The trajectories of the MD simulated system allow for calculations of dynamic and structural observables. Although, the methodology of calculations differs, the outcome is very proficient in both cases as well as important within the concepts of the theory of liquids [182].

#### 3.5.1 Dynamic observables

For a dynamical quantity  $A$  which represents time-dependent properties of the system, the PBC must be removed which will expend the trajectories, then, by averaging the value of  $A$  over the range of initial time, the instantaneous mean value of  $A$  at time step  $t$  can be derived by

$$\langle A(t) \rangle = \frac{1}{NM} \sum_{t_1} \sum_{t_2-t_1=t} A(t_1 - t_2) \quad (3.6)$$

Overall, the dynamic state of liquid is characterized by correlation functions [183].

##### 3.5.1.1 Self-Intermediate Scattering Function, SISF

This density-density correlation function is of great importance in the study of liquids as it probes the single-particle translational dynamics of the system and characterizes its structural relaxation phenomena. It can be directly compared to experimental data from inelastic scattering of neutron and/or X-ray.

Its main part is the van Hove function [183] which represents the probability density of finding a particle  $i$  in the vicinity of  $\mathbf{r}$  at the time  $t$  which originated at  $t = 0$ .

$$G_s(\mathbf{r}, t) = \frac{1}{N} \left\langle \sum_i^N \delta(\mathbf{r} - \mathbf{r}_i(0) - \mathbf{r}_i(t)) \right\rangle \quad (3.7)$$

The SISF is defined as the spatial Fourier transform of van Hove function, i.e.

$$F_s(\mathbf{q}, t) \equiv \int G_s(\mathbf{r}, t) e^{-i\mathbf{q}\cdot\mathbf{r}} d\mathbf{r} \quad (3.8)$$

By rewriting the SISF function in a specific form, it can be directly calculated from the atomic trajectories of the MD simulations. In fact, this function is the autocorrelation function of the Fourier components of the local density in the  $\mathbf{q}$  space

$$F_s(\mathbf{q}, t) = \frac{1}{N} \langle \rho_{\mathbf{q}}(t) \rho_{-\mathbf{q}}(0) \rangle = \left\langle \frac{1}{N} \sum_{i=1}^N e^{i\mathbf{q}\cdot(\mathbf{r}_i(t) - \mathbf{r}_i(0))} \right\rangle \quad (3.9)$$

where  $N$  is the number of particles,  $\mathbf{r}_i(t)$  is the position of the  $i$ -th particle at time  $t$ .

### 3.5.1.2 Mean Square Displacement, MSD

The Mean Square Displacement (MSD) is related to the velocity autocorrelation function [183] and is defined as

$$\langle \Delta r^2(t) \rangle \equiv \left\langle \frac{1}{N} \sum_{i=1}^N (r_i(t) - r_i(0))^2 \right\rangle \quad (3.10)$$

where  $N$  is the number of particles,  $\mathbf{r}_i(t)$  is the position of the  $i$ -th particle at time  $t$ .

To determine MSD experimentally, neutron scattering, and photon correlation spectroscopy are employed.

### 3.5.2 Structural observables

To characterize the local structure of liquid water and its tetrahedral arrangement, a broad spectrum of geometric order parameters is utilized.

For a structural quantity  $A$  with an instantaneous position and/or velocities of the system function  $N$ , the mean value of  $A$  at each configuration  $i$  is calculated first and then averaged over  $N$  stored configurations, i.e.

$$\langle A \rangle = \frac{1}{N} \sum_{i=0}^N A_i(\mathbf{r}^N, \mathbf{p}^N) \quad (3.11)$$

Some popular structural order parameters for analysis of MD simulations of water are Radial Distribution Function,  $g(r)$ ; Structural Order Parameter,  $P(\zeta)$ ; Orientational Tetrahedral Parameter,  $P(q)$ ; Translational Tetrahedral Parameter,  $S_k$ ; and Local Structure Index, LSI.

---

It has been shown that these structural order parameters are weakly correlated and probe various distortions, such as the angular vs. radial disorders [184].

### 3.5.2.1 Radial Distribution Function, RDF

A fundamental idea in the theory of liquids, in general, is that of a *Distribution Function* which gives the probability of finding a particle (molecule or ion) in a given position relative to another particle.

In simple pure liquids the Distribution Function has *radial symmetry*, i.e., it depends only on the distance between the particles, and not on their mutual orientation. It shows a marked peak at the distance corresponding to the nearest neighbour, i.e., to the first layer of molecules surrounding the central molecule. This is followed by one or two subsidiary peaks, and thereafter, the *Radial Distribution Function* (RDF) flattens out to an effectively constant value, which means that there are no preferred positions for molecules more than a few diameters distant from the central molecule under consideration [185].

RDF is denoted in equation by the term  $g(r)$  which defines the probability of finding a particle or a pair of particles (atoms) at distance  $r$  apart relative to the probability expected for completely uniform distribution at same density [183]. It strongly depends on the type of matter under study and is widely incorporated in the MD simulations as it is highly proficient in describing the structure of a liquid system.

The important highlights of the RDF are:

- it considers only pairs of atoms, i.e., it is a pair correlation function
- it delivers structural information of the system under study
- it is equipped to provide information about dynamical change of structure, yet it doesn't reveal the transport properties, i.e., how fast the atoms move
- it depicts the formation of the atoms in a system as they are radially packed around each other (on average)
- it is particularly effective in describing the structure of disordered molecular systems, such as liquids.

In a liquid, the average point density is referred to as the *bulk density*,  $\rho$ , which is always the same for a given liquid. The density of the liquid at a given distance  $r$  of one molecule to another is called the *local density*,  $\rho(r)$ , and is dependent on the structure of individual liquid [182].

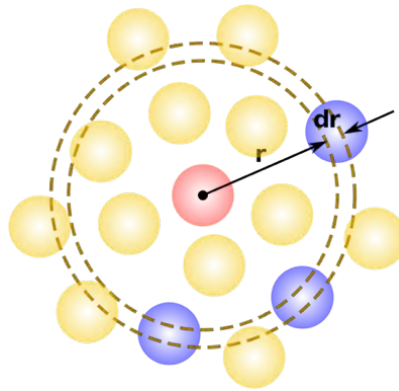


Figure 9: RDF schematics.

More explicitly, the RDF can be evaluated as

$$g(r) = \frac{dn_r}{4\pi r^2 dr * \rho} \quad (3.12)$$

where  $dn_r$  is a function that computes the number of particles within a shell of thickness  $dr$ .

The discrete expression for RDF is

$$g(r) = \frac{\langle N(r \pm \frac{\Delta r}{2}) \rangle}{\Omega(r \pm \frac{\Delta r}{2}) \rho} \quad (3.13)$$

where the numerator of the first fraction represents the number of atoms in the interval  $r \pm \frac{\Delta r}{2}$ , and the denominator represents volume of the shell,  $dr$ .

The number of particles that lie in a spherical shell of radius  $r$  and thickness  $dr$  is  $g(r)2\pi r^2 dr$ .

Since  $g(r)$  is the correlation function which relates the bulk density to the local density, the local density can be calculated as

$$\rho(r) = \rho^{bulk} g(r) \quad (3.14)$$

Figure 10 below depicts the RDF for water molecules where the distance  $r$  is the distance between the oxygen atoms of two water molecules.

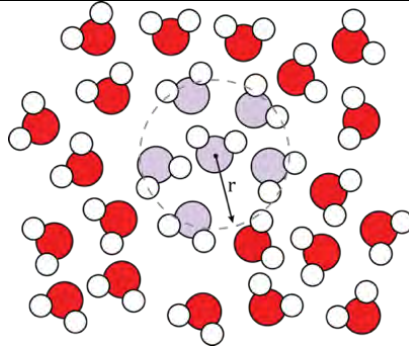


Figure 10: Graphical representation of RDF for water molecules.

Liquids cannot maintain constant structure and, hence, lose all of their long-range structure. As a rule, the first coordination sphere for a liquid will occur at  $\sigma$ . When the values of  $r$  become large enough, molecular dependence on each other dissipates and RDF returns to the bulk density:  $g(r) = 1$ . In general, upon obtaining graphical representation for RDF results in MD simulation of a liquid, the first peak will be the sharpest as it represents the first coordination sphere of a liquid.

In a graphical representation of  $g(r)$  the first peak represents a nearest neighbour shell, followed by a minimum, then a second peak corresponding to the second shell of neighbours, etc. For large distances the  $g(r)$  decays to 1 with damped oscillations.

Example of RDF-shell relations for two temperatures is presented in Figure 11. The first two peaks provide the locations of the first and the second shells that surround the atom in the origin.

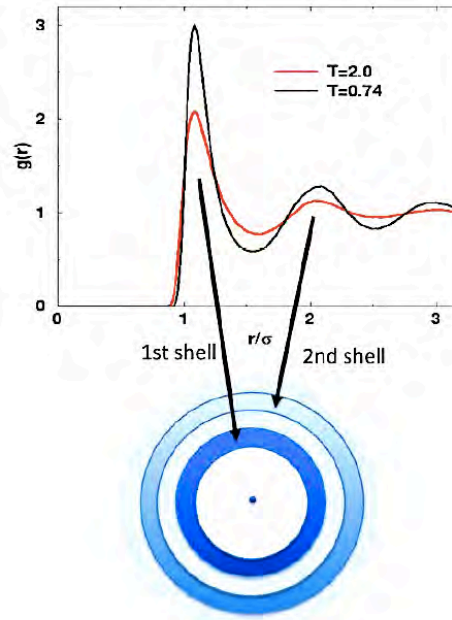


Figure 11: RDF of a LJ liquid for two temperatures.

The position and the height of the peaks are determined from the potential features and the thermodynamic conditions. The oscillations at large  $r$  could persist in a liquid to distances of the order of  $10 \text{ \AA}$ . The decrease of the temperature enhances the height of the peaks while their positions usually remain constant. A similar effect is obtained at constant temperature by increasing the density [182].

To determine how many liquid molecules are found in the range of each coordination sphere, the coordination number must be obtained, i.e.

$$n(r') = 4\pi\rho \int_0^{r'} g(r)r^2 dr \quad (3.15)$$

Notably, liquids which contain hydrogen bonding and electrostatic interactions, such as water, have a much lower coordination number

(Figure 12): in the first sphere water's coordination number is 4-5 versus 12 for liquids with optimal packing of hard spheres.

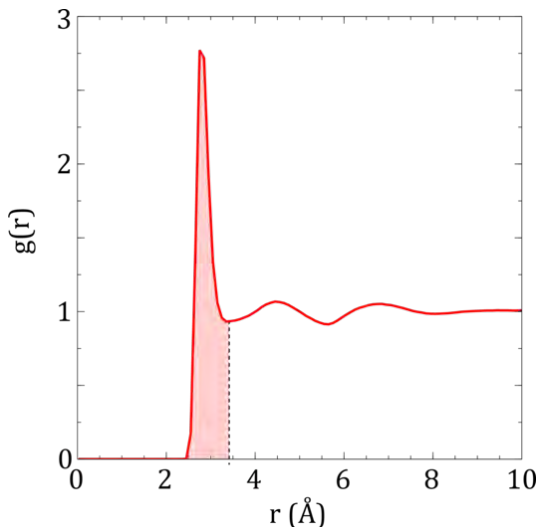


Figure 12: The first coordination sphere of water molecule indicated on the O-O RDF.

For determining RDF, the volume of the sampling shell is

$$\delta V = \frac{4}{3}\pi(r + \delta r)^3 - \frac{4}{3}\pi r^3 = 4\pi r^2 \delta r \quad (3.16)$$

For a perfectly uniform distribution, the number of particle pairs at a particular  $r$  will depend on the concentration and volume space in the sample

$$d_{\text{uniform}}(r) = \frac{N(N-1)}{V} 4\pi r^2 \delta r \quad (3.17)$$

where  $\frac{N(N-1)}{V}$  is the number of pairs per volume, and  $4\pi r^2 \delta r$  is the volume sampled at  $r$ .

Thus, the RDF is fully calculated for each frame and then averaged

$$g(r) = \frac{\sum_{\text{frames}} d(r)}{N_f d_{\text{uniform}}(r)} = \frac{V}{4\pi N_f N(N-1)r^2 \delta r} \sum_{\text{frames}} \sum_i \sum_{j \neq i} \delta(r - r_{ij}) \quad (3.18)$$

Overall, RDF indicates if there is a local structure in the fluid. A uniform distribution of particles would have  $g(r) = 1$  for all  $r$ . Accumulation of particles shows up as  $g(r) > 1$  and depletion of particles shows up as  $g(r) < 1$ .

Given that the RDF is a pair correlation function, it can be also represented as an ensemble average over pair, i.e.

$$g(r) = \frac{V}{N^2} \langle \sum_i \sum_{j \neq i} \delta(r - r_{ij}) \rangle \quad (3.19)$$

where  $\sum_i \sum_{j \neq i} \delta(r - r_{ij})$  is the distribution of particles at a particular instant (particular frame),  $N$  is the particle number and  $V$  is the volume of the system.

#### 3.5.2.1.1 Statistics for RDF

RDF error estimation is calculated by [184]

$$R(t) = \frac{C(t)}{C(0)} \pm \sqrt{\frac{2\tau}{T} \left[ 1 - \frac{C(t)}{C(0)} \right]} \quad (3.20)$$

where  $\frac{C(t)}{C(0)}$  is the normalized correlation function,  $\tau$  is the relaxation time of this correlation function, and  $T$  is the total simulation time.

This estimation was derived under assumption that  $C(t)$  is a random Gaussian variable, and is also a good order-of-magnitude estimate of the correlation function of a non-Gaussian velocity distribution [185].

In computing self-correlation function  $R(t)$  for each of the  $N$  atoms and the average of them, this error has to be divided by an additional factor  $\sqrt{N}$ .

### 3.5.2.2 Orientational Tetrahedral Parameter, $P(Q)$

Orientation Tetrahedral Order (OTO) is the angular tetrahedral order parameter which measures the local structure in the first coordination shell of water. Graphically, the orientational tetrahedral parameter is given by the probability density  $P(Q)$  of finding a molecule with tetrahedral index  $Q$ .

It was originally proposed by Chau and Hardwick [186], and subsequently rescaled by Errington and Debenedetti [187], so the average value of  $Q$  varies from 0 for ideal gas to 1 for regular tetrahedron.

The tetrahedral index  $Q$  focuses on the four nearest water oxygen neighbours and is defined as

$$Q = 1 - \frac{3}{8} \sum_{j=1}^3 \sum_{k=j+1}^4 \left( \cos \psi_{jk}(i, t) + \frac{1}{3} \right)^2 \quad (3.21)$$

where  $\psi_{jk}(i, t)$  is the angle between the lines connecting the oxygen molecule  $i$  with those of its nearest molecules  $j$  and  $k$  at time  $t$ . Then,  $-3 \leq$

---

$q(i, t) \leq 1$ , and a high value indicates that molecule  $i$  has a good tetrahedral order [188].

From established framework of this parameter, it is only sensitive to the angular order and not to the radial order.

Notably, the angular tetrahedral order parameter has been widely used in research of the structure of supercooled water [189, 190, 191, 192] and in determining the changes in the local structure of water with various solutes and surfaces [189, 193, 194].

### 3.5.2.3 Local Structure Index, LSI

The Local Structure Index (LSI) focuses on translational order, and it probes local structure beyond the first hydration shell, i.e., it aims to measure the extent of the gap between the first and the second hydration shells surrounding water molecule. It was proposed by Shiratani and Sasai [196] who associated a local structure index to each molecule to quantify the degree of local order. Graphically, LSI is given by the probability density  $P(I)$  of finding a molecule with local structure index  $I$ .

The key observation is the existence of certain molecules which show an unoccupied gap between 3.2 Å and 3.8 Å in their radial neighbour distribution for certain period of time. Such low-density molecules are well structured and coordinated in a highly tetrahedral manner with other four water molecules. Occupancy of such gap increases the local density and distorts the tetrahedral order of the central molecule [194].

The LSI is defined as  $I(i, t)$  for molecule  $i$  at time  $t$ . For each molecule  $i$  one orders the rest of the molecules depending on the radial distance  $r_j$  between the oxygen of the molecule  $i$  and the oxygen of molecule  $j$ :

$$r_1 < r_2 < r_j < r_{j+1} < \dots < r_{n(i,t)+1} \quad (3.22)$$

where the cutoff is chosen so that

$$r_{n(i,t)} < r_{th} = 3.7 \text{ \AA} < r_{n(i,t)+1} \quad (3.23)$$

Then,  $I(i, t)$  is defined as [196]

$$I(i, t) = \frac{1}{n(i, t)} \sum_{j=1}^{n(i,t)} [\Delta(j; i, t) - \bar{\Delta}(i, t)]^2 \quad (3.24)$$

where  $\Delta(j; i, t) = r_{j+1} - r_j$  and  $\bar{\Delta}(i, t)$  is the average over all molecules of  $\Delta(j; i, t)$  and  $n(i, t)$  is the normalization factor. Thus,  $I(i, t)$  expresses the inhomogeneity in the radial distribution within the sphere of radius around  $3.7 \text{ \AA}$ . A high value of  $I(i, t)$  implies that molecule  $i$  at time  $t$  is characterized by a tetrahedral local order and a low-local density, while on contrary, values of  $I(i, t) \sim 0$  indicate a molecule with defective tetrahedral order and high-local density.

The LSI has been extensively employed in investigations of the structure of supercooled water [198, 199, 200]. The idea is to apply the LSI analysis to inherent structure of water. In the study of supercooled liquids it is useful to consider the potential energy landscape (PEL) of the system obtained by the interactions between the molecules. The PEL has a very complex structure with minima marked by the different depth. The inherent structures are the collection of minima classified according to

their depths. With appropriate quenching procedures it is possible to determine the inherent structures by looking to the minima in the PEL. The inherent structures are obtained by quenching the instantaneous structure to the nearest local minimum in the PEL.

Each minima would be a sort of basin of attraction for a number of configurations. It has been found that the LSI analysis applied to the inherent structure in simulations of supercooled water reveals a structural bimodality in the underlying potential energy surface on which the thermal motion evolves corresponding to the LDL and HDL components of water. In the figure the LSI obtained with the TIP4P/2005 model for water where  $P(I)$  is the probability density of finding a molecule with local structure index  $I$  for water.

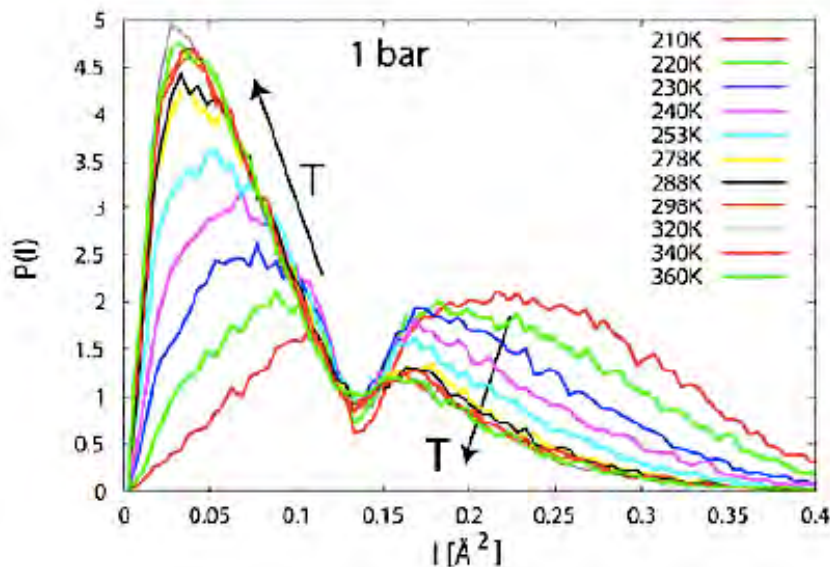


Figure 13: Evolution with temperature of the probability distribution of LSI values,  $I(i)$ , computed for inherent structures (IS) at different isobars [194].

The analysis of the results shows that the peak located to the right of the center in the plot represents the LDL component while the peak found to the left of the center indicates the presence of the HDL component.

#### 3.5.2.4 Angular Distribution Function, $P(\cos \gamma)$

In order to analyze the local structure around a water molecule, the arrangement of nearest neighbour molecules can be investigated by employing the distribution of the angle  $\gamma$  which is the angle between the two vectors from an oxygen atom of water molecule with the oxygen atoms of the two closest water neighbours. The distribution of the values of angles  $\gamma$  is estimated by the water molecules and are characteristic to those of a short-range bulk liquid water order. Hence, by monitoring  $\gamma$ , the clear picture of perturbation on the water HB network due to the attraction of ions can be perceived.

At high temperature a significant amount of water molecules is bonded with two, three, four and even five HBs to other water molecules. Notably, as the temperature of the system decreases the number of water molecules that form four HBs with other water molecules drastically increases.

The angle  $\gamma$  is defined as the H – O ... O angle of three water molecules. The angular distribution function,  $P(\cos \gamma)$ , is usually calculated for a system defined by  $N_W$ . In general, the distribution of the values of  $\gamma$  angles is taken according to the H<sub>2</sub>O molecules.

The distribution function for bulk water at ambient conditions, from both, experimental and computer simulations data, shows a well-defined peak at  $\gamma \approx 109.5^\circ$  ( $\cos \gamma \approx -0.26$ ), representing the tetrahedral order, and a secondary peak at  $\gamma \approx 54^\circ$  ( $\cos \gamma \approx 0.6$ ), which is attributed to the neighbours located in the cavities of the HB network [120].

---

Since RDF of water demonstrates the distortion of the HB network in aqueous solution, angular distribution function,  $P(\cos \gamma)$  has been found to be very effective tool in probing the HB network. Thus, by examining this quantity, the perturbation of water's HB network due to addition of ions is possible to observe [194].

### 3.5.2.5 Structural Order Parameter, $P(\zeta)$

Structural Order Parameter  $P(\zeta)$  is used to determine the local structure of water molecule by measuring the distance between first and second coordination shells by considering hydrogen bonding [194].

This parameter is sensible in detecting high translational and tetrahedral order in both oxygen and hydrogen atoms [185].

The positive value of  $\zeta$  indicates well separated first and second hydration shells, which, in turn, represents well developed tetrahedral hydrogen bond (HB) network.

The Structural Order Parameter,  $P(\zeta)$  is obtained as the distribution function of

$$\zeta = d_{-\text{HB}} - d_{\text{HB}} \quad (3.25)$$

where  $d_{\text{HB}}$  is the distance to the furthest HB neighbour, and  $d_{-\text{HB}}$  is the distance to the nearest non-HB neighbour.

---

### 3.5.2.6 Translational Tetrahedral Order Parameter, $S_k$

Translational Tetrahedral Order (TTO) parameter is the radial tetrahedral parameter which measures the variance of the radial distance between central water oxygen atom and the four nearest neighbouring water oxygen atoms [188].

It is defined as

$$S_k = 1 - \frac{1}{3} \sum_{k=1}^4 \frac{(r_k - \bar{r})^2}{4\bar{r}^2} \quad (3.26)$$

where  $r_k$  is the radial distance from central oxygen atom to the  $k$ th peripheral oxygen atom, and  $\bar{r}$  is the arithmetic mean of the four radial distances.

$S_k$  increases upon an increase of the local tetrahedral order. It reaches a maximum value of 1 for perfect tetrahedron.

Although, the Translational Tetrahedral Order is less used than the Orientation Tetrahedral Order, it has been shown to be more sensitive to density fluctuation [200, 201].

---

## Chapter 4

### LiCl:RH<sub>2</sub>O solutions in a supercooled water regime



The liquid water is understood by the dynamic behaviour of its molecules, in particular by the hydration of the solute genus. Dissolved ions in aqueous solutions are ubiquitous in many systems, but in water the addition of the ions crucially impacts its properties. Here, the factors, such as the ion type and concentration, play critical role in amending the structural and dynamical properties of water. Based on existing counteractive observations of the extent of the specific ion affect from which different microscopic images of ionic hydration emerge, the hydration of ionic solutes remains intriguing. In fact, at room temperature the electrolyte solution materializes when a vast number of ionic crystals is dissolved in normal liquid water. Au counterair, very tiny amount of electrolytes are dissolved in the glassy and crystalline water due to the quenching of the molecular diffusion of water [202, 203]. Deeply supercooled liquid water can be prepared by heating the *hyperquenched glassy water* (HGW) or *amorphous solid water* (ASW) above the glass transition temperature ( $T_g = 136$  K). The MD simulations provide much knowledge about the fluctuation of the local structure in the HDL and LDL

---

and the behaviour of water in the supercooled region upon its solvation of electrolytes. Lithium chloride, LiCl, aqueous solutions play particularly important role here due to their ease in supercooling. Moreover, since LiCl has an outstanding ability to dissolve in water and effects on the tetrahedral molecular structure of water molecule, it is particularly advantageous for studying the properties of water in the supercooled regime in bulk conditions.

This Chapter covers the Significance of the LiCl:RH<sub>2</sub>O solutions (4.1) and describes LiCl:RH<sub>2</sub>O as a gateway for probing water in supercooled regime (4.2).

#### 4.1 Significance of the LiCl:RH<sub>2</sub>O solutions

The influence of ions on the structure and dynamics of water is paramount in understanding of their role in many physical, chemical and biological processes. Hence, the effects of ions, in general, on the structure and dynamics of water have been widely studied experimentally, theoretically and by means of the MD simulations [124, 199, 204, 205, 206, 207, 208, 209, 210, 211, 212, 213, 214, 215, 216, 253, 267].

Aqueous solutions of salts have been long investigated for the purpose of determining a way to lower the freezing point of water. The precise salt concentration for which the solution remains to be in the liquid state up till its lowest temperature is *eutectic*. The lowest eutectic properties of temperature of 200 K, corresponding to a salt molar fraction of 20% concentration (6.76 M) are in LiCl [221, 222].

---

When ions are dissolved in water, the structural and dynamic properties of water deviate from neat water depending on the ion-water interaction. For bulk water, the complex HB network structure spans the whole space, and it critically impacts the unique behaviour and unusual characteristics of water. As the number of ions increases, the ion-water interaction becomes more significant than the water-water interaction. Consequently, the HB network in water is interrupted by ions. Notably, the disrupted HB network is different from bulk water.

Based on the notion that the local structure, adopted by the water molecule, is modified by the presence of ions in solution, depending on salt concentration, the thermodynamic properties of aqueous LiCl solution are indeed resemble those of bulk water [199, 223, 224, 225, 226, 227].

Due to its small cation, LiCl is the most soluble salt in water. In fact, solutions of LiCl are the most studied binary aqueous systems in experiments, as well as an effective probe to study polyamorphism of water in the supercooled regime via computer simulations [228, 229].

Aqueous solutions of LiCl are also of a great use in probing the properties of bulk water in the supercooled state up to 200 K (eutectic temperature), far into the no man's land. Moreover, different physical hypothesized scenarios for behaviour of water [228] and its anomalies [231, 232, 233, 234, 235] can be tested, as well as the existence of the Widom line and the corresponding LLCP [236] can be verified.

---

#### 4.1.1 Features of LiCl: $RH_2O$ solutions

Aqueous solutions of LiCl are widely used as a salt model to study properties of water due to its very high solubility in water and ample knowledge of its structure and physiochemical properties.

Some of the known features and observed behaviour of LiCl:  $RH_2O$  solutions (where  $R$  is the water-salt molar mass ratio) are:

- glass-forming liquid with a glass transition temperature ( $T_g$ ) of 135 K
- peculiarity of avoiding crystallization
- ease on supercooling directly to glass transition without thermal/kinetic restrictions
- persistence in liquid state over large temperature drop
- freezing point of  $H_2O$  can be lowered by adding LiCl - most famous thermodynamic property
- persistence to remain in the liquid state throughout a large temperature decreasing range - one of the most significant property [236]
- increase in ionic association constant at higher temperatures and low densities [238]
- perturbation of  $H_2O$  structure beyond first hydration shell with similar effect as applying pressure on pure  $H_2O$
- preservation of water's HBs in the system and strong effects on tetrahedral HB network
- strong temperature dependence of ionic structure for long distance behaviour of RDF [199]
- lesser distortion of O-O structure in bulk  $H_2O$  at low concentrations of LiCl:  $RH_2O$  [199]
- presence of the second CP at low concentrations of LiCl:  $RH_2O$  [239]

---

#### 4.1.2 Influence of LiCl on dynamics of water

The liquid water can be identified by the dynamical behaviors of its molecules, such as hydration of solute species. In fact, one of the most characteristic features of normal liquid water at room temperature is the formation of concentrated electrolyte solutions by dissolution of a large number of ionic crystals. On the other hand, since tiny amount of electrolytes dissolve in the glassy and crystalline water due to quenching of the molecular diffusion, more insights into the properties of amorphous water in the deeply supercooled region would be gained from the studying interaction of water with electrolytes [239].

Many studies have shown that the ionic effects on the properties of water strongly depend on the specific type of ions. Both, experimental and simulation studies showed that the dynamics of water is suppressed or enhanced by the presence of a different types of ions, which is induced by the subtle change in the structure of water by the ions [240, 241].

The effects of the salt concentration on the forming and breaking of the HB in water result in the two different behaviors in the fast and slow HB dynamics for all anions. The dynamics of water with dissolved ions can be understood by envisioning a molecular picture in which a water molecule rotates faster on a certain molecular axis, but it translates much slower with the given surrounding conditions for higher salt concentrations [242].

The hydrophilicity of the aqueous LiCl solutions is of importance. As a rule, the more hydrophilic the solute the less of it is required to reduce the nucleation temperature to a target value and/or to remove the possibility of crystallization altogether. The general consequence of high hydrophilicity is that the structures responsible for the interesting

---

anomalies of water are quickly destructed. Since LiCl is a hydrophilic solute, it lowers the nucleation temperature rapidly, leading to noncrystallizing solution.

#### 4.1.3 Impact of LiCl on the molecular structure of water molecules

There have been many attempts in the past to classify the structure of aqueous solutions (compositions over the liquidus lines of the phase diagram) into distinct regions over the whole concentration range from pure water to pure salt. The 5 classes classification by Braunstein is very efficient, and it was later simplified by Emonz to 4 classes [244].

Recently, two more regions were added by Yim [245]: the pure water (called 0) and pure molten salt (called V) as reference points. Thus, the solution structure is then divided into 6 distinct regions:

0—Pure solvent: No ion present and solvent structure is dominated by dipole-dipole interactions with no long-range order but short-range order with a lot of free volume for ions to fit in. In the case of water, the structure is dominated by tetrahedrally, the HB network that at low temperature freezes to various ordered structures of ice.

I—Dilute solutions: In this region the Debye-Hückel limiting law applies in the most diluted region (0.01 M) and where ions are completely solvated by water. At higher concentrations ions re-arrange the solvent structure based on their charge and size ( $z/r^2$ ), so introducing more short-range order around ions but the long-range order of the HB network remains intact. Hence, at low temperature ice still forms along with salt hydrates.

---

II—Concentrated solutions: This is the region where significant ion association occurs and extended Debye-Hückel-Onsager law applies. More ions introduce more short-range order locally and less long-range order in the bulk, but the HB network remains intact. Thus, at low temperature ice still forms along with salt hydrates. Small and large ionic species including clusters form, but the solution still has enough solvent (water) molecules to keep a less dynamic but otherwise a HB network intact, which means that at low temperature ice still forms along with salt hydrates.

III—Molten salt hydrates: In Braunstein's classification this region is split into two (III and IV). The dilute end of this region (IIIA: the hydrate melts sub-region) the number of water molecules is low but sufficient to form complete hydration shells around ions while in the second (IIIB) sub-region at the concentrated end ions do not have enough number of water molecules to form complete hydration shells. The structure is believed to resemble that of a molten salt. This is the region where the HB network breaks down and therefore ice does not form at low temperature and only salt hydrates do.

IV—Hydrous melts: This region consists of molten salt with small amounts of water molecules which are integrated into the lattice structure.

V—Pure salt: The solid is made up of a crystalline lattice that upon melting remains intact but becomes loose and ions become more mobile.

The structure/phase diagram relationship of the solutions  $\text{LiCl}:\text{RH}_2\text{O}$  is depicted in Figure 1.

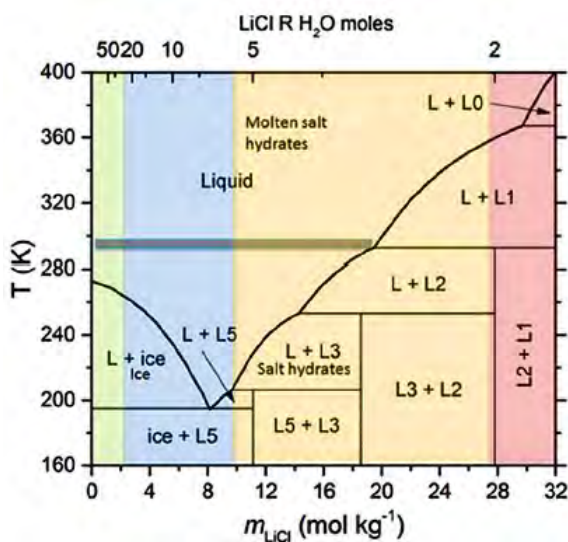
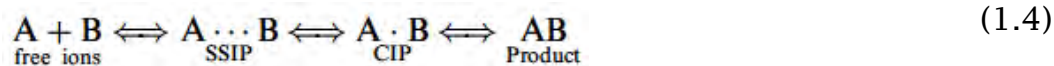


Figure 1: Phase diagram of the solutions  $\text{LiCl}:\text{RH}_2\text{O}$  adopted from *Yim et al., 2018* [245].

The structural properties of  $\text{LiCl}:\text{RH}_2\text{O}$  solution can also be probed by examining its *ionic association*.

Ionic association mechanism scheme was proposed by Fuoss [246] and Winstein [247], i.e.



where A and B represent  $\text{Li}^+$  and  $\text{Cl}^-$ , respectively, in the aqueous solutions and the two intermediate states are defined in the process of dissolving the salt product (AB) into free ions (A + B): a contact ion pair (CIP:  $\text{A} \cdot \text{B}$ ) and a solvent separated ion pair (SSIP:  $\text{A} \cdots \text{B}$ ).

The MD study by Zhang determined that at CIP state ( $r = 2.2 \text{ \AA}$ ) each ion occupies the expected hydration position of another ion and chloride ion forms a well-defined tetrahedron around lithium ion along with another

---

three water molecules. At high temperatures and low densities of dilute solutions, this kind of structure for ionic association will dominate and, therefore, this electrolyte is considered as a stable neutral ion pair [245].

At SSIP state ( $r = 4.5 \text{ \AA}$ ), a well-defined tetrahedral structure of lithium hydration shell was identified. Moreover, it was observed that simultaneously one of the hydrating water molecules interacted directly with  $\text{Cl}^-$  and was defined as a *bridging* molecule.

Zhang identified two intermediate states of ionic association of  $\text{Li}^+$  and  $\text{Cl}^-$  (CIP and SSIP) which revealed strong hydration effect of lithium ion and the bridge role of the lithium hydrating complex. Furthermore, the co-assembly between CIP and SSIP was found to be asymmetric with the trend of SSIP gradually becoming more pronounced at higher temperature and low density.

The distinctive properties of water can be extensively explained in terms of electrostatic forces arising from the charge distribution of the water molecule, in addition to its nearly tetrahedral bond angle [246].

Considering that the simple ions possess dimensions and charges in comparison to water molecule, it is only rational to expect that molecular structure of water will be considerably modified in ionic solutions.

From a series of measurements of the difference in movement between the number of molecules of water moving with the cation and with an anion, in various electrolytes, the hydration number can be allocated to each ion (provided  $\text{Cl}^-$  is used). Extensive study of this concept unequivocally confirmed the order of the hydration values for the monovalent cations [247]:

$$\text{Li}^+ > \text{Na}^+ > \text{K}^+ > \text{Cs}^+ > \text{H}^+ \quad (2.4)$$

When water molecules are in direct interaction with the charged ions in solution, the number of water molecules in their first hydration shell is smaller in comparison to those water molecules that are not in direct interaction with the charged ions. Water molecules in pure water exhibit same pattern of behaviour. Thus, the water number density around these molecules is lower. If the water partial RDFs in the salt solutions are not corrected for inhomogeneity, the derived from simulations heights of the peaks will be decreased in comparison to neat water.

In electrolyte solution, the distribution of ions occurs due to the competition between Coulomb (long-range) electrical forces and the thermal motions. This distribution is not random by all means, including at substantially considerable distances [246].

On the other hand, the water molecules that are in direct interaction with the charged ions have a lower value of the Orientational Tetrahedral Parameter,  $P(q)$ . Hence, in order to determine water structural perturbations in the ionic solutions, relative to the neat water, the close interactions of water molecules with the ions must be ignored. However, for the large anions, the water molecules at the outer edge of the first ionic hydration shall are not in direct interchange with the anions and, thus, are able to form four water-water HBs.

Moreover,  $\text{Cl}^-$  tends to replace oxygen atom in  $\text{H}_2\text{O}$  network, coordination shells of  $\text{Li}^+$  shift to longer distances with respect to  $\text{Cl}^-$ . Thus,  $\text{Li}^+$  has most relevant effect on  $\text{H}_2\text{O}$  than  $\text{Cl}^-$ . Diversification on long range order between these two ions is attributed to their different sizes (Figure 2).

Hence, the collapse of the second hydration shell is directly associated with angular perturbation of tetrahedral network of H<sub>2</sub>O.

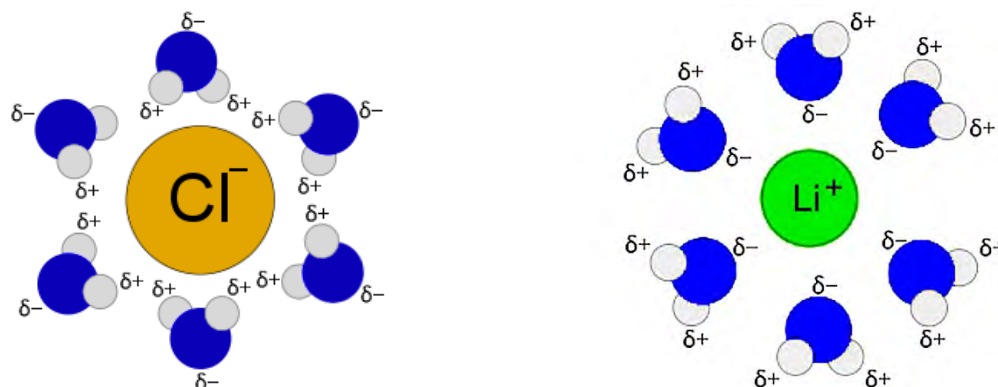


Figure 2: First hydration shell of Cl<sup>-</sup> and Li<sup>+</sup> ions in H<sub>2</sub>O.

As long as the chloride ions do not enter the second coordination shell of lithium ions the solution tetrahedral structure remains intact and transport is vehicular, and conductivity increases with concentration. As it enters the second shell ( $R < 11$ ), the ions become closer to each other and start feeling their electrical fields very strongly. Herein, the conductivity starts to stagnate, approaches maximum and when it enters the first shell ( $R < 3$ ) the conductivity decreases. [242].

At low salt concentrations, the halide anions, e.g., Cl<sup>-</sup>, slightly increase the tetrahedrality of the HB network of water in the second anionic hydration shell. But at higher concentrations, the dominant disruptive effect of Li<sup>+</sup> cancels the anionic effects, including in the anionic second hydration shell.

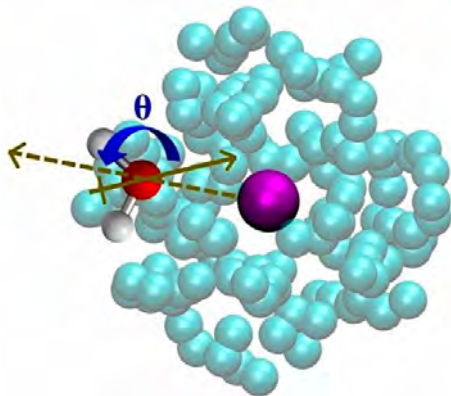


Figure 3: Hydration shell around an ion and representation of the polarization angle between water dipole and ion-water intermolecular axis.

The ionic effects on water are usually described in terms of a concept of the *structure-maker* and *structure breaker* [246] where ions could partake in either strengthening or weakening the HB network of water.

#### 4.1.3.1 Properties of aqueous ionic solutions: ionic hydration

Since the ionic field of water is controlled by the electrostatic field of the dipoles, the introduction of charged ions considerably modifies that field. The effect is roughly proportional to the polarizing power of the ion, i.e., its charge divided by its radius. Steaming from the hypothesis of the hydration of ions, large monovalent ion,  $\text{Cl}^-$ , will have the least effect while small highly charged ion,  $\text{Li}^+$ , will have the greatest effect [116].

The hydration of an ion occurs when the potential energy of water molecule forming part of the coordination shell around an ion is less than that of a molecule in free water. In free water every molecule has four neighbours and a single molecule coordinated to an ion has three neighbours - the ion and two water molecules on the other side. This follows because the charge of the ion must be expected to attract the two

---

H-nuclei or the two vacant places in the water molecule symmetrically and, from the point of view of further coordination, occupy them both. The coordination for an ion having at least one coordinated water molecule is therefore that the potential energy for a water molecule due to the ion is less than that due to two other water molecules.

#### 4.1.3.2 Effects on the HB network: Hofmeister classification scheme for anions and cations in the HB network of H<sub>2</sub>O

The concept of Hofmeister series contains a famous classification of ions in order of their ability to salt out or salt in proteins. It has been widely used in the interpretation of the properties of ionic solutions. In the Hofmeister classification scheme anions and cations are ordered according to their properties of enhancing (*structure makers*) or weakening (*structure breakers*) the HB network of water.

For the structure makers, the idea is that they are strongly hydrated since they break the HB in surrounding water molecules while the rest of the water molecules are able to rearrange themselves in an ordered hydration structure. Au contraire, the structure breaker ions interact weakly with water, hence, induce a disorder in the HB network of water molecule [252].

The existing evidence from both, experimental and computer simulations, shows that ions disturb the structure of water molecules beyond the first hydration shell similarly to when pressure is applied on pure water [251, 252, 253].

The tetrahedral structure of the water molecule is perturbed by the Li<sup>+</sup> cation and Cl<sup>-</sup> anion. Specifically, since Li<sup>+</sup> cation is enhancing the

---

tetrahedral structure it is determined to be the structure maker, whereas the  $\text{Cl}^-$  anion is disrupting the tetrahedral structure of the water molecule and, therefore, is designated to be the structure breaker [254].

#### 4.2 $\text{LiCl}:\text{RH}_2\text{O}$ solutions: a gateway for probing water in supercooled regime

The presence of salt is presumed to modify the behaviour of the supercooled water, reveal water's behaviour in no man's land and explain its anomalies. For example, it has been established that upon addition of salt to water its freezing point lowers. Thus, studying reactions mechanism and behaviour of ionic aqueous solutions is of a great interest.

$\text{LiCl}$  ionic solution is a glass forming liquid with unique feature to remain in the liquid state over a large temperature drop which results in its innate ease in supercooling [235].

Large number of studies exist on  $\text{LiCl}:\text{RH}_2\text{O}$  solutions due to the particular interest in extrapolating the information from the structure of the eutectic concentrations at low temperature to bypass the no-man's land region, which precludes the understanding of the water structure at low temperature.

Evidence of the presence of the supercooled liquid water can be obtained by the dissolution of  $\text{LiCl}$  in the deeply supercooled regime. The resulting  $\text{LiCl}$  solution may be connected to the  $\text{LiCl}$  solutions at room temperature [252]. It has been established that the concentrated  $\text{LiCl}$  solutions can be supercooled without phase separation [256]. Yet, dilute  $\text{LiCl}$  solutions ( $R > 12$ ) are seldomly obtained [257] since at low temperatures they are found

---

to be unstable and split into two phases: concentrated solution and hyperquenched glassy amorphous water (HW) [258, 259].

The study by Aouizerat-Elarby *et al.* on metastable crystallization products of the glassy and supercooled aqueous ionic solutions of LiCl [221] determined that by varying temperature, concentration or salt, three different states can be defined and explored, i.e.: (i) the supercooled liquid above  $T_g$  before ice crystals are detected; (ii) the faulty cubic ice structure; (iii) the cubic to hexagonal ice transformation. In addition, upon examining the hydration, the observation was made that for  $R > 12$ , ice crystallized on quenching which means that the hydration shell of both ions was completed for  $R = 12$ . For  $12 > R > 6$ , the value for  $T_g$  was found to remain constant and nucleation of ice was obtained under appropriate treatment (at  $T \sim 170$  K by precipitation of LiCl:5H<sub>2</sub>O in thermal equilibrium). It was concluded that for those concentrations, the water in excess of the value LiCl:6H<sub>2</sub>O is weakly bound and at  $R = 6$ , all the water molecules are probably shared by the hydration shells of both ions, while for  $R = 5$ , some LiCl ion pairs could already be formed.

The LiCl:6H<sub>2</sub>O ionic solution is of a great interest hence it is a topic of several studies. It is a glass-forming liquid solution which is effortlessly supercooled with an ease of the maintenance of the liquid phase over a large descend in the temperature range which allows to gain an understanding of the anomalies in supercooled water [199].

Given the system with four crystalline hydrates with  $R = 1, 2, 3, 5$  and eutectic point at 1 bar is at  $T_e = 199$  K, near the eutectic concentrations, at  $R \sim 6$ , where  $R$  is the water-salt molar mass ratio, i.e.,

$$R = N_{H_2O \text{ molecules}} / N_{ions} \quad (3.4)$$

the liquid can be supercooled directly to the glass transition, avoiding thermal or kinetic interferences. This can be successfully achieved by changing the cooling rate of the solution when the concentrations are varied from  $R = 4$  to  $R = 7$  [197].

#### 4.2.1 Recent experimental findings

The phase diagrams of the aqueous ionic solutions in the supercooled region show that the addition of salt perturbs the LDL structure of water and stabilizes the HDL phase. Based on  $H_2O$  anomalies from two-state model, LiCl enhances HDL of  $H_2O$  with respect to LDL [215, 220], as well as modifies  $RDF_O$  and  $ADF_{HB}$ .

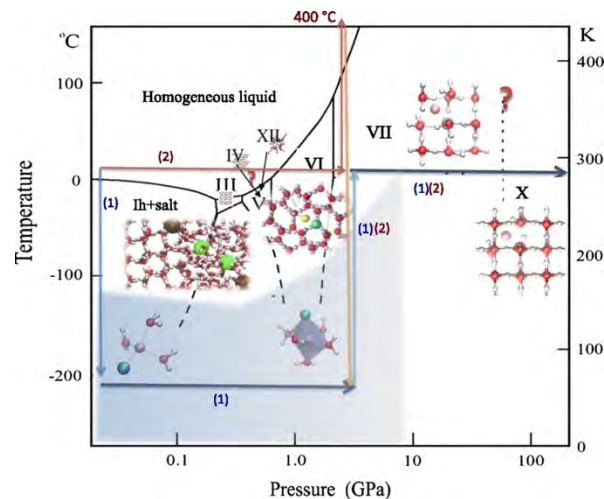


Figure 4: Temperature diagram of salty ice.

It has been observed that dilute LiCl solution ( $R > 50$ ) is formed when deeply supercooled liquid water interacts with LiCl at the very beginning of the glass-liquid transition. Furthermore, this liquid phase is short-lived

---

and merges into the second liquid phase that is characterized by a much higher solubility of LiCl [240].

It has been established that the supercooled liquid water (LDL) is accessible from the low-temperature side by heating the ASW (which is identical to LDA after annealing) above  $T_g$  and has a poor solubility of electrolytes [240]. Moreover, the second phase of supercooled liquid water, characterized by the long-range diffusivity of molecules, can dissolve a vast amount of LiCl and the LDL is short-lived, since it develops into supercooled normal liquid or freezes into crystalline ice  $I_c$  [237].

The local structure of LDA is quite similar to (largely different from) that of crystalline ice  $I_h$  (liquid water) [205]. This fact suggests that the LDL is characterized by a poor solubility of electrolytes. Moreover, it has been determined that the long-range translational diffusion of water molecules occurs due to the evolution of deeply supercooled liquid water. This evidence was attributed to the fact that LiCl dissolves in the fluidized water film after structural relaxation. It was also found that the dilute LiCl solution evolves first and then the concentrated one follows. The former is hardly accessible by quenching the aqueous LiCl solutions formed at room temperature due to the phase separation, whereas the latter is basically identical to the quenched LiCl solutions. This result suggested that two distinct liquid phases exist in the deeply supercooled regime; the first liquid phase, characterized by a poor solubility of LiCl and a high solubility of hydrophobes, is thought to be LDL, and the second liquid phase may be linked directly to the normal liquid water, as inferred from the high solubility of LiCl. The glass-liquid transition at 136 K is followed by the liquid-liquid transition in the deeply supercooled region. It is thus demonstrated that the supercooled aqueous solutions can be prepared by heating the water-deposited thin films of solute species above  $T_g$  and that

---

the slowed-down molecular dynamics of the aqueous solution can be explored on real time under vacuum conditions [237].

The presence of two supercooled liquid phases coincides with the second CP hypothesis, i.e., pure water separates into LDL and HDL phases, and then in its deeply supercooled region LDL and HDL turn into LDA and HDA at low temperatures. As mentioned before, this hypothesis is rarely evidenced experimentally by using bulk water because of the crystallization of the liquid water [238].

Furthermore, experiments in glass transition of pure water showed that the evolution of deeply supercooled liquid water should be responsible for the dissolution of LiCl. Due to the ice nucleation, the supercooled liquid phases are unstable for both, pure water and LiCl solutions. However, there are present broad metastable regions for supercooled LiCl solutions due to the slow ice crystallization within hours or days [215, 258]. Even though, the lifetime of the pure supercooled water is shorter than the lifetime of the LiCl solutions, the highly concentrated LiCl solutions are not likely to form unless the supercooled liquid is predominant to the crystal ice,  $I_c$ , over  $T_g$ .

By using time-of-flight secondary ion mass spectrometry (TOF-SIMS), the presence of deeply supercooled water has manifested by dissolution of LiCl in the pure amorphous water films heated at 140-155 K and the formation of aqueous LiCl solutions. Two phases of deeply supercooled water, that lead to the dilute and concentrated LiCl solutions, were clearly identified. It was deduced that the former is short-lived and merges into the latter, whereas the latter is basically identical to normal liquid water as far as the solubility of LiCl is concerned [237].

---

The volume of the LiCl-H<sub>2</sub>O solution during the decompression was also examined. It was found that the sudden volumetric change occurred in the liquid solution just above the  $T_g$  and, by employing X-ray and Raman spectroscopy, the amorphous phase and the ice phases,  $I_c$  and  $I_h$  were confirmed. Overall, the observed decompression-included volumetric change of the dilute LiCl aqueous solution was interpreted from the polyamorphic point of view regarding water as a solvent which coincides with hypothesis that water behaves as a polyamorphic phase divider [226].

Additional experiments on melting of precipitated ice IV in supercooled LiCl-H<sub>2</sub>O solution proposed the existence of polyamorphism in water based on the premise that LiCl is dissolved primarily in the HDL water [262, 263].

#### 4.2.2 Latest MD simulations results

Nowadays, the structural and dynamic properties of aqueous ionic solutions, such as LiCl:RH<sub>2</sub>O, in supercooled regime are extensively probed by MD computer simulation method.

The solubility of an electrolyte is associated, at the microscopic level, with a local phase separation (type of nucleation) which, in fact, can be the initial step of a phase transition. Therefore, it is important to gain an understanding of the local properties, i.e., structure, of the system in order to determine the phase transition [264] by employing the calculations of the RDFs.

For instance, the O-O structure is strongly dependent on the ionic concentration while the HB is well preserved. The results showed that

---

increasing the ion concentration is analogous to increase pressure on pure water [266].

MD simulation studies also determined that the anomalous behaviour of water in supercooled regime is contained in aqueous ionic solutions at low and moderate concentrations with a shift of hypothetically predicted second CP of water which has been probed experimentally [213, 214].

Singh *et al.* studied structure and diffusivity of aqueous LiCl solutions in the entire range by the MD simulations and found a strong solvation of monovalent ions in water and cluster formation at higher salt concentrations [271]. Also, the diffusion coefficient of LiCl was found to decrease depending on the coordination number and geometry that change with the salt concentration.

In the MD simulation study of LiCl aqueous solutions, Degrève *et al.* observed that the ion hydration structure is progressively lost with increasing concentration. At  $c = 1.0$  M, the ions were aggregated in small clusters, and as the concentration was increased to 5.0 M and 10.0 M, almost all ions were clustered in one cluster which did not present a crystal-like structure. Therefore, the high solubility of LiCl in aqueous solutions was subsequently attributed to the large radii difference between the anion and the cation which results in the instability of the ionic aggregates. This makes the formation of crystal seeds very difficult [270].

Aouizerat-Elarby *et al.* also studied the structure and diffusion in LiCl solutions over the whole concentration range. They showed that in the range  $0 < R < 3$  the solution is predominantly ionic in nature. For  $R$  values close to 6 and 4, there is no defined compound and deep eutectics are

---

formed. Their structural analysis showed a complete hydration sphere for  $R = 6$  and a direct anion-cation interaction for  $R = 4$ . This explained the diffusion coefficient values for Li, Cl, and water that were similar above  $R = 100$  where water structure is still intact. This changes around  $R = 90$  to  $100$  where chloride ions modify the structure and again different values occur at  $R = 3$  and  $R = 12$  indicating dependence on the presence of chloride in the first or second solvation shell [269].

In a very recent work, Prasad *et al.* studied the structural and dynamic changes and thermodynamic properties of aqueous LiCl solutions over the whole range and connected them to the experimental phase diagram. They observed by MD simulation the breakdown of the HB network of water as the LiCl concentration crosses the eutectic composition and they showed pronounced monotonic decrease in diffusivities of  $\text{H}_2\text{O}$ ,  $\text{Li}^+$  and  $\text{Cl}^-$ , accompanied by an increase in viscosity. They also compared the structural asymmetries of  $\text{H}_2\text{O}$  (tetrahedral) and LiCl (cubic) to that of  $\text{BeF}_2$  (tetrahedral) and LiF (cubic) and suspected a breakdown of the tetrahedral structure as the origin of the V-shape of the binary phase diagram [272].

In the study of the anionic effects on the structure and dynamics of water in superconcentrated aqueous electrolytes for various LiCl concentrations by Han *et al.*, additional MD simulations results were obtained [243]. These results demonstrated that a certain amount of salt is needed to show the different properties of water caused by the presence of different types of anion; below the cutoff concentration, most features of water show the same characteristics in spite of the presence of different anions; in the superconcentrated limit, a full disruption of the HB network between water molecules occurs for most anions investigated, indicating that the effect of the water-water interaction becomes negligible. However, a certain type of anion could enhance an ion-pairing of cations and anions and the

---

water-water interaction remains considerable even in the superconcentrated limit. In addition, the cationic and anionic hydration shell structures and dynamics were investigated and their dependence on the anion type and the salt concentration was revealed. Finally, it was observed that the anionic effects on water extend to the dynamics of water molecules, such as an anionic dependence of the onset of subdiffusive translation and anisotropic rotation [243].

Most recently, Camisasca *et al.* has carried out the MD simulations on LiCl:6H<sub>2</sub>O [199], in which the dynamical and structural properties of LiCl:6H<sub>2</sub>O solution (LiCl concentration of 9.25 mol/kg) upon supercooling were investigated. The relaxation time of the self-density correlation function was examined from ambient to 200 K temperature range and it showed that the system under study was in correlation with the mode coupling theory and exhibited fragile liquid behaviour. The structural properties were obtained by calculation of the RDF,  $g(r)$ , for  $g_{OX}(r)$  where  $X = \text{Li, Cl}$  and were compared to the two selected temperatures,  $T = 300 \text{ K}$  and  $T = 200 \text{ K}$ . Specifically, to determine the effect of ions on the structure of water molecules, the calculated RDFs for water in LiCl:6H<sub>2</sub>O were compared to corresponding functions of bulk TIP4P/2005 potential of water at ambient pressure. The comparison of those RDFs clearly revealed that the presence of LiCl in aqueous solutions strongly effects the structure of water molecule, i.e., it preserves the HB in the system, while it strongly modifies the tetrahedral HB network due to changes in O-O correlation. It was found that Li<sup>+</sup> contributes more relevant effect on H<sub>2</sub>O than Cl<sup>-</sup>. Therefore, it was determined that Li<sup>+</sup> is a structure maker and, as such, it increases HDL component in two-state H<sub>2</sub>O. The RDF and angular distribution of water,  $P(\gamma)$ , of the HB were probed in conjunction of the interpretation of water anomalies in terms of two-state model. It was deduced that in the presence of LiCl in aqueous solutions the high-

---

density liquid component of water increases with respect to the low-density component. Furthermore, the solution under study was determined as the one that is easily supercooled and driven to glassy state, as well as overall concluded that structure maker/braker role of ionic participants depends on the concentration of the solution and the liquid behaves as fragile liquid for all temperatures investigated.

---

## Chapter 5

### Water and hydrated ions correlations: investigating structural properties



MD simulations of aqueous solutions of LiCl is of a great interest because of its high solubility due to its small-size cation being responsible for excellent solvation properties of salt.

Up to date, vast number of experimental studies had investigated structural properties of highly, mid-concentrated and dilute LiCl:RH<sub>2</sub>O solutions. The most frequently applied experimental methods for structure determination of LiCl:RH<sub>2</sub>O solutions are the diffraction techniques, such as X-ray diffraction (XRD) and neutron diffraction (ND) mostly with isotropic substitution.

Multiple results of XDR showed clearly and significantly that LiCl produces an extensive rearrangement of water molecules upon solution. In particular, the existence of well-oriented hydration shells about Li<sup>+</sup> and Cl<sup>-</sup> ions has been firmly established. The Li<sup>+</sup> ions appeared to engage a lone pair of oxygen thus producing a tetrahedral environment about oxygen of one Li<sup>+</sup>, two hydrogens and, presumably, the HB to a neighbouring H<sub>2</sub>O

molecule or, at high LiCl concentrations, to a neighbouring  $\text{Cl}^-$  ions. On the other hand, chloride ions appeared to coordinate water by the HB as an acceptor atom [273, 274, 275]. X-ray diffraction study on aqueous lithium chloride solution in the temperature range 138-373 K was performed by Yamanaka *et al.* and the results showed that with lowering temperature the water-water correlation within the hydration shell of  $\text{Li}^+$  ions decreased, while the hydration shell of  $\text{Cl}^-$  ions was more structured in the supercooled and glassy states [276]. Probing the local order in aqueous lithium chloride solutions of various concentrations by X-ray scattering had revealed a decrease of the HB in liquid water as compared with pure fluid and that the presence of ions also leads to a weakness of the association structure of the solvent, i.e., both  $\text{Li}^+$  and  $\text{Cl}^-$  are dissolved by water molecules at the expense of the breakdown of the HBs of water molecule. Furthermore, it was observed that the hydration number of  $\text{Li}^+$  ions decreased with increased salt concentration. Also, the probability of contact ions increased and that of solvent-separated ion pair formation decreased [277]. X-ray scattering studies support the notion that as the salt concentration increases, the degree of the HB in liquid water clearly decreases, whereas the coordination number of  $\text{H}_2\text{O}$  molecule in solution increases. Overall, the basic feature in ionic solutions is the perturbation of water's HBs and the appearance of electrostatic interactions between ions and water, i.e., both cations and anions are dissolved by water molecules at the expense of the breakdown of the HB network [278]. A significant T-mode XAS study by Waluyo *et al.* explored the role of alkali cation as a player of a structure-breaker in water which weakens the HB network and the collapse of the second shell due to the breakdown of the tetrahedral structure. As a member of alkali and halide ion series, the structure-making and structure-breaking property is usually depends on the ion size. Contrary to common belief that the small lithium cation is designated to be structure-maker, this study determined that lithium

cation indeed breaks water-water HB network as well as increases the population of HDL species. In addition, this study concluded that structure-breaking character of LiCl is enhanced at lower temperature [279].

Experimental ND studies have also been delivering great findings in structural properties of ionic LiCl aqueous solutions. For instance, ND study by Harsányi *et al.* showed the presence of Li<sup>+</sup> cations with only 3 (or less) coordinated H<sub>2</sub>O molecules around them and revealed that at the highest concentration, one counter-ion has been found to penetrate the first hydration sphere of the ions [280]. The structure of nearest hydration shell has been probed by ND and results revealed that the coordination number for Li<sup>+</sup> is 4 and for Cl<sup>-</sup> is 6 in the LiCl aqueous solution; the average ion-oxygen distances for Li<sup>+</sup> are  $1.90 \pm 0.05$  Å and  $3.10 \pm 0.05$  Å; around cations the configuration of the water molecules is that of orientation of the axis of one of two lone-pair hybrids on a straight line joining an oxygen atom and a cation [281].

Several other experimental techniques also have been used to study structure of aqueous LiCl solutions. These are, but not limited to: X-ray Raman scattering spectroscopy which is rather efficient for understanding the changes that ions cause to the HB network [282]; X-ray Compton scattering is sensitive predominantly to the ion-ion and ion-oxygen bond-length distributions as well as to the hydration number and ion pairing [283]; dielectric relaxation spectroscopy which allows to study contact ion pairs over the concentration range [284], heat pulse technique and nuclear magnetic resonance (NMR). For the temperature range from 313 K down to 173 K the LiCl:7H<sub>2</sub>O solution, NMR study using ultrahigh magnetic field gradient was conducted revealing behaviour of the viscosity, electrical conductance and reorientational correlation time of water [285]. The

---

nuclear spin relaxation times  $\tau_1$  and  $\tau_2$  of concentrated aqueous LiCl solution over a wide range of temperatures has been obtained using NMR showing that the relaxation is mainly attributed to dipolar coupling between water protons and lithium ions, and  $\tau_1$  and  $\tau_2$  at temperatures higher than the glass transition point are governed by the translational motion of the hydrated lithium ions [286].

In order to investigate structural properties of aqueous ionic solutions the MD simulations were performed in this thesis with two ionic concentrations: LiCl:7H<sub>2</sub>O and LiCl:24H<sub>2</sub>O over a range of temperature from 300 K down to 200 K upon supercooling. The goal of these analysis was to determine the change in behaviour of bulk water in the presence of Li<sup>+</sup> and Cl<sup>-</sup> ions upon supercooling. In particular, the main issue was to study how the ions affect the LDL/HDL composition of water.

This Chapter covers the MD simulation parameters (5.1); Water interaction (5.2); Structural properties of aqueous ionic solutions (5.3); Calculations of structural trajectories and variables (5.4); and finally, investigation of the Hydrogen Bond network (5.5).

## 5.1 MD simulations

All the investigations of the structural properties of the correlations of water and hydrated charged ions, i.e., Li<sup>+</sup> and Cl<sup>-</sup>, were obtained by employing MD simulations technique with appropriate model potential and applicable setup of initial space configuration of the system's constituents.

### 5.1.1 Model potential

The potential model used in this study [181, 287] is a combination of the TIP4P/2005 site potential and the Joung and Cheatham (JC) [179] force field for the ions-water interaction. The JC-TIP4P/2005 site potential model showed good agreement with the RDF obtained in experiments.

The detailed description of the JC-TIP4P/2005 potential model was presented in Chapter 3, Section 3.4.1.

The JC-TIP4P/2005 ion-water and ion-ion parameters for the LJ form of the potential used in this study are presented in Table 1.

Table 1: Water-water, ion-water, ion-ion LJ interaction parameters in JC-TIP4P/2005 potential [260].

Atom pair	$\epsilon_{ij}$ (kJ/mol)	$\sigma_{ij}$ (nm)
O-O	0.77490	0.31589
Li <sup>+</sup> -Li <sup>+</sup>	0.43509	0.14397
Cl <sup>-</sup> -Cl <sup>-</sup>	0.04879	0.49178
Li <sup>+</sup> -O	0.58065	0.22993
Li <sup>+</sup> -Cl <sup>-</sup>	0.27392	0.29626
Cl <sup>-</sup> -O	0.19444	0.40383

### 5.1.2 Simulation constituents

Two systems were studied: the higher concentration (concentrated) LiCl:7H<sub>2</sub>O and lower concentration (dilute) LiCl:24H<sub>2</sub>O. All-atoms MD simulations of both systems were performed at constant pressure  $p = 1$

bar and the temperatures ranging from  $T = 300$  K down to  $T = 200$  K. The cubic simulation box with a length approximately  $L = 2.6$  nm at  $T = 300$  K contained 490 water molecules, 70  $\text{Cl}^-$  ions, and 70  $\text{Li}^+$  ions for  $R = 7$  concentrated solution which gives a concentration of 12.5% corresponding to  $c \approx 7.94$  mol/kg. Similarly, for  $R = 24$  dilute solution the cubic simulation box contained 480 water molecules, 20  $\text{Cl}^-$  ions, and 20  $\text{Li}^+$  ions which gives a concentration of 4% corresponding to  $c \approx 2.31$  mol/kg.

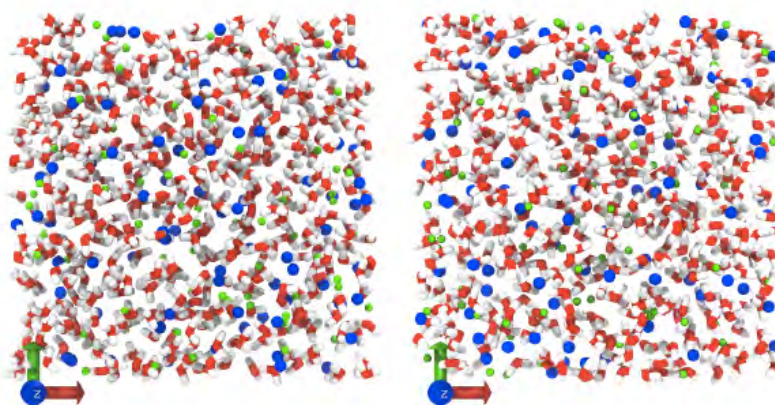


Figure 1: Cubic simulation boxes for  $T = 300$  K (left) and  $T = 200$  K (right).

The study parameters for both concentrations are listed in Table 2.

Table 2: Parameters for TIP4P/2005 and JC-TIP4P/2005 potential models in the study.

MD potential model	TIP4P/2005/JC-TIP4P/2005
Simulation application	GROMACS
Pressure	1 bar
Temperatures	Range: 200 K to 300 K
1 - $\text{H}_2\text{O}$ particles number, $N$ ( $N_{\text{H}_2\text{O}}$ )	490
1 - LiCl concentration ( $x_{\text{LiCl}}$ )	7.94 mol/kg
1 - LiCl ions number, $N$ ( $N_{\text{Li}^+}, N_{\text{Cl}^-}$ )	$\text{Li}^+ = 70, \text{Cl}^- = 70$
1 - $R$	7 (concentrated)
2 - $\text{H}_2\text{O}$ particles number, $N$ ( $N_{\text{H}_2\text{O}}$ )	480
2 - LiCl concentration ( $x_{\text{LiCl}}$ )	2.31 mol/kg
2 - LiCl ions number, $N$ ( $N_{\text{Li}^+}, N_{\text{Cl}^-}$ )	$\text{Li}^+ = 20, \text{Cl}^- = 20$
2 - $R$	24 (diluted)

The cutoff radius for the non-bonded van der Waals interactions was set to 9.5 Å (0.95 nm). The Coulombic interaction was truncated at 9.5 Å (0.95 nm). The correction contribution was evaluated by using the Particle Mesh Ewald (PME) method [288]. The equations of motion were integrated with a time-step of 1 fs using Verlet leap-frog algorithm (Section 2.2.1). To handle both, temperature and pressure of the system, Berendsen method was employed. The MD simulations were performed using parallelized version of GROMACS 4.5.5 (Section 3.3) simulation package. The optimized parameters for TIP4P/2005 model are listed in Table 3.

Table 3: Optimized parameters for TIP4P/2005 model.

Model	$\epsilon/k$ (K)	$\sigma$ (Å)	$q_H$ (e)	$d_{OM}$ (Å)
TIP4P/2005	0.7749	0.31589	0.5564	0.01546

Table 4 contains the summary of the thermodynamic state points probed in the study. Information is given for the density of the system,  $\rho$ , the potential energy,  $U$ , and the simulation times for the equilibration,  $t_{eq}$ , and for the production,  $t_{prod}$ , runs. The internal energies,  $U$ , are given per mol of particles  $N_{H_2O} + N_{Li^+} + N_{Cl^-}$ . To ensure that the system of water and ions equilibrate properly at each temperature, particularly upon cooling, equilibration runs are typically longer than the production runs. In fact, the length of the production run is set to specifically produce enough statistics for the calculations of the static and dynamics density correlators.

Table 4. Summary of the simulated state points at  $p = 1$  bar containing the temperature  $T$ , density  $\rho$ , and potential energy  $U$  for both, LiCl:7H<sub>2</sub>O and LiCl:24H<sub>2</sub>O systems. At each temperature, the equilibration length of the run,  $t_{\text{eq}}$  is followed by the data collection for a time of the production run,  $t_{\text{prod}}$ .

$T$ (K)	LiCl:7H <sub>2</sub> O				LiCl:24H <sub>2</sub> O			
	$\rho$ (g/cm <sup>3</sup> )	$U$ (kJ/mol)	$t_{\text{eq}}$ (ns)	$t_{\text{prod}}$ (ns)	$\rho$ (g/cm <sup>3</sup> )	$U$ (kJ/mol)	$t_{\text{eq}}$ (ns)	$t_{\text{prod}}$ (ns)
300	1.110	-136.69	40	30	1.037	-78.69	40	40
290	1.113	-137.22	50	30	1.040	-79.28	50	50
280	1.115	-137.77	50	40	1.042	-79.88	50	40
270	1.120	-138.23	80	40	1.043	-80.50	80	40
260	1.122	-138.76	80	50	1.044	-81.11	80	60
250	1.123	-139.36	80	50	1.043	-81.73	80	60
240	1.125	-139.85	80	50	1.041	-82.38	80	50
230	1.126	-140.36	80	50	1.037	-82.99	80	60
220	1.128	-140.88	60	60	1.033	-83.65	120	60
210	1.129	-141.37	60	60	1.028	-84.27	120	60

The total computational time amounted to approximately 1680 ns for the entire simulated isobars. The simulations were carried out on the INFN-Grid Roma Tre cluster.

## 5.2 Structure and thermodynamics of water in presence of ions

This subsection contains the results of investigation of the behaviour of the Temperature of Maximum Density (TMD) anomaly in the presence of the two aqueous ionic solutions: one dilute and one concentrated. Also, the structural properties of water molecule, which were calculated from

---

the equilibrated and stored trajectories in the production run, are presented and analyzed.

### 5.2.1 Correlation between TMD anomaly and ionic concentrations

The temperature at which density of water exhibits a maximum is 277 K and is known as a *temperature of maximum density* (TMD). As mentioned in Chapter 1 in relation to water's anomalies, the TMD line serves as a border between a simple liquid water state and an anomalous liquid water state which expands upon cooling. For each value of the pressure, water shows a maximum that towards lower temperature as pressure increases. Yet, density is known to decrease upon cooling at constant pressure otherwise.

The TIP4P/2005 (Section 3.3.4.2) potential model which is employed in this study delivers big improvement in probing the TMD quantity. As shown in Figure 2, for the potential used in the study, for the bulk water the value of TMD falls around 271 K, which is in good agreement with known value of 277 K with only 2.2% error.

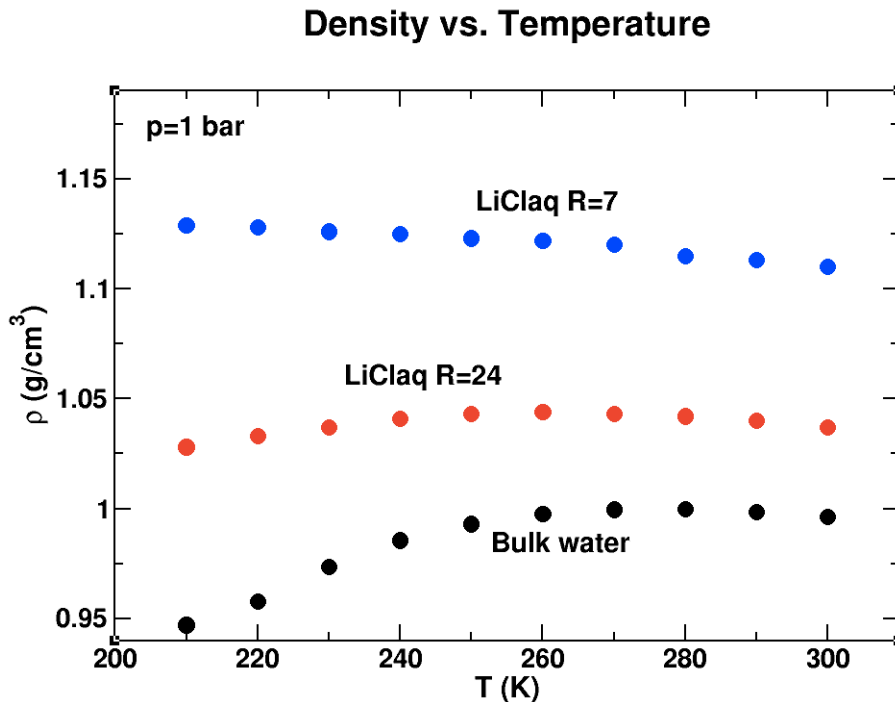


Figure 2: Density vs. Temperature plot for Bulk water (black dots), LiClaq for  $R = 24$  (red dots), and LiClaq for  $R = 7$  (blue dots). Pressure was held constant at 1 bar. The TMD for Bulk water falls at 271 K.

Upon addition of dilute LiCl,  $R = 24$ , the TMD shifts slightly towards lower temperature and a severe drop of the curve is seen. When examining the behaviour of concentrated LiCl,  $R = 7$ , the TMD anomaly disappears, thus we no longer have its features. Therefore, it is beneficial to use two different LiCl concentrations in the study: the dilute  $R = 24$  which exhibits TMD anomaly of water and the concentrated  $R = 7$  which does not. This allows for comparative observations of their behaviour from which the decision about what percentage of ions must be added into the solution in order to have water anomalies disappear.

## 5.2.2 Structural properties of water

The local internal structural properties of water in the two electrolyte solutions in the study were determined by calculating three RDFs,  $g_{ij}(r)$ , where  $i, j$  are the oxygen and hydrogen atoms, i.e.,  $i, j = \text{O}, \text{H}$ . More precisely, the three RDFs are:  $g_{\text{OO}}(r)$ ,  $g_{\text{OH}}(r)$ ,  $g_{\text{HH}}(r)$ .

In this study, it was adopted the geometry criterion for the definition of a HB between two water molecules is given in Figure 3.

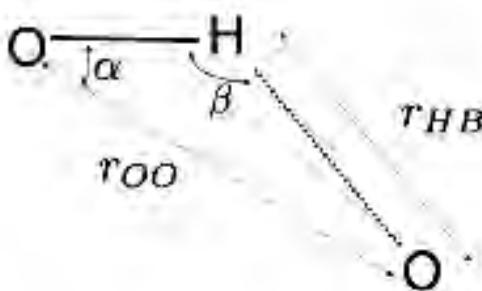


Figure 3: Geometry of the O–H group of the donor  $\text{H}_2\text{O}$  molecule and the oxygen atom of the acceptor  $\text{H}_2\text{O}$  molecule partaking in the HB.

As noted in Chapter 1, Section 1.2, a HB between a donor and an acceptor can be characterized by different geometrical and energetic principles. Here, geometrical criterion is employed to establish the existence of a HB in the systems under investigation. The method holds that a donor oxygen atom and an acceptor oxygen atom are H-bonded when:

- the distance between them,  $r_{\text{OO}}$ , is less than a cutoff distance
- the acceptor-donor-hydrogen angle,  $\alpha = \text{H} - \widehat{\text{O}} \cdots \text{O}$ , is less than or equal to a cutoff angle (Figure 3)

The cutoff distance is usually determined by the first minimum of the RDF between the donor and the acceptor atoms. And the cutoff angle is

typically chosen to facilitate the linearity of the HB inside specific cone value. In this study the HBs between H<sub>2</sub>O molecules are adopted and used from [279], i.e.:

$$\begin{aligned} r_{00} &< 3.5 \text{ \AA} \\ \alpha &< 30^\circ \end{aligned} \tag{5.1}$$

The conditions of Eq. 5.1 hold for  $r_{\text{HB}} < 2.7 \text{ \AA}$  and  $\beta > 140^\circ$  [273].

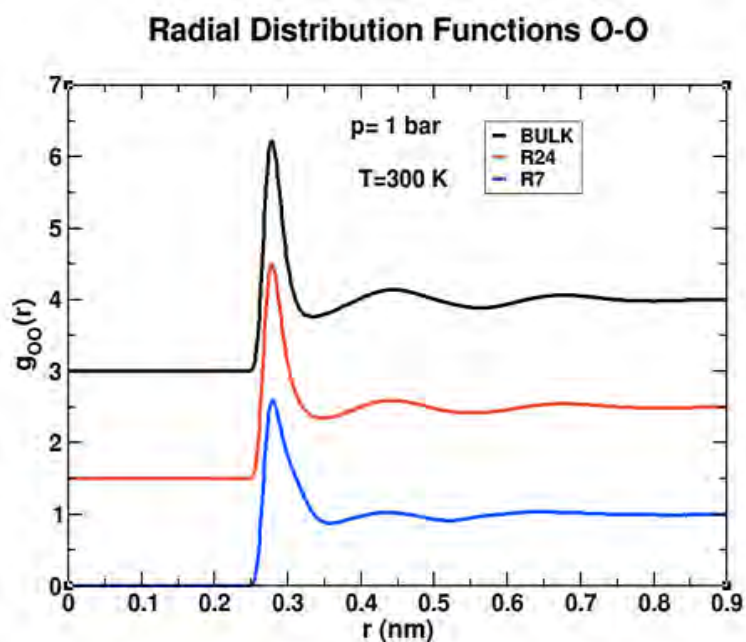
The calculations were executed between an atom pair  $i, j$  which does not belong to the same molecule. The  $i, j$  pair gives the probability of simultaneously finding atom  $i$  in a unit volume located at  $r_i$  and atom  $j$  in a unit volume at  $r_j$ . By placing the coordinate system's origin in an atom and integrating over the space accessible to that kind of atom, a distribution function  $g(r_j - r_i)$  is derived. Moreover, the obtained  $g_{ij}(r)$  does not contain the intramolecular peaks that are not relevant for our study.

The calculations of RDFs were performed at 11 different temperatures: from 300 K down to 200 K. For the purpose of discussion, the plots for three temperatures:  $T = 300 \text{ K}$ ,  $T = 240 \text{ K}$  and  $T = 210 \text{ K}$  are presented. The intermolecular peak positions for probing structural properties of water derived by the correlations of the LiCl:24H<sub>2</sub>O and LiCl:7H<sub>2</sub>O systems at  $T = 300 \text{ K}$ ,  $T = 240 \text{ K}$  and  $T = 210 \text{ K}$  are given in Appendix D, Tables 7 through 19.

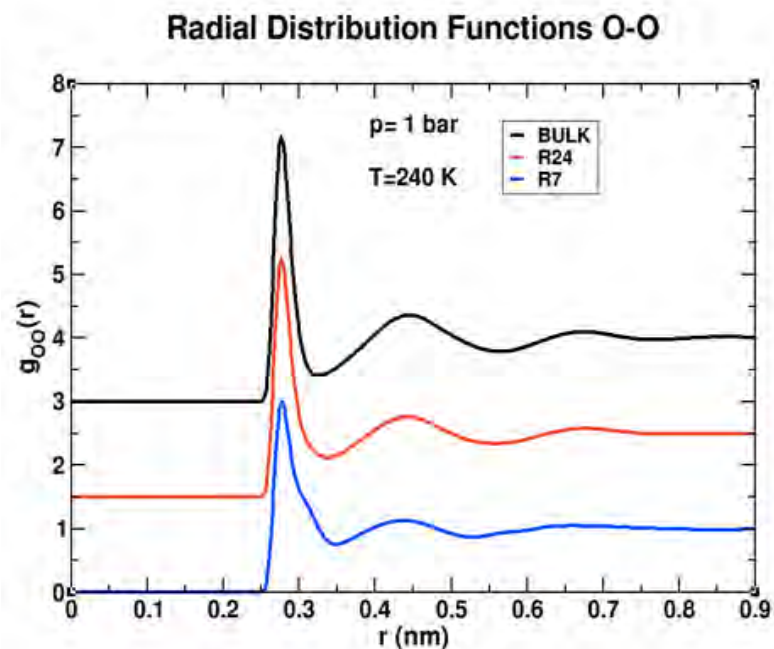
## 5.2.2.1 RDFs for O-O

Figure 4 presents  $g_{OO}(r)$  for  $T = 300$  K,  $T = 240$  K and  $T = 210$  K. Comparison between these three temperatures reveals that the local maxima of each RDF are generally sharper and alternates to deeper minima. In fact, this behaviour is characteristic of a pair correlation function upon cooling.

(a)  $g_{OO}(r)$  for  $T = 300$  K



(b)  $g_{OO}(r)$  for  $T = 240$  K



(c)  $g_{OO}(r)$  for  $T = 210$  K

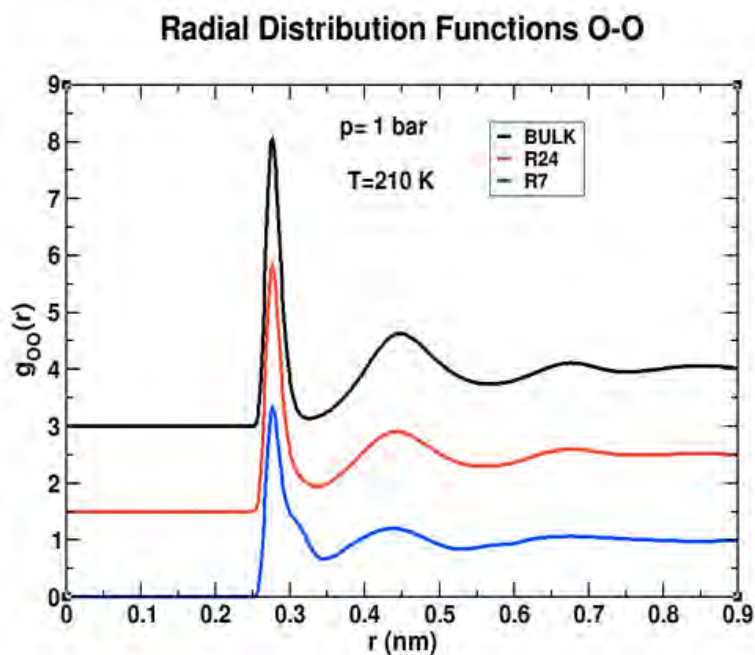


Figure 4: RDFs for oxygen-oxygen at three different temperatures and pressure of 1 bar for bulk water (black line), LiCl:24H<sub>2</sub>O -  $R = 24$  from here on (red line), and LiCl:7H<sub>2</sub>O -  $R = 7$  from here on (blue line).

More specifically, in Figure 4 (a) at  $T = 300$  K, all, bulk,  $R = 24$  and  $R = 7$  LiCl aqueous solutions have only one pronounced peak at 0.28 nm. The

effect of salt is relevant as the peaks of the solutions are lower and  $R = 7$  the first peak is also wider to that one of bulk with the presence of a shoulder. For intermediate  $T = 240$  K the shoulder slightly raised. This represents the presence of the possible distortion of the short-range order of oxygen atoms due to the interaction with ions in the more concentrated solution. Plot (c) for  $T = 210$  K also has main peaks at  $2.8 \text{ \AA}$  but here for  $R = 7$  the effect of decreasing temperature results in a more pronounced shoulder to the right of the first peak and a decrease of the height of second peak with respect to bulk and low ionic concentration. This indicates that the increase of ionic concentration implies an increase of the distortion effect on short-range order of oxygen atoms. Nevertheless, given that the position of maxima and minima remains rather unchanged within the temperature range under investigation, neither the short-range nor the long-range order of  $\text{H}_2\text{O}$  molecules is significantly affected by the drop in temperature.

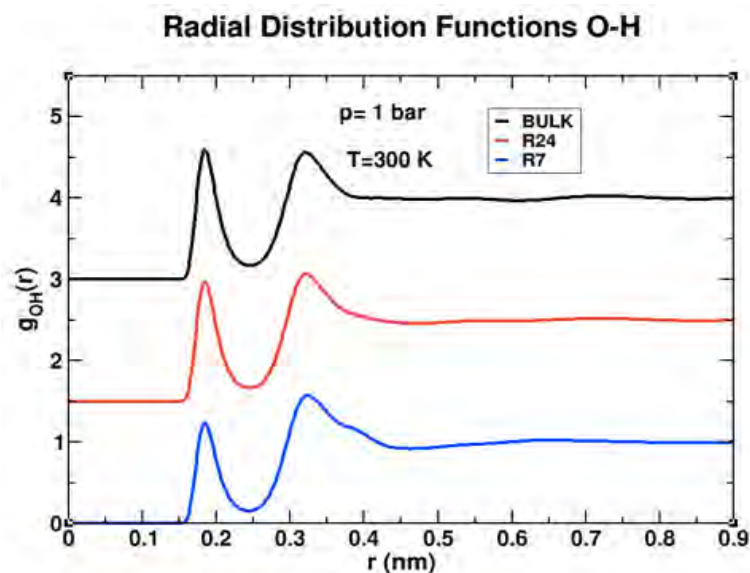
Although, the HBs are preserved, the changes in the O-O correlations manifest a distortion of the HB network of water for  $R = 7$ . The modification of the second shell of the oxygen in other ionic solutions has already been seen. We confirm the effect of ions being present with an increase of pressure on water.

#### 5.2.2.2 RDFs for O-H

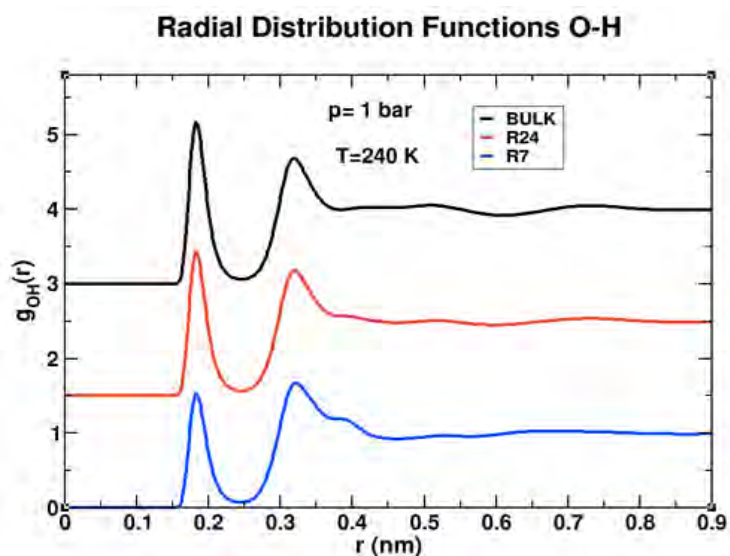
RDFs for oxygen-hydrogen,  $g_{\text{OH}}(r)$  are presented in Figure 5. The first intermolecular peak at  $1.8 \text{ \AA}$  belongs to the H-bonded water molecules. For all species the position of this peak is very similar. There are also present very pronounced second peaks at  $3.2 \text{ \AA}$  corresponding to the second shell. For lower temperature the maximum of the second shell is slightly reduced.

In general, with higher increase of the density of the ions, more structural modifications occur. Notably, these modifications occur from the third shell onwards. Overall, they are connected to the HB as the first two shells remain similar in bulk water.

(a)  $g_{\text{OH}}(r)$  for  $T = 300$  K



(b)  $g_{\text{OH}}(r)$  for  $T = 240$  K



(c)  $g_{\text{OH}}(r)$  for  $T = 210$  K

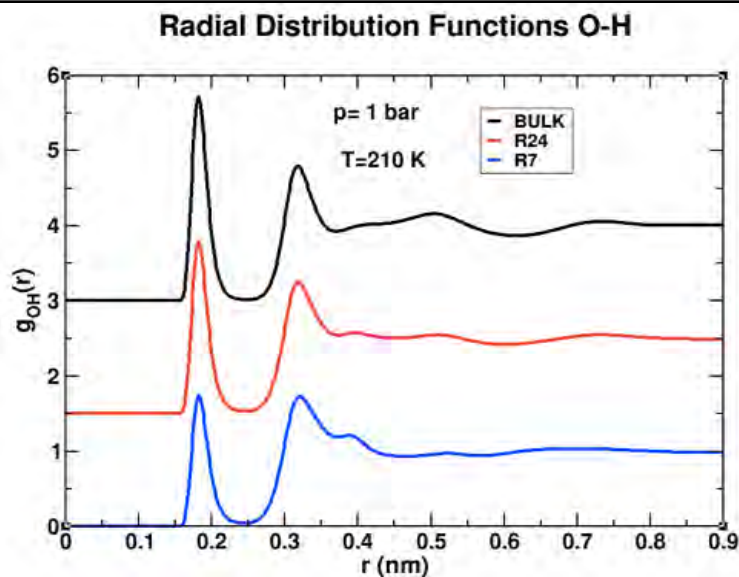
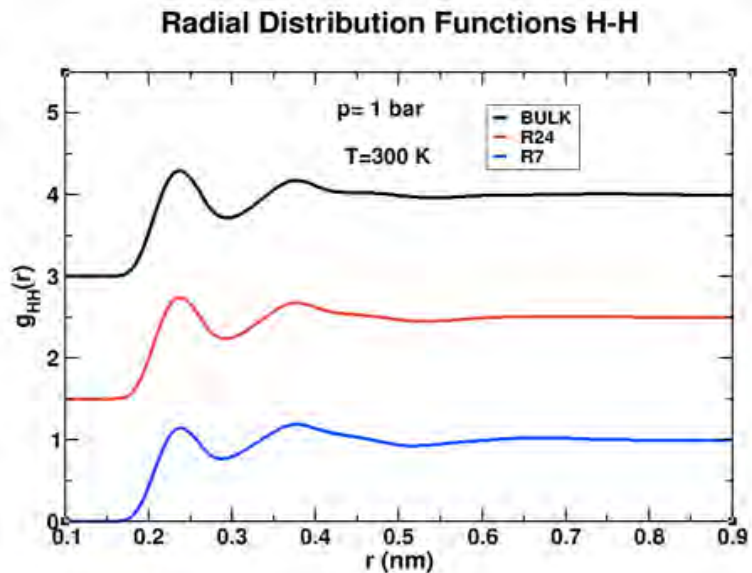
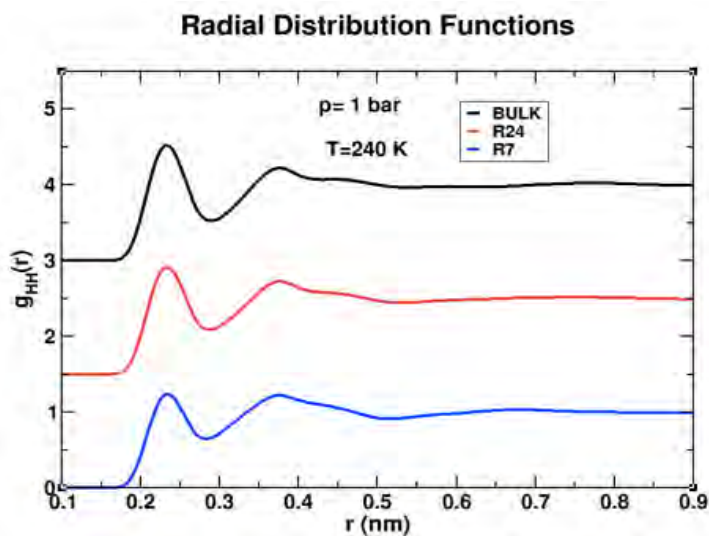
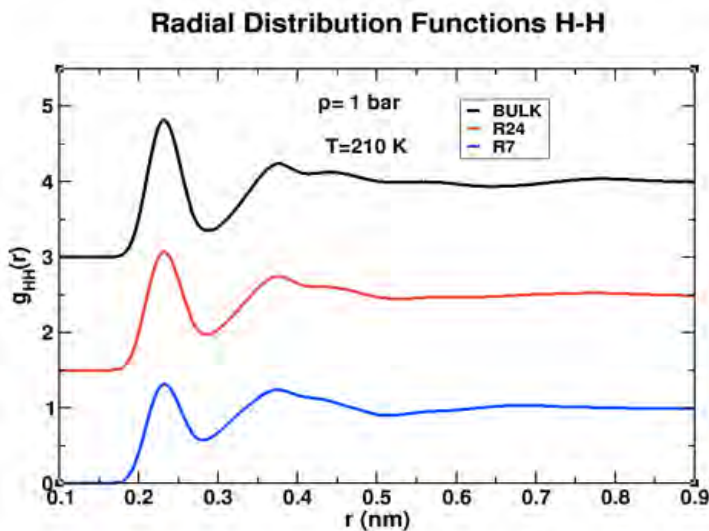


Figure 5: RDFs for oxygen-hydrogen at three different temperatures and pressure of 1 bar for bulk water (black line),  $R = 24$  (red line), and  $R = 7$  (blue line).

### 5.2.2.3 RDFs for H-H

Figure 6 contains RDFs for  $g_{\text{HH}}(r)$  at three temperatures,  $T = 300$  K,  $T = 240$  K and  $T = 210$  K, for dilute and concentrated aqueous solutions as well as for bulk water. The RDF of H-H represents the orientational correlation between neighbouring molecules of pure water. It behaves similarly to the RDF of O-H in aqueous solutions, i.e., in the solution the first peak is less-defined, and the consecutive shells show some difference with respect to bulk. These results display the preservation of the HBs between water molecules in the system.

(a)  $g_{HH}(r)$  for  $T = 300$  K(b)  $g_{HH}(r)$  for  $T = 240$  K(c)  $g_{HH}(r)$  for  $T = 210$  K

---

Figure 5: RDFs for hydrogen-hydrogen at three different temperatures and pressure of 1 bar for bulk water (black line),  $R = 24$  (red line), and  $R = 7$  (blue line).

For all three species the only pronounced peak occurs at 2.4 Å and corresponds to first shell. The overall hydrogen atoms correlations across temperatures range are less sensitive to the temperature drop except for formation of a small second peak-like shoulders at  $T = 210$  K. Like for  $g_{00}(r)$ , neither short- nor long-range order of H<sub>2</sub>O molecules is significantly influenced by the decrease in temperature. The H-H correlations are indicative of the orientation correlation between the neighbouring pure water molecules. Here, in the aqueous solution they remain essentially unchanged which means that the HBs between water molecules are preserved in the system, while the changes in the H-H correlations manifest a distortion of the HB network of water.

### 5.3 Ion-water correlations

The main structural units in the MD study are those of the first coordination shells, i.e., the H-bonded water molecules, the hydrated ions (through Li-O and Cl-H pairs) and the contact ion pairs. The proportion of these units is concentration dependent. These units are crucial to the understanding of the structure of aqueous LiCl solutions as not only the first coordination shells of the ions and water can be described through them, but the medium range structure (second and third nearest neighbours) is also determined by the ratio of these basic pairs.

In this study, a further understanding of the structural properties of aqueous ionic solutions can be acquired by examining the RDFs for Cl-X, Li-X and ion-H for concentrated and dilute solutions in all the range of

temperatures. The intermolecular peak positions for probing structural properties of aqueous ionic solutions derived by the correlations of the LiCl:24H<sub>2</sub>O and LiCl:7H<sub>2</sub>O systems at T = 300 K, T = 240 K and T = 210 K are given in Appendix D, Tables 7 through 12.

### 5.3.1 RDFs for Cl-X

The first coordination shell of Cl<sup>-</sup> ions contains water molecules and lithium ions. The water molecules turn towards the ion by positively charged hydrogen atoms.

Figure 7 shows RDFs,  $g_{\text{Cl-X}}(r)$ , for  $R = 24$  dilute LiCl aqueous solution at high, intermediate and low temperatures where X is either Li or Cl. Lithium is the closest to chloride with first pronounced peak of  $g_{\text{CLi}}(r)$  at 2.3 Å and second peak at 4.5 Å for all three temperatures. The second RDF is for Cl-O,  $g_{\text{ClO}}(r)$ , with first peak at 3.2 Å and second peak at 4.9 Å for T = 300 K, 3.2 Å and 4.8 Å for T = 240 K, and 3.1 Å and 4.9 Å for T = 210 K. The third RDF for  $g_{\text{ClCl}}(r)$  is noted with first peak at 3.9 Å and second peak at 5.1 Å at T = 300 K; only one peak of Cl-Cl is observed at 5.1 Å at T = 240 K and at T = 210 K. This is an indication that Cl<sup>-</sup> ions' hydration shell is more structured in supercooled water. Overall, for  $R = 24$  the structure is more stable as a function of time because at the presence of large amount of Cl, stable network is formed which is preserved upon cooling. In addition, this is a very good potential because it does not have cluster of Cl.

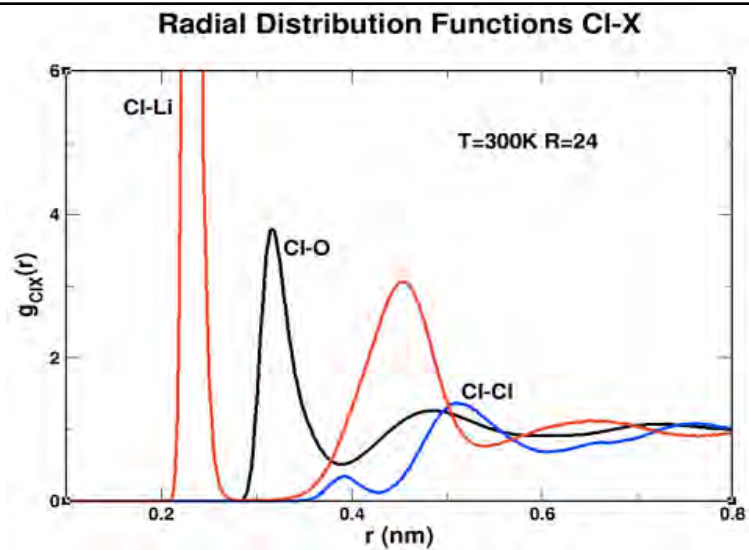
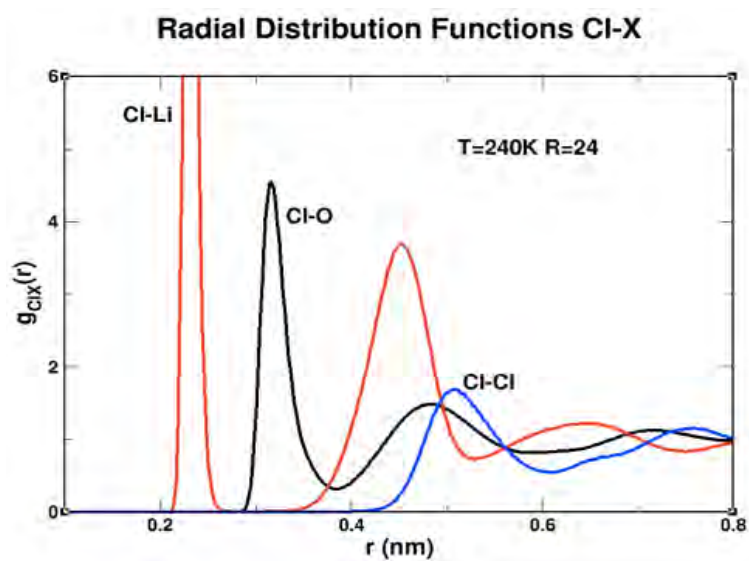
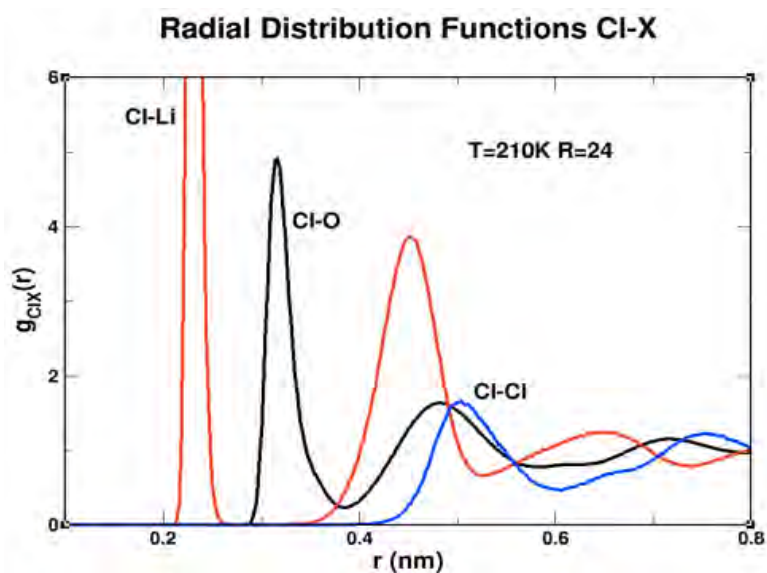
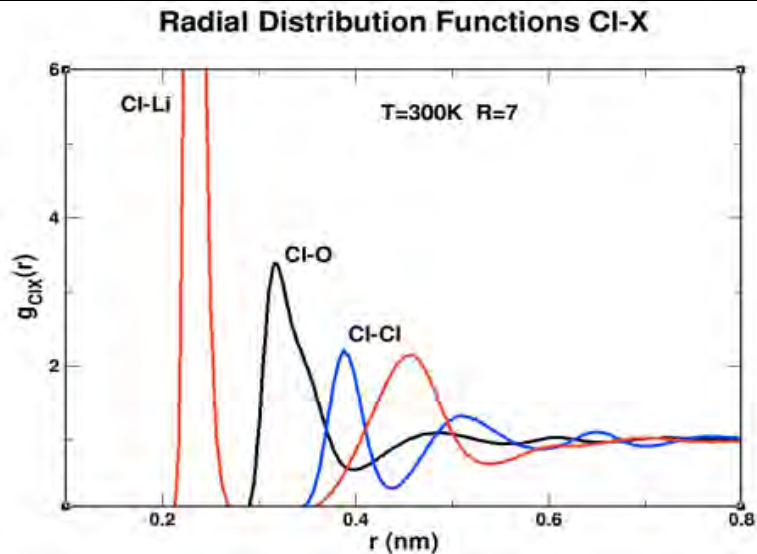
(a)  $g_{\text{Cl-X}}(r)$  for  $T = 300$  K(b)  $g_{\text{Cl-X}}(r)$  for  $T = 240$  K(c)  $g_{\text{Cl-X}}(r)$  for  $T = 210$  K

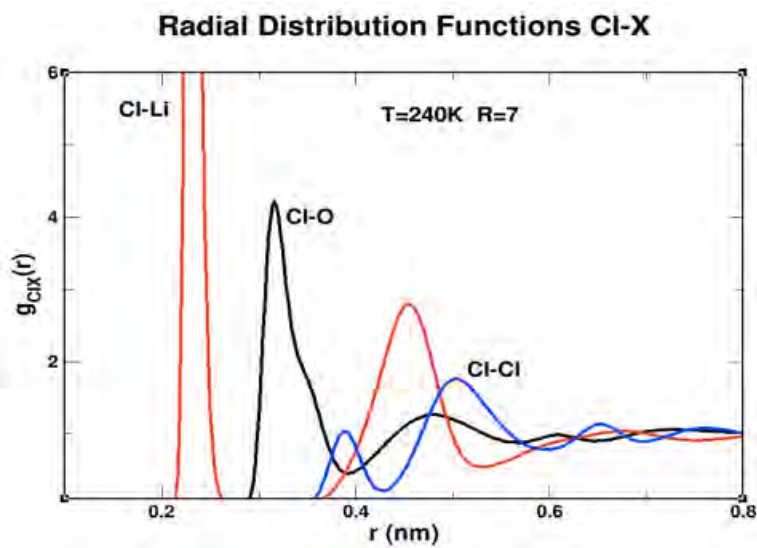
Figure 7: RDFs for Cl-X at  $R = 24$  at three different temperatures and pressure of 1 bar for Cl-Li (red line), Cl-O (black line), and Cl-Cl (blue line).

For concentrated  $R = 7$  the RDFs,  $g_{\text{Cl-X}}(r)$ , are shown in Figure 8. At  $T = 300$  K the first peak of Cl-Li at 2.3 Å is very pronounced while second peak at 4.6 Å is less pronounced than at lower temperatures. Similarly, the two peaks for Cl-O (3.2 Å and 4.8 Å) are lower at this higher temperature than at lower ones. The longer-distanced Cl-Cl peaks (3.9 Å and 5.1 Å) are interesting as the first is much higher at this temperature than at the lower ones. At  $T = 240$  K the first Cl-Li peak at 2.3 Å is high while the second peak at 4.6 Å is higher, just as the peaks for Cl-O (3.2 Å and 4.8 Å). Here the Cl-Cl peaks are different with first (3.9 Å) being smaller and second (5.1 Å) being taller and wider. Finally, at  $T = 210$  K the Cl-Li peaks (2.3 Å and 4.6 Å) are higher than at higher temperatures; Cl-O peaks (3.2 Å and 4.8 Å) are also higher and more pronounced, and Cl-Cl peaks much smaller at 3.9 Å and slightly higher at 5.0 Å. Thus, for Cl-Cl first peak is much higher at higher temperature and is significantly shrank upon supercooling. Since in the supercooled and glassy water  $\text{Cl}^-$  tends to form a rigid hydration shell, it is feasible to deduct that big structural change occurs with a change in temperature which must be reflected in the structure of water.

(a)  $g_{\text{Cl-X}}(r)$  for  $T = 300$  K



(b)  $g_{\text{Cl-X}}(r)$  for  $T = 240$  K



(c)  $g_{\text{Cl-X}}(r)$  for  $T = 210$  K

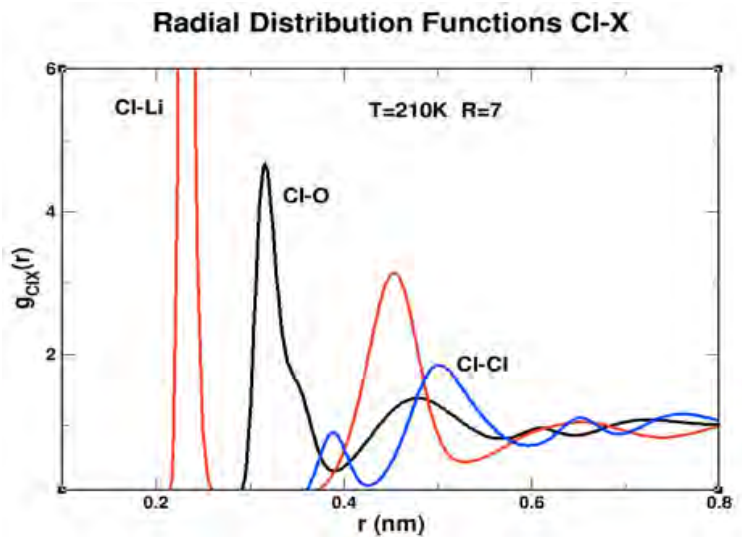


Figure 8: RDFs for Cl-X at  $R = 7$  at three different temperatures and pressure of 1 bar for Cl-Li (red line), Cl-O (black line), and Cl-Cl (blue line).

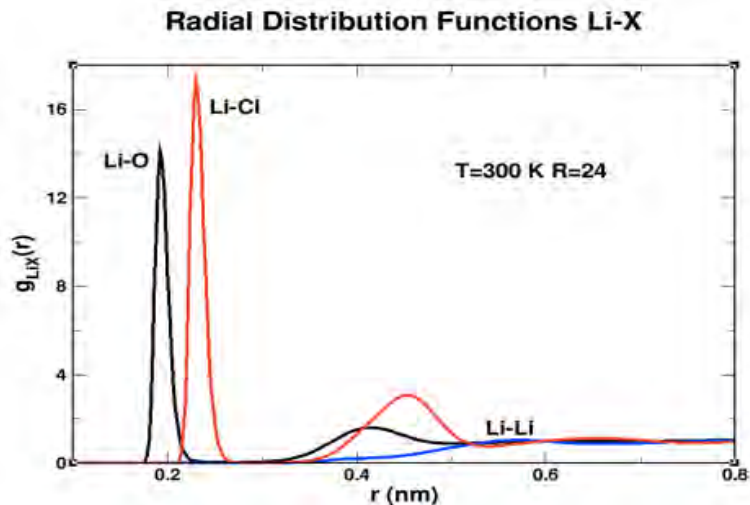
### 5.3.2 RDFs for Li-X

In case of the nearest neighbours of  $\text{Li}^+$  ions, the first coordination shell of lithium ions consists of water molecule and chloride ions at both concentrations, i.e., clearly established shell of Li atoms is formed around oxygen, followed by the sharp high peak of Li-Cl and a barely pronounced shallow peak for Li-Li for both concentrations at three temperatures, as seeing in Figure 9 for  $R = 24$ .

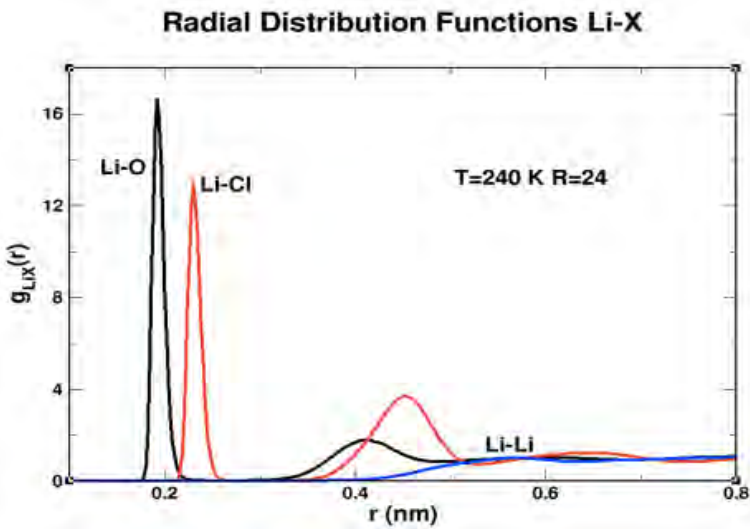
For  $R = 24$  at all three temperatures,  $T = 300$  K,  $T = 240$  K and  $T = 210$  K, the  $g_{\text{LiO}}(r)$  and  $g_{\text{LiCl}}(r)$  curves have well-defined first peaks (around  $r_{\text{max,LiO}}$  and  $r_{\text{max,LiCl}}$ ) at 1.9 Å and 2.3 Å, respectively, followed by a region where the neighbouring particles are completely missing. Thus, the  $N_{\text{LiO}}$  and  $N_{\text{LiCl}}$  coordination numbers (the number of the particles in the first coordination shell, a.k.a. the number of the nearest neighbours) is determined by counting particles up to the first minimum of the curves ( $r_{\text{min,LiO}}$  and  $r_{\text{min,LiCl}}$ ). The second maxima for both Li-O and LiCl at 4.1 Å and 4.5 Å, respectively, are much lower at three temperatures. The total coordination number of  $\text{Li}^+$  is the sum of the two values,  $N_{\text{Li}} = N_{\text{LiO}} + N_{\text{LiCl}}$  and is determined to be 4 which is consistent with experimental results. Notably, the  $r_{\text{max,LiCl}}$  is higher at  $T = 300$  K, lower at  $T = 240$  K and slightly higher at  $T = 210$  K. It represents the orientation of  $\text{H}_2\text{O}$  molecules in hydration shells of ions. Also, the separation between first and second Li-Cl peaks indicates the presence of  $\text{H}_2\text{O}$  molecule between two ions. Finally,

the lone peak of Li-Li at 5.7 Å for all three temperatures indicates that it is less structured system in which ions are moving freely.

(a)  $g_{\text{Li-X}}(r)$  for  $T = 300$  K



(b)  $g_{\text{Li-X}}(r)$  for  $T = 240$  K



(c)  $g_{\text{Li-X}}(r)$  for  $T = 210$  K

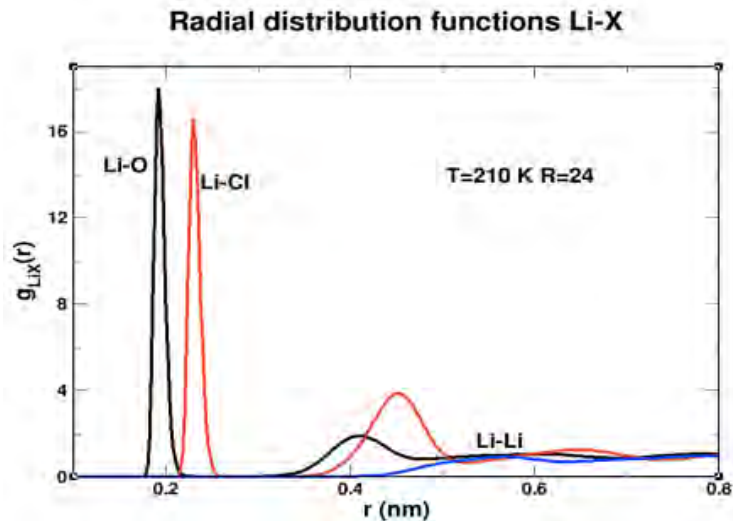
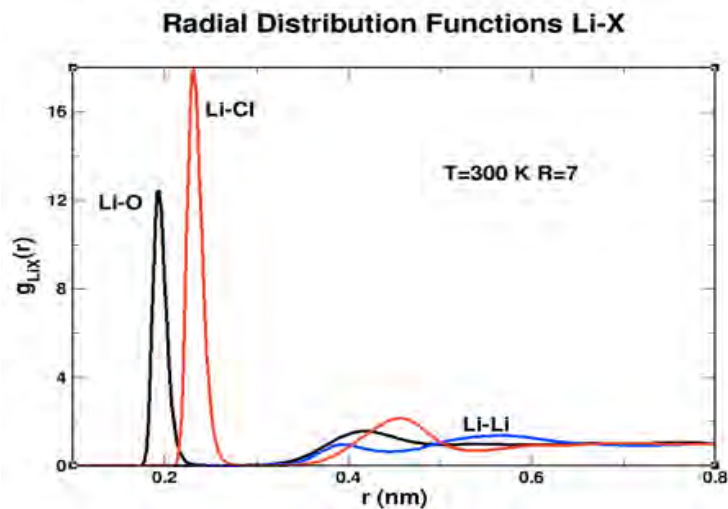


Figure 9: RDFs for Li-X at  $R = 24$  at three different temperatures and pressure of 1 bar for Li-O (black line), Li-Cl (red line), and Li-Li (blue line).

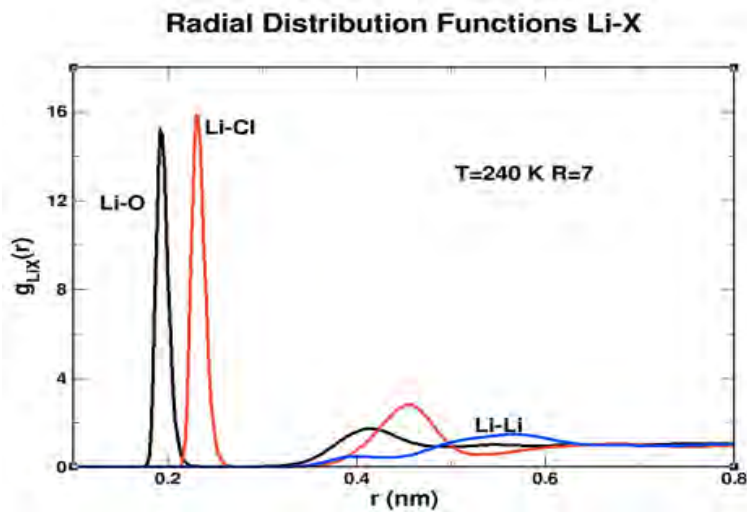
Figure 10 contains  $g_{\text{Li-X}}(r)$  for higher concentration of  $R = 7$  at three temperatures similar scenario occurs, i.e., the  $g_{\text{LiO}}(r)$  and  $g_{\text{LiCl}}(r)$  curves have well-defined first peaks (around  $r_{\text{max,LiO}}$  and  $r_{\text{max,LiCl}}$ ) at 1.9 Å and 2.3 Å, respectively, followed by a region where the neighbouring particles are completely missing. The second maxima for the  $g_{\text{LiO}}(r)$  and  $g_{\text{LiCl}}(r)$  shallow curves occur at 4.2 Å and 4.6 Å, once again, indication coordination number of  $\text{Li}^+$  to be 4. At higher temperature the first maximum is higher, at low temperature is lower and at supercooled temperature is even lower. This may be related to the fact that the first hydration shell of  $\text{Li}^+$  becomes ordered at high temperature and the number of oxygens in the first coordination shell of Li is decreasing and the number of  $\text{Cl}^-$  ions is increasing as the concentration increases. Finally, similar to  $R = 24$ , the Li-Li peaks for all three temperatures are shifted far to the right of spectrum away from Li-O and Li-Cl peaks and are barely pronounced at 4.0 Å. This also indicates that there are more ions moving around and when comparing  $R = 24$  and  $R = 7$  potentials, not much change is observed.

Moreover, since here is not much change in potentials with change in temperature, this indicates great confirmation of a trend.

(a)  $g_{\text{Li-X}}(r)$  for  $T = 300$  K



(b)  $g_{\text{Li-X}}(r)$  for  $T = 240$  K



(c)  $g_{\text{Li-X}}(r)$  for  $T = 210$  K

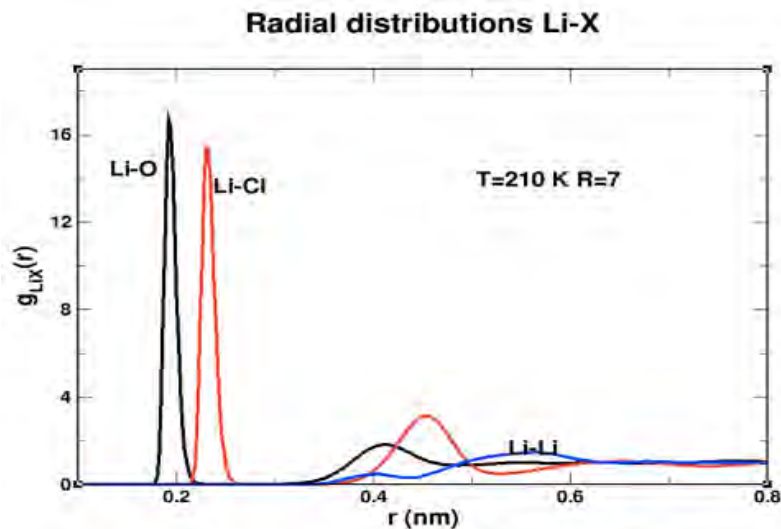
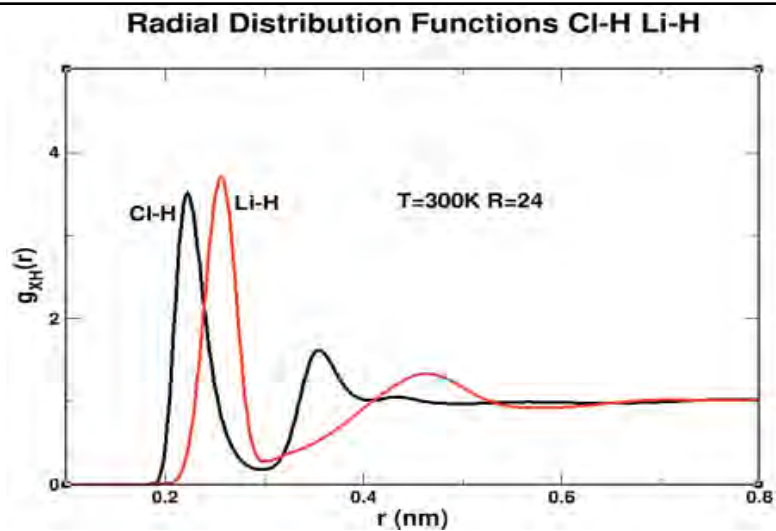


Figure 10: RDFs for Li-X at  $R = 7$  at three different temperatures and pressure of 1 bar for Li-O (black line), Li-Cl (red line), and Li-Li (blue line).

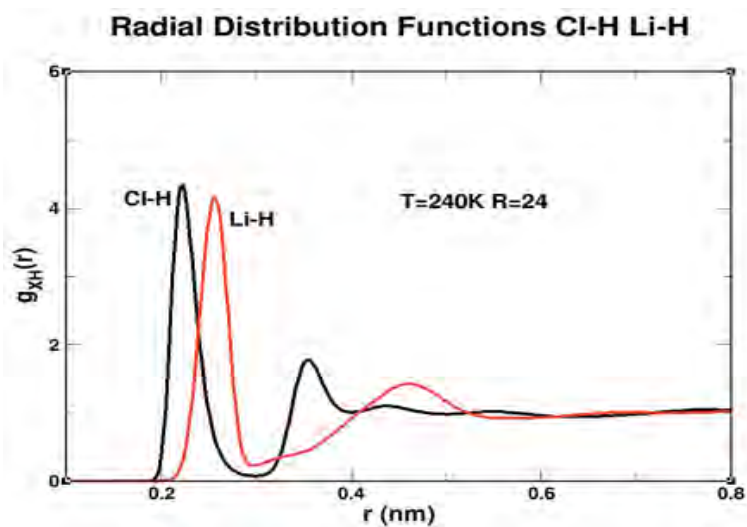
### 5.3.3 RDFs for ion-H

For  $R = 24$  in all three temperatures (Figure 11) the  $\text{Cl}^- - \text{H}$  pairs result in the first peak of  $g_{\text{ClH}}(r)$  at  $2.2 \text{ \AA}$ . The boundary of the shell is not well defined at  $T = 300 \text{ K}$  as in case of the Li-O and Li-Cl because  $g_{\text{ClH}}(r)$  is not equal zero at any  $r$  distance. Thus, the uncertainty of the  $N_{\text{ClH}}$  coordination number is higher. Nevertheless, given that the second peak for Cl-H is located at  $3.6 \text{ \AA}$ , the coordination number of  $\text{H}^+$  is 2. For  $g_{\text{LiH}}(r)$  the peaks are located at  $2.6 \text{ \AA}$  and  $4.6 \text{ \AA}$  resulting in higher coordination number. Overall, the peaks for both, Cl-H and Li-H look very much alike across the temperature range, i.e., their heights shapes and shoulders are close enough. Hence, at this concentration the decrease in temperature does not produce any changes in RDFs. Also, similar to ion-O, the location of first maximum of ion-H represents orientation of  $\text{H}_2\text{O}$  molecules in hydration shells of ions.

(a)  $g_{X-H}(r)$  for  $T = 300$  K



(b)  $g_{X-H}(r)$  for  $T = 240$  K



(c)  $g_{X-H}(r)$  for  $T = 210$  K

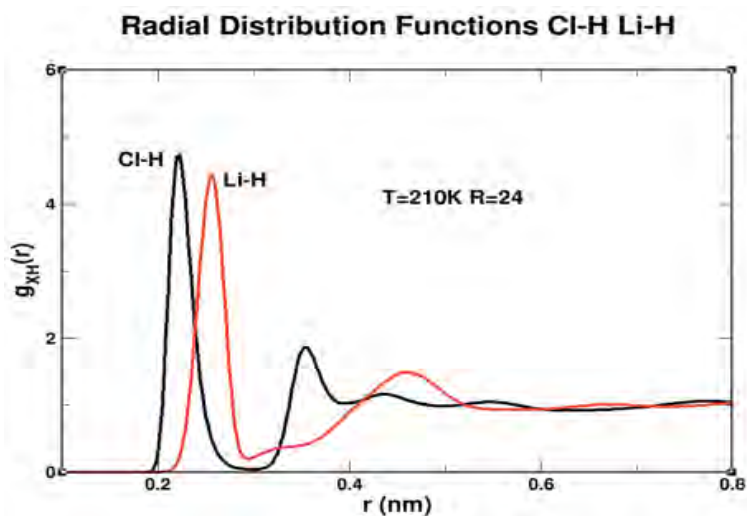
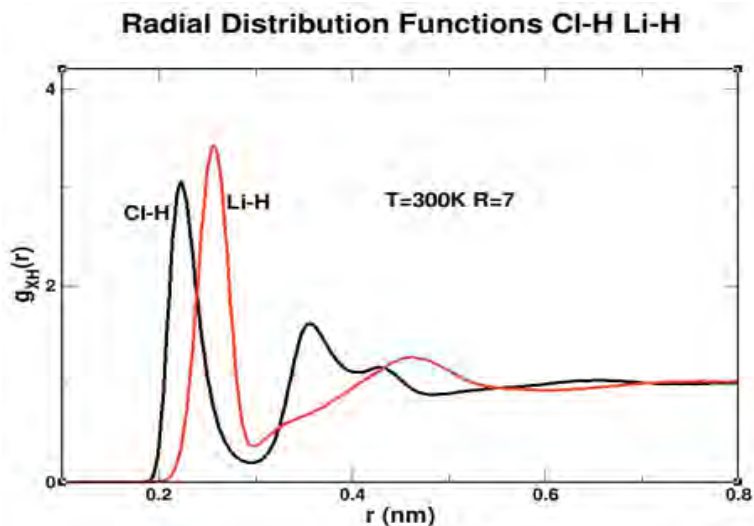


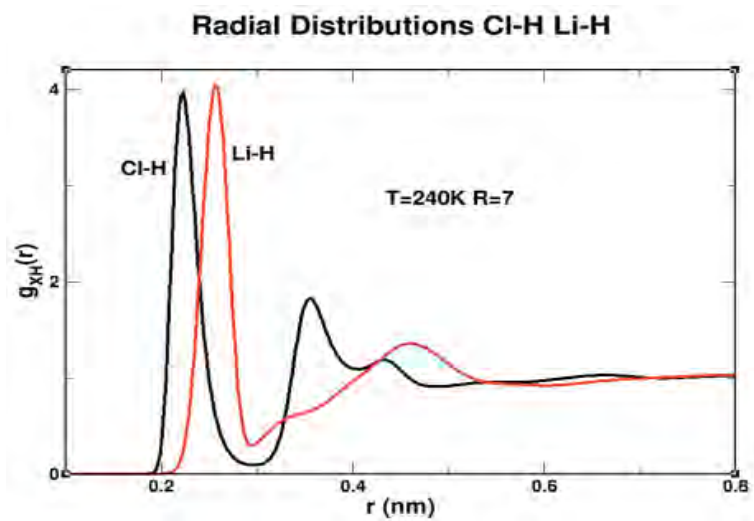
Figure 11: RDFs for X-H at  $R = 24$  at three different temperatures and pressure of 1 bar for Cl-H (black line) and Li-H (red line).

For  $g_{X-H}(r)$  for  $R = 7$  (Figure 12), at all three temperatures two peaks are observed for both, Cl-H at 2.2 Å and 3.6 Å and Li-H at 2.6 Å and 4.6 Å, resulting in similar scenario as for lower concentration. Although, the maxima of the peaks are registered at the same positions, the height of the peaks is clearly lower for the high temperature, high for the intermediate temperature and mid-high for the coldest system. However, overall, there is not much difference in  $R = 24$  and  $R = 7$  potentials with change in temperature.

(a)  $g_{X-H}(r)$  for  $T = 300$  K



(b)  $g_{X-H}(r)$  for  $T = 240$  K



(c)  $g_{X-H}(r)$  for  $T = 210$  K

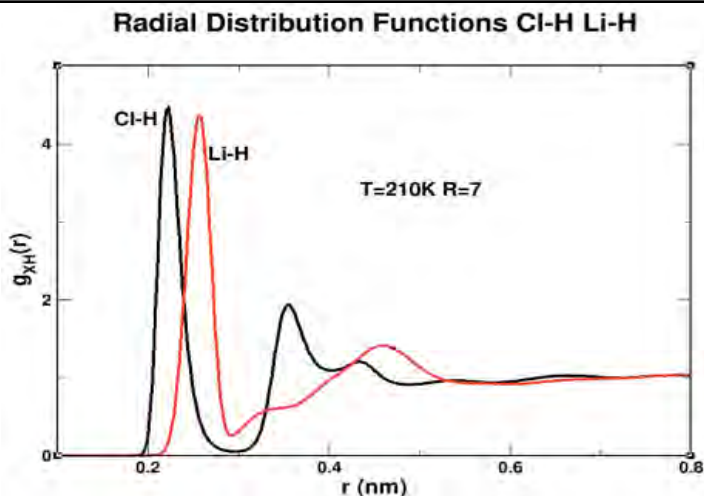


Figure 12: RDFs for X-H at  $R = 7$  at three different temperatures and pressure of 1 bar for Cl-H (black line) and Li-H (red line).

## 5.4 Calculations of structural trajectories and variables

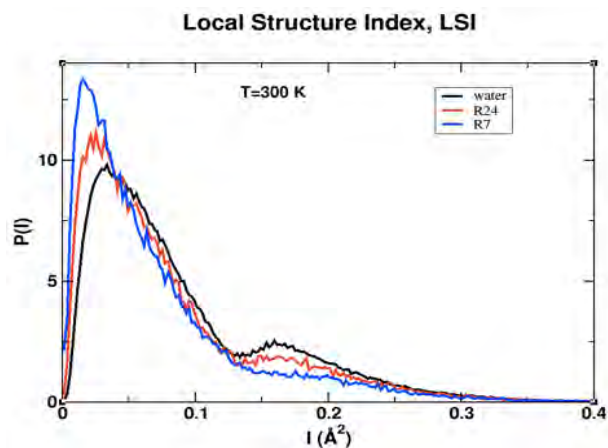
### 5.4.1 Local Structure Index, LSI

The Local Structure Index (LSI) aims to measure the extent of the gap between the first and the second hydration shells surrounding water molecule and is abbreviated as  $P(I)$ . The LSI focuses on translational order and probes local structure beyond the first hydration shell (Section 3.5.2.3). The LSI analysis has been performed on the inherent structures (IS) of supercooled water and aqueous solutions, the IS are obtained by quenching the systems to extremely low temperatures.

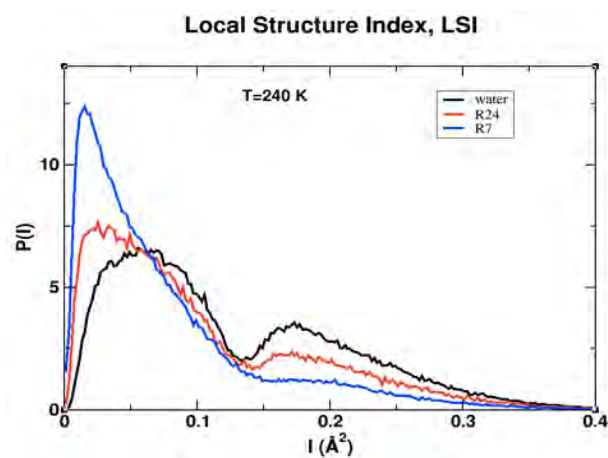
The probability density  $P(I)$  of finding a molecule with local structure index  $I$  for water, and dilute and concentrated aqueous LiCl solutions in the study for three temperatures used in the analysis are shown in Figure 13. As a rule, the peak that is located on the right in the plot represents LDL; and the peak found to the left indicates HDL.

Complete data for  $P(I)$  for water, LiCl:24H<sub>2</sub>O and LiCl:7H<sub>2</sub>O systems at  $T = 300$  K,  $T = 240$  K and  $T = 210$  K is given in Appendix E, Tables 13 through 17.

(a)  $P(I)$  for  $T = 300$  K



(b)  $P(I)$  for  $T = 240$  K



(c)  $P(I)$  for  $T = 210$  K

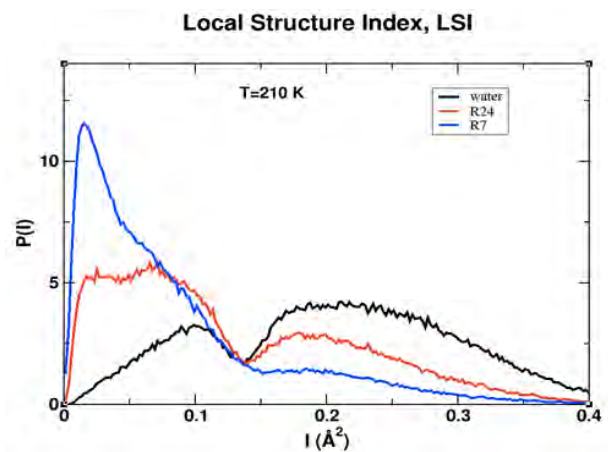


Figure 13:  $P(I)$  at three different temperatures and pressure of 1 bar for bulk water (black line),  $R = 24$  (red line), and  $R = 7$  (blue line).

For  $T = 300$  K bulk water shows a first peak at  $0.03 \text{ \AA}^2$  and a second peak at  $0.16 \text{ \AA}^2$ ; for  $R = 24$  the first peak is also located at  $0.03 \text{ \AA}^2$  but it is higher with respect to bulk water. Instead, the second peak at  $0.18 \text{ \AA}^2$  is lower than the second peak in bulk water. For  $R = 7$  it is found a first very tall peak at  $0.02 \text{ \AA}^2$  and a very shallow tale-like second peak at  $0.20 \text{ \AA}^2$ . Overall, at this temperature for all three species the HDL component is dominant, particularly for  $R = 7$  for which LDL is almost absent.

Upon cooling at intermediate temperature  $T = 240$  K, behaviour of all three systems is different as all first three peaks at  $I = 0.06 \text{ \AA}^2$  for water, and shorter at  $I = 0.03 \text{ \AA}^2$  for  $R = 24$  and  $I = 0.02 \text{ \AA}^2$  for  $R = 7$  and the second peaks become higher and more pronounced. The second peaks at  $0.17 \text{ \AA}^2$  for water and  $R = 24$  shows clear strong increase of the LDL. Also, since the second peak for  $R = 7$  ( $I = 0.20 \text{ \AA}^2$ ) is much larger with respect to bulk the HDL is already dominating at this intermediate temperature.

When the system is further cooled and becomes supercooled at  $T = 210$  K, the behaviour of all three systems becomes very different. What is interesting is that water's first peak at  $0.10 \text{ \AA}^2$  is much lower and wider while very pronounced taller and much wider second peak at  $0.22 \text{ \AA}^2$  clearly indicates the presence and dominance of LDL. Similarly, for  $R = 24$  the first (taller than water) peak at  $0.07 \text{ \AA}^2$  indicates presence of HDL while rather pronounced second peak at  $0.20 \text{ \AA}^2$  (shoulder than that of water) also confirms the LDL nature. For  $R = 7$ , although lower than for preceding temperatures, the big peak at  $0.02 \text{ \AA}^2$  clearly indicates the dominance of HDL. This implies that the liquid  $R = 7$  introduces novel configuration for water is in the HDL state with very little amount of LDL water.

For all three temperatures and for all three systems, lower values of the first peaks indicate molecules with very defective tetrahedral order and high-local density; whereas higher values of the second peaks imply that the molecules are characterized by better tetrahedral local order and a low-local density.

For a visual comparison of the behaviour of each solution as a function of temperature, Figure 14 contains LSI's for LiCl:24H<sub>2</sub>O and LiCl:7H<sub>2</sub>O systems at T = 300 K, T = 240 K and T = 210 K.

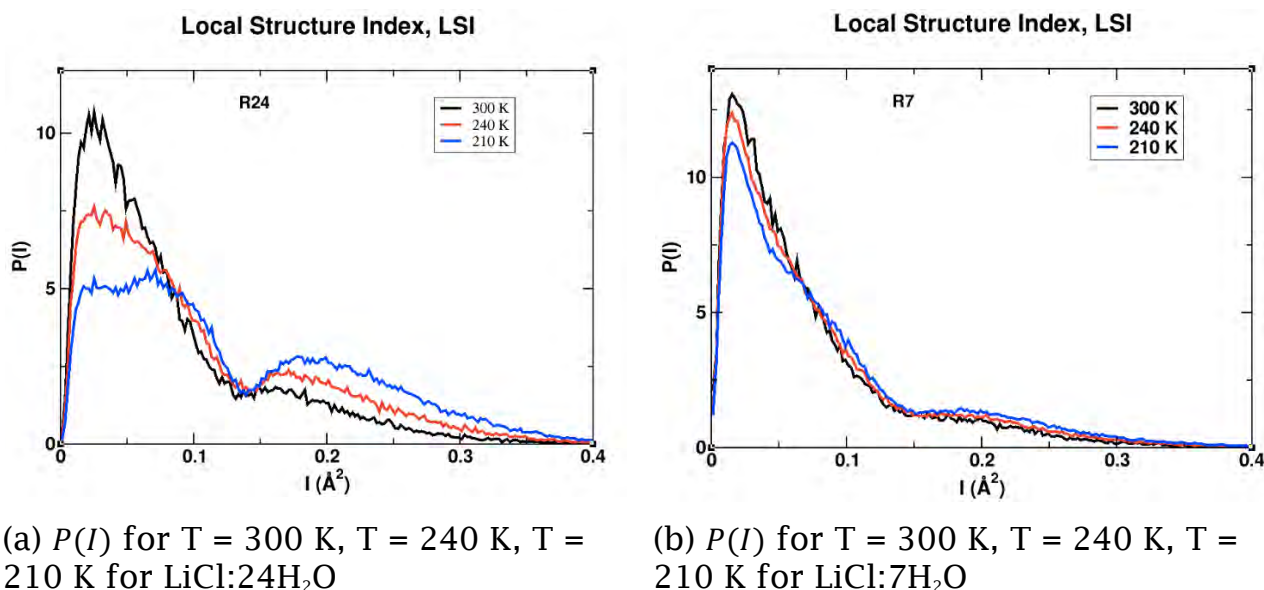


Figure 14:  $P(I)$  for LiCl:24H<sub>2</sub>O and LiCl:7H<sub>2</sub>O systems at T = 300 K (black), T = 240 K (red) and T = 210 K (blue).

For  $R = 24$  at all three temperatures the HDL is present with higher content at T = 300 K, lesser content at the intermediate T = 240 K, and lower content at T = 210 K. The second peaks, reflecting the presence of LDL, are higher for the lower temperature, medium for intermediate and lower for higher temperature. The behaviour of  $R = 7$  system is very different and very interesting. Here, the HDL maxima for all three temperatures is

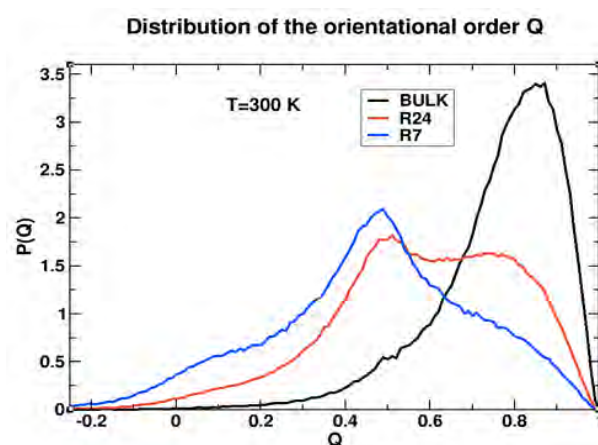
clearly pronounced at  $0.02 \text{ \AA}^2$  with  $T = 300 \text{ K}$  being the highest and  $T = 210 \text{ K}$  the lowest in probability but the distribution shows mild dependence on temperature.

#### 5.4.2 Tetrahedral Parameter, $P(Q)$

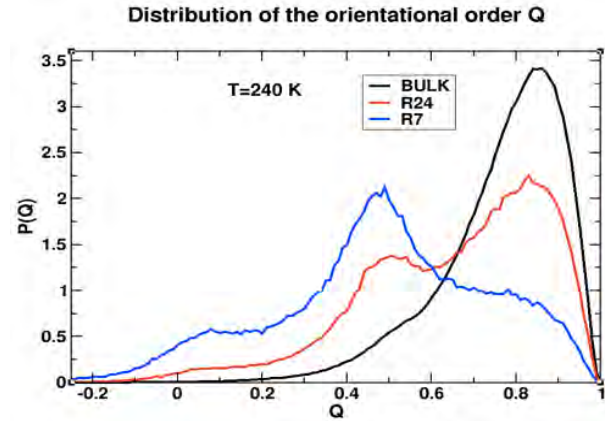
The Tetrahedral Parameter,  $P(Q)$ , a.k.a. Orientation Tetrahedral Order (OTO) is the angular tetrahedral order parameter which measures the local inner structure in the first coordination shell of water (Section 3.5.2.2) and focuses on the four nearest water oxygen neighbours. Parameter  $Q$  ranges from 0 to 1 and is only sensitive to the angular order. In analysis of  $P(Q)$ , bulk water is always used as a point of reference.

Figure 15 presents probability density  $P(Q)$  of finding a molecule with tetrahedral index  $Q$  for bulk, LiCl:24H<sub>2</sub>O and LiCl:7H<sub>2</sub>O solutions at  $T = 300 \text{ K}$ ,  $T = 240 \text{ K}$  and  $T = 210 \text{ K}$ . Complete data for  $P(Q)$  for bulk, LiCl:24H<sub>2</sub>O and LiCl:7H<sub>2</sub>O systems at  $T = 300 \text{ K}$ ,  $T = 240 \text{ K}$  and  $T = 210 \text{ K}$  is given in Appendix F, Tables 18 through 21.

(a)  $P(q)$  for  $T = 300 \text{ K}$



(b)  $P(q)$  for  $T = 240$  K



(c)  $P(q)$  for  $T = 210$  K

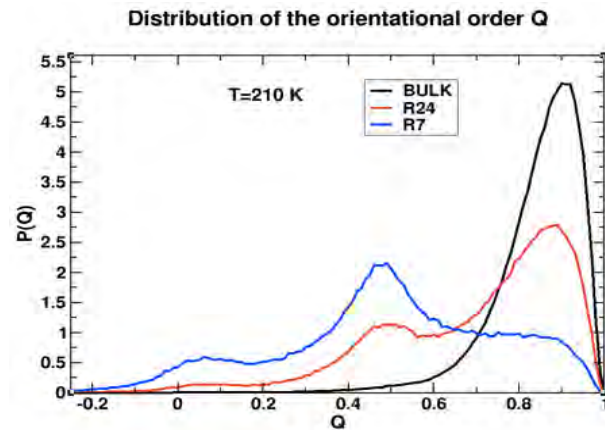


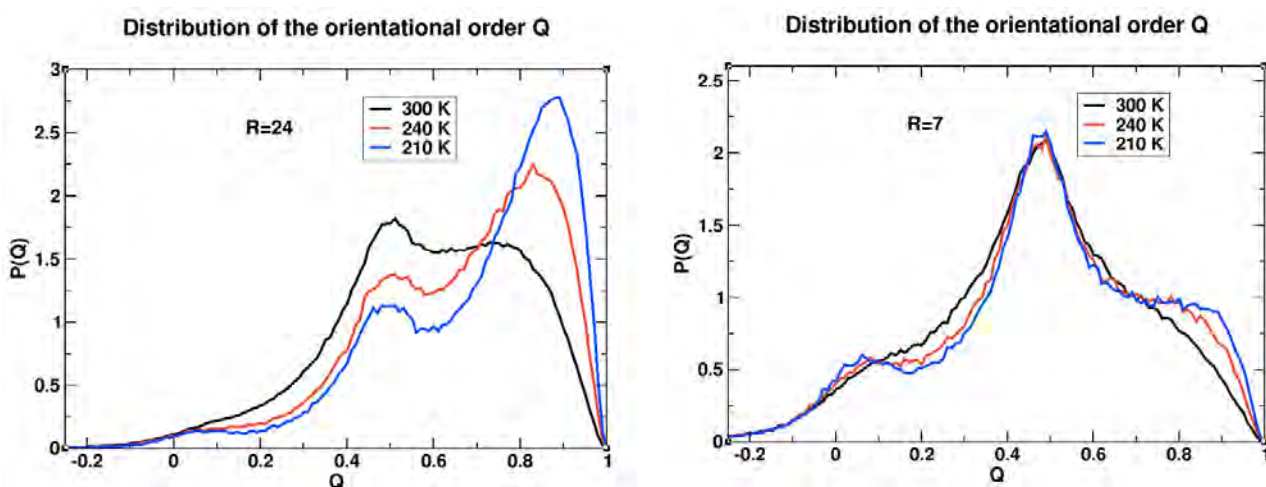
Figure 15:  $P(Q)$  at three different temperatures and pressure of 1 bar for bulk water (black line),  $R = 24$  (red line), and  $R = 7$  (blue line).

For  $T = 300$  K, bulk has a high single peak at  $Q = 0.87$ , whether  $R = 24$  has two very broad peaks at  $Q = 0.50$  and  $0.75$ ; and  $R = 7$  has one pronounced wide peak at  $Q = 0.49$ . For  $T = 240$  K, bulk also has only one wide and tall peak at  $Q = 0.85$ ;  $R = 24$  has two wide and shorter peaks at  $Q = 0.51$  and  $0.83$ ; and  $R = 7$  has one wide peak at  $Q = 0.49$ . For  $T = 210$  K, bulk has only one sharp and tall peak at  $Q = 0.91$ ;  $R = 24$  has two short and taller peaks at  $Q = 0.49$  and  $0.89$ ; and  $R = 7$  has two even shorter and wider peaks at  $Q = 0.06$  and  $0.48$ .

Hence, when passing from higher temperature at  $T = 300$  K to supercooled temperature of  $T = 210$  K, bulk becomes more tetrahedral. The tetrahedrality also remains for  $R = 24$  when cooling from  $T = 300$  K to  $T =$

210 K. The peak around 0.48 at both temperatures is indicative of the presence of interstitial  $\text{H}_2\text{O}$  and relates to bulk water while the peak around 0.06 which is closer to 0 is present as a result of ions. Similarly, weaker tetrahedrality remains for  $R = 7$  with three peaks - second being  $\sim 0.50$  as an indication of interstitial  $\text{H}_2\text{O}$ .

Figure 16 shows the distribution of the orientational order,  $Q$ , for  $\text{LiCl}:24\text{H}_2\text{O}$  and  $\text{LiCl}:7\text{H}_2\text{O}$  systems at  $T = 300\text{ K}$ ,  $T = 240\text{ K}$  and  $T = 210\text{ K}$ .



(a)  $P(Q)$  for  $T = 300\text{ K}$ ,  $T = 240\text{ K}$ ,  $T = 210\text{ K}$  for  $\text{LiCl}:24\text{H}_2\text{O}$

(b)  $P(Q)$  for  $T = 300\text{ K}$ ,  $T = 240\text{ K}$ ,  $T = 210\text{ K}$  for  $\text{LiCl}:7\text{H}_2\text{O}$

Figure 16: Distribution of the orientational order,  $Q$ , for  $\text{LiCl}:24\text{H}_2\text{O}$  and  $\text{LiCl}:7\text{H}_2\text{O}$  systems at  $T = 300\text{ K}$  (black),  $T = 240\text{ K}$  (red) and  $T = 210\text{ K}$  (blue).

As seen in Figure 16 (a) for  $\text{LiCl}:24\text{H}_2\text{O}$  system, the tetrahedrality is lesser at  $T = 300\text{ K}$  (broad distribution) and is increased for the supercooled  $T = 210\text{ K}$ . Figure 16 (b) shows an interesting picture of the  $\text{LiCl}:7\text{H}_2\text{O}$  system's tetrahedrality as for all three temperatures there is one strong peak at  $\sim 0.50$ . Once again, here is a good indication of interstitial  $\text{H}_2\text{O}$  at all three temperatures. Overall, this is the configuration that water adopts is

influenced by the presence of ions and the appeared peak is slightly related to ions. This is more evident at higher concentration.

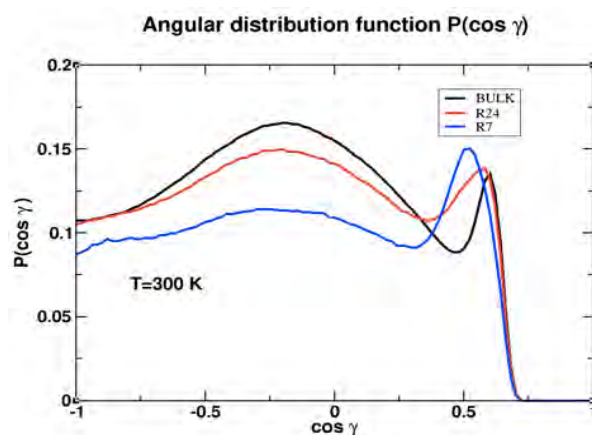
## 5.5 Hydrogen Bond network

### 5.5.1 Angular Distribution Function, $P(\cos \gamma)$

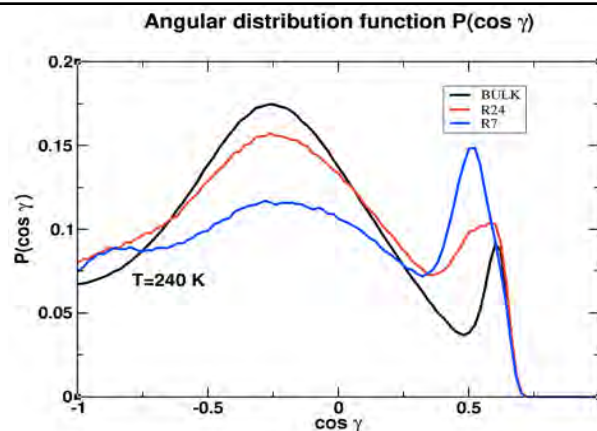
Angular Distribution Function,  $P(\cos \gamma)$  measures the H – O ... O angle between three water molecules (Section 3.5.2.4). In bulk water, particularly at low temperature, the  $\cos \gamma$  is anticipated to have a defined peak at approximately tetrahedral value of  $\gamma = 109.5^\circ$  and a secondary peak at about  $54^\circ$  occurring in interstitial  $\text{H}_2\text{O}$  molecules.

The resulting water angular distribution  $P(\cos \gamma)$  in  $\text{LiCl}:24\text{H}_2\text{O}$  and  $\text{LiCl}:7\text{H}_2\text{O}$  solutions at  $T = 300 \text{ K}$ ,  $T = 240 \text{ K}$  and  $T = 210 \text{ K}$  are shown in Figure 17. Complete data for Angular Distribution Function  $P(\cos \gamma)$  for bulk,  $\text{LiCl}:24\text{H}_2\text{O}$  and  $\text{LiCl}:7\text{H}_2\text{O}$  systems at  $T = 300 \text{ K}$ ,  $T = 240 \text{ K}$  and  $T = 210 \text{ K}$  is given in Appendix G, Tables 22 through 26.

(a)  $P(\cos \gamma)$  for  $T = 300 \text{ K}$



(b)  $P(\cos \gamma)$  for  $T = 240$  K



(c)  $P(\cos \gamma)$  for  $T = 210$  K

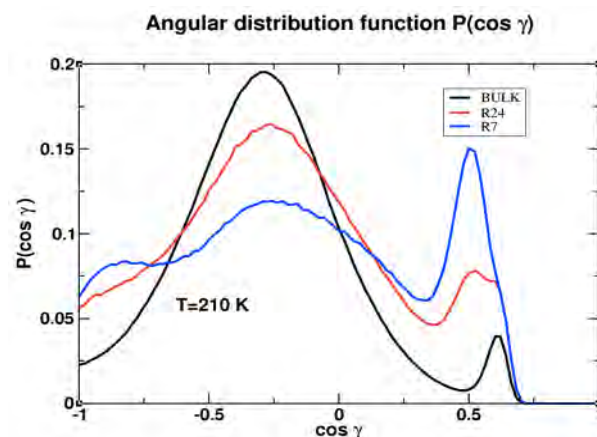


Figure 17: Normalized angular distribution function  $P(\cos \gamma)$  of the angle between oxygen of three nearest neighbour water molecules at three different temperatures and pressure of 1 bar for bulk water (black line),  $R = 24$  (red line), and  $R = 7$  (blue line).

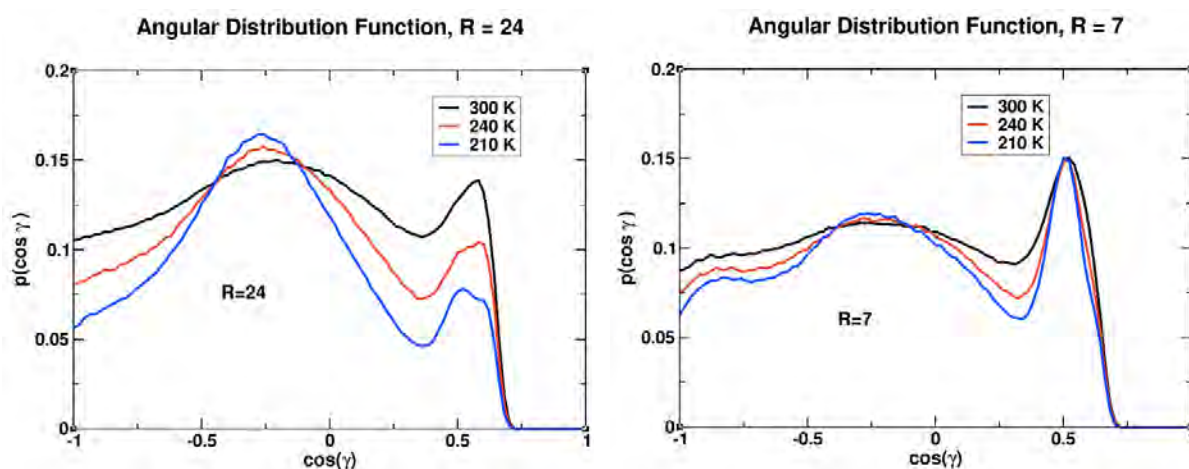
At  $T = 300$  K, the first peaks for all, bulk,  $R = 24$  and  $R = 7$ , are narrow and wide with bulk being the tallest maximum at  $100.4^\circ$ , second tallest for  $R = 24$  at  $101.5^\circ$  and shortest one for  $R = 7$  at  $100.4^\circ$ . The second peaks at this high temperature are much sharper and narrower, i.e., sharp lower peak at  $53.1^\circ$  for bulk, higher one at  $54.5^\circ$  for  $R = 24$  and tall sharp peak at  $59.3^\circ$  for  $R = 7$ . Notably, the second peak for  $R = 24$  at  $54.5^\circ$  suggests perfect tetrahedrality of the second shell. This second peak is interstitial and is characteristic of presence of more HDL.

At  $T = 240$  K, bulk also exhibits tetrahedral structure with pronounced high first peak at  $105.1^\circ$  and smaller sharp second peak at  $52.4^\circ$ . For  $R = 24$ , the first wide and pronounced peak is also found at  $105.1^\circ$  but it is shorter than that for bulk, while second, wider and taller than that for bulk, peak is found at  $53.1^\circ$ . Finally, for  $R = 7$ , the first, wide and lower than the other two, peak is seen at  $106.3^\circ$  and the second, sharper and taller, peak is seen at  $53.3^\circ$ . Notably, the first peak here at  $106.3^\circ$  is the closest to the tetrahedral value of  $\gamma = 109.5^\circ$  occurring in bulk  $\text{H}_2\text{O}$  molecules. Here, for both  $R = 24$  and  $R = 7$  two novel features are present. First, for both concentrations, second peaks - both at  $53.1^\circ$  are increasing, especially for higher concentration, i.e., with temperature decrease, the height of the peaks increases. Second, the angles of these second peaks are very low which is indicative of *electrostrictivity* for  $R = 7$ . This means that the angle between three molecules is very small, i.e., molecules are very tightly packed together, and the ions are somewhat squeezing water locally as opposed to oxygens of water being apart normally. Ions of this type are electrostrictive [275], i.e., they mimic the effect of applied pressure with their charge caused by anharmonicity of ion pair potential.

At  $T = 210$  K, the tetrahedral structure of water is also confirmed by the first peak of bulk at  $106.9^\circ$  and a second peak at  $52.4^\circ$  with the first peak being wide and tall and the second one being sharp and small. For  $R = 24$ , the tetrahedral structure is observed as well with wide and less tall first peak at  $105.7^\circ$  and wider and taller than bulk second peak at  $58.7^\circ$ . The behaviour of  $R = 7$  solution is very interesting at this temperature. The first main peak at  $105.1^\circ$  is low and wide, while the second peak at  $60.0^\circ$  is sharp and very tall. Overall, the values for the first peaks are close enough to that of bulk-like HBs indicating that these systems do indeed contain tetrahedral HB network. This indeed is intact with assumption that

tetrahedrality of the HB network is present in high concentration aqueous ionic solutions at low temperatures, and the solution is more LDL-like. As for the second peaks, the observed highly pronounced increase with decrease in temperature is indicative of a continuous trend of an electrostrictivity.

The normalized angular distribution function  $P(\cos \gamma)$  of the angle between oxygen of three nearest neighbour water molecules for  $R = 24$  is shown in Figure 18 (a) and for  $R = 7$  in Figure 18 (b).



(a)  $P(\cos \gamma)$  for  $T = 300$  K,  $T = 240$  K,  $T = 210$  K for  $\text{LiCl}:24\text{H}_2\text{O}$  (b)  $P(\cos \gamma)$  for  $T = 300$  K,  $T = 240$  K,  $T = 210$  K for  $\text{LiCl}:7\text{H}_2\text{O}$

Figure 18: normalized angular distribution function  $P(\cos \gamma)$  of the angle between oxygen of three nearest neighbour water molecules for  $R = 24$  and  $R = 7$  with  $T = 300$  K (black),  $T = 240$  K (red) and  $T = 210$  K (blue).

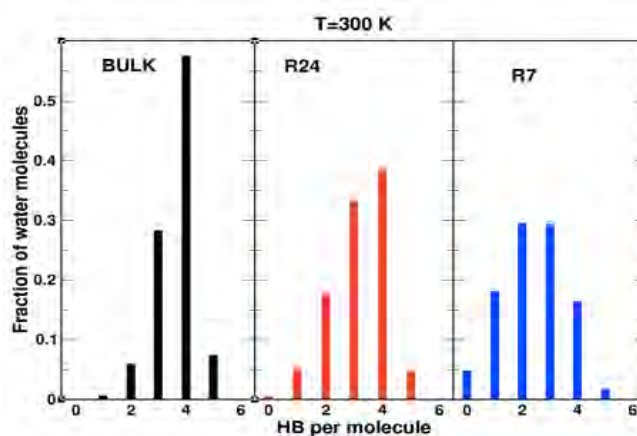
Once again, here of an interest the presence of tetrahedral value of  $\gamma$  at approximately  $109.5^\circ$  and a secondary peak at about  $54^\circ$  which occur in interstitial  $\text{H}_2\text{O}$  molecules. These values are taken as point reference values in the analysis and determining tetrahedrality. For  $R = 24$ , the tetrahedrality of the first peak is less than  $109.5^\circ$  yet getting closer to it at  $T = 210$  K. The second peak at both  $T = 300$  K and  $T = 240$  K is almost  $54^\circ$

(54.5°) which is in excellent agreement with hypothesized value. For  $R = 7$ , the angle value for the first peak (106.3°) at  $T = 240$  K is the closest to the reference value out of all. The values for the second peak at all three temperatures are nevertheless in the vicinity of the point reference value. Overall, Figure 18 depicts a strong signaling of tetrahedral structural arrangement for both concentrations at three temperatures.

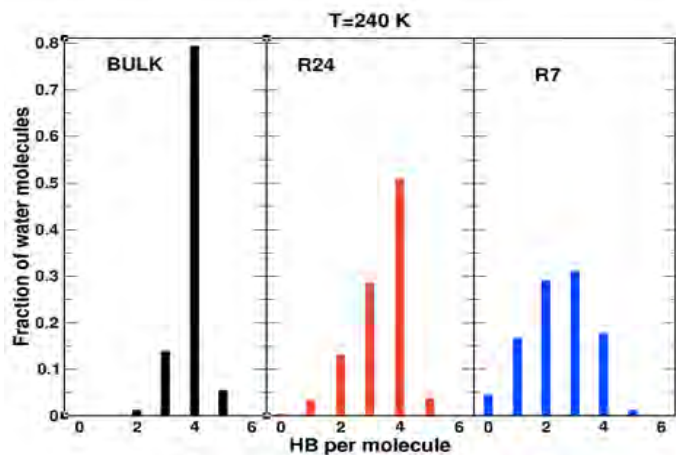
### 5.5.2 HBs distribution

By adopting the same geometry criterion as the one for the definition of HB between two water molecules where the O-O distance is less than 3.5 Å and the H – O...O angle is less than or equal to 30°, the distribution of HBs in the system was derived. Figure 19 contains graphical representation of the number of HBs per water molecule for bulk and both concentrations,  $R = 24$  and  $R = 7$ , at three temperatures. Complete data for bulk, LiCl:24H<sub>2</sub>O and LiCl:7H<sub>2</sub>O systems at  $T = 300$  K,  $T = 240$  K and  $T = 210$  K is given in Appendix H, Tables 27 through 29.

(a) HBs for  $T = 300$  K



(b) HBs for  $T = 240$  K



(c) HBs for  $T = 210$  K

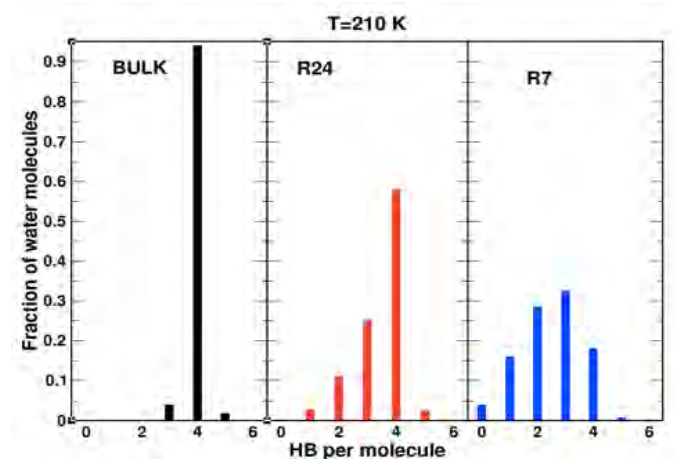


Figure 19: HBs distribution per molecule vs. fraction of water molecules for bulk (black), LiCl:24H<sub>2</sub>O (red) and LiCl:7H<sub>2</sub>O (blue) for three temperatures.

In Figure 19 (a) the distribution of water population engaged in  $n = 0, 1, 2, 3, 4, 5$  HBs with another water molecules is seen at  $T = 300$  K with five HBs with a maximum at  $n = 4$  for bulk and six HBs for both,  $R = 24$  and  $R = 7$ . In Figure 19 (b) for  $T = 240$  K, three  $n$ 's are present for bulk with  $n = 4$  being the tallest, and six HBs are present for  $R = 24$  and  $R = 7$ , respectively. Finally, in Figure 19 (c) for  $T = 210$  K, only three HBs are present for bulk with, once again, the tallest one being at position  $n = 4$  and six HBs are present for  $R = 24$  and  $R = 7$ . Overall, when comparing the trend of HBs distribution per molecule with temperature decrease from  $T = 300$  K down to  $T = 210$  K for bulk, the number of HBs decreases as the

---

temperature decreases and the height of the fraction of water molecules at  $n = 4$  increases with decrease in temperature. The other values of  $n$  for bulk are significantly diminished upon cooling. For  $R = 24$ , with the temperature drop the number of  $n$ 's remains the same and the fraction of water molecules decreases only slightly. Since two or three  $n$ 's are diminished, only two or three HBs are fully formed. Similar situation is seen for  $R = 7$ , but the fraction of water molecules is more decreased with decreased temperature. Again, only two or three HBs are formed which indicates potential distortion of water network in the solution since the fourth HB is missing. This indicates that the adopted in the study geometrical constraints are not met due to the higher angle in water molecule. This is to be regarded as the non-zero population of water is embodied in zero HB.

---

## Conclusion



Using MD simulations, the structural properties of water in correlations between water molecules and hydrated LiCl ions have been studied upon cooling [Bashta, I., Rovere, M. and Gallo, P. Structure of water in LiCl solutions versus salt concentration, interplay between low density and high density liquid. In preparation, 2022]. The MD simulations were performed for two concentrations - LiCl:24H<sub>2</sub>O and LiCl:7H<sub>2</sub>O under ambient pressure  $p = 1$  bar for temperatures ranging in the interval from 300 - 200 K. The intermolecular interactions of atoms and molecules contained in solution was described by the JC-TIP4P/2005 potential in which water is depicted with the four-site TIP4P/2005 potential. To better reproduce experimental properties of the system at ambient condition, the ion-ion interaction modified Lorentz-Berthelot mixing rules were implemented.

To investigate the TMD anomaly of water in the study, using two concentrations of LiCl was beneficial as the dilute  $R = 24$  solution exhibited TMD anomaly of water and the concentrated  $R = 7$  solution did not. This allows for comparative observations of their behaviour from

---

which the decision about what percentage of ions must be added into the solution in order to have water anomalies disappear.

Water interactions were examined by investigating correlation between TMD anomaly and ionic concentrations and structural properties of water were probed by corresponding RDFs,  $g_{OO}(r)$ ,  $g_{OH}(r)$ , and  $g_{HH}(r)$ .

For  $g_{OO}(r)$ , the HBs were preserved, the changes in the O-O correlations manifested a distortion of the HB network of water for  $R = 7$ . The modification of the second shell of the oxygen in other ionic solutions has already been confirmed and the effect of ions has been interpreted as an increase of pressure on water.

For  $g_{OH}(r)$ , in general, with higher increase of the density of the ions, more structural modifications occur. Notably, these modifications occurred from the third shell onwards. Overall, they were found to be connected to the HB as the first two shells remain similar in bulk water.

The  $g_{HH}(r)$  was found to behave similarly to the RDF of the O-H in aqueous solutions, i.e., in the solution the first peak is less-defined, and the consecutive shells show some difference with respect to bulk. These results display the preservation of the HBs between water molecules in the system.

Notably, the H-H correlations are indicative of the orientation correlation between the neighbouring pure water molecules. In this study, in the aqueous solution they remained essentially unchanged which means that the HBs between water molecules are preserved in the system, while the changes in the H-H correlations manifested a distortion of the HB network of water.

---

Further understanding of the structural properties of aqueous ionic solutions in this study was acquired by examining the RDFs for Cl-X, Li-X, where X are O and H, and ion-H for concentrated and dilute solutions in all the range of chosen temperatures.

For  $g_{\text{Cl-X}}(r)$ , the two concentrations were studied. Overall, for  $R = 24$  the structure was found to be more stable as a function of time because at the presence of large amount of Cl, stable network was formed which is preserved upon cooling. In addition, this is considered to be a very good potential because it does not have cluster of Cl. For  $R = 7$  the observed behaviour is as follows: since in the supercooled and glassy water  $\text{Cl}^-$  tends to form a rigid hydration shell, it is feasible to deduct that big structural change occurs with a change in temperature which must be reflected in the structure of water.

For  $g_{\text{Li-X}}(r)$ ,  $R = 24$  indicated that it is less structured system where ions are moving freely. In addition, this also indicated that there are more ions moving around and when comparing  $R = 24$  and  $R = 7$  results, not much change was observed.

For  $g_{\text{ion-H}}(r)$ , at  $R = 24$  concentration the decrease in temperature did not produce any changes in RDFs. Also, similar to the ion-O, the location of first maximum of the ion-H represented orientation of  $\text{H}_2\text{O}$  molecules in hydration shells of the ions. Overall, there were not much difference in  $R = 24$  and  $R = 7$  potentials with change in temperature observed.

In order to get more insight on the structure and properties of the LiCl aqueous solutions, the structural trajectories and variables were employed with the Local Structure Index, LSI, Tetrahedral Parameter,  $P(Q)$ , Angular Distribution Function,  $P(\cos \gamma)$  and HBs distribution.

The LSI for bulk water shows two peaks. The first peak represents HDL component and the second peak represents the LDL component. We see that upon increase of the ions concentration water loses tetrahedrality at both high and low temperatures. This loss of tetrahedrality becomes more evident at low temperatures while bulk water becomes locally very tetrahedral. In addition, for lower concentration of ions ( $R = 24$ ), the peak of LDL is still observed upon decrease in temperature although less than the in bulk. For higher concentration of ions ( $R = 7$ ) the two peaks practically do not change upon decrease in temperature meaning that the tendency to form the LDL is completely inhibited.

For the lower concentration, the structure of  $P(Q)$  at ambient temperature appears quite different from the bulk, yet similar to LSI upon decrease in temperature. The first tetrahedral peak grows and the peak corresponding to interstitial water peak around  $Q = 0.5$  decreases upon cooling. This confirms that water anomalies are still present. For the higher concentration, the  $P(Q)$  appears very different from bulk - it shows a third peak around  $Q = 0.1$ . The tetrahedral peak is very low and the overall shape is mildly dependent on temperature.

For angular distribution function,  $P(\cos \gamma)$ , we observe similar trend to that of the other two indicators. With  $P(\cos \gamma)$  we can relate the peaks directly to the angle among three oxygens and we see that as the concentration increases, the peak at 0.5 increases and shifts to the lower values with respect to bulk. In addition, it also sharpens and increases in intensity as the temperature decreases. These features tell us that water molecules are very tightly packed together, and the ions somewhat are squeezing water locally exerting electrostriction effect on water molecule and mimicking the effect of applied pressure with their charge caused by anharmonicity

---

of ion pair potential. Interestingly, this indicator,  $P(\cos\gamma)$ , is more sensitive to the modification of structure of water and we note that the tetrahedrality in water molecule does not appear to be disrupted even for higher concentration  $R = 7$ . Indeed, it shows more sensitivity in temperature for higher concentration. Overall, the fact that we show that water is still becoming more tetrahedral even at  $R = 7$ , might imply that the anomalies are still weakly present even for high LiCl concentration.

For the HBs distribution, overall, when increasing percent of ions in water, it becomes more HDL. Similar trend has been observed in NaCl [207, 208]. For  $R = 24$  solution the fraction of water molecules having less than 3 HBs becomes significant. Nonetheless, the number of water molecules having 4 HBs dominates upon cooling although less than in the bulk. In the  $R = 7$  solution the number of HBs is distributed prevalently between 1 and 4 but for this solution  $n = 2$  and  $n = 3$  dominate and the distribution does not substantially change with temperature.

In conclusion, the results presented in this thesis indicate how strong is the tendency of water to preserve its behaviour in spite of the strong influence exerted by LiCl ions. The tetrahedral network is only partially disrupted in  $R = 24$  solution, and even in  $R = 7$  solution we see some remains of tetrahedrality. These results point to the fact that water's anomalous behaviour is to be considered is also when water is in solution.

---

## References

- [1] Reece, J. B., Urry, L. A., Cain, M. L., Wasserman, S. A., Minorsky, P. V., Jackson, R. B. *Cambell Biology* (p.44). 10<sup>th</sup> Edition, Mass. Pearson Boston, 2013.
- [2] Henry, M. The State of Water in Living Systems: From the Liquid to the Jellyfish Cell. *Mol. Biol.* **51**, 677-702, 2005.
- [3] Caldecott, J. *Water: Life in Every Drop*. Virgin Digital, 2008.
- [4] Encrenaz, T. Water in the solar system. *Annu. Rev. Astron. Astrophys.*, **46**, 57-87, 2008.
- [5] Gallo, P. and Rovere, M. *Physics of Liquid Matter*. Elsevier, 2021.
- [6] Gallo, P., Amann-Winkel, K., Angell, C. A., Anisimov, M. A., Caupin, F., Chakravarty, C., Lascaris, E., Loerting, T., Panagiotopoulos, A. Z., Russo, J., Sellberg, J. A., Stanley, H. E., Tanaka, H., Vega, C., Xu, L., and Pettersson, L. G. M. Water: A Tale of Two Liquids. *Chem. Rev.* **116**, 7463-7500, 2016.
- [7] Chaplin, M. *Water Structure and Science*. 2016.
- [8] Poole, P. H., Bowles, R. K., Saika-Voivod, I., Sciortino, F. Free energy surface of ST2 water near the liquid-liquid phase transition. *J. Chem. Phys.* **138**, 034505, 2013.
- [9] Loerting, T., Salzmann, C., Kohl, I., Mayer, E., Hallbrucker, A. A second distinct structural "state" of high-density amorphous ice at 77 K and 1 bar. *Phys. Chem. Chem. Phys.* **3**, 5355, 2001.
- [10] Lina, C., Smitha, J. S., Sinogeikina, S. V., Shena, G. Experimental evidence of low-density liquid water upon rapid decompression. *PNAS* **115**, 2010-2015, 2018.
- [11] Bullock, G., Molinero, V. Low density liquid water is the mother of ice: on the relation between mesostructured, thermodynamics and ice crystallization in solutions. *Faraday Discuss.* **167**, 371, 2013.
- [12] Tanaka, H. A self-consistent phase diagram for supercooled water. *Nature* **380**, 328330, 1996.

- 
- [13] Smallenburg, F., Fillion, L., Sciortino, F. Erasing no-mans land by thermodynamically stabilizing the liquid-liquid transition in tetrahedral particles. *Nature Phys.* **10**, 653657, 2014.
- [14] Palmer, J. C., Martelli, F., Liu, Y., Car, R., Panagiotopoulos, A. Z., Debenedetti, P. G. Metastable liquid-liquid transition in a molecular model of water. *Nature*, **510**, 385, 2014.
- [15] Nomuraa, K., et al. Evidence of low-density and high-density liquid phases and isochore end point for water confined to carbon nanotube. *PNAS* **114**, 4066-4071, 2017.
- [16] Holten, V., Bertrand, C. E., Anisimov, M. A., and Sengers, J. V. Thermodynamics of supercooled water. *J. Chem. Phys.* **136**, 094507, 2012.
- [17] Sciortino, F. Which way to low-density liquid water? *PNAS* **114**, 8141-8143, 2017.
- [18] Le, L., Molinero V. Nanophase Segregation in Supercooled Aqueous Solutions and Their Glasses Driven by the Polyamorphism of Water. *J. Phys. Chem. A* **115**, 5900-5907, 2011.
- [19] Moore, E. B., Molinero V. Ice crystallization in waters no-mans land. *J. Chem. Phys.* **132**, 244504, 2010.
- [20] Moore, E. B., Molinero V. Structural transformation in supercooled water controls the crystallization rate of ice. *Nature* **479**, 506-509, 2011.
- [21] Pereyra R. G., Szleifer, I., Carignano, M. A. Temperature dependence of ice critical nucleus size. *J. Chem. Phys.* **135**, 044508, 2011.
- [22] Li, T., Donadio, D., Russoc, G., Galli, G. Homogeneous ice nucleation from supercooled water. *Phys. Chem. Chem. Phys.* **13**, 19807-19813, 2011.
- [23] Limmer, D. T., Chandler, D. The Putative Liquid-Liquid Transition Is a Liquid-Solid Transition in Atomistic Models of Water. *J. Chem. Phys.* **135**, 134503, 2011.
- [24] Limmer, D. T., Chandler, D. The putative liquid-liquid transition is a liquid-solid transition in atomic models of water II. *J. Chem. Phys.* **138**, 214504, 2013.

- 
- [25] Tanaka, H. Bond orientational order in liquids: Towards a unified description of water-like anomalies, liquid-liquid transition, glass transition, and crystallization. *Eur. Phys. J. E. Soft Matter*, **35**, 113, 2012.
- [26] Prasad, S., Chakravanty, C. and Kashyap, H. K. Concentration-dependent structure and dynamics of aqueous LiCl solutions: A molecular dynamics study. *Journal of Molecular Liquids*, **225**, 240, 2017.
- [27] Riddick, J. *Organic Solvents Physical Properties and Methods of Purification - Techniques of Chemistry*. Wiley-Interscience, 1970.
- [28] Linstrom, P., Mallard, W. G. (eds). *NIST Chemistry WebBook*, NIST Standard Reference Database Number **69**, National Institute of Standards and Technology, Gaithersburg (MD), 2016.
- [29] Bernal, J. D. and Fowler, R. H. A theory of water and ionic solution, with particular reference to hydrogen and hydroxyl ions. *J. Chem. Phys.* **1**, 8, 515-548, 1933.
- [30] Greenwood, N. N., Eamshaw, A. *Chemistry of the Elements* (p. 620). 2<sup>nd</sup> Edition, Butterworth-Heinemann, 1997.
- [31] Weingärtner, H., Teermann, I., Borchers, U., Balsaa, P., Lutze, H. V., Schmidt, T. C., Franck, E. U., Wiegand, G., Dahmen, N., Schweltdt, G., Frimmel, F. H., Gordalla, B. C. *Water 1. Properties, Analysis, and Hydrological Cycle*. Ullman's Encyclopedia of Industrial Chemistry. Wiley-VCH Verlag GmbH & Co. KGaA, 2016.
- [32] de Oliveira, M. J. *Equilibrium Thermodynamics*, 2<sup>nd</sup> Edition. Springer-Verlag Berlin Heidelberg, 2017.
- [33] Murphy, D. M., Koop, T. Review of the vapour pressures of ice and supercooled water for atmospheric applications. *Quarterly Journal of the Royal Meteorological Society*, **131**, 608, 2005.
- [34] Fennell, C. J., Bizjak, A., Vlachy, V., Dill, K. A. Ion Pairing in Molecular Simulations of Aqueous Alkali Halide Solutions. *J. Phys. Chem. B*, **113**, 6782-6791, 2009.
- [35] Pople, J. A. *Molecular Association in Liquids. II. A Theory of the Structure of Water*. Proc. R. Soc. London, Ser. A, 1951.

- 
- [36] Pople, J. A. *Molecular Association in Liquids. II. A Theory of the Structure of Water*. Proc. R. Soc. London, Ser. A, 1951.
- [37] Franks, F. *The Physics and Physical Chemistry of Water*. Hasted, J. *Liquid water: Dielectric properties*. Springer, pp. 255-309, 1972.
- [38] Eisenberg, D. and Kauzmann, W. *The structure and properties of water*, 1969.
- [39] Clausius, R. Ueber die bewegende Kraft der Wärme und die Gesetze, welches ich daraus für die Wärmelehre selbst abeiten lassen. *Annalen der Physik*, **155**, 500-524, 1850.
- [40] Clausius, R. Ueber die bewegende Kraft der Wärme und die Gesetze, welches ich daraus für die Wärmelehre selbst abeiten lassen. *Annalen der Physik*, **155**, 500-524, 1850.
- [41] Liu, L., Chen, S. H., Faraone, A., Yen, C. W., Mou, C. Y. Pressure dependence of fragile to strong transition and a possible second critical point in supercooled confined water. *Phys. Rev. Lett.* **95**, 117802, 2005.
- [42] Chaplin, M. F. Water: its importance to life. *Biochem. and Molec. Biol. Educat.*, **29**, 2, 54-59, 2001.
- [43] Eisenberg, D. and Kauzmann, W. *The structure and properties of water*. OUP Oxford, 2005.
- [44] Maréchal, Y. *The Hydrogen Bond and the Water Molecule*. Elsevier, 2007.
- [45] Császár, A. G., Czakó, G., Furtenbacher, T., Tennyson, J., Szalay, V., Shirin, S. V., Zobov, N. F., and Polyansky, O. L. On equilibrium structures of the water molecule. *J. Chem. Phys.* **122**, 214305, 2005.
- [46] Molnar, C. and Gair, J. *Concepts of Biology*, 1<sup>st</sup> Canadian Edition. Pressbooks, 2012.
- [47] Ball, P. Water - an enduring mystery. *Nature*, **452**, 291-292, 2008.
- [48] Debenedetti, P. G. Supercooled and Glassy Water. *J. Phys. Condens. Matter*, **15**, 2003.
- [49] Debenedetti, P., Stillinger, F. Supercooled Liquids and the Glass Transition. *Nature*, **410**, 259, 2001.

- [50] Kell, G. S. Density thermal expansivity, and compressibility of liquid water from 0 °C to 150 °C: correlations and tables for atmospheric pressure and saturation reviewed and expressed on 1968 temperature scale. *J. Chem. Eng. Data* **20**, 97-105, 1975.
- [51] Zheleznyi, B. V. The density of supercooled water. *Russ. J. Phys. Chem.* **43**, 1311-1311, 1969.
- [52] Debenedetti, P. G. *Metastable Liquids: Concepts and Principles*. Princeton University Press, 1996.
- [53] Wagner, W., Prub, A. The IAPWS Formulation 1995 for the Thermodynamic Properties of Ordinary Water Substance for General and Scientific Use. *J. Phys. Chem. Ref. Data*, **31**, 387-535, 2002.
- [54] Lynden-Bell, R. M., Morris, S. C., Barrow, J. D., Finney, J. L. and Harper, JR, C., L. (edit). *Water and Life: The Unique Properties of H<sub>2</sub>O*. CRC Press, Taylor & Francis Group, 2010.
- [55] Huang, C., et al. The Inhomogeneous Structure of Water at Ambient Conditions. *Proc. Natl. Acad. Sci. U. S. A.*, **106**, 15214-15218, 2009.
- [56] Franks, F. *Water: A Matrix of Life*, 2<sup>nd</sup> Edition, Royal Society of Chemistry, Cambridge, UK. 2000.
- [57] Singh, L. P., Issenmann, B., Caupin, F. Pressure Dependence of Viscosity in Supercooled Water and a Unified Approach for Thermodynamic and Dynamic Anomalies of Water. *Proc. Natl. Acad. Sci. U. S. A.*, **114**, 4312-4317, 2017.
- [58] Sciortino, F., Poole, P. H., Stanley, H. E., Havlin, S. Lifetime of the Bond Network and Gel-Like Anomalies in Supercooled Water. *Phys. Rev. Lett.*, **64**, 1686, 1990.
- [59] Mishima, O., Stanley, H. E. The Relationship Between Liquid, Supercooled and Glassy Water. *Nature*, **396**, 329-335, 1998.
- [60] Nilsson, A., Huang, C. & Pettersson, L. G. M. Fluctuations in ambient water. *J. Mol. Liq.* **176**, 2-16, 2012.
- [61] Nilsson, A., Pettersson, L. G. M. The structural origin of liquid water. *Nat. Commun.* **6**, 8998, 2015.

- 
- [62] Kell, G. S. Isothermal compressibility of liquid water at 1 atm. *J. Chem. Eng. Data*, **15**, 119-122, 1970.
- [63] Speedy, R. J. and Angell, C. A. Isothermal compressibility of supercooled water and evidence for a thermodynamic singularity at -45° C. *J. Chem. Phys.* **65**, 851, 1976.
- [64] Angell, C. A., Sichina, W. J. & Oguni, M. Heat capacity of water at extremes of supercooling and superheating. *J. Phys. Chem.*, **86**, 998-1002, 1982.
- [65] Kumar, P., Han, S. & Stanley, H. E. Anomalies of water and hydrogen bond dynamics in hydrophobic nanoconfinement. *J. Phys. Condens. Matter* **21**, 504108, 2009.
- [66] DeFries, T., Jonas, J. Pressure Dependence of NMR Proton Spin-Lattice Relaxation Times and Shear Viscosity in Liquid Water in the Temperature Range-15 - 10° C. *J. Chem. Phys.*, **66**, 896-901, 1977.
- [67] Prielmeier, F., Lang, E., Speedy, R., Lüdemann, H.-D. The Pressure Dependence of Self Diffusion in Supercooled Light and Heavy Water. *Ber. Bunsenges. Phys. Chem.*, **92**, 1111-1117, 1988.
- [68] Kumar, A., Kuchhal, P., Dass, N., Pathak, P. Anomalous Behaviour in Sound Velocity of Water. *Phys. Chem. Liq.*, **49**, 453-458, 2011.
- [69] Angell, C. A., Shuppert, J., and Tucker, J. C. Anomalous properties of supercooled water. Heat capacity, expansivity, and proton magnetic resonance chemical shift from 0 to -38%. *J. Phys. Chem.* **77**, 3092-3099, 1973.
- [70] Pi, H. L., Aragonés, J. L., Vega, C., Noya, E. G., Abascal, J. L. F., Gonzalez, M. A. and McBride, C. Anomalies in water as obtained from computer simulations of the TIP4P/2005 model: density maxima, and density, isothermal compressibility and heat capacity minima. *Molecular Physics*, **107**, 4-6, 2009.
- [71] Einstein, A. Zur Elektrodynamik bewegter Körper. *Annalen der Physik*, **10**, 322, 891-921, 1905.
- [72] Starr, F. W., Harrington, S., Sciortino, F. and Stanley, H. E. Slow dynamics of water under pressure. *Phys. Rev. Lett.* **82**, 3629, 1999.

- 
- [73] Scala, A., Starr, F. W., La Nave, E., Sciortino, F. and Stanley, H. E. Configurational entropy and diffusivity of supercooled water. *Nature*, **406**, 166-169, 2000.
- [74] Nilsson, A. & Pettersson, L. G. M. Perspective on the structure of liquid water. *Chem. Phys.* **389**, 1-34, 2011.
- [75] Kühne, T. D. & Khaliullin, R. Z. Electronic signature of the instantaneous asymmetry in the first coordination shell in liquid water. *Nat. Commun.* **4**, 1450, 2013.
- [76] Leetmaa, M. *et al.* Diffraction and IR/Raman data do not prove tetrahedral water. *J. Chem. Phys.* **129**, 084502, 2008.
- [77] Russo, J. and Tanaka, H. Understanding water's anomalies with locally favoured structures. *Nat. Commun.* **3**, 3556, 2014.
- [78] Soper, A. K. & Ricci, M. A. Structures of high-density and low-density water. *Phys. Rev. Lett.* **84**, 2881-2884, 2000.
- [79] Bellissent-Funel, M. C. Is there a liquid-liquid phase transition in supercooled water? *Europhys. Lett.* **42**, 161-166, 1998.
- [80] Errington, J. R. and Debenedetti, P. G. Relationship between structural order and anomalies of liquid water. *Nature*, **409**, 318-321, 2001.
- [81] Simeoni, G. G., Bryk, T., Gorelli, F., Krisch, M., Ruocco, G., Santoro, M., and Scopigno, T. The Widom line as the crossover between liquid-like and gas-like behaviour in supercritical fluids. *Nat. Phys.* **6**, 503-507, 2010.
- [82] Gallo, P., Corradini, D., and Rovere, M. Widom line and dynamical crossover as routes to understanding supercritical water. *Nat. Commun.* **5**, 5806, 2014.
- [83] Yue, Y.-Z., Angell, C. A. Clarifying the Glass-Transition Behaviour Of water by comparison with hyperquenched inorganic glasses. *Nature*, **427**, 717-720, 2004.
- [84] del Rosso, L., Celli, M., Ulivi, L. New porous water ice metastable at atmospheric pressure obtained by emptying a hydrogen-filled ice. *Nat. Commun.*, **7**, 13394, 2016.
- [85] Burton, E. F., Oliver, W. F. The crystal structure of ice at low temperatures. *Proc. R. Soc. London, Ser. A* **153**, 166, 1935.

- [86] Brüggeller, P., Mayer, E. Complete vitrification in pure water and dilute aqueous solutions. *Nature*, **288**, 569, 1980.
- [87] Tulk, C. A. *et al.* Structural studies of several distinct metastable forms of amorphous ice. *Science* **297**, 1320-1323, 2002.
- [88] Mishima, O., Calvert, L. D., Whalley, E. 'Melting ice' I at 77 K and 10 kbar: a new method of making amorphous solids. *Nature*, **310**, 393, 1984.
- [89] Loerting, T., Salzmann, C., Kohl, I., Mayer, E., Hallbrucker, A. A second distinct structural "state" of high-density amorphous ice at 77 K and 1 bar. *Phys. Chem. Chem. Phys.* **3**, 5355, 2001.
- [90] Sellberg, J. A., Huang, C., McQueen, T. A., Loh, N. D., Laksmono, H., Schlesinger, D., Sierra, R. G., Nordlund, D., Hampton, C. Y., Starodub, D., *et al.* Ultrafast X-ray probing of water structure below the homogeneous ice nucleation temperature. *Nature*, **510**, 381-384, 2014.
- [91] Vonnegut, K. *Cat's Cradle*. Holt, Rinehart and Winston, New York, 1953.
- [92] Hallbrucker, A., Mayer, E. Calorimetric study of the vitrified liquid water to cubic ice phase transition. *J. Phys. Chem.* **91**, 503-505, 1987.
- [93] Xu, L., Kumar, P., Buldyrev, S. V., Chen, S-H., Poole, P. H., Sciortino, F., and Stanley, H. E. Relation between the Widom line and the dynamic crossover in systems with a liquid-liquid phase transition. *Proc. Natl. Acad. Sci. U. S. A.* **102**, 16558-16562, 2005.
- [94] Franzese, G. and Stanley, H. E. The Widom line of supercooled water. *J. of Phys.: Condensed Matter*, **19**, 20, 205126, 2007.
- [95] Handle, P. H., Loerting, T., Sciortino, F. Supercooled and glassy water. *Proceedings of the National Academy of Sciences*, **114**, 51, 13336-13344, 2017.
- [96] Gallo, P., Corradini, D. & Rovere, M. Widom line and dynamical crossover as routes to understand supercritical water. *Nat. Commun.*, **5** (1), 1 - 6, 2014.

- 
- [97] Appignanesi, G. A., Rodriguez Fris, J. A., and Sciortino, F. Evidence of a two-state picture for supercooled water and its connections with glassy dynamics. *Eur. Phys. J. E* **29**, 305-310, 2009.
- [98] Holten, V. and Anisimov, M. A., Entropy-driven liquid-liquid separation in supercooled water. *Sci. Rep.* **2**, 713, 2012.
- [99] Tanaka, H. Simple physical explanation of the unusual thermodynamic behavior of liquid water. *Phys. Rev. Lett.* **80**, 5750, 1998.
- [100] Holten, V., Palmer, J. C., Poole, P. H., Debenedetti, P. G. and Anisimov, M. A. Two-state thermodynamics of the ST2 model for supercooled water. *J. Chem. Phys.* **140**, 104502, 2014.
- [101] Bosio, L., Teixeira, J. & Bellissent-Funel, M. C. Enhanced density fluctuations in water analyzed by neutron scattering. *Phys. Rev. A* **39**, 6612-6613, 1989.
- [102] Kim, K. H., Späh, A., Pathak, H., Perakis, F., Mariedahl, D., Amann-Winkel, K., Sellberg, J. A., Lee, J. H., Kim, S., Park, J., Nam, K. H., Katayama, T., Nisson, A. Maxima in the thermodynamic response and correlation functions of deeply supercooled water. *Science*, **22**, 358 (6370), 1589-1593, 2017.
- [103] Gallo, P. and Stanley, H. E. Supercooled water reveals its secrets. *Science*, **358**, 6370, 1543-1544, 2017.
- [104] Abascal, J. L. F. and Vega, C. Widom line and liquid-liquid critical point for the TIP4P/2005 water model. *J. Chem. Phys.*, **133**, 234502, 2010.
- [105] Luck, W. A. P. *The Hydrogen Bond*. Amsterdam: North-Holland, 1976.
- [106] Mishima, O. Reversible first-order transition between two H<sub>2</sub>O amorphs at ~0.2 GPa and ~135 K. *J. Chem. Phys.* **100**, 5910, 1994.
- [107] Smith, J. D., Cappa, C. D., Wilson, K. R., Cohen, R. C., Geissler, P. L., Saykally, R. J. Unified Description of Temperature-Dependent Hydrogen-Bond Rearrangements in Liquid Water. *Proc. Natl. Acad. Sci. U. S. A.*, **102**, 14171-14174, 2005.
- [108] Geissler, P. L. Temperature Dependence of Inhomogeneous Broadening: on the Meaning of Isosbestic Points. *J. Am. Chem. Soc.*, **127**, 14930-14935, 2005.

- 
- [109] Sciortino, F., Geiger, A., Stanley, E. Isochoric Differential Scattering Functions in Liquid water: the fifth neighbor as a network defect. *Phys. Rev. Lett.*, **65**, 3452, 1990.
- [110] Liu, Y., Panagiotopoulos, A. Z. and Debenedetti, P. G., Low-temperature fluid Phase behavior of st2 water, *J. Chem. Phys.*, **131**, p.104508, 2009.
- [111] Azouzi, M. E. M., Ramboz, C., Lenain, J-F., Caupin, F. A coherent picture of water at extreme negative pressure. *Nat. Phys.*, **9**, 38, 2013.
- [112] Amann-Winkel, K., Gainaru, C., Handle, P. H., Seidl, M., Nelson, H., Böhmer, R., Loerting, T. Waters second glass transition. *Proc. Natl. Acad. Sci. U. S. A.*, **110**, 17720-17725, 2013.
- [113] Pallares, G., El Mekki Azouzi, M., González, M. A., Aragonés, J. L., Abascal, J. L., Valeriani, C., Caupin, F. Anomalies in bulk supercooled water at negative pressure. *Proc. Natl. Acad. Sci. U. S. A.*, **111**, 7936-7941, 2014.
- [114] Smallenburg, F., Sciortino, F. Tuning the liquid-liquid transition by modulating the hydrogen-bond angular flexibility in a model for water. *Phys. Rev. Lett.*, **115**, 015701, 2015.
- [115] Yang, H-C., Ge, Y-C., Su, K-H., Chang, C-C., Lin, K-C., Aquilanti, V. & Kasai, T. Temperature effect on water dynamics in tetramer phosphofructokinase matrix and the super-arrhenius respiration rate. *Sci. Reports*, **11**, 383, 2021.
- [116] Nishiyama, M., Klejin, S., Aquilanti, V. & Kasai, T. Temperature dependence of respiration rate of leaves, <sup>18</sup>O-experiments and super-Arrhenius kinetics. *Chem. Phys. Lett.* **482**, 325-329, 2009.
- [117] Holten, V., Bertrand, C. E., Anisimov, M. A., and Sengers, J. V. Thermodynamics of supercooled water. *J. Chem. Phys.* **136**, 094507, 2012.
- [118] Schwegler, E., Galli, G., Gygi, F. Water under pressure. *Phys. Rev. Lett.* **84**, 2429, 2000.
- [119] Teboul, V. Pressure dependence of dynamical heterogeneity in water. *J. Physics: Condens. Matter* **20**, 244116, 2008.

- 
- [120] Harting, C., Witschel, W., Spohr, E., Gallo, P., Ricci, M. A. and Rovere, M. Modifications of the hydrogen bond network of liquid water in a cylindrical SiO<sub>2</sub> pore. *J. Mol. Liquids* **85**, 1-2, 127-137, 2000.
- [121] Gallo, P. and Rovere, M. Mode coupling and fragile to strong transition in supercooled TIP4P water. *J. Chem. Phys.*, **137**, 16, 164503, 2012.
- [122] Faraone, A. Fragile-to-strong liquid transition in deeply supercooled confined water. *J. Chem. Phys.*, **121**, 10843, 2004
- [123] De Marzio, M., Camisasca, G., Rovere, M. and Gallo, P. Mode coupling theory and fragile to strong transition in supercooled TIP4P/2005 water. *J. Chem. Phys.*, **144**, 074503, 2016.
- [124] Gallo, P., Corradini, D. and Rovere, M. Fragile to strong crossover at the Widom line in supercooled aqueous solutions of NaCl. *J. Chem. Phys.*, **139**, 204503, 2013.
- [125] Alder, B. J., and Wainwright, T. E., Studies in Molecular Dynamics. I. Genera Method, *The Journal of Chemical Physics*, vol. **31**, no. 2, pp. 459-466, 1959.
- [126] Rahman, A., Correlations in the Motion of Atoms in Liquid Argon, *Phys. Rev.*, vol. 136, pp. A405-A411, Oct 1964.
- [127] de Laplace, P.S., *A Philosophical Essay on Probabilities*, (transl.) Dover, New York, 1951.
- [128] Rapaport, D. C., *The Art of Molecular Dynamics Simulations*, 2<sup>nd</sup> edition, Cambridge University Press, 2003.
- [129] Goldstein, H., *Classical Mechanics*, Addison-Wesley, Reading, MA, 2<sup>nd</sup> edition, 1980.
- [130] Schlick, T. *Modeling and Simulation: An Interdisciplinary Guide*, Vol. 21, 2<sup>nd</sup> ed., Springer, New York, 2010.
- [131] Metropolis, N., Rosenbluth, A. W., Rosenbluth, M. N., Teller, A. H. and Teller, E., Equation of state calculations by fast computing machines, *The Journal of Chemical Physics*, **21**, pp. 1087-1092, 1953.
- [132] Alder, B. and Wainwright, T., Phase transition for a hard sphere system, *The Journal of Chemical Physics*, **27**, p. 1208, 1957.

- 
- [133] Satoh, A., *Introduction to Practice of Molecular Simulation*, Akita Prefectural University, Japan, 2010.
- [134] Ciccotti, G., Frenkel, D., and McDonald, I. R., eds., *Simulation of Liquids and Solids. Molecular Dynamics and Monte Carlo Methods in Statistical Mechanics*, North-Holland, Amsterdam, 1987.
- [135] Levesque, D. and Weis, J. J., *Recent progress in the simulation of classical fluids*, Springer, Berlin, 1992.
- [136] Allen, M. P. and Tildesley, D. J., *Computer Simulations of Liquids*, Oxford University Press, 1989.
- [137] Leach, A. R., *Molecular modelling: principles and applications*. Pearson Education, 2001.
- [138] Verlet, L., Computer “experiments” on classical fluids. I. Thermodynamical Properties of Lennard-Jones molecules. *Phys. Rev.* **159**, 98-103, 1967.
- [139] Hoover, W. G., Canonical dynamics: equilibrium phase-space distributions, *Physical Review A*, **31**, p. 1695, 1985.
- [140] Berendsen, H. J., Postma, J. v., van Gunsteren, W. F., Di-Nola, A., and Haak, J., Molecular dynamics with coupling to an external bath, *The Journal of Chemical Physics*, **81**, pp. 3684-3690, 1984.
- [141] Evans, D. J. and Morriss, O., Non-newtonian molecular dynamics, *Computer Physics Reports*, **1**, pp. 297-343, 1984.
- [142] Melchionna, S., Ciccotti, G., and Lee Holian, B., Hoover npt dynamics for System varying in shape and size, *Molecular Physics*, **78**, pp. 533-544, 1993.
- [143] Frenkel, D., and Smit, B., *Understanding molecular simulation: frog algorithm to applications*, Academic press, 2001.
- [144] Van Gunsteren, W. F and Berendsen, H. JC. A leap-frog algorithm for stochastic dynamics. *Molecular Simulation* **1,3**, 173-185, 1988.
- [145] Toukmaji, Abdulnour Y., Board, John A., Jr., Ewald summation techniques in Perspective: a survey, *Computer Physics Communications*, **95**, pp. 73-92, 1996.

- 
- [146] von Ewald, P. P., Die Berechnung optischer and electrostatischer Gitterpotentiale, *Ann. Phys.* **369** (3), pp. 253-287, 1921.
- [147] Knopp, K., *Theorie und Anwendung der unendlichen Reihen*, Springer, 1964 (English translation: Blackie, 1951 & Dover, Reprint, 1990).
- [148] Wells, Brad A. and Chaffee, Alan L., Ewald Summation for Molecular Simulations, *Journal of Chemical Theory and Computation*, **11**, pp. 3684-36-95, 2015.
- [149] González, M. A. Force fields and molecular dynamics simulations. *Collection de la Société Française de la Neutronique*, **12**, 169-200, 2011.
- [150] Jorgensen, W. L., Maxwell, D. S. and Tirado-Rivers, J. Development and testing of the OPLS all-atom force field on conformational energies and properties of organic liquids. *J. Am. Chem. Soc.*, **118**, 11225-11236, 1996.
- [151] Jones, J. E. On the determination of molecular fields. - I. From the variation of the viscosity of a gas with temperature. *Proceedings of the Royal Society of London. Series A, Containing Papers of a Mathematical and Physical Character*, **106** (738), 441-462, 1924.
- [152] Jones, J. E. On the determination of molecular fields. - II. From the equation of state of gas. *Proceedings of the Royal Society of London. Series A, Containing Papers of a Mathematical and Physical Character*, **106** (738), 463-477, 1924.
- [153] Lennard-Jones, J. E. Cohesion. *Proceedings of the Physical Society*, **43** (5), 461-482, 1931.
- [154] Vega, C., Abascal, J. L. F., Conde, M. M., and Aragones, J. L. What ice can teach us about water interactions: a critical comparison of the performance of different water models. *Faraday Discuss.*, **141**, 251-276, 2009.
- [155] Jorgensen, W. L. Quantum and statistical mechanical studies of liquids. 10. Transferable intermolecular potential functions for water, alcohols, and Ethers. Application to liquid water. *J. Am. Chem. Soc.* **103**, 335-340, 1981.
- [156] Berendsen, H. J. C., Postman, J. P. M., van Gunsteren, W. F. and Hermans, J. *Intermolecular Forces*, edited by Pullman, B., p. 331, Dordrecht, R., 1981.

- 
- [157] Molinero, V. & Moore, E. B. Water modeled as an intermediate element between carbon and silicon. *J. Phys. Chem. B*, **113**, 4008-4016, 2019.
- [158] Jorgensen, W. L., Chandrasekhar, J., Madura, J. D., Impey, R. W., Klein, M. L. Comparison of simple potential functions for simulating liquid water. *J. Chem. Phys.* **79**, 926-935, 1983.
- [159] Berendsen, H. J. C., Grigera, J. R. and Straatsma, T. P. The Missing Term In Effective Pair Potentials. *J. Phys. Chem.* **91**, 6269-6271, 1987.
- [160] Bernal, J. D., Fowler, R. H. A Theory of Water and Ionic Solution, with Particular Reference to Hydrogen and Hydroxyl Ions. *J. Chem. Phys.*, **1**, 515, 1933.
- [161] Horn, H. W., Swope, W. C., Pitner, J. W., Madura, J. D., Dick, T. J., Hura, G. L. and Head-Gordon, T. Development of an improved four-site water model for biomolecular simulations: TIP4P-Ew. *J. Chem. Phys.* **120**, 9665-9678, 2004.
- [162] Abascal, J. L. F., Sanz, E., García Fernández, R. and Vega, C. A potential model for the study of ices and amorphous water: TIP4P/Ice. *J. Chem. Phys.* **122**, 234511, 2005.
- [163] Abascal, J. L. F. and Vega, C. A general purpose model for the condensed phases of water: TIP4P/2005. *J. Chem. Phys.* **123**, 234505, 2005.
- [164] Mahoney, M. W., Jorgensen, W. L. A five-site model liquid water and the reproduction of the density anomaly by rigid, non-polarizable models. *J. Chem. Phys.* **112**, 8910-8922, 2000.
- [165] Rick, S. W. A reoptimization of the five-site water potential (TIP5P) for use with Ewald sums. *J. Chem. Phys.* **120**, 6085-6093, 2004.
- [166] Marechal, Y. *The Hydrogen Bond and the Water Molecule: The Physics and Chemistry of Water, Aqueous and Bio Media*. Elsevier: Oxford, U.K., 2007.
- [167] Pronk, S., Páll, S., Schulz R., Larsson, P., Bjelkmar, P., Apostolov, R., Shirts, M., R., Smith, J. C., Kasson, P. M., van der Spoel, D., Hess, B., and Lindahl, E. GROMACS 4.5: a high-throughput and highly parallel open source molecular simulation toolkit. *Bioinformatics* **29**, 845-854, 2013.

- 
- [168] Izadi, S., Anandakrishnan, R. and Onufriev V. Building Water Models: A Different Approach. *J. Phys. Chem. Lett.*, **5**, 21, 3863-3871, 2014.
- [169] Butt, H. J, Graf, K., Kappl, M., Physics and Chemistry of Interfaces, 2006.
- [170] Berendsen, H. J. C., Postma, J. P. M., Gunsteren, W. F. V., and Hermans, J. *Interaction models for water in relation to protein hydration* pp. 331-342. Springer Netherlands Dordrecht, 1981.
- [171] Jorgensen, W. L. and Madura, J. D. Temperature and size dependence for Monte Carlo simulations of TIP4P water. *Mol. Phys.* **56**, 1381-1392, 1985.
- [172] Duboué-Dijon, E., Fogarty, A. C., Laage, D. Temperature Dependence of Hydrophobic Hydration Dynamics: From Retardation to Acceleration. *J. Phys. Chem. B* **118**, 1574-1583, 2014.
- [173] Samios, J. and Durov. V. (editors). *Novel Approaches to the Structure and Dynamics of Liquids: Experiments, Theories and Simulations. II.* Mathematics, Physics and Chemistry - Vol. 133, NATO Science Series, 2002.
- [174] Dixon, M. and Sangster, M. J. L., The structure of molten NaCl from a Simulation Model which allows for the polarization of both ions. *J. Phys.* **C9**, L 5-9, [1.3.2, 11.4], 1976.
- [175] Ferrara, P., Apostolakis, J. and Caflisch, A. Evaluation of a Fast Implicit Solvent Model for Molecular Dynamics Simulations. *PROTEINS: Structure, Function, and Genetics* **33**, 24-46, 2002.
- [176] Burgess, J. *Metals Ion in Solution*. John Wiley & Sons: Chichester and New York, 1979.
- [177] Brooks, B. R., Bruccoleri, R. E., Olafson B. D., States, D. J., Swaminathan, S., Karplus, M. CHARMM: a program for macromolecular energy, minimization, and dynamics calculations. *J. Comput. Chem.* **4**, 187-217, 1983.
- [178] Aragones, J. L., Rovere, M., Vega, C., and Gallo, P. Computer simulation study of the structure of LiCl aqueous solutions: Test of non-standard mixing rules in the ion interaction. *J. Phys. Chem. B* **118**, 7680-7691, 2014.

- 
- [179] Joung, I. S. and Cheatham, T. E. Determination of alkali and halide monovalent ion parameters for use in explicitly solvated biomolecular simulations. *J. Phys. Chem. B* **112**, 9020-9041, 2008.
- [180] Eyring, H. and Hirschfelder, J. The Theory of the Liquid State. *J. Phys. Chem.* **41**, 2, 249-257, 1937.
- [181] Hansen, J. P. and McDonald, I. R. *Theory of Simple Liquids*. 3<sup>rd</sup> Edition Academic Press, 2006.
- [182] Duboué-Dijon, E. and Laage, D. Characterization of the Local Structure in Liquid Water by Various Order Parameters. *J. Phys. Chem. B*, **119**, 26, 8406-8418, 2015.
- [183] Shi, R. and Tanaka, H. Microscopic structural descriptor of liquid water. *J. Chem. Phys.* **148**, 124503, 2018.
- [184] Zwanzig, R. and Ailawadi, N. K. Statistical error due to finite time averaging in computer experiments. *Phys. Rev.*, **182**, 280-283, 1969.
- [185] Bitsanis, I., Tirrell, M. and Davis, H. T. Statistics of correlation functions from molecular dynamics. *Phys. Rev. A.*, **36**, 958-961, 1987.
- [186] Chau, P. L., Hardwick, A. J. A New Order Parameter for Tetrahedral Configurations. *Mol. Phys.* **93**, 511-518, 1998.
- [187] Errington, J. R., Debenedetti, P. G. Relationship Between Structural Order and the Anomalies of Liquid Water. *Nature* **409**, 318-321, 2001.
- [188] Giovambattista, N., Rossky, P. J., Debenedetti, P. G. Effect of Temperature on The Structure and Phase Behavior of Water Confined by Hydrophobic, Hydrophilic, and Heterogeneous Surfaces. *J. Phys. Chem. B* **113**, 13723-13734, 2009.
- [189] Giovambattista, N., Debenedetti, P. G., Sciortino, F., Stanley, H. E. Structural Order in Glassy Water. *Phys. Rev. E* **71**, 061505, 2005.
- [190] Nayar, D., Chakravarty, C. Water and Water-like Liquids: Relationships Between Structure, Entropy and Mobility. *Phys. Chem. Chem. Phys.* **15**, 14162-14177, 2013.
- [191] Jedlovszky, P., Pártay, L. B., Bartók, A. P., Voloshin, V. P., Medvedev, N. N., Garberoglio, G., Vallauri, R. Structural and Thermodynamic

- 
- Properties of Different Phases of Supercooled Liquid Water. *J. Chem. Phys.* **128**, 244503, 2008.
- [192] Moore, E. B., Molinero, V. Growing Correlation Length in Supercooled Water. *J. Chem. Phys.* **130**, 24405, 2009.
- [193] Galamba, N. Water's Structure Around Hydrophobic Solutes and the Iceberg Model. *J. Phys. Chem. B* **117**, 2153-2159, 2013.
- [194] Shiratani, E., Sasai, M. Growth and Collapse of Structural Patterns in the Hydrogen Bond Network in Liquid Water. *J. Chem. Phys.* **104**, 7671-7680, 1996.
- [195] Accordino, S. R., Rodriguez Fris, J. A., Sciortino, F., and Appignanesi, G. A. Quantitative investigation of the two-state picture for water in the normal liquid and the supercooled regime. *Eur. Phys. J. E* **34**, 48, 2011.
- [196] Shiratnani, E., Sasai, M. Molecular Scale Precursor of the Liquid-Liquid Phase Transition of Water. *J. Chem. Phys.* **108**, 3264-32-76, 1998.
- [197] Wikfeldt, K.T., Nisson A. and Pettersson, L. G. M. Spatially Inhomogeneous Bimodal Inherent Structure of Simulated Liquid Water. *Phys. Chem. Chem. Phys.* **13**, 44, 19918-19924, 2011.
- [198] Nilsson, A., Huang, C., Pettersson, L. G. Fluctuations in Ambient Water. *J. Mol. Liq.* **176**, 2-16, 2012.
- [199] Camisasca, G., De Marzio, M., Rovere, M. and Gallo, P. High density liquid structure enhancement in glass forming aqueous solution of LiCl. *J. Chem. Phys.* **148**, 222829, 2018.
- [200] Jedlovszky, P., Mezei, M., Vallauri, R. A Molecular Level Explanation of the Density Maximum of Liquid Water from Computer Simulations with a Polarizable Potential Model. *Chem. Phys. Lett.* **318**, 155-160, 2000.
- [201] Caleman, C., van der Spoel, D. Temperature and Structural Changes of Water Clusters in Vacuum Due to Evaporation. *J. Chem. Phys.* **125**, 154508, 2006.
- [202] Conde, M. M., Rovere, M. and Gallo, P. Spontaneous NaCl-doped ice at seawater conditions: focus on the mechanisms of ion inclusion. *Phys. Chem. Chem. Phys.*, **19**, 14, 9566-9574, 2017

- 
- [203] Conde, M. M., Rovere, M., Gallo, P. Spontaneous NaCl-doped ices I<sub>h</sub>, I<sub>c</sub>, III, V and VI. Understanding the mechanism of ion inclusion and its dependence on the crystalline structure of ice. *Phys. Chem. Chem. Phys.*, **23**, 40, 22897-22911, 2021.
- [204] Kropman, M. F. and Bakker, H. J. Dynamics of Water Molecules in Aqueous Solvation Shells. *Science*, **291**, 2118-2120, 2001.
- [205] Smith, J. D., Saykally, R. D. and Geissler, P. L. The effects of dissolved halide anions on hydrogen bonding in liquid water. *J. Am. Chem. Soc.*, **129**, 13847-13856, 2007.
- [206] Mancinelli, R., Botti, A., Bruni, F., Ricci, M. A. and Soper, A. K. Hydration of sodium, potassium, and chloride ions in solution and the concept of structure maker/breaker. *J. Phys. Chem. B*, **111**, 13570-13577, 2007.
- [207] Bakker, H. J. Structural Dynamics of Aqueous Salt Solutions. *Chem. Rev.*, **108**, 1456-1473, 2008.
- [208] Markus, Y. Effect of Ions on the Structure of Water: Structure Making and Breaking. *Chem. Rev.*, **109**, 1346-1370, 2009.
- [209] Fayer, M. D., Moilanen, D. E., Wong, D., Rosenfeld, D. E., Fenn, E. E. and Park, S. Water Dynamics in Salt Solutions Studied with of Ultrafast 2D IR Vibrational Echo Spectroscopy. *Acc. Chem. Res.*, **42** (9): 1210-1219, 2009.
- [210] Tielrooij, K. J., Garcia-Araez, N., Bonn, M. and Bakker, H. J. Cooperativity in Ion Hydration. *Science*, **328**, 1006-1009, 2010.
- [211] Oleinikova, A. and Brovchenko, T. Hydrogen-bonded network of hydration water around model solutes. *Phys. Chem. Chem. Phys.*, **14**, 5686-5694, 2012.
- [212] Tse, Y.-L. S., Voth, G. A. and Witten, T. A. An analysis of hydrated proton diffusion in *ab initio* molecular dynamics. *J. Chem. Phys.*, **142**, 184905, 2015.
- [213] Gaiduk, A. P. and Galli, G. Local and global effects of dissolved sodium chloride on the structure of water. *J. Phys. Chem. B*, **8**, 1496-1502, 2017.
- [214] Han, S. Dynamic features of water molecules in superconcentrated aqueous electrolytes. *Sci. Rep.*, **8**, 9347, 2018.

- [215] Corradini, D., Rovere, M., and Gallo, P. Structural Properties of High and Low Density Water in a Supercooled Aqueous Solution of Salt. *J. Phys. Chem. B* **115**, 1461, 2011.
- [216] Corradini, D., Gallo, P. and Rovere, M. Molecular dynamics studies on the thermodynamics of supercooled sodium chloride aqueous solution at different concentrations. *J. Phys.: Condens. Matter* **22**, 284104, 2010.
- [217] Corradini, D., Rovere, M., Gallo, P. A route to explain water anomalies from results on an aqueous solution of salt. *J. Chem. Phys.*, **132**, 13, 134508, 2010.
- [218] Conde, M. M., Rovere, M., Gallo, P. Molecular dynamics simulations of freezing-point depression of TIP4P/2005 water in solution with NaCl. *J. Mol. Liquids*, **261**, 513-519, 2018.
- [219] Gallo, P., Corradini, D., Rovere, M. Excess entropy of water in a supercooled solution of salt. *Mol. Phys.*, **109**, 23-24, 2969-2979, 2011.
- [220] Corradini, D., Rovere, M., Gallo, P. Structural properties of high and low density water in supercooled aqueous solution of salt. *J. Phys. Chem. B*, **115**, 6, 1461-1468, 2011.
- [221] Aouizerat-Elarby, A., Jal, J.-F., Chieux, P., Letoffe, J. M., Claudy, P., Dupuy, J. Metastable crystallization products and metastable phase diagram of the glassy and supercooled aqueous ionic solutions of LiCl. *J. Non-Cryst. Solids*, **104**, 203, 1988.
- [222] Maurin, P. O. *et al.*, Dynamics and structure in good glass formers LiCl-RH<sub>2</sub>O: A NMR and quasielastic neutron scattering study. *Prog. Theor. Phys. Suppl.*, **126**, 141, 1997.
- [223] Gallina, M. E. *et al.* The low frequency phonons dynamics in supercooled LiCl, 6H<sub>2</sub>O. *J. Chem. Phys.*, **131**, 124504, 2009.
- [224] Bove, L., Dreyfus, C., Torre, R. and Rick, R. M. Observation of nanophase segregation in LiCl aqueous solutions from transient grating experiments. *J. Chem. Phys.*, **139**, 044501, 2013.
- [225] Santucci, S. C. *et al.* Onset of the  $\alpha$ -relaxation in the glass-forming solution LiCl-6H<sub>2</sub>O revealed by Brillouin scattering techniques. *J. Chem. Phys.*, **131**, 154507, 2009.

- [226] Turton, D. A., Corsaro, C., Martin, D. F., Mallamace, F. and Wynne, K. The dynamic crossover in water does not require bulk water. *Phys. Chem. Chem. Phys.*, **14**, 8067, 2012.
- [227] Turton, D. A., *et al.* The structure and terahertz dynamics of water confined in nanoscale pools in salt solutions. *Faraday Discuss.*, **150**, 493, 2011.
- [228] Mishima, O. Phase separation in dilute LiCl-H<sub>2</sub>O solution related to the polymorphism of liquid water. *J. Chem. Phys.*, **126**, 244507, 2007.
- [229] Mallamace, F. The liquid water polymorphism. *Proc. Natl. Acad. Sci. U. S. A.*, **106**, 15097, 2009.
- [230] Archer, D. G. and Carter, R. W. Thermodynamic Properties of the NaCl + H<sub>2</sub>O System. 4. Heat Capacities of H<sub>2</sub>O and NaCl(aq) in Cold-Stable and Supercooled States. *J. Phys. Chem. B.*, **104**, 8563, 2000.
- [231] Mallamace, F., Corsaro, C. and Stanley, H. E. Possible relation of water structural relaxation to water anomalies. *Proc. Natl. Acad. Sci. U. S. A.*, **110**, 4899, 2013.
- [232] Mallamace, F., *et al.* Thermodynamic properties of bulk and confined water. *J. Chem. Phys.*, **141**, 18C504, 2014.
- [233] Mallamace, F., Corsaro, C., Mallamace, D., Vasi, C. and Stanley, H. E. The thermodynamical response functions and the origin of the anomalous behavior of liquid water. *Faraday Discuss.*, **167**, 95, 2013.
- [234] Russo, J. and Tanaka, H. Understanding water's anomalies with locally favoured structures. *Nat. Commun.* **3**, 3556, 2014.
- [235] Cupane, A., Fomina, M., Piazza I., Peters, J. and Schiró, G. Experimental evidence for a liquid-liquid crossover in deeply cooled confined water. *Phys. Rev. Lett.*, **113**, 215701, 2014.
- [236] Poole, P. H., Sciortino, F., Essmann, U., Stanley, H. E. Phase Behaviour of Metastable Water. *Nature*, **360**, 324-328, 1992.
- [237] Moran, H. E. System lithium chloride-water. *J. Phys. Chem.*, **60**, 1666, 1956.

- 
- [238] Kim, K. H. et al., Experimental observation of the liquid-liquid transition in bulk supercooled water under pressure. *Science*, **270**, 6519, 978-982, 2020.
- [239] Zhang, Z., Duan, Z. Lithium chloride ionic association in dilute aqueous solution: a constrained molecular dynamics study. *Chem. Phys.*, **297**, 221-233, 2004.
- [240] Souda, R. Evidence of Deeply Supercooled Water in Interaction with LiCl. *J. Phys. Chem. B.*, **110**, 14787-14791, 2006.
- [241] Kim, J. S., Wu, Z., Morrow, A. R., Yethiraj, A. and Yethiraj, A. Self-diffusion and viscosity in electrolyte solutions. *J. Phys. Chem. B.*, **116**, 12007-12013, 2012.
- [242] Ding, Y., Hassanali, A. A. and Parrinello, M. Anomalous water diffusion in salt solutions. *Proc. Natl. Acad. Sci. U. S. A.*, **111**, 3310-3315, 2013.
- [243] Han, S. Anionic effects on the structure and dynamics of water in superconcentrated aqueous electrolytes. *RSC Adv.*, **9**, 609, 2019.
- [244] Braunstein, J., Mamantov, G., Smith, G. P. (ed.). *Advances in Molten Salt Chemistry*: Vol. 3. Plenum Press, New York and London, 1975.
- [245] Yim, C.-H., Abu-Lebdeh, Y. A. Connection between phase diagram, structure and ion transport in liquid, aqueous electrolyte solutions of lithium chloride. *J. Electrochem. Soc.*, **165**, A547-A556, 2018.
- [246] Sadek, H., Fuoss, R. M. Electrolyte-solvent interaction. VI. tetrabutylammonium bromide in nitrobenzene-carbon tetrachloride mixtures. *J. Am. Chem. Soc.*, **76**, 5905, 1954.
- [247] Winstein, S., Clippinger, E., Fainberg, A. H., Robinson, G. C. Salt effects and ion pairs in solvolysis. *J. Am. Chem. Soc.*, **76**, 2597, 1954.
- [248] Oelkers, E. H., Helgeson, H. C. Calculation of activity coefficients and degrees of formation of neutral ion pairs in supercritical electrolyte solutions. *Geochim. Cosmochim. Acta*, **55**, 1235, 1991.
- [249] Robinson, R. A., Stokes, R. *Electrolyte Solutions*. 2<sup>nd</sup> Revised Edition. Dover Publications, Inc., 2002.
- [250] Bockris, J. O'M. Ionic solvation. *Quart. Rev.*, **3**, 173, 1949.

- 
- [251] Gurney, R. W. *Ionic Process in solution*, McGraw-Hill, New York, 1953.
- [252] Hofmeister, F. Zur Lehre von der Wirkung der Salze. *Arch. Exp. Pathol. Pharmacol.*, **XXV**, 1-30, 1888.
- [253] Hribar, B., Southall, N. T., Vlachy, V. and Dill, K. A. How ions affect the structure of water. *J. Am. Chem. Soc.*, **124**, 12302, 2002.
- [254] Gallo, P., Corradini, D. and Rovere, M. Ion hydration and structural properties of water in aqueous solutions at normal and supercooled conditions: a test of the structure making and breaking concept. *Phys. Chem. Chem. Phys.*, **13**, 19814, 2011.
- [255] Soper, A. K. and Weckström, K. Ion solvation and water structure in potassium halide aqueous solutions. *Biophys. Chem.*, **124**, 180, 2006.
- [256] Leberman, R. and Soper, A. K. Effect of high salt concentrations on water structure. *Nature*, **378**, 364, 1995.
- [257] Collins, K. D. Charge density-dependent strength of hydration and biological structure. *Biophys. J.*, **72**, 65, 1997.
- [258] Bachler, J., Handle, P. H., Giovambattista, N. and Loering, T. Glass polymorphism and liquid-liquid phase transition in aqueous solutions: experiments and computer simulations. *Phys. Chem. Chem. Phys.*, **21**, 233238, 2019.
- [259] Mishima, O. Phase separation in dilute LiCl-H<sub>2</sub>O solution related to the polyamorphism of liquid water. *Jour. Chem. Phys.*, **126**, 244507, 2007.
- [260] Prevel, B., Jal, J. F., Dupuy-Philon, J., Soper, A. K. Structural characterization of an electrolytic aqueous solution, LiCl · 6H<sub>2</sub>O, in the glass, supercooled liquid, and liquid states. *J. Chem. Phys.* **103**, 1886, 1995.
- [261] Angell, C. A., Sare, E. J. Liquid-Liquid Immiscibility in Common Aqueous Salt Solutions at Low Temperatures. *J. Chem. Phys.*, **49**, 4713, 1968.
- [262] Suzuki, Y., Mishima, O. Two distinct Raman profiles of glassy dilute LiCl solution. *Phys. Rev. Lett.*, **85**, 1322, 2000.

- 
- [263] Finney, J.L., Hallbrucker, A., Kohl I., Soper, A. K., Bowron, D. T. Structures of high and low density amorphous ice by neutron diffraction. *Phys. Rev. Lett.*, **88**, 225503, 2002.
- [264] Mishima, O. Melting of the Precipitated Ice IV in LiCl Aqueous Solution and Polyamorphism of Water. *J. Phys. Chem. B* **115**, 14064-14067, 2011.
- [265] Suzuki, Y., Mishima, O. Sudden Switchover Between the Polyamorphic Phase Separation and the Glass-to-Liquid Transition in Glassy LiCl Aqueous Solutions. *J. Chem. Phys.* **138**, 084507, 2013.
- [266] Armitage, D. and Price, F. P. Size and surface effects on phase transitions. *Chem. Phys. Lett.*, **44**, 305, 1976.
- [267] Bellissent-Fund, M.-C. and Neilson, G. W. (edit.), *The Physics and Chemistry of Aqueous Ionic Solutions*. D. Reidel Publishing Co., 1986.
- [268] Gallo, P., Corradini, D., Rovere, M. Do ions affect the structure of water? The case of potassium halides. *J. Mol. Liquids*, **189**, 52-56, 2014.
- [269] Aouizerat-Elarby, A., Dez, H., Prevel, B., Jal, J. F., Bert, J. and Dupuy-Philon, J. Diffusion processes in LiCl, R H<sub>2</sub>O solutions. *Journal of Molecular Liquids*, **84**, 289, 2000.
- [270] Degrève, L. and Mazzè, F. M. Molecular simulation of LiCl aqueous solutions. *Mol. Phys.*, **101** (10), 1443-1453, 2003.
- [271] Singh, M. B., Dalvi, V. H. and Gaikar, V. G. Investigations of clustering of ions and diffusivity in concentrated aqueous solutions of lithium chloride by molecular dynamic simulations. *RSC Advances*, **5**, 15328, 2015.
- [272] Prasad, S., Chakravanty, C. and Kashyap, H. K. Concentration-dependent structure and dynamics of aqueous LiCl solutions: A molecular dynamics study. *Journal of Molecular Liquids*, **225**, 240, 2017.
- [273] Brady, G. W. Structure in Ionic Solutions II. *J. Chem. Phys.* **28**, 464-469, 1958.
- [274] Kruh, R. F. Diffraction Studies of the Structure of Liquids. *Chem. Rev.* **62**, 4, 219-346, 1962.

- 
- [275] Narten, A. H. Diffraction pattern and structure of aqueous lithium chloride solutions. *J. Chem. Phys.* **58**, 11, 1973.
- [276] Yamanaka, K., Yamagami, M., Takamuku, T., Yamaguchi, T., Wakita, H. X-ray diffraction study on aqueous lithium chloride solution in the temperature range 138-373 K. *J. Phys. Chem.* **97**, 10835-10839, 1993.
- [277] Bouazizi, S., Nasr, S. Local order in aqueous lithium chloride solutions as studied by X-ray scattering and molecular dynamics simulations. *J. Mol. Struct.* **837**, 206-213, 2007.
- [278] Bouazizi, S., Nasr, S. Structural investigations of high concentrated aqueous LiCl solutions: X-ray scattering and MD simulations approach. *J. Mol. Struct.* **875**, 121-129, 2008.
- [279] Waluyo, I., Nordlund, D., Bergmann, U., Schlesinger, D., Pettersson, L. G. M., and Nilsson, A. A different view of structure-making and structure-breaking in alkali halide aqueous solutions through x-ray absorption spectroscopy. *J. Chem. Phys.* **140**, 244506, 2014.
- [280] Harsányi, I., Temleitner, L., Beuneu, B., Pusztai, L. Neutron and X-ray diffraction measurements on highly concentrated aqueous LiCl solutions. *J. Mol. Liq.* **165**, 94-100, 2012.
- [281] Ohtomo, N., Arakawa, K. Neutron Diffraction Study of Aqueous Ionic Solutions. I. Aqueous Solutions of Lithium Chloride and Caesium Chloride. *Bull. Chem. Soc. Jpn.* **52**, 2755-2759, 1979.
- [282] Juurinen, I. *et al.* Saturation Behaviour in X-ray Raman Scattering Spectra of Aqueous LiCl. *J. Phys. Chem. B* **117**, 16506-16511, 2013.
- [283] Nygård, K. *et al.* Ion hydration studied by x-ray Compton scattering. *Phys. Rev. B* **73**, 24208, 2006.
- [284] Wachter, W., Fernandez, Š., Buchner, R., Hefter, G. Ion Association and Hydration in Aqueous Solutions of LiCl and Li<sub>2</sub>SO<sub>4</sub> by Dielectric Spectroscopy. *J. Phys. B* **111**, 9010-9017, 2007.
- [285] Feiweier, T., Isfort, O., Ceil, B., Fujara, F. and Weingärtner, H. Decoupling of lithium and proton self-diffusion in supercooled LiCl:7H<sub>2</sub>O: A nuclear magnetic resonance study using ultrahigh magnetic field gradients. *J. Chem. Phys.* **105**, 5737, 1996.

- 
- [286] Hasebe, T., Tamamushi, R., Tanaka, K. Nuclear magnetic resonance and thermal studies of concentrated aqueous solutions of lithium chloride. *J. Chem. Soc. Faraday Trans.* **88**, 205, 1992.
- [287] Gallo, P., Rapinesi, M., and Rovere, M. Confined water in the low hydration regime. *J. Chem. Phys.* **117**, 359, 2002.
- [288] Petersen, H. G. Accuracy and efficiency of the particle mesh Ewald method. *J. Chem. Phys.* **103**, 3668 (1995).

## Appendices

### Appendix A

Table 1: Selected Physiochemical Properties of Liquid Water<sup>1</sup>.

Property	Value
Density	997.047013 kg m <sup>-3</sup>
Molar mass	18.015 g mol <sup>-1</sup>
Molar volume	18.0685 cm <sup>3</sup> mol <sup>-1</sup>
Molar concentration	55.345 mol dm <sup>-3</sup>
Molality	55.508472 mol kg <sup>-1</sup>
Boiling point	373.12 K (at 101.3 kPa)
Melting point	273.15 K
Enthalpy of vaporization	40.657 kJ mol <sup>-1</sup> (at boiling)
Entropy of vaporization	108.95 J mol <sup>-1</sup> K <sup>-1</sup>
Critical temperature	647.1 K
Critical pressure	22.06 MPa
Critical molar volume	55.9 cm <sup>3</sup> mol <sup>-1</sup>
Critical density	322 kg m <sup>-3</sup>
Critical compressibility	0.229
Adiabatic compressibility	0.4477 GPa <sup>-1</sup>
Isothermal compressibility	0.4599 GPa <sup>-1</sup>
Dielectric constant	78.375
Magnetic susceptibility	-1.64 × 10 <sup>-10</sup> m <sup>3</sup> mol <sup>-1</sup>
Electric conductivity	0.05501 × 10 <sup>-6</sup> Ω <sup>-1</sup> cm <sup>-1</sup>
Limiting molar conductivity	H <sup>+</sup> : 349.19 cm <sup>2</sup> Ω <sup>-1</sup> mol <sup>-1</sup> OH <sup>-</sup> : 199.24 cm <sup>2</sup> Ω <sup>-1</sup> mol <sup>-1</sup>
Ionic mobility	H <sup>+</sup> : 3.623 × 10 <sup>-7</sup> m <sup>2</sup> V <sup>-1</sup> s <sup>-1</sup> OH <sup>-</sup> : 2.064 × 10 <sup>-7</sup> m <sup>2</sup> V <sup>-1</sup> s <sup>-1</sup>
Thermal conductivity	0.610 W m <sup>-1</sup> K <sup>-1</sup>
Speed of sound	1496.69922 m s <sup>-1</sup>
Reflective index	1.33286 (λ = 589.26 nm)
pH	6.9976
pK <sub>w</sub>	13.995
Surface tension	0.07198 N m <sup>-1</sup>
Kinematic viscosity	0.8935 × 10 <sup>-6</sup> m <sup>2</sup> s <sup>-1</sup>
Dynamic viscosity	0.8909 mPa s
Bulk viscosity	2.47 mPa s
Diffusion coefficient	0.2299 Å <sup>2</sup> ps <sup>-1</sup>
Dipole moment	2.95 D (at 27 °C)
<sup>1</sup> Specific heat capacity, C <sub>v</sub>	74.539 J mol <sup>-1</sup> K <sup>-1</sup>

---

<sup>1</sup> Specific heat capacity, $C_p$	75.3 J mol <sup>-1</sup> K <sup>-1</sup>
Expansion coefficient	0.000253 °C <sup>-1</sup>
Adiabatic elasticity	2.44 GPa
Joule-Thomson coefficient	0.214 K MPa <sup>-1</sup>
Vapor pressure	3.165 kPa
Cryoscopic constant	1.8597 K kg mol <sup>-1</sup>
Ebullioscopic constant	0.5129 K kg mol <sup>-1</sup>
Polarizability	1.636 × 10 <sup>-40</sup> F m <sup>2</sup>

---

<sup>1</sup>Quantities depend on temperature and/or pressure are given at 25 °C and 101.325 kPa [34].

## Appendix B

Table 2: Crystal Structure and Density of Various Ice Forms<sup>2</sup>.

Ice form	Crystal structure	Density [g cm <sup>-3</sup> ]
I <sub>h</sub>	hexagonal	0.92
I <sub>c</sub>	cubic	0.93
II	rhombohedral	1.17
III	tetragonal	1.14
IV	rhombohedral	1.27
V	monoclinic	1.23
VI	tetragonal	1.31
VII	cubic	1.50
VIII	tetragonal	1.46
IX	tetragonal	1.16
X	cubic	2.51
XI	orthorhombic	0.92
XII	tetragonal	1.29
XIII	monoclinic	1.23
XIV	orthorhombic	1.29
XV	pseudoorthorhombic	1.30
XVI	cubic	0.81

<sup>2</sup>Data collected from ref. [40].

## Appendix C: Parameters and Calculated Properties for Some Water Models.

Table 3: The parameters for some water models.

The water-water pair interaction potential ( $u_{ww}$ ) for polarizable pointcharge water model is calculated using the parameters from Equation 5.2:

$$u_{ww} = 4\epsilon \left[ \left( \frac{\sigma}{r_{00}} \right)^{12} - \left( \frac{\sigma}{r_{00}} \right)^6 \right] + \sum_{i < j} \frac{q_i q_j}{4\pi\epsilon_0 r_{ij}} \quad (5.2)$$

where  $r_{00}$  is the distance between two oxygens, and  $r_{ij}$  is a distance between charges  $q_i$  and  $q_j$ , located on different water molecules.

Table 4: Parameters of Some Water Molecular Models<sup>1</sup>

Model	Type	$\sigma$ [Å]	$\epsilon$ [kJ mol <sup>-1</sup> ]	$l_1$ [Å]	$l_2$ [Å]	$q_i$ [ $e_0$ ]	$\theta$ [deg]	$\phi$ [deg]
SPC	a	3.166	0.65	1	–	–0.82	109.47	–
SPC/E	a	3.166	0.65	1	–	–0.85	109.47	–
TIP4P	b	3.154	0.648	0.957	0.15	–1.04	104.52	52.26
TIP4P-Ew	b	3.164	0.681	0.957	0.125	–1.05	104.52	52.26
TIP4P/2005	b	3.159	0.775	0.957	0.155	–1.11	104.52	52.26

<sup>1</sup>Data collected from [39].

Table 5: Physical and molecular parameters of SPC/E and TIP4P/2005 potential models for H<sub>2</sub>O.

<i>Model</i>	<i>Interaction sites</i>	$L_{OH}$	$L_{OM}$	$\alpha$ (H-O-H)	<i>O position</i>		<i>H position</i>
					<i>Point charge</i>	<i>LJ interaction</i>	<i>Point charge</i>
SPC/E	coplanar	1 Å	---	105.5°	$q_O = -0.8476e$	$\epsilon_{OO} = 0.650$ kJ/mol $\sigma_{OO} = 3.166$ Å	$q_H = +0.4238e$
TIP4P/2005	4	0.957 2 Å	0.15 46 Å	104.52° $q_M = -2q_H$	$q_O = 0$	$\epsilon_{OO} = 0.7749$ kJ/mol $\sigma_{OO} = 3.1589$ Å	$q_H = +0.5564e$

Table 6: Calculated Physical properties of Some Water Models at 25 °C and 101.3 kPa<sup>1</sup>

Model	Dipole moment [D]	Dielectric constant	Self-diffusion, $10^{-5}$ [cm <sup>2</sup> s <sup>-1</sup> ]	Density maximum [°C]	Expansion coefficient, $10^{-4}$ [°C <sup>-1</sup> ]
SPC	2.27	65	3.85	-45	7.3 <sup>2</sup>
SPC/E	2.35	71	2.49	-38	5.14
TIP4P	2.18	53	3.29	-25	4.4
TIP4P-Ew	2.32	62.9	2.4	1	3.1
TIP4P/2005	2.305	60	2.08	5	2.8

<sup>1</sup>Data collected from [39]. <sup>2</sup>At 27 °C.

## Appendix D: Intermolecular peak positions.

Table 7: Intermolecular peak positions in nm for bulk, LiCl:24H<sub>2</sub>O and LiCl:7H<sub>2</sub>O systems at T = 300 K.

Type	R = 24		R = 7		Bulk	
	1 <sup>st</sup> (nm)	2 <sup>nd</sup> (nm)	1 <sup>st</sup> (nm)	2 <sup>nd</sup> (nm)	1 <sup>st</sup> (nm)	2 <sup>nd</sup> (nm)
O-O	0.28	–	0.28	–	0.28	–
O-H	0.18	0.32	0.18	0.33	0.18	0.32
H-H	0.24	–	0.24	–	0.24	–
Li-Cl	0.23	0.45	0.23	0.46		
Li-O	0.19	0.41	0.19	0.42		
Li-H	0.26	0.47	0.26	0.46		
Li-Li	0.57	–	0.40	–		
Cl-O	0.32	0.49	0.32	0.48		
Cl-H	0.22	0.36	0.22	0.36		
Cl-Cl	0.39	0.51	0.39	0.51		
Cl-Li	0.23	0.45	0.23	0.46		
Cl-H	0.22	0.36	0.22	0.36		
Li-H	0.26	0.46	0.26	0.46		

Table 8: Intermolecular peak positions in Å derived by the correlations of the Bulk, LiCl:24H<sub>2</sub>O and LiCl:7H<sub>2</sub>O systems at T = 300 K.

Type	R = 24		R = 7		Bulk	
	1 <sup>st</sup> (Å)	2 <sup>nd</sup> (Å)	1 <sup>st</sup> (Å)	2 <sup>nd</sup> (Å)	1 <sup>st</sup> (Å)	2 <sup>nd</sup> (Å)
O-O	2.8	–	2.8	–	2.8	–
O-H	1.8	3.2	1.8	3.3	1.8	3.2
H-H	2.4	–	2.4	–	2.4	–
Li-Cl	2.3	4.5	2.3	4.6		
Li-O	1.9	4.1	1.9	4.2		
Li-H	2.6	4.7	2.6	4.6		
Li-Li	5.7	–	4.0	–		
Cl-O	3.2	4.9	3.2	4.8		
Cl-H	2.2	3.6	2.2	3.6		
Cl-Cl	3.9	5.1	3.9	5.1		
Cl-Li	2.3	4.5	2.3	4.6		
Cl-H	2.2	3.6	2.2	3.6		
Li-H	2.6	4.6	2.6	4.6		

Table 9: Intermolecular peak positions in nm derived by the correlations of the LiCl:24H<sub>2</sub>O and LiCl:7H<sub>2</sub>O systems at T = 240 K.

Type	R = 24		R = 7		Bulk	
	1 <sup>st</sup> (nm)	2 <sup>nd</sup> (nm)	1 <sup>st</sup> (nm)	2 <sup>nd</sup> (nm)	1 <sup>st</sup> (nm)	2 <sup>nd</sup> (nm)
O-O	0.28	–	0.28	–	0.28	–
O-H	0.18	0.32	0.18	0.32	0.18	0.32
H-H	0.23	–	0.23	–	0.23	–
Li-Cl	0.23	0.45	0.23	0.46		
Li-O	0.19	0.41	0.19	0.42		
Li-H	0.26	0.46	0.26	0.46		
Li-Li	0.57	–	0.40	–		
Cl-O	0.32	0.48	0.32	0.48		
Cl-H	0.22	0.36	0.22	0.36		
Cl-Cl	0.51	–	0.39	0.51		
Cl-Li	0.23	0.45	0.23	0.46		
Cl-H	0.22	0.35	0.22	0.36		
Li-H	0.26	0.46	0.26	0.46		

Table 10: Intermolecular peak positions in Å derived by the correlations of the Bulk, LiCl:24H<sub>2</sub>O and LiCl:7H<sub>2</sub>O systems at T = 240 K.

Type	R = 24		R = 7		Bulk	
	1 <sup>st</sup> (Å)	2 <sup>nd</sup> (Å)	1 <sup>st</sup> (Å)	2 <sup>nd</sup> (Å)	1 <sup>st</sup> (Å)	2 <sup>nd</sup> (Å)
O-O	2.8	–	2.8	–	2.8	–
O-H	1.8	3.2	1.8	3.2	1.8	3.2
H-H	2.3	–	2.3	–	2.3	–
Li-Cl	2.3	4.5	2.3	4.6		
Li-O	1.9	4.1	1.9	4.2		
Li-H	2.6	4.6	2.6	4.6		
Li-Li	5.7	–	4.0	–		
Cl-O	3.2	4.8	3.2	4.8		
Cl-H	2.2	3.6	2.2	3.6		
Cl-Cl	5.1	–	3.9	5.1		
Cl-Li	2.3	4.5	2.3	4.6		
Cl-H	2.2	3.5	2.2	3.6		
Li-H	2.6	4.6	2.6	4.6		

Table 11: Intermolecular peak positions in nm derived by the correlations of the LiCl:24H<sub>2</sub>O and LiCl:7H<sub>2</sub>O systems at T = 210 K.

Type	R = 24		R = 7		Bulk	
	1 <sup>st</sup> (nm)	2 <sup>nd</sup> (nm)	1 <sup>st</sup> (nm)	2 <sup>nd</sup> (nm)	1 <sup>st</sup> (nm)	2 <sup>nd</sup> (nm)
O-O	0.28	–	0.28	–	0.28	–
O-H	0.18	0.32	0.18	0.32	0.18	0.32
H-H	0.23	–	0.23	–	0.23	–
Li-Cl	0.23	0.45	0.23	0.46		
Li-O	0.19	0.41	0.19	0.42		
Li-H	0.26	0.46	0.26	0.46		
Li-Li	0.56	–	0.40	–		
Cl-O	0.31	0.49	0.32	0.48		
Cl-H	0.22	0.35	0.22	0.36		
Cl-Cl	0.39	0.51	0.39	0.50		
Cl-Li	0.23	0.45	0.23	0.46		
Cl-H	0.22	0.36	0.22	0.36		
Li-H	0.26	0.46	0.26	0.46		

Table 12: Intermolecular peak positions in Å derived by the correlations of the Bulk, LiCl:24H<sub>2</sub>O and LiCl:7H<sub>2</sub>O systems at T = 210 K.

Type	R = 24		R = 7		Bulk	
	1 <sup>st</sup> (Å)	2 <sup>nd</sup> (Å)	1 <sup>st</sup> (Å)	2 <sup>nd</sup> (Å)	1 <sup>st</sup> (Å)	2 <sup>nd</sup> (Å)
O-O	2.8	–	2.8	–	2.8	–
O-H	1.8	3.2	1.8	3.2	1.8	3.2
H-H	2.3	–	2.3	–	2.3	–
Li-Cl	2.3	4.5	2.3	4.6		
Li-O	1.9	4.1	1.9	4.2		
Li-H	2.6	4.6	2.6	4.6		
Li-Li	5.6	–	4.0	–		
Cl-O	3.1	4.9	3.2	4.8		
Cl-H	2.2	3.5	2.2	3.6		
Cl-Cl	3.9	5.1	3.9	5.0		
Cl-Li	2.3	4.5	2.3	4.6		
Cl-H	2.2	3.6	2.2	3.6		
Li-H	2.6	4.6	2.6	4.6		

Appendix E: Data for Local Structure Index (LSI) for water, LiCl:24H<sub>2</sub>O and LiCl:7H<sub>2</sub>O systems at T = 300 K, T = 240 K and T = 210 K.

Table 13: Local Structure Index (LSI) for water, LiCl:24H<sub>2</sub>O and LiCl:7H<sub>2</sub>O systems at T = 300 K.

System	I (Å <sup>2</sup> )		I (Å)		P (I)	
	1 <sup>st</sup> peak	2 <sup>nd</sup> peak	1 <sup>st</sup> peak	2 <sup>nd</sup> peak	1 <sup>st</sup> peak	2 <sup>nd</sup> peak
Water	0.03	0.16	0.17	0.40	9.89	2.59
R = 24	0.03	0.18	0.17	0.42	11.34	1.83
R = 7	0.02	0.20	0.14	0.45	13.40	1.07

Table 14: Data for Local Structure Index (LSI) for water, LiCl:24H<sub>2</sub>O and LiCl:7H<sub>2</sub>O systems at T = 240 K.

System	I (Å <sup>2</sup> )		I (Å)		P (I)	
	1 <sup>st</sup> peak	2 <sup>nd</sup> peak	1 <sup>st</sup> peak	2 <sup>nd</sup> peak	1 <sup>st</sup> peak	2 <sup>nd</sup> peak
Water	0.06	0.17	0.24	0.41	6.66	3.59
R = 24	0.03	0.17	0.17	0.41	7.78	2.42
R = 7	0.02	0.20	0.14	0.45	12.42	1.22

Table 15: Data for Local Structure Index (LSI) for water, LiCl:24H<sub>2</sub>O and LiCl:7H<sub>2</sub>O systems at T = 210 K.

System	I (Å <sup>2</sup> )		I (Å)		P (I)	
	1 <sup>st</sup> peak	2 <sup>nd</sup> peak	1 <sup>st</sup> peak	2 <sup>nd</sup> peak	1 <sup>st</sup> peak	2 <sup>nd</sup> peak
Water	0.10	0.22	0.32	0.47	3.20	4.28
R = 24	0.07	0.20	0.26	0.45	5.92	2.93
R = 7	0.02	0.20	0.14	0.45	11.63	1.49

Table 16: Data for Local Structure Index (LSI) for LiCl:24H<sub>2</sub>O for T = 300 K, T = 240 K and T = 210 K.

T, K	I (Å <sup>2</sup> )		I (Å)		P (I)	
	1 <sup>st</sup> peak	2 <sup>nd</sup> peak	1 <sup>st</sup> peak	2 <sup>nd</sup> peak	1 <sup>st</sup> peak	2 <sup>nd</sup> peak
300	0.06	0.18	0.24	0.42	10.92	1.78
240	0.03	0.17	0.17	0.41	7.74	2.45
210	0.07	0.20	0.26	0.45	5.71	2.81

Table 17: Data for Local Structure Index (LSI) for LiCl:7H<sub>2</sub>O for T = 300 K, T = 240 K and T = 210 K.

T, K	I (Å <sup>2</sup> )		I (Å)		P (I)	
	1 <sup>st</sup> peak	2 <sup>nd</sup> peak	1 <sup>st</sup> peak	2 <sup>nd</sup> peak	1 <sup>st</sup> peak	2 <sup>nd</sup> peak
300	0.02	–	0.14	–	13.13	–
240	0.02	–	0.14	–	12.14	–
210	0.02	–	0.14	–	11.29	–

Appendix F: Data for the distribution of the orientational order,  $Q$ , for water, LiCl:24H<sub>2</sub>O and LiCl:7H<sub>2</sub>O systems at T = 300 K, T = 240 K and T = 210 K.

Table 18: Data for the distribution of the orientational order,  $Q$ , for water, LiCl:24H<sub>2</sub>O and LiCl:7H<sub>2</sub>O systems at T = 300 K.

System	$Q$		$P(Q)$	
	1 <sup>st</sup> peak	2 <sup>nd</sup> peak	1 <sup>st</sup> peak	2 <sup>nd</sup> peak
Bulk	–	0.87	–	3.42
$R = 24$	0.50	0.75	1.83	1.64
$R = 7$	–	0.49	–	2.11

Table 19: Data for the distribution of the orientational order,  $Q$ , for water, LiCl:24H<sub>2</sub>O and LiCl:7H<sub>2</sub>O systems at T = 240 K.

System	$Q$		$P(Q)$	
	1 <sup>st</sup> peak	2 <sup>nd</sup> peak	1 <sup>st</sup> peak	2 <sup>nd</sup> peak
Bulk	–	0.85	–	3.43
$R = 24$	0.51	0.83	1.38	2.25
$R = 7$	–	0.49	–	2.15

Table 20: Data for the distribution of the orientational order,  $Q$ , for water, LiCl:24H<sub>2</sub>O and LiCl:7H<sub>2</sub>O systems at T = 210 K.

System	$Q$		$P(Q)$	
	1 <sup>st</sup> peak	2 <sup>nd</sup> peak	1 <sup>st</sup> peak	2 <sup>nd</sup> peak
Bulk	–	0.91	–	5.15
$R = 24$	0.49	0.89	1.15	2.79
$R = 7$	0.06	0.48	0.60	2.16

Table 21: Data for the distribution of the orientational order,  $Q$ , for LiCl:24H<sub>2</sub>O and LiCl:7H<sub>2</sub>O systems at T = 300 K, T = 240 K and T = 210 K.

$T, K$	$R = 24$				$R = 7$			
	$Q$		$P(Q)$		$Q$		$P(Q)$	
	1 <sup>st</sup> pk	2 <sup>nd</sup> pk						
300	0.51	–	1.83	–	0.49	–	2.08	–
240	0.51	0.83	1.38	2.27	0.49	–	2.12	–
210	0.48	0.89	1.14	2.78	0.49	–	2.16	–

Appendix G: Data for Angular Distribution Function  $P(\cos \gamma)$  for water,  
LiCl:24H<sub>2</sub>O and LiCl:7H<sub>2</sub>O systems at T = 300 K, T = 240 K and  
T = 210 K.

Table 22: Data for Angular Distribution Function  $P(\cos \gamma)$  for water,  
LiCl:24H<sub>2</sub>O and LiCl:7H<sub>2</sub>O systems at T = 300 K.

System	$\cos \gamma$		$\gamma$ (°)		$P(\cos \gamma)$	
	1 <sup>st</sup> peak	2 <sup>nd</sup> peak	1 <sup>st</sup> peak	2 <sup>nd</sup> peak	1 <sup>st</sup> peak	2 <sup>nd</sup> peak
Bulk	-0.18	0.60	100.4	53.1	0.17	0.14
$R = 24$	-0.20	0.58	101.5	54.5	0.15	0.13
$R = 7$	-0.18	0.51	100.4	59.3	0.11	0.15

Table 23: Data for Angular Distribution Function  $P(\cos \gamma)$  for water,  
LiCl:24H<sub>2</sub>O and LiCl:7H<sub>2</sub>O systems at T = 240 K.

System	$\cos \gamma$		$\gamma$ (°)		$P(\cos \gamma)$	
	1 <sup>st</sup> peak	2 <sup>nd</sup> peak	1 <sup>st</sup> peak	2 <sup>nd</sup> peak	1 <sup>st</sup> peak	2 <sup>nd</sup> peak
Bulk	-0.26	0.61	105.1	52.4	0.17	0.09
$R = 24$	-0.26	0.60	105.1	53.1	0.16	0.10
$R = 7$	-0.28	0.51	106.3	53.3	0.12	0.15

Table 24: Data for Angular Distribution Function  $P(\cos \gamma)$  for water,  
LiCl:24H<sub>2</sub>O and LiCl:7H<sub>2</sub>O systems at T = 210 K.

System	$\cos \gamma$		$\gamma$ (°)		$P(\cos \gamma)$	
	1 <sup>st</sup> peak	2 <sup>nd</sup> peak	1 <sup>st</sup> peak	2 <sup>nd</sup> peak	1 <sup>st</sup> peak	2 <sup>nd</sup> peak
Bulk	-0.29	0.61	106.9	52.4	0.20	0.04
$R = 24$	-0.27	0.52	105.7	58.7	0.16	0.08
$R = 7$	-0.26	0.50	105.1	60.0	0.12	0.15

Table 25: Data for Angular Distribution Function  $P(\cos \gamma)$  for LiCl:24H<sub>2</sub>O at T = 300 K, T = 240 K and T = 210 K.

$T, K$	1 <sup>st</sup> peak			2 <sup>nd</sup> peak		
	$\cos \gamma$	$\gamma$ (°)	$P(\cos \gamma)$	$\cos \gamma$	$\gamma$ (°)	$P(\cos \gamma)$
300	-0.21	102.1	0.15	0.58	54.5	0.14
240	-0.26	105.1	0.16	0.58	54.5	0.10
210	-0.27	105.7	0.17	0.52	58.7	0.08

Table 26: Data for Angular Distribution Function  $P(\cos \gamma)$  for LiCl:7H<sub>2</sub>O at T = 300 K, T = 240 K and T = 210 K.

$T, K$	1 <sup>st</sup> peak			2 <sup>nd</sup> peak		
	$\cos \gamma$	$\gamma$ (°)	$P(\cos \gamma)$	$\cos \gamma$	$\gamma$ (°)	$P(\cos \gamma)$
300	-0.27	105.7	0.11	0.53	58.0	0.15
240	-0.28	106.3	0.12	0.51	59.3	0.15
210	-0.26	105.1	0.12	0.50	60.0	0.15

Appendix H: Data for the number of HBs per water molecule for bulk,  
LiCl:24H<sub>2</sub>O and LiCl:7H<sub>2</sub>O at T = 300 K, T = 240 K and T = 210  
K.

Table 27: Data for the number of HBs per water molecule for bulk,  
LiCl:24H<sub>2</sub>O and LiCl:7H<sub>2</sub>O at T = 300 K.

Species	HB per molecule						Fraction of H <sub>2</sub> O molecules					
Bulk	–	1.0	2.0	3.0	4.0	5.0	–	0.01	0.06	0.28	0.57	0.07
R = 24	0.0	1.0	2.0	3.0	4.0	5.0	0.00	0.05	0.18	0.33	0.39	0.05
R = 7	0.0	1.5	2.0	3.0	4.0	5.0	0.05	0.18	0.29	0.29	0.16	0.02

Table 28: Data for the number of HBs per water molecule for bulk,  
LiCl:24H<sub>2</sub>O and LiCl:7H<sub>2</sub>O at T = 240 K.

Species	HB per molecule						Fraction of H <sub>2</sub> O molecules					
Bulk	–	–	2.0	3.0	4.0	5.0	–	–	0.01	0.14	0.79	0.05
R = 24	0.0	1.0	2.0	3.0	4.0	5.0	0.00	0.03	0.13	0.28	0.51	0.04
R = 7	0.0	1.5	2.0	3.0	4.0	5.0	0.04	0.17	0.29	0.31	0.18	0.01

Table 29: Data for the number of HBs per water molecule for bulk,  
LiCl:24H<sub>2</sub>O and LiCl:7H<sub>2</sub>O at T = 210 K.

Species	HB per molecule						Fraction of H <sub>2</sub> O molecules					
Bulk	–	–	–	3.0	4.0	5.0	–	–	–	0.04	0.94	0.02
R = 24	0.0	1.0	2.0	3.0	4.0	5.0	0.00	0.03	0.11	0.26	0.58	0.02
R = 7	0.0	1.5	2.0	3.0	4.0	5.0	0.04	0.16	0.29	0.33	0.18	0.01

---

## Vita

### Biography

Inna Bashta was born in the Ukraine. She was raised in the UK and attended private school from which she graduated with Gold Medal Honours. She was trained in classical ballet and spent many years performing as a renowned ballerina worldwide. Upon moving to the USA, she dedicated herself to combining her performing career with getting her higher education in sciences. She concluded her performing career to become a scientist.

### Academic Credentials

PhD Student, Theoretical Condensed Matter Physics,  
Università degli Studi Roma Tre  
Thesis: Structural anomalies of supercooled water in LiCl solution  
Advisor: *Professor P. Gallo*

Graduate Research Student, Nuclear Physics and RadioChemistry, UNLV  
Project: Nuclear Transmutation of  $^{238}\text{U}$  and  $^{235}\text{Pu}$  at the Yucca Mt. Nuclear  
Waste Repository  
Advisor: *Professor K. Czerwinski*

BS/MS Summa Cum Laude, Chemistry, UNLV | ALS LBNL, Berkeley, CA  
Thesis: Challenging the Dipole Approximation: Showcase Valence Shell  
Photoionization of Nitrogen at Low Photon Energies  
Mentor: *Dr. O. Hemmers*, Advisor: *Professor D. W. Lindle*

Fellowship in Particle Physics, Nuclear and RadioChemistry |  
DOE/DOD/NSF | SUNY | RHIC BNL, NY  
Mentor: *Professor G. Friedländer*

### Relevant Research Experience

Performed and presented to INFN task: NSW-SM1 Final Summary on Mesh  
Production at RM3 Site and Mesh Integration on Drift Panels at LNF

Became a member of ATLAS Experiment at CERN

### Languages, Teaching, Leadership and Public Service

Languages: English, Ukrainian, Russian, Spanish | Creative Writing |  
Teaching: Sciences, Languages, Memory | Business Owner | Charities and  
Fundraisers | Public Figure | Military Service Volunteer, Ukraine